SSCL-SR-1054
UC-414

Superconducting Super Collider Laboratory

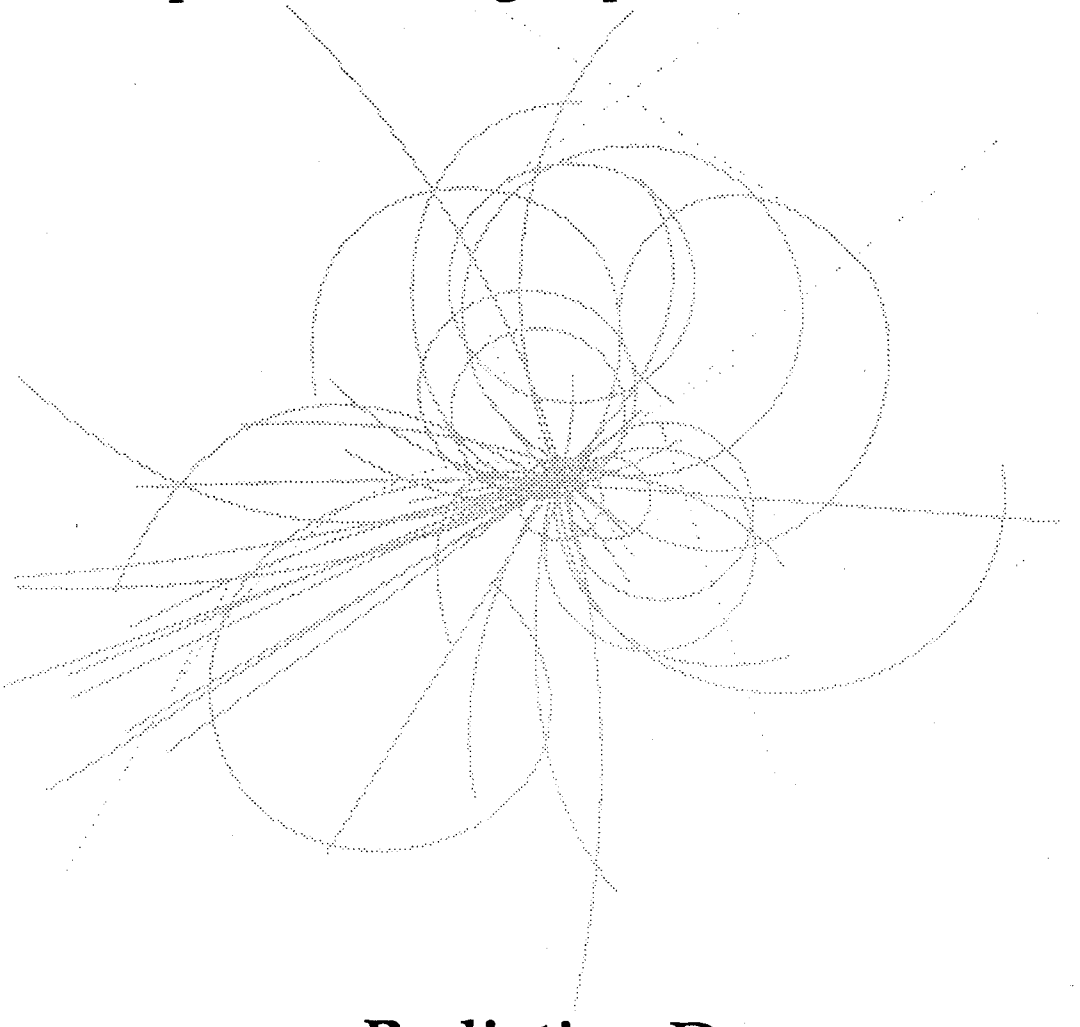

Radiation Damage Testing at the SSC

W. Chinowsky and R. Thun, Editors

June 1990

SSCL-SR-1054

RADIATION DAMAGE TESTING AT THE SSC

Task Force Report

W. Chinowsky and R. Thun, Editors

Superconducting Super Collider Laboratory*

Physics Research Division

2550 Beckleymeade Avenue

Dallas, TX 75237

June 1990

* Operated by Universities Research Association, Inc. under contract with the U.S. Department of Energy.

SUMMARY

A Task Force on Radiation Damage Testing met at the SSC Laboratory on March 5–6, 1990. This Task Force was asked to assess the availability of appropriate facilities for radiation damage tests of SSC detector materials and components. The Task Force was also instructed to review the techniques and standards for conducting such tests. Semiconductors were considered separately from other detector materials. Radiation damage tests of electronic devices generally require exposures to both ionizing radiation and neutrons, whereas non-electronic components such as plastic scintillating materials, adhesives, cable insulation, and other organic polymers are adequately tested with ionizing radiation only.

The Task Force compiled listings of existing radiation facilities. Suitable radioactive sources include ^{60}Co for ionizing particles and ^{252}Cf for neutrons. Ionizing particles and neutrons are also available at accelerator laboratories with primary proton and electron beams and at nuclear reactors. While many sources and beams are available, the Task Force recommends that the SSC Laboratory purchase at least one ^{252}Cf source to facilitate the testing of electronic components. This source should be located at an existing, easily accessible, and properly instrumented laboratory site.

Test standards were discussed with respect to irradiation techniques, environmental factors, dosimetry, and mechanisms whereby various materials are damaged. It was emphasized that radiation sources should be chosen to duplicate as much as possible the expected SSC environment and that the effects from ionizing particles and from neutrons be investigated separately. Radiation damage tests at reactors must be designed with particular care since complex spectra of neutrons and gamma rays are produced at such facilities. It is also essential to investigate dose-rate effects since they are known to be important in many cases. The required irradiations may last several months and are most easily carried out with dedicated radioactive sources. Environmental factors such as the presence of oxygen when testing plastic scintillators, or temperature when measuring semiconductor annealing effects, must also be taken into account. The importance of reliable dosimetry was stressed and suitable references cited. Finally, it was noted that an understanding of the mechanisms for radiation damage in semiconductor and other materials is important in planning irradiations and evaluating results.

TABLE OF CONTENTS

1. GENERAL DISCUSSION 1
2. RECOMMENDATIONS ON SOURCES AND STANDARDS 6
3. RADIATION SOURCE FACILITIES AT MAJOR U.S. LABORATORIES 9
4. RADIATION DAMAGE STANDARDS FOR ORGANIC MATERIALS USED IN SSC DETECTORS 11
TASK FORCE CHARGE 13
TASK FORCE MEMBERSHIP 14

APPENDICES
1. "Radiation Levels in Detectors at the SSC," D. Groom 17
2. "Experience with IEC Standard 544 to Assess Radiation Damage of Organic Insulating Materials," H. Schonbacher and M. Tavlet . . . 25
3. "Radiation Sources for Material Testing in Europe," H. Schonbacher and M. Tavlet 42
4. "Overview of Radiation Effects on Polymers," R. L. Clough and K. T. Gillen 58
5. "Recommended Total-Dose Radiation Test Guidelines for SSC Detector Applications," P. S. Winokur and D. M. Fleetwood 71
6. "Standards for Electronics Radiation Testing and Remarks about SSC Displacement Damage Testing," E. L. Petersen and P. W. Marshall108
7. "Radiation Studies in Iron Calorimeter Structures," J. S. Russ . . . 136
8. "Comments on Radiation Damage Tests with Neutron Sources and Other Available Sources," H. W. Kraner 152
9. "Rad-Hard Electronics Development Program for SSC Liquid-Argon Calorimeters," A. Stevens, J.Dawson, H. Kraner, V. Radeka, and S. Rescia 163
10. "Radiation Damage Tests with Neutron and Proton Sources," H. F.-W. Sadrozinski 174
11. "Irradiation Facilities at the Los Alamos Meson Physics Facility," V. Sandberg 185
12. "Guidelines for Measurements of Radiation Effects in SSC Semiconductor Detectors and Electronics," H. Spieler 222
13. "Electron Accelerators as Irradiation Facilities," S. Majewski . . . 229
14. "Radiation Displacement Damage Testing at JPL," G. Soli 244

1. GENERAL DISCUSSION

This is the third in a series of reports that address the problems of radiation damage to detector components at the SSC. In the first (Ref. [1]), estimates were presented of the radiation environment expected at the SSC. It was shown that beam-beam collisions will be the major source of radiation at the detectors. The assumptions and methods for estimating radiation levels are summarized by Groom in Appendix 1. The two major components of radiation are ionizing particles and neutrons. A primary flux of ionizing particles is produced by the proton-proton collisions and is then amplified by interactions in the electromagnetic and hadronic calorimeters. Neutrons with an energy-weighted spectrum that peaks at about 1 MeV are produced copiously in hadronic showers and tend to spread throughout the whole detector volume. For SSC operating at 40 TeV and at a standard luminosity of 10^{33} cm^{-2} sec^{-1}, the yearly dose from ionizing radiation in a tracking element 10 cm from the beam axis is about 0.4 Mrad; within an electromagnetic calorimeter at small angles (5 degrees) this can exceed 10 Mrad. The annual neutron fluence is of order 10^{12} cm^{-2} near the collision point and reaches 10^{14} cm^{-2} inside the forward portion of the hadronic calorimeter.

The second report (Ref. [2]) described the deleterious effects of this radiation on detector components. The radiation levels expected at the SSC are such that significant damage can occur in many of the detectors now under consideration. These include silicon tracking devices, wire chambers, scintillators, optical media, electronic circuitry, and insulating materials used in signal feedthroughs and cables. It is essential that SSC detector materials be chosen and evaluated to insure successful operation and survival in the SSC radiation environment. A body of knowledge already exists regarding the effects of radiation on materials and electronic devices. However, results have sometimes been inconsistent or not directly applicable to specific SSC detector issues. In many cases, the required research has not yet been carried out. It is therefore recognized that additional,

systematic studies must be performed under controlled and well-understood exposure conditions that duplicate as much as possible the situation expected at the SSC. In particular, careful attention must be given to dosimetry and, in the case of irradiating neutrons, to measurements of their energy spectrum.

One of the primary goals of this third report is to provide a listing and evaluation of existing sources suitable for radiation damage tests of SSC detector components. The reports by Schonbacher and Tavlet (Appendix 3), Winokur and Fleetwood (Appendix 5), Peterson and Marshall (Appendix 6), Kraner (Appendix 8), Stevens et alii (Appendix 9), Sandberg (Appendix 11), and Majewski (Appendix 13) give extensive lists of radiation sources. Descriptions of additional sources can be found in several other appendices as well. A summary of the radiation facilities located at several major U.S. laboratories is given Section 3.

Three kinds of sources are available: accelerators, nuclear reactors, and radioactive materials. Each can provide useful particle types, energies, and doses. All have been used in previous studies. There are, however, significant differences in accessibility, convenience, and cost of irradiations. Operation at accelerators and reactors may require substantial preparation and, in some cases, elaborate instrumentation. Unless such operation is parasitic (such as behind beam stops), it must be scheduled within an often crowded program at the particular facility. It is therefore often preferable to use dedicated radioactive sources, especially when long exposures are required. However, in some instances the greater penetration possible with high-energy particle beams may be necessary to make realistic measurements of radiation effects on detector systems or modules. For example, electromagnetic showers produce a characteristic pattern of energy deposit inside a calorimeter that cannot be duplicated with radiation from low-energy radioactive sources. Radiation effects on such detector systems will require study with higher energy beams that can mimic more closely the pattern of radiation damage within the system volume. This point is discussed by Majewski in Appendix 13.

Accelerator beams of protons or electrons are suitable for radiation damage tests. Representative beams are described by Sandberg in Appendix 11 and Majewski in Appendix 13. Accelerators can also generate suitable neutron beams such as those at the Intense Pulsed Neutron Source (IPNS) at Argonne National Laboratory described by Stevens et alii in Appendix 9. This beam is created by exposing a uranium target to a beam of 500 MeV protons. The resulting spectrum of spallation and fission neutrons closely matches that of neutrons produced at the SSC. An excellent spectrum match is also provided by the neutrons emerging from the beam stop of the Radiation Effects Facility at Los Alamos as discussed in Appendices 10 and 11.

Nuclear reactors also provide intense sources of neutrons and ionizing radiation. An extensive listing of reactors is given in Ref. [3]. A typical example of a conveniently accessible reactor is the University of Michigan facility which routinely provides exposures for radiation damage tests. Users of nuclear reactors must exercise care to insure that the irradiation spectrum and composition matches that expected at the SSC. For example, thermal neutrons, which are produced copiously at reactors but less so at the SSC, may require the use of cadmium-lined containers as filters when performing certain irradiations at reactors.

Ionizing radiation and neutrons can also be generated with radioactive sources. The gamma rays from ^{60}Co decays are commonly used to produce ionizing radiation. Facilities for carrying out irradiations with ^{60}Co or other equivalent sources exist at many laboratories as indicated in the appendices. When using ^{60}Co sources it is important to consider dose-enhancement effects and charged-particle equilibrium of the Compton electrons (Ref. [4]–[6]). Neutron sources with appropriate intensities are less readily available. Such sources exist in two generic types: Be in combination with alpha emitters such as Am which produce neutrons via (α, n) reactions, and fission sources such as ^{252}Cf. The energy spectrum of neutrons produced in (α, n) reactions has a broad peak

around 4-5 MeV which is higher than the typical 1 MeV energy at the SSC. The ^{252}Cf spectrum which peaks at around 2 MeV gives a closer match.

Radiation damage tests have been and will be carried out at many different facilities. This raises the question of the comparability of results obtained in such diverse radiation environments. The report by Petersen and Marshall (Appendix 6) notes that the concept of non-ionizing energy loss (NIEL) allows one to relate the displacement damage in semiconductors from any particle to that produced by 1 MeV neutrons. Although the calculations may not yield conversion factors with adequate accuracy for precise quantitative scaling, this concept does offer the prospect of using a conveniently available source and calibrating it to provide results valid for the radiation field of the SSC.

The second major goal of this report is the establishment of standards appropriate for radiation damage tests of SSC detector components. A number of existing general standards may have specific application to the SSC program. Petersen and Marshall give a very extensive listing in Appendix 6 of American Society of Testing and Materials (ASTM) Standards as well as of Military Standards. The report by Schonbacher and Tavlet in Appendix 2 describes experience with IEC Standard 544 used for rating organic insulating materials. That report, as well as the one by Clough and Gillen in Appendix 4, stresses the importance of dose rate in predicting radiation damage. For a fixed total dose, many organic materials show much more severe damage when exposed at low dose rates. The time dependence of annealing effects at the oxide-silicon interface of electronic devices is discussed by Winokur and Fleetwood in Appendix 5 and also in Ref. [4]. The observation that significant changes in material properties can occur over long time periods after irradiation introduces a further complication in the study of radiation damage effects. The Task Force on Radiation Damage Testing at the SSC thought it neither appropriate nor possible in the time available to suggest specific standards for the SSC. General recommendations on this subject are given in Section 2.

The Task Force also considered briefly the difficult and complicated topic of dosimetry. Accurate dosimetry is essential for obtaining reproducible radiation damage test results and for comparing data from different irradiations. For example, the report by Russ in Appendix 7 describes the use of activation foils to measure the energies and fluences of neutrons produced in hadronic shower cascades. Besides activation foils, techniques for dose measurements include thermoluminescent dosimetry (TLD), the use of alanine (Ref. [7]), and the determination of radiation-induced PIN diode leakage currents.

Thermoluminescent dosimetry has become the preferred technique at many facilities especially in applications involving ionizing radiation (Ref. [8]). Lithium fluoride is the prinicipal TLD material because the dose effect is stable over long time periods, is linear in response between 10^{-2} and 10^{3} rad, and has a known saturated response at higher doses. It may also be applied to neutron dosimetry by the incorporation of ^{6}Li in the crystal. Thermoluminescent dosimetry is inexpensive (each TLD element can be reused after a short annealing period), easy to read out, and available commercially as a system.

Alanine dosimetry is based on the creation of stable free radicals under ionizing radiation. These radicals are detected reliably, even long after exposure, with electron spin resonance (ESR) techniques. The required equipment is not widely available, however, and is rather expensive to acquire.

As with test standards, the Task Force thought it appropriate to give only general recommendations on dosimetry, as indicated in Section 2. Detailed discussions of dosimetry for irradiations of electronic devices, for example, can be found in Refs. [4]and [6].

2. RECOMMENDATIONS ON SOURCES AND STANDARDS

The Task Force on Radiation Damage Testing at the SSC makes the following general recommendations:

a) Non-electronic detector components such as plastic scintillators, cable insulation, optical fibers, adhesives, wire chambers, and calorimeter active media can be tested adequately with ionizing radiation alone. A ^{60}Co source is appropriate for such irradiations in most but not all cases. Particle beams and reactors are also useful but generally require additional care in dosimetry. It is important to note that beams of high-energy (>1 GeV) particles will be required to provide realistic radiation exposure patterns for tests of calorimeter modules or systems.

b) Electronic devices such as solid-state detectors, amplifiers, and integrated circuits should be tested for both ionization effects and displacement damage. Ionization effects typically occur at oxide-silicon interfaces, whereas displacement damage affects bulk properties, for example, in depletion regions. ^{60}Co is a convenient source of ionizing radiation if proper precautions are taken (Refs. [4, 5]). Displacement damage can be induced by neutron or proton irradiations. Neutrons of about 1 MeV are a good choice since they match the spectrum of the calorimeter background, are practically free of ionization effects, and can be scaled to the effects of charged-particle irradiations. ^{252}Cf is a suitable neutron source. Spallation sources and reactors are also useful for performing neutron damage tests. The use of proton beams with momenta below 1 GeV/c is described by Sadrozinski in Appendix 10. It should be noted that ^{60}Co gamma rays also produce displacement damage; for some measurements this must be taken into account (Ref. [9]).

c) Annealing effects in semiconductors and in materials such as plastic scintillators make radiation damage dependent on both dose rate and on total

dose. It is, therefore, essential to perform irradiations at different dose rates to allow extrapolations to the expected life span of the experiments.

d) Systematic dose rate studies may require the acquisition of sources specifically dedicated to SSC detector testing. In particular, the Task Force recommends that a ^{252}Cf neutron source be purchased and located at an existing, accessible laboratory. The SSC detector R&D budgets should also provide for appropriate user fees to insure that radiation damage tests can be carried out at existing facilities.

e) Possible radiation damage requirements for the use of organic materials in SSC detectors are given in Section 4 as an example of what might be attempted in formulating standards. Electronics standards would be highly application and device dependent and are not easily summarized. It is the responsibility of the experimenter to estimate, for each component of a particular detector, the expected dose rate and total dose and to insure, on the basis of reproducible damage tests, that the component can perform its function during the lifetime of the SSC experiment.

f) Accurate dosimetry is essential for obtaining reproducible radiation damage test results. Detector physicists who perform radiation tests are advised to become familiar with the dosimetry techniques at the irradiation facilities where the tests are performed. Information is also available in a number of references and at the National Institute of Standards and Technology (NIST).

g) Radiation damage can depend in a complicated way on the type of radiation, total dose, dose rate, environment (temperature, presence of oxygen), and may even vary from sample to sample because of minor changes in configuration or chemical composition. Tests should be designed to determine how these various factors affect the damage mechanism.

REFERENCES

1. "Radiation Levels in the SSC Interaction Regions," SSC-SR-1033, edited by D. E. Groom (SSC Central Design Group, 1988).
2. "Radiation Effects at the SSC," SSC-SR-1035, edited by M.G.D. Gilchriese (SSC Central Design Group, 1988).
3. *Research, Training, Test and Production Reactor Directory, United States of America,* edited by R. R. Burn (American Nuclear Society, 1988).
4. *Ionizing Radiation Effects in MOS Devices and Circuits*, edited by T. P. Ma and P. V. Dressendorfer (Wiley, New York, 1989).
5. J. R. Srour et al., *Radiation Effects on and Dose Enhancement of Electronic Materials* (Noyes Publications, Park Ridge, 1984).
6. G. C. Messenger and M. S. Ash *The Effects of Radiation on Electronic Systems* (Van Nostrand Reinhold, New York, 1986).
7. F. Coninckx et al., "Alanine Dosimetry as Reference Dosimetric System in Accelerator Radiation Environment," Appl. Rad. Iso. **40** (10-12), 977-983 (1989).
8. Glenn F. Knoll, *Radiation Detection and Measurement* (Wiley, New York, 1979).
9. J. R. Srour et al., "Radiation Damage Coefficients for Silicon Depletion Regions," IEEE Trans. Nucl. Sci. **NS-26**, 4784-4791 (1979).

3. RADIATION SOURCE FACILITIES AT MAJOR U.S. LABORATORIES

We list below some of the radiation sources available at several major U.S. laboratories. The reader is referred to the appropriate appendices for more detailed information. Appendix 6 by Petersen and Marshall lists facilities at some additional sites. Schonbacher and Tavlet give an extensive listing of European radiation sources in Appendix 3.

Argonne National Lab (Ref: A. Stevens et alii, Appendix 9)

(1) Intense Pulsed Neutron Source (IPNS)

Generates 10^{12} neutrons cm^{-2} sec^{-1} in a spallation target bombarded by 500 MeV protons. The neutron energy spectrum peaks near 1 MeV.

(2) ^{60}Co Source

Produces as much as 2 Mrad(Si)/hr

(3) 22-MeV Electron Linac

Provides beam currents up to 50 μamp with variable beam spot size as small as 0.6 cm in diameter.

(4) Fast Neutron Generator

Produces 2.5 MeV neutrons with a flux up to 10^{10} cm^{-2} sec^{-1} by accelerating 7 MeV deuterons onto a Be target.

Brookhaven National Lab (Ref: H. Kraner, Appendix 8)

(1) AGS Linac

Generates 10^{14} protons/pulse at a repetition rate of 5 pulses/sec with energies adjustable from 100 to 200 MeV.

(2) Tandem Van de Graaff

A single-event upset facility that provides nuclei (protons to uranium) with energies from 35 to 350 MeV and flux 10^2 to 10^{12} cm^{-2}.

(3) ^{60}Co Source

Doses of 200 krad/hr will be available.

(4) Neutron source

Provides 10^7 to 10^8 neutrons/sec with a 0.5-8 MeV energy spectrum via Be(α, n) reaction.

Lawrence Berkeley Lab (Ref: H. Spieler, Appendix 12)

(1) ^{60}Co Source

Doses up to 10 krad(Si)/hr are available.

Los Alamos National Lab (Ref: V. Sandberg, Appendix 11)

(1) Radiation Effects Facility

Generates 10^6 to 6×10^{13} neutrons cm^{-2} sec^{-1} with energies near 1 MeV by absorbing 800 MeV protons in a beam stop.

(2) WNR-PSR-LANSCE

Spallation neutrons from 0.1 ev to greater than 750 MeV are available.

Sandia National Laboratories (Ref: P. S. Winokur and D. M. Fleetwood, Appendix 5)

(1) ^{60}Co Source

Doses of 2 Mrad(Si)/hr are available.

(2) ACRR, SPR-II, and SPR-III reactors

Neutron irradiation facilities.

(3) HERMES II

10 MeV electron beam used for generating bremsstrahlung gamma rays with a repetition rate of 3 pulses/hr and peak dose of 70 krad(Si).

4. RADIATION DAMAGE STANDARDS FOR ORGANIC MATERIALS USED IN SSC DETECTORS

The following is presented as a prototype of a possible set of general radiation damage standards for organic materials used in SSC detectors. More detailed standards and characteristics of different materials can be found in Appendices 2 and 4.

Material	Critical Properties	Environment (*)	Damage Criteria	Remarks
scintillators	scintillating efficiency; transmission loss	atmosphere (oxygen?); 30°C; dose rate: 1 krad/hr to 1 Mrad/hr (annealing?)	operational at 1 to 30 Mrad, depending on position in detector	need a substantial R&D effort quickly
electrical insulation	flexural strength; elongation	air; 50°C; dose rate: 10 krad/hr to 1 Mrad/hr	>50% of initial value (or >50% absolute for elongation) at 10 Mrad	large data base; well understood
optical fibers	attenuation	air; 50°C; 10 krad/hr to 10 Mrad/hr	20-100 dB/km at 1 Mrad	promising materials; needs some more work
adhesives	sheer strength; peel strength	air; 50°C; 10 krad/hr to 10 Mrad/hr	>50% of initial value at 10 Mrad	materials available; no major problems
composites	mechanical strength; resin-matrix interface integrity	air; 50°C; 10 krad/hr to 10 Mrad/hr	not established	some data exist; needs more work

General recommendation: exclude or minimize halogen-containing materials

(*) The above table excludes cryogenic environments for simplicity. Materials that are to be used in high-radiation regions inside superconducting magnets or inside calorimeters that use liquified noble gases must be tested in the corresponding environment (e.g. liquid argon for components used inside a liquid-argon calorimeter).

TASK FORCE CHARGE:
TASK FORCE ON RADIATION DAMAGE TESTING AT THE SSC

The radiation levels at the SSC will present unprecedented challenges to detector technology. The Task Force is charged to:

1) Catalogue existing radiation sources and evaluate their suitability for performing radiation damage studies of SSC detector components. The listing should include appropriate accelerator, reactor, and radioactive source facilities.

2) Provide recommendations to the SSC Laboratory for optimal use of existing resources in the U.S.

3) Provide recommendations, if necessary, to the Laboratory about the purchase of new sources and the implementation of improvements at existing facilities.

4) Describe the standards and techniques for making dose/fluence measurements.

5) Propose standards for radiation damage measurements that are specifically applicable to SSC requirements. Such standards could be applied in the approval process for SSC experiments. The Task Force will produce a written report containing its conclusions and recommendations.

TASK FORCE MEMBERSHIP:
TASK FORCE ON RADIATION DAMAGE TESTING AT THE SSC

1) Professor Willi Chinowsky
SSC Laboratory
Physics Research
2550 Beckleymeade Avenue
Dallas, TX 75237
(on leave from Berkeley)

Tel: 214-708-6024
FAX: 214-708-0006
woc@SSCVX1

2) Dr. Roger Clough
Sandia National Laboratories
Org. 1811
Albuquerque, NM 87185

Tel: 505-844-3492
FAX: 505-844-9624

3) Dr. John Dawson
High Energy Physics, Bldg. 362
Argonne National Laboratory
9700 South Cass Avenue
Argonne, IL 60439

Tel: 708-972-6541
jwd@ANLHEP

4) Dr. Donald E. Groom
Lawrence Berkeley Laboratory
50-308
Berkeley, CA 94720

Tel: 415-486-6788
deg@LBL or CSA::DEG

5) Dr. Hobart Kraner
535B Instrumentation Division
Brookhaven National Laboratory
Upton, LI, NY 11973

Tel: 516-282-4238
kraner@BNLCL1

6) Dr. Stanley Majewski
CEBAF
Physics Division
12000 Jefferson Avenue
Newport News, VA 23606

Tel: 804-249-7448
majewski@CEBAFVAX

7) Dr. Edward Peterson
Code 4711
Naval Research Laboratory
Washington DC 20375

Tel: 202-767-3939
FAX: 202-767-3709

8) Professor James Russ
Physics Department
Carnegie-Mellon University
Pittsburgh, PA 15213

Tel: 412-268-2755
russ@CMPHYS

9) Dr. Hartmut Sadrozinski
Institute for Particle Physics
Nat. Sci. 2
University of California
Santa Cruz, CA 95064

Tel: 408-459-4670
hfws@SLACVM

10) Dr. Vernon Sandberg
M.S. H846
Group MP4
Los Alamos National Laboratory
Los Alamos, NM 87545

Tel: 505-667-7268
FAX: 505-665-1712
sandberg@LAMPF

11) Dr. Helmut Schonbacher
CERN
1211 Geneva 23
Switzerland

Tel: 011-41-22-767-61-11
schonbac@CERNVM

12) Dr. George Soli
MS 303/220
JPL
4800 Oak Grove Dr.
Pasadena, CA 91109

Tel: 818-354-3937
FAX: 818-393-4559

13) Dr. Helmuth Spieler
Lawrence Berkeley Laboratory
50B-6208
Berkeley, CA 94720

Tel: 415-486-6643
hgspieler@LBL

14) Professor Rudolf Thun
SSC Laboratory
Physics Research Division
2550 Beckleymeade Avenue
Dallas, TX 75237
(on leave from the U. of Michigan)

Tel: 214-708-6026
FAX: 214-708-0006
thun@SSCVX1

15) Dr. Peter Winokur
Sandia National Laboratories
P.O. Box 5800
Division 2147
Albuquerque, NM 87185

Tel: 505-846-2998
FAX: 505-846-5004

also participating:

16) Dr. Joseph Coyne
NIST
Center for Radiation Research
Gaithersburg, MD 20899

Tel: 301-975-5555
FAX: 301-869-7682

APPENDIX 1

Radiation Levels in Detectors at the SSC

Radiation Levels in Detectors at the SSC*

Donald E. Groom†

Lawrence Berkeley Laboratory 50-308, Berkeley CA 94720

Estimates of ionizing dose and neutron fluence have been made for typical SSC detector configurations exposed to radiation from *p-p* collisions. Using a description of "average events" in conjunction with simulations of secondary processes, it is found for calorimetry that the ionizing dose (D) or neutron fluence (ϕ) can be adequately expressed as

$$D \text{ (or } \phi) = \frac{A}{r^2 \sin^{2+\alpha} \theta} \, .$$

Here A depends on the process and exposure time, α is slightly less than unity, and r is the distance from the interaction point. Under nominal operating conditions, a metallic calorimeter element 2 m from interaction point and 6° from the beam line is subjected to an annual dose of 30 kGy at electromagnetic shower maximum and an annual neutron fluence of $10^{14}\,\mathrm{cm}^{-2}$ at hadronic cascade maximum.

This report includes provisional correction of an error in electromagnetic dose discovered in the Task Force Report.‡

1. Introduction

An SSC Central Design Group task force was formed to assess radiation levels to be expected in SSC detectors. Its findings are available in a thick report[1], and short versions have also been published[2]. Radiation *effects* were addressed by a separate task force[3]. In this report we present a very brief discussion of radiation levels.

2. Assumptions

On the basis of SSC design parameters and extrapolation from S$\bar{\text{p}}$pS and Tevatron operating experience, the following assumptions were made:

- The machine luminosity at $\sqrt{s} = 40$ TeV is $\mathcal{L} = 10^{33}$ cm^{-2}s^{-1}, and the *p-p* inelastic cross section is $\sigma_{\text{inel}} = 100$ mb. This luminosity is effectively achieved for 10^7 s yr^{-1}. The interaction rate is thus 10^8 s^{-1}, or 10^{15} yr^{-1}.

---

* This report is based on a version published in the *Proceedings of the ECFA Conference on Future Accelerators,* Madrid, Spain (Sept. 1989), but differs from it in three important respects: Table 1 in that report was wrong, and has now been corrected, the electromagnetic dose has been corrected (see the footnote below), and a figure showing the neutron flux in the central cavity as a function of the minimum calorimeter angle has been added.

† For the SSC Central Design Group Task Force on Radiation Levels in the SSC Interaction Regions: F. S. Alsmiller, R. G. Alsmiller, Jr., S. Ban, J. E. Brau, K. W. Edwards, A. Fassò, H. Fesefeldt, T. A. Gabriel , M. G. D. Gilchriese (Chairman), D. E. Groom, H. Hirayama, H. Kowalski, H.W. Kraner, N. V. Mokhov, D. R. Nygren, F. E. Paige, J. Ranft, J. S. Russ, H. Schönbacher, T. Stanev, G. R. Stevenson, A. Van Ginneken, E. M. Wang, R. Wigmans, and T. P. Wilcox, Jr.

‡ The maximum dose in the electromagnetic calorimeter due to incident photons from primary π^0 decay, as reported in Ref. 1 and in numerous conference proceedings, was high by a factor of three because of a trivial conversion error in Appendix 7. Corrected results given here. They are thought to be correct for the metallic part of the calorimeter, but to obtain the dose in the active part of the calorimeter they should probably be corrected upward by the stopping power ratio for the two media. For lead/scintillator the ratio is about 1.6.

- All radiation comes from p-p collisions at the interaction point. For the SSC, the nominal luminosity contributes $(300\ \mathrm{hr})^{-1}$ to the reciprocal current lifetime, so p-p collisions contribute as much radiation as dumping one of the beams into the apparatus every 6 days. Moreover, any process of comparable importance would prevent normal operation of the machine.
- The charged particle distribution is (a) flat in pseudorapidity for $|\eta| < 6$ and (b) has a momentum distribution whose perpendicular component is independent of rapidity, or approximately independent of pseudorapidity:

$$\frac{d^2 N_{\mathrm{ch}}}{d\eta dp_\perp} = H\ f(p_\perp) \tag{1}$$

  (where $p_\perp = p \sin\theta$). Integrals involving $f(p_\perp)$ are simplified by replacing $f(p_\perp)$ by $\delta(p_\perp - \langle p_\perp \rangle)$; in the worst case this approximation introduces an 8% error.
- Gamma rays from π^0 decay are as abundant as charged particles. They have approximately the same η distribution, but half the mean momentum.
- The values $H \approx 7.5$ and $\langle p_\perp \rangle \approx 0.6$ GeV/c for $\sqrt{s} = 40$ TeV are obtained by extrapolating experimental results[4, 5], and are in good agreement with results obtained with standard fragmentation models. These values together with Eq. (1) are thought to describe particle production at the SSC within a factor of two or better.

3. Dose from direct particle production

Since $d\eta/d\Omega = (2\pi \sin^2\theta)^{-1}$, it follows from Eq. (1) that the flux of charged particles from the interaction point passing through a normal area da located a distance $r_\perp$ from the beam line is given by

$$\frac{dN_{\mathrm{ch}}}{da} = \frac{1.2 \times 10^8\ \mathrm{s}^{-1}}{r_\perp^2}\ . \tag{2}$$

In a typical organic material, a relativistic charged particle flux of $3 \times 10^9\ \mathrm{cm}^{-2}$ produces an ionizing radiation dose of 1 Gy, where 1 Gy $\equiv$ 1 joule kg^{-1} (= 100 rads). The above result may then be rewritten as

$$\dot{D} = \frac{0.4\ \mathrm{MGy\ yr}^{-1}}{r_\perp^2} \tag{3}$$

for an absorber much thinner than a nuclear interaction length, where $r_\perp$ is in cm.

In the presence of a magnetic field, low-energy particles make multiple passes through a test sample and so contribute to the dose more than once. This increases dose by about a factor of two.

4. Dose and fluence in a calorimeter

In a medium in which cascades can develop, the ionizing dose or neutron flux is at least roughly proportional to the particle energy striking unit area at a distance r from

the interaction point. The charged particle flux is proportional to $(r^2 \sin^2\theta)^{-1}$, and the energy carried by the particles is proportional to $\langle E\rangle \approx p = p_\perp/\sin\theta$. The dose or fluence at cascade maximum is hence proportional to $1/(r^2\sin^3\theta)$. Symbolically, this logic flow is as follows:

$$\left.\begin{array}{l}\left.\begin{array}{l}\dfrac{dN_{\rm ch}}{d\eta} = \text{Const}\\[2ex] \dfrac{d\eta}{d\Omega} = \dfrac{1}{2\pi\sin^2\theta}\end{array}\right\} \dfrac{dN_{\rm ch}}{d\Omega} = \dfrac{\text{Const}}{\sin^2\theta}\\[2ex] E \approx p = \dfrac{p_\perp}{\sin\theta}\end{array}\right\} \dfrac{dE}{d\Omega} = \dfrac{\text{Const}}{\sin^3\theta}$$

$$\left.\begin{array}{l}\dfrac{dE}{d\Omega} = \dfrac{\text{Const}}{\sin^3\theta}\\[2ex] \dfrac{d\Omega}{da} \propto \dfrac{1}{r^2}\end{array}\right\} \begin{array}{l}\text{Neutron fluence}\\ \text{or ionizing dose}\end{array} = \dfrac{K}{r^2\sin^3\theta} \tag{4}$$

This result is incomplete for a number of reasons. In the first place, the constant K must come from Monte Carlo simulations, hopefully supplemented by experimental measurements. Secondly, since showers lengthen with energy the maximum amplitude is not quite proportional to the incident energy density, so that the power of $\sin\theta$ is a little less than three. This is true for both electromagnetic and hadronic cascades. Finally, hadronic activity increases less rapidly than linearly with energy because π^0 production progressively "bleeds off" more and more energy to the electromagnetic channel as the incident energy increases, further reducing the power of $\sin\theta$ for processes such as neutron production. Even in this case, the combined effect is to reduce the exponent to about 2.7, so the above equation still provides guidance. The inverse r^2 dependence remains rigorously true, providing a serious constraint on detector design.

We rewrite the result as

$$\begin{array}{l}\text{Neutron fluence}\\ \text{or ionizing dose}\end{array} = \sigma_{\rm inel}\int \mathcal{L}dt\,\frac{H\,\langle p_\perp\rangle^\alpha}{r^2}\frac{\text{Const.}}{\sin^{2+\alpha}\theta} = \frac{A}{r^2}\cosh^{2+\alpha}\eta \tag{5}$$

where the dependence on some machine-dependent parameters is made explicit. The second form is obtained with the aid of the identity $\cosh\eta = \sin\theta$.

Values of A and α are given in Table 1 for several relevant situations. The constant A includes factors evaluated with cascade simulation programs as well as constants describing particle production at the interaction point. It is felt that each could introduce an error as large as a factor of two in the results.

For calorimeters the maximum neutron flux, ionizing dose from incident photons, and maximum ionizing dose from incident hadrons are shown in Figs. 1 and 2. The curves are calculated using Eq. (5) and the constants in Table 1.

Under all conditions so far studied, the neutron spectrum shows a broad log-normal distribution peaking at just under 1 MeV, as might be expected for neutron boiloff fol-

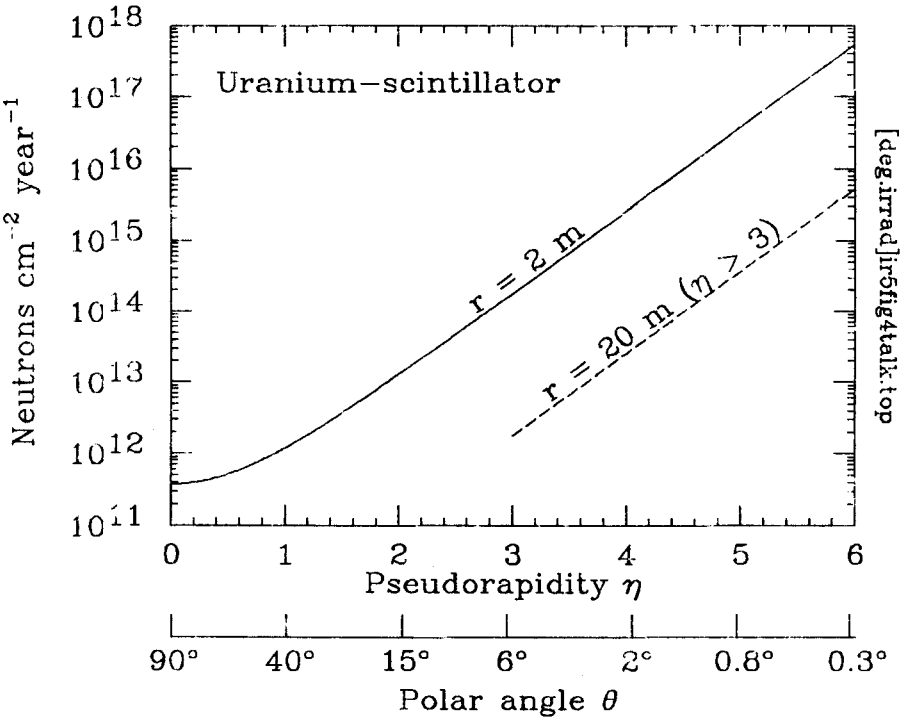

FIG. 1. The maximum neutron flux for a 1:1 uranium:scintillator calorimeter. The solid curve shows the result assuming the maximum occurs at a radius of 200 cm. Also shown is the result for a radius of 20 m, typical of forward detectors, for pseudorapidity > 3.

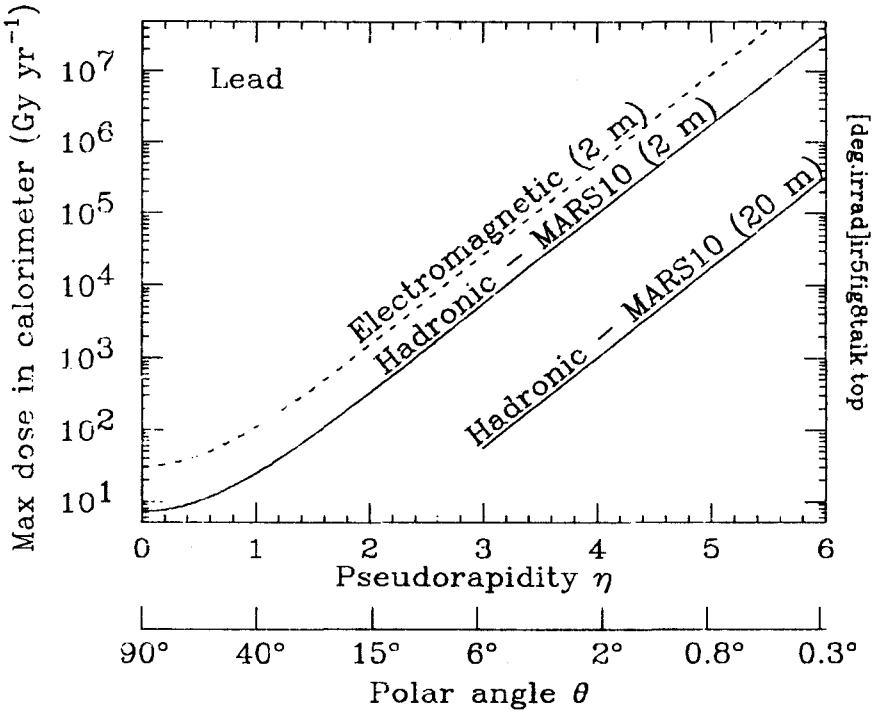

FIG. 2. The maximum hadronic dose as a function of pseudorapidity for a lead sphere, assuming that the maximum dose occurs at the indicated radius. The maximum electromagnetic dose in 1:1 uranium:scintillator is shown by the dashed line. Since the radiation length, nuclear interaction length, and density are nearly identical for the two materials, dose (but not neutron flux) results may be compared directly. The electromagnetic dose has been corrected downward by a factor of three, as described in an earlier footnote. Doses are for the high-Z absorber in the calorimeter, and should probably be corrected upward by a stopping power ratio (1.4 for silicon and 1.6 for scintillator) to obtain the dose in the sensitive material.

lowing nuclear excitation. In the 2 m radius central cavity of a detector with coverage down to $|\eta| = 3$, the average neutron flux is 2×10^{12} cm^{-2}yr^{-1}, including reflection.

Table 1

Coefficients $A/(100\text{ cm})^2$ and α for the evaluation of radiation levels at cascade maximum in SSC calorimetry under nominal operating conditions. At a distance r and angle θ from the interaction point the annual fluence or dose is $A/(r^2 \sin^{2+\alpha}\theta)$.

Quantity	$A/(100\text{ cm})^2$	Units	$\langle p_\perp \rangle$	α
Neutron flux	1.5×10^{12}	cm^{-2}yr^{-1}	0.6 GeV/c	0.67
Dose rate from photons	124*	Gy yr^{-1}	0.3 GeV/c	0.93
Dose rate from hadrons	29	Gy yr^{-1}	0.6 GeV/c	0.89

*Corrected value.

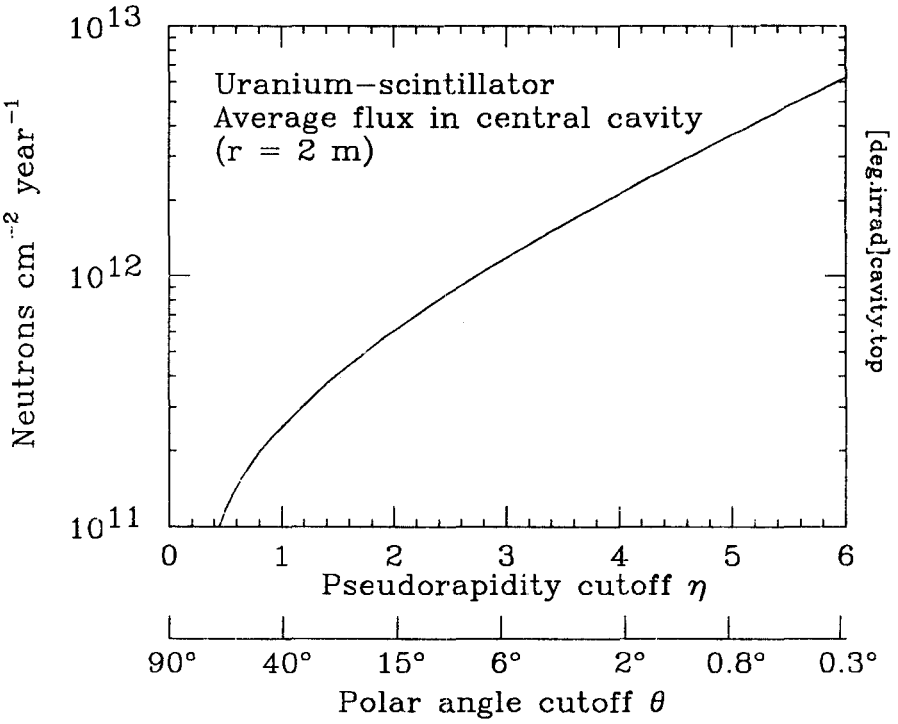

FIG. 3. Average neutron flux in a spherical central cavity with 200 cm radius under nominal SSC operating conditions, in the absence of reflections. Reflections increase the flux by a factor of about two, and the flux scales inversely as the square of characteristic dimensions.

5. Neutrons in the central cavity

Neutrons in the calorimeter may be thought of as a gas in a leaky container. Some (the "albedo neutrons") diffuse back into the central cavity. These have the same "1 MeV" spectrum as do all other neutrons in the environment. Since cascade maxima occur deeper in the calorimeter with increasing energy, the number of albedo neutrons scales only weakly (as about the 0.5 power) with the energy of an incident hadron. The number of neutrons injected per event per pseudorapidity interval is approximately given by

$14.5 \cosh^{0.5} \eta$, as shown in Fig. 5-3 of Ref. 1. The average flux in the cavity is obtained by integrating this function over the region subtended by the central detector. The result is shown in Fig. 3 for a spherical detector with a 200 cm inside radius, in the absence of secondary scattering ("reflection"). Note that most contributions to the integral come from the smallest-angle parts of the calorimeter. Scattering enhances the average flux by a factor of about two, and tends to make it more uniform. With realistic reflection and a cutoff at $|\eta| = 3$, the flux near the ends of the cavity is nearly three times the flux at the center, and the flux near the calorimeter at 90° is about 60% lower than at the center (Wilcox, p. 191 of Ref. 1).

Gabriel and Lillie have investigated the effect of a polyethylene "liner" on the inside surface of the calorimeter[6]. The found that a 10 cm liner reduces the flux in the cavity by an order of magnitude. Matthews has pointed out[7] that most of the reduction can probably be achieved if the hydrogenous layer only covers a small region near the minimum angles, but detailed simulations have yet to be made.

The flux in the cavity scales as the inverse square of the characteristic dimensions, but for a different reason than for the flux in the calorimeter: it is proportional to the average path length of a neutron in the cavity divided by the volume.*

6. Scaling to other machines

Using the scaling discussed in connection with Eq. (5) above, examples of scaling to other accelerators are given in Table 2. It should be noted that the assumption that all radiation comes from the interaction point does not apply to the present generation of accelerators.

Table 2

A rough comparison of beam-collision induced radiation levels in calorimetry at the Tevatron, УНК, high-luminosity LHC, and SSC.

	Tevatron	УНК-3	LHC	SSC
$\sqrt{s}$ (TeV)	1.8	6	16	40
$\mathcal{L}_{\rm nom}$ (cm^{-2}s^{-1})	2×10^{30}	4×10^{32}	$4 \times 10^{34\dagger}$	1×10^{33}
$\sigma_{\rm inel}$	59 mb	80 mb	86 mb	100 mb
H	4.1	4.5	6.3	7.5
$\langle p_\perp \rangle$ (GeV/c)	0.46	0.52	0.55	0.60
Scale factor‡	5×10^{-4}	0.2	27	1

† High-luminosity option.

‡ Proportional to $\mathcal{L}_{\rm nom}\, \sigma_{\rm inel}\, H\, \langle p_\perp \rangle^{0.7}$

* In the approximation of constant flux, this path length may be replaced by the mean chord. For a solid whose surface everywhere has curvature with the same sign, the mean chord is equal to four times the volume divided by the surface area[8].

7. References

1. "Report of the Task Force on Radiation Levels in the SSC Interaction Regions," ed. by D. E. Groom, SSC Central Design Group Report SSC-SR-1033 (June 1988).
2. D. E. Groom, Nucl. Instrum. Methods **A279**, 1 (1989);
   D. E. Groom, pp. 711–716 in *Proc. of the 1988 Summer Study on High Energy Physics in the 1990's*, Snowmass CO, June 27–July 15, 1988, ed. S. Jensen, World Scientific (1989);
   D. E. Groom, *Proc. of the Workshop on Calorimetry for the Superconducting Super Collider*, Tuscaloosa, Alabama, 13–17 March 1989, ed. by R. Donaldson and M. G. D. Gilchriese, World Scientific (to be published, June 1990).
3. "Radiation Effects at the SSC," ed. by M. G. D. Gilchriese, SSC Central Design Group Report SSC-SR-1035 (June 1988).
4. F. Abe *et al.* (CDF), Phys. Rev. Lett. **61**, 1819 (1988).
5. G. J. Alner *et al.* (UA5), Z. Phys. C **33**, 1-6 (1986).
6. T. A. Gabriel and R. A. Lillie, SSC Central Design Group Note SSC-N-545 (1988).
7. J. A. J. Matthews, private communication (1990).
8. A. Cauchy, "Memoire sur la rectification des courbes et la quadrature des surfaces courbes" (1850); reprinted in *Ouvres Completes*, Vol. 2, Gauthier Villard, Paris (1908);
   E. Czuber, "Zur Theorie der geometrischen Wahrscheinlichkeiten," Sitzungsber. Akad. Wiss. Wien Abt. 2, **90**, 719-742 (1884).

APPENDIX 2

Experience with IEC Standard 544 to Assess
Radiation Damage of Organic Insulating Materials

EXPERIENCE WITH IEC STANDARD 544 TO ASSESS RADIATION DAMAGE OF ORGANIC INSULATING MATERIALS

by

H. SCHÖNBACHER and M. TAVLET

CERN, CH - 1211 GENEVA 23, SWITZERLAND

ABSTRACT

The essential topics of IEC Standard 544 are presented which contains four parts: I Radiation interaction, II Procedures for irradiation, III Test procedures for permanent effects and IV Classification system for service in radiation environments. The topics described include test procedures, critical parameters and end-point criteria, dose rate and the Radiation Index. Experience at CERN is reported which is based on radiation testing of many hundreds of organic insulating materials supplied by a large number of different manufacturers. The experience with rigid plastics, eg. epoxy resins, were extremely positive, whereas with flexible plastics, mainly cable insulation and sheath materials, several difficulties did occur. It was however found that the recommended procedure to assess the dose rate effect clearly allows to identify materials where this effect is of importance and that the Radiation Index is a simple and clearly defined tool to rank materials according to their radiation resistance.

1. INTRODUCTION

Several national and international bodies such as ASTM, IEEE, DIN, ISO and IEC issue standards on radiation testing of materials. Since more than 20 years CERN has aligned its activity in the field to IEC Standard 544 because it is essentially devoted to insulating materials and issued by an international commission. Further CERN staff and CERN experience has been instrumental in the elaboration of the series of IEC Standard 544.

In this report we give a short summary of the essential parts of the Standard and concentrate then on CERN experience with its application. This experience has mainly been gained during the construction of the CERN Large Electron Positron storage ring from 1982 to 1989 (LEP). In this high energy particle accelerator tunnel of 27 km circumference hundreds of kilometres of cables and tons of magnet coil insulations are installed and exposed to high radiation levels.

2. THE ESSENTIAL PARTS OF IEC STANDARD 544

The "Guide for determining the effects of ionizing radiation on insulating materials", Publication 544 [1] of the International Electro-technical Commission (IEC) contains four parts:

Part I : Radiation interaction
Part II : Procedures for irradiation
Part III: Test procedures for permanent effects
Part IV : Classification system for service in radiation environments

The present report concentrates on Part II, III and IV.

Part I contains an introduction to the problems that may be encountered with this type of tests and detailed information on dosimetry.

2.1. Test procedures

Mechanical properties are very sensitive to radiation, and experience shows that electrical breakdown of insulating materials is usually a consequence of severe mechanical deterioration [2, 3]. Therefore the recommended test procedures for permanent effects are tests of mechanical properties. Eg. tensile tests (ISO/R 527 and R 37) on flexible plastics and flexural tests (ISO 178) on rigid plastics.

2.2. Critical parameter and end-point criteria

For normal application the most restrictive property is:

- flexional stress at maximum load for rigid plastics
- elongation at break for flexible plastics and elastomers

The recommended end-point criterium is 50 % of the initial value.

2.3. Dose-rate

It is known that radiation damage does not depend only on the total integrated dose; it may also depend on the dose rate as well as on environmental parameters such as humidity and temperature.

Therefore, the IEC standard recommends irradiations at two dose rates:

- high-dose rate irradiations at 3 to 30 Gy/s,
- low-dose rate irradiations at 30 mGy/s.

2.4. Radiation Index

In the fourth part of Standard IEC 544 a classification system is defined to categorize the radiation endurance of insulating materials in radiation environments, with the purpose to provide a guide for the selection and indexing of these materials. The material is assigned a "Radiation Index". To qualify for a particular Radiation Index, a material must satisfy one of the above defined end-point criteria after being irradiated by the classification dose and dose rate.

The Radiation Index will be determined by the logarithm ($\log_{10}$) of the absorbed dose (Gy, rounded down to the two significant figures) above which the appropriate critical property value has changed to the end-point criterion under specified conditions. For example, a material which satisfies a particular end-point criterion to a dose of $2 \cdot 10^4$ Gy has a Radiation Index of 4.3 [i.e. $\log(2 \cdot 10^4) = 4.306$]

The Radiation Index is given with qualifiers indicating the dose rate and the temperature at which it was obtained, since it may depend on these parameters.

3. EXPERIENCE WITH IEC STANDARD 544

Radiation tests on many hundred insulating materials both rigid and flexible ones have been tested at CERN. A large amount of these data have been compiled and published [4]. The experience with rigid plastics, mainly epoxy resins used for magnet coil insulation were extremely positive, whereas with flexible plastics, mainly cable insulation and sheath materials, several difficulties did occur. The reason for this may be their increased sensitivity to radiation dose and dose rate. The presentation in this report will therefore concentrate on cable materials.

3.1. End-point criteria

It shall be noted that before 1980 the CERN specification required for cable materials an absolute value of elongation at break of 100 % at 10^6 Gy. As for safety reason halogen free materials were imposed (to replace PVC) the mineral fillers reduced the initial value of elongation of many materials so that the above specification was no longer applicable. At that time we aligned with the IEC recommendation and specified 50 % of initial value of elongation at 5×10^5 Gy. In practice we accept any material which irradiated at high dose rate (30Gy/s) satisfy one of the following conditions:

- Elongation > 100 % asbsolute value at 10^6 Gy
- Elongation > 50 % initial value at 5 x 10^5 Gy (RI > 5.7)

The following example is based on 280 tested materials out of which:

- 132 pass either the one or the other requirement (47 %)
- 121 have an RI > 5.7 based on initial value (43 %)
- 62 have an RI > 6.0 based on absolute value (22 %)
- 51 pass both requirements (18 %)

In Appendix 1 we list these materials with values of elongation at zero, 5 x 10^5 and 1 x 10^6 Gy and the RI (30 Gy/s) based on 50 % of initial value. In the following tables we discuss some specific cases.

Table 1 is an example of materials with a high initial elongation. This type of materials usually tend to satisfy the first of the above requirements, an absolute value of 100 % at 10^6 Gy. None of them satisfies the present specification of RI > 5.7 based on initial value. In table 2 we summarize materials with low initial elongation. These are usually highly mineral filled halogen-free cable sheath materials. As mentioned above none of these would satisfy the 100 % elongation requirement but they all have a RI > 5.7.

Comparing now tables 1 and 2 one would by strict application of the RI > 5.7 specification have to accept all in table 2 and refuse all in table 1. The latter have to be refused although in absolute terms the elongation at 5 x 10^5 Gy and 1 x 10^6 Gy is in all cases higher than for the materials in table 2. In many cases the elongation after irradiation is even higher than for the other material at zero dose!

This example shows that a combination of the two requirements as it is practiced at CERN (although the RI > 5.7 only is specified) seems to be a good compromise and that strict application of the one or the other would clearly unfavour otherwise satisfactory materials.

Experience also shows that specification of an absolute value may give rise to less troubles if the values are properly set, eg. 100 % or 50 % at 5 x 10^5 Gy. In the latter case however, almost all of the 280 materials included in this study (94 %) would pass. This clearly would not be enough selective.

Table 3 finally gives some examples of very radiation sensitive materials which pass none of the above specification requirements.

3.2. Dose rate

The effect of dose rate on insulating materials has been extensively treated in literature and is also well discussed and to a large extent taken into account of in the series of IEC Standard 544. Since 1982 long term irradiations as recommended by IEC at 100 Gy/h are carried out on a routine basis on cable materials and the results are compared with short term irradiations at 10^5 Gy/h [5].

For a representative group of materials results are presented in table 4. In this table the elongation at break at zero dose and 5.10^5 Gy for both accelerated and long-term tests is given, as well as the ratio of the two, defined as the "Long-Term Factor at 5.10^5 Gy". This factor allows the assessment of the error made by estimating the life performance of the cable-insulating materials by accelerated tests.

The results in table 4 show that the LT factor is in general between 0.5 and 1.0 (hence within a factor 2) for EPR type materials, whereas for Polyolefins values down to 0.1 and lower are found. This is also clearly seen from fig. 1, where the LT factor (at 5.10^5 Gy)is plotted as a function of percentage of elongation at break at 5.10^5 Gy compared to elongation at break at zero dose. As an example, a material that fulfils CERN specification requirements, with an elongation of 50 % of initial value at 5.10^5 Gy but with a LT factor of 0.1, will after long-term irradiation only show 5 % of initial elongation at that dose.

In fig. 2 we give for elongation E/Eo = 0.5 the long term factor of radiation index as a function of the radiation index and the end-point dose of short term irradiations. It must be stressed that the RI has been obtained in many cases by extrapolation to lower doses than the lowest measurement point or by extrapolation to higher doses. The error involved may therefore be important (see fig. 3). Because of these extrapolations the presentation of the LT factor in fig. 1 is much closer to reality and can be used with more confidence.

It is clear that the procedure recommended by IEC can not precisely predict the life performance of the material. This could according to our present knowledge only be obtained by irradiation at service dose rate. The examples shown allow however to determine the overall performance of a group of materials (eg. PUR is better than EPR or PE) and identify materials which are particularly sensitive to dose rate effects (eg. polyolefins). This is demonstrated in fig. 4.

At present, we carry out at CERN also irradiations at an intermediate dose rate of about 5000 Gy/h. With 3 data points it shall then be possible to find a relation between end-point dose and dose rate and investigate whether it is possible to extrapolate to lower dose rates. This method is at present subject of a proposal for a new IEC recommendation [6].

3.3. Radiation Index

Since the issue of IEC 544 part 4 in 1985 all CERN data published contain the Radiation Index. As shown in Section 2.4. this is clearly defined and easy to assess. It can therefore be considered as a valuable recommendation. From a practical point of view, it might have been easier understandable if the end-point dose would be given as such and not the logarithm of it.

4. DISCUSSION

In the complex field of radiation testing of insulating materials much work is done under well defined laboratory experiments. IEC Standards must however also be applicable in field work. In this respect, the results obtained at CERN represent a valuable experience since assessments of radiation resistance have been made on materials

which come from different manufacturers, have different sample sizes and to a large extend an unknown composition. They are installed in large quantities in high radiation areas. From this experience we can conclude the following:

- to specify as end-point criterion 50 % of initial value at 5 x 10^5 Gy unfavours materials with high initial elongation. Specification of two conditions seems to be a reasonable compromise eg. at 5.10^5 Gy:
  elongation > 100 % in absolute value
  OR elongation > 50 % of initial value

- the recommendation to assess dose rate effects is certainly not perfect from a scientific point of view, but clearly allows to identify materials with a high dose rate effect,

- the Radiation Index is a simple and clearly defined tool to rank materials according to their radiation resistance. However to assess the dose rate effect a comparison of absolute values gives more accurate results than the Radiation Index.

REFERENCES

[1] Guide for determining the effect of ionizing radiation on insulating materials, Part I: Radiation interaction (1977), Part II: Procedures for irradiation (1979), PART III: Test procedures for permanent effects (1979), Part IV: Classification system for service in radiation environments (1985), Publication 544, International Electrotechnical Commission, Geneva.

[2] STUETZER, O., Correlation of electrical cable failure with mechanical degradation, SANDIA Report SAND 83-2622 (1984).

[3] LIPTAK, G., et al., Radiation tests on selected electrical insulating materials for high power and high-voltage application CERN 85-02 (1985).

[4] SCHONBACHER, H., BEYNEL, P., STOLARZ-YZICKA, A., Compilation of radiation damage test data, Part 1: cable-insulating materials, CERN 79-08, (1979), Part 2: Thermosetting and thermoplastic resins, CERN 79-08/1979, Part 3: Materials used around high-energy accelerators, CERN 82-10, (1982).

[5] SCHONBACHER, H., TAVLET, M., Routine long term radiation tests on cable insulating materials CERN Internal Report TIS-RP/IR/86-27 (1986).

[6] WÜNDRICH, K., Proposal for a new part of IEC 544: Test procedure for determining long time degradation, unpublished.

Table 1. Materials with high initial values where elongation at 10^6 Gy > 100 % but RI is below 5.7

	PE C 678	Th.pl. C 615	Th.pl. C 672	EPR C 574	EPR C 808	EPDM C 578	EPDM C 633
dose 0	680	520	684	360	415	562	716
5.10^5 Gy	126	162	166	178	181	218	196
1.10^6 Gy	116	122	103	106	111	104	119
OI (%)	19	29	26	22	24	26	37

Table 2. Materials with low initial values of elongation where RI > 5.7

	PE C 716	Th.pl. C 734	Th.pl. C 790	EPR C 759	EPR C 701	EPDM C 571	EPDM C 729
dose 0	131	84	121	142	158	136	107
5.10^5 Gy	81	79	91	103	98	79	52
1.10^6 Gy	51	39	51	80	72	56	38
OI (%)	40	/	39	28	35	32	57

Table 3. Materials very sensitive to radiation

	PE C 548	Th.pl. C 553	Th.pl. C 569	EPR C 751	EPR C 540	EPDM C 703	EPDM C 721
dose 0	423	573	505	550	520	540	344
5.10^5 Gy	150	95	92	18	41	46	88
1.10^6 Gy	43	27	22	12	30	41	30
5.10^6 Gy	17	12	15	6	14	20	/

Table 4

Elongation at break at zero dose and $5x10^5$ Gy
for accelerated and long-term tests
for different groups of base polymers

TIS num.	Material / Type	Elongation (%) dose zero E_0	$5x10^5$ Gy short E_S	long E_L	L.T. factor E_L/E_S
633	EPDM	716	196	114	0.58
717	EPR basis LFHS 5060	288	90	91	1.01
728	EPR EPDM	182	74	50	0.68
729	EPR	150	69	49	0.71
730	EPR EPDM	184	79	85	1.07
736	EPR Sheath	264	52	28	0.54
737	EPR Insulation	352	130	164	1.26
738	EPDM Pyrofil	99	46	39	0.85
760	EPR	520	191	183	0.96
763	EPR + Copolymer (XL)	352	210	215	1.02
767	EPR 3 G	276	115	47	0.41
806	EPR	375	95	43	0.45
807	EPR	160	90	70	0.77
808	EPR	416	182	45	0.25
809	EPR	294	124	162	1.30
484	EPR + Copolymer (TP)	620	378	180	0.48
505	PE MCA 245	634	306	144	0.47
545	EVA 4/7	212	134	144	1.07
546	EVA 4/7L	760	236	276	1.17
652	EVA MCA 319	612	378	58	0.15
653	Polyolefin MCA 320	660	404	264	0.65
658	EVA Lupolen	520	386	65	0.17
684	Polyolefin	200	78	46	0.59
687	EVA	666	351	64	0.18
690	EVA Sioplas 407	130	110	93	0.85
696	EVA G 840	147	87	91	1.05
716	Polyolefin LFHS 5040	131	81	20	0.25
731	Polyolefin	334	60	31	0.52
732	Polyolefin	612	254	8	0.03
733	Polyolefin	408	300	82	0.27
734	Polyolefin	84	79	2	0.03
735	Polyolefin	222	44	32	0.73
739	Polyolefin Radox	124	59	54	0.92
744	Polyolefin	146	46	7	0.15
759	XLPE	142	104	53	0.51
762	EVA	112	60	4	0.06
764	EVA	569	403	42	0.10
766	EVA D 2983 FR	583	397	6	0.01
768	EVA	123	62	36	0.58
769	XLPE	307	239	30	0.12
790	PE News 1386	121	92	7	0.07
791	EPDM + EVA	551	177	17	0.10
706	Polyester - PUR	548	557	459	0.82
707	Polyether - PUR	556	568	478	0.84

CABLE MATERIALS - RESULTS

TIS Num	Materials	ELONGATIONS (%) 0 Gy	5.10^5	1.10^6	R.I.	Remarks
409	EPDM LD BY 92	255	142	120	5.8	1
410	EPDM LD 37 34	260	150	124	5.8	1
411	EPR	434	180	108		2
412	EPR 1239	132	93	75	6.1	1+
414	Flamtrol Insul.	443	194	112		2
415	Flamtrol Sheath	441	120	50	5.7	1
420	EPDM	220	133	95	5.8	1
421	EPDM	233	131	72	5.7	1
424	EPR	382	163	90	/	
425	Polyolefin	275	152	105	5.8	1 2
430	PUR-Polyether	606	605	576	> 6	1+ 2
431	PUR-Polyester	566	676	618	> 6	1+ 2
432	PUR-Polyester	592	578	508	> 6	1+ 2
433	EPR	490	250	212	5.7	1 2
434	Polyolefin 801	620	40	32	< 5	
442	EPR	252	150	108	5.9	1 2
443	EPR	217	127	99	5.7	1 (2)
455	XLPE 909	239		104	5.9	1
464	EPR	293	150	123	5.7	1 2
465	EPR	220	136	101	5.8	1 2
466	EPR	275	150	107	5.7	1 2
469	Polyolefin	205	120	93	5.8	1
472	Polyolefin	132	23	17	< 5	
473	EVA Sioplas	132	114	96	> 6	1+
475	EPDM	113		63	>6	1+
483	VAC + EPR T1	642	418	130	5.8	1 2
484	VAC + EPR T2	620	378	129	5.7	1 2
485	VAC + EPR T3	573	310	72	5.7	1
486	VAC + EPR T4	342	142	64	/	
498	EPDM	616	270	104	5.6	2
507	EVA Silampex	164	132	64	5.8	1
511	EPR	254	150	108	5.8	1
514	EVA Lupolen	434	87	38	< 5	
519	Polyolefin 236	527	302	222	5.8	1 2
520	Polyolefin 245	634	350	162	5.7	1 2
521	Polyolefin 245	481	250	146	5.7	1 2
536	EVA Lupolen	470	68	37	< 5	
537	EPR	64	26	20	/	!
538	EPR	258	105	80	/	
539	EPR	82	57	43	6.0	1+ !
540	EPR	520	41	30	< 5	
541	Polyolefin	210	138	106	6.0	1+2
544	Polyol. AFT/R1	252	167	139	5.9	1 2
545	EVA 4/7	212	134	102	5.9	1 2
546	EVA 4/7L	760	236	130	/	2
549	PE (LDPE)	581	270	99	/	2
550	EPDM	384	121	63	/	
551	EVA Lupolen	433	99	41	/	
552	Polyolefin	621	105	19	< 5	

TIS Num	Materials	ELONGATIONS (%) 0 Gy	5.10^5	1.10^6	R.I.	Remarks
553	EVA Lupolen	573	95	27	< 5	
555	EPR	408	198	109	5.6	(1) 2
556	EPR	291	124	86	/	
557	EEA (MCA 280)	501	264	172	5.7	1 2
558	XLPE	547	296	170	5.7	1 2
559	EPR	357	111	62	/	
560	Polyolefin	324	197	147	5.9	1
561	EPR	280	172	116	5.8	1 2
568	EVA Sioplas	103	84	70	> 6	1+
569	EVA Lupolen	505	92	22	< 5	
575	EVA 4 G	264	176	110	5.8	1 2
576	XLPE Insulation	461	310	138	5.8	1 2
577	XLPE Semicond.	214	118	84	5.7	1
578	EPDM	562	218	104	/	2
579	EPDM	531	136	88	/	
581	EVA	165	76	51	5.6	
582	SIR	531	41	21	< 5	
583	EVA	191	130	78	5.8	1
584	EVA	156	100	77	6.0	1+
585	EPDM IE 606	202	117	70	5.7	1
586	EPDM IE 606	284	177	109	5.8	1 2
587	Thermoplastic	219	112	64	5.7	1
615	Thermoplastic	520	162	122	/	2
616	Thermoplastic	290	62	56	/	
617	Radox 110	309	193	150	6.0	1+
618	Radox 110 A	178	124	95	6.0	1+
619	Radox 110	179	95	75	5.8	1
620	EPDM	171	56	17	/	
624	EPR AT/2	242	77	28	/	
625	EPR AT/3	325	92	28	/	
626	EPR	160	62	22	/	
627	Toxfree 1	304	100	48	/	
628	Toxfree 2	276	89	39	/	
629	Toxfree 3	156	69	32	5.6	
630	EVA HFI/20	716	417	272	5.8	1 2
631	EPDM	382	114	70	/	
652	EVA MCA 319	610	378	160	5.8	1 2
658	EVA Lupolen	520	386	88	5.8	1
659	EVA 4/7	152	88	21	5.7	1
660	EVA 4/7	181	82	23	/	
661	EVA 5/2	284	134	43	5.6	
663	EVA HFI/36	720	440	315	5.9	1 2
664	EVA HFI/38	711	417	156	5.7	1 2
672	EVA 5/2	684	166	103	/	2
674	Vamac	131	82	55	5.8	1
677	EPDM/PE	51	13	16	/	!
678	PE DFDS 6032	680	126	116	/	2
682	EPR 1202	110	56	34	5.7	1
683	EPR 1106	162	80	65	5.65	1
684	Polyolefin	200	78	53	/	
686	EVA HFI/36	657	345	140	5.7	1 2
687	EVA HFI/38	666	351	57	5.7	1

TIS Num	Materials	ELONGATIONS (%) 0 Gy	5.10^5	1.10^6	R.I.	Remarks
690	EVA Sioplas	130	110	92	6.2	1+
696	EVA G 810	147	87	58	5.8	1
699	EVA	748	140	84	<	
700	EVA	695	154	96	/	(2)
701	EVA KX 712	158	98	72	5.9	1
706	PUR polyester	556	568	466	6.2	1+
707	PUR polyether	548	557	462	6.2	1+
716	Polyolefin 5040	131	81	51	5.8	1
717	PE + EPR 5060	288	90	71	/	
726	PE DFDK 4960	28	22	12	5.9	1 !
727	Polyol. AFT/R1	224	144	102	5.9	1
730	EPR-EPDM	184	79	59	/	
736	EPR ext. sheath	264	52	32	<	
737	EPR inner sheath	352	130	82	/	
739	Radox	124	59	31	5.65	(1)
746	Megolon S 2	224	49	32	/	
747	Megolon I	445	160	66	/	
751	Polyolefin 802	550	18	12	< 5	
752	EVA 3917 BASF	516	408	324	6.1	1+ 2
753	EVA D 2083 FR	440	168	69	/	
754	Polyolefin	243	140	76	5.7	1
759	XLPE charged	142	103	80	6.2	1+
760	EPR	520	190	125	/	2
762	EVA compound	112	59	33	5.7	1
763	VAC XL	351	210	145	6.3	1+
764	VAC thermoplastic	569	404	280	6.3	1+
766	D 2983 FR	583	397	60	5.7	1
767	EPR 3 G	276	115	68	/	
769	XLPE	308	240	101	5.8	1 2
780	XLPE 4201	530	362	195	5.9	1 2
781	Semi-conductor	294	177	126	5.8	1 2
782	XLPE 931	341	235	95	5.8	1
783	PE 972	609	358	190	5.9	1 2
784	Polyolefin XL 244	94	57	47	6.0	1+ !
785	Polyolefin XL 251	216	109	40	5.7	1
786	Polyolefin 270	161	130	67	5.9	1
788	Polyolefin XL	109	66	42	5.8	1
790	PE NEWS 1386	121	91	51	5.9	1
791	Cogegum AFR/1	551	177	112	/	2
798	PE Silythene	540	237	85	5.6	
799	Toxfree M 2	126	61	37	5.7	1
800	Toxfree M 2	163	95	66	5.8	1
801	Toxfree G 10	178	74	54	/	
802	Toxfree G 5	222	133	78	5.8	1
803	Toxfree G 9	136	93	57	5.9	1
804	Polyolefin AFR/1	550	152	56	/	
805	Vamac ZFI3H1p	276	116	66	/	
806	EPR DU 1202	375	95	63	/	
807	EPR DU 1106	160	90	60	5.8	1
808	EPR 5009	415	181	111	5.6	2
809	EPR DU 191	294	123	79	/	

TIS Num	Materials	ELONGATIONS (%) 0 Gy	5.10^5	1.10^6	R.I.	Remarks
812	EVA 4 G	185	96	58	5.7	1
813	PE copolymer	174	118	80	5.9	1
814	PE copolymer	172	106	74	5.8	1
818	EPR	155	103	78	6.0	1+
819	EVA	255	142	111	5.8	1 2
836	EPR 4-56680-04	138	89	70	6.0	1+
840	Rubber Acryl Sh.	142	73	52	5.7	1
841	EVA X 2502 19	218	131	82	5.8	1
856	XLPE G2-EC-MD	342	174	64	5.7	1
860	EVA D 2983 FR	465	37	21	< 5	
862	Polyolefin 5040	140	90	65	5.9	1
868	Rheyhalon KF2U	202	44	21	5.4	
872	VAC + EPR T2	653	250	91	5.5	
884	EPR	126	70	52	5.8	1
885	EVA D 2983 FR	670	393	63	5.7	1
886	Polyolefin 2979FR	535	374	190	5.8	1 2
888	TPR 799 nat	138	34	15	/	
891	Megolon S 1	194	57	33	/	
892	Megolon S 1'	97	50	33	5.7	1
893	Megolon S 300	125	62	32	5.65	(1)
897	EPDM/EVA	127	58	48	5.6	
899	EPDM	104	64	49	5.9	1
900	EPDM	128	75	60	5.9	1
903	EVA Ceanotox	162	87	61	5.7	1
904	EPR Ceanotox	161	51	40	5.3	
908	PE News 1386	127	95	47	5.9	1
914	Cogegum AFR/2	273	115	26	5.5	
915	VAC thermoplastic	657	391	231	5.8	1 2
922	VAC thermoplastic	608	527	340	6.0	1+ 2
925	EPR 3 GZ 340	483	259	176	5.7	1 2
926	EPR DM 021	588	335	220	5.8	1 2
931	Polyolefin DF632	517	10	4	5.3	
937	Polyolefin ZH 33	121	54	28	5.6	
951	Sioplas	118	63	52	5.8	1
952	EPR G 5	110	63	48	5.8	1
953	Megol.S300-15	171	122	102	> 6.	1+ 2
954	Megol.S300-10	154	112	87	> 6.	1+
955	Megolon S 2-1	415	169	118	5.6	2
956	Megolon S 2-5	486	226	164	5.6	2
961	Cogegum AFR 11	560	383	24	5.8	1
982	VAC thermoplastic	628	487	27	5.8	1
983	VAC thermoplastic	607	96	12	5.5	
988	VAC thermoplastic	668	371	134	5.7	1 2
989	VAC XL	458	92	57	5.5	
990	VAC XL	483	263	62	5.7	1

Explanation of remarks : 1 = RI > 5.7
1+ = RI > 6.0
2 = elongation at 1 MGy > 100 %
! = initial absolute values are low

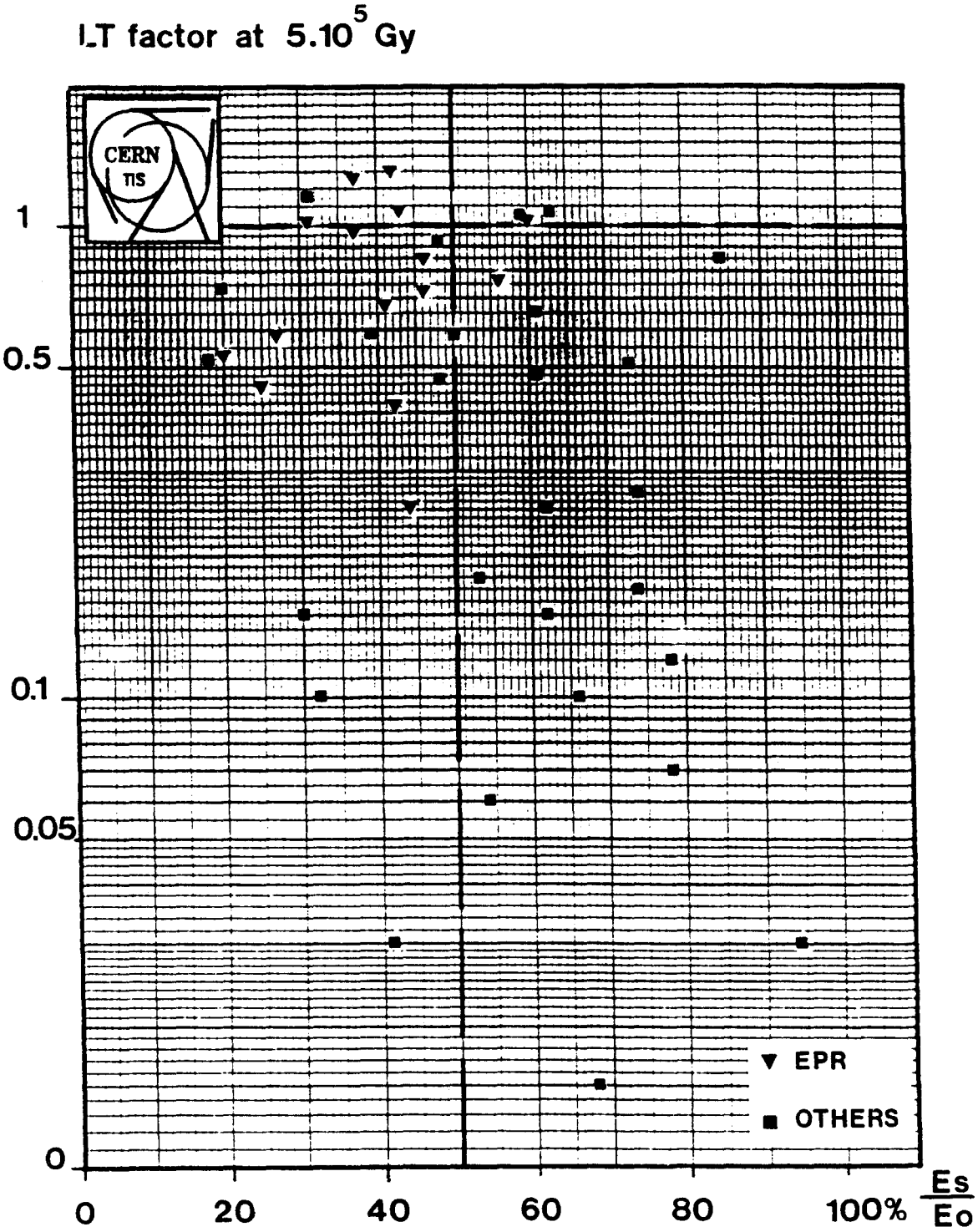

Fig. 1: Long Term factor (LT) at 5.10^5 Gy (ratio of elongation at break for long-term and short-term tests) versus ratio of elongation at break at 5.10^5 Gy and initial elongation (E/E_0) for short-term tests.

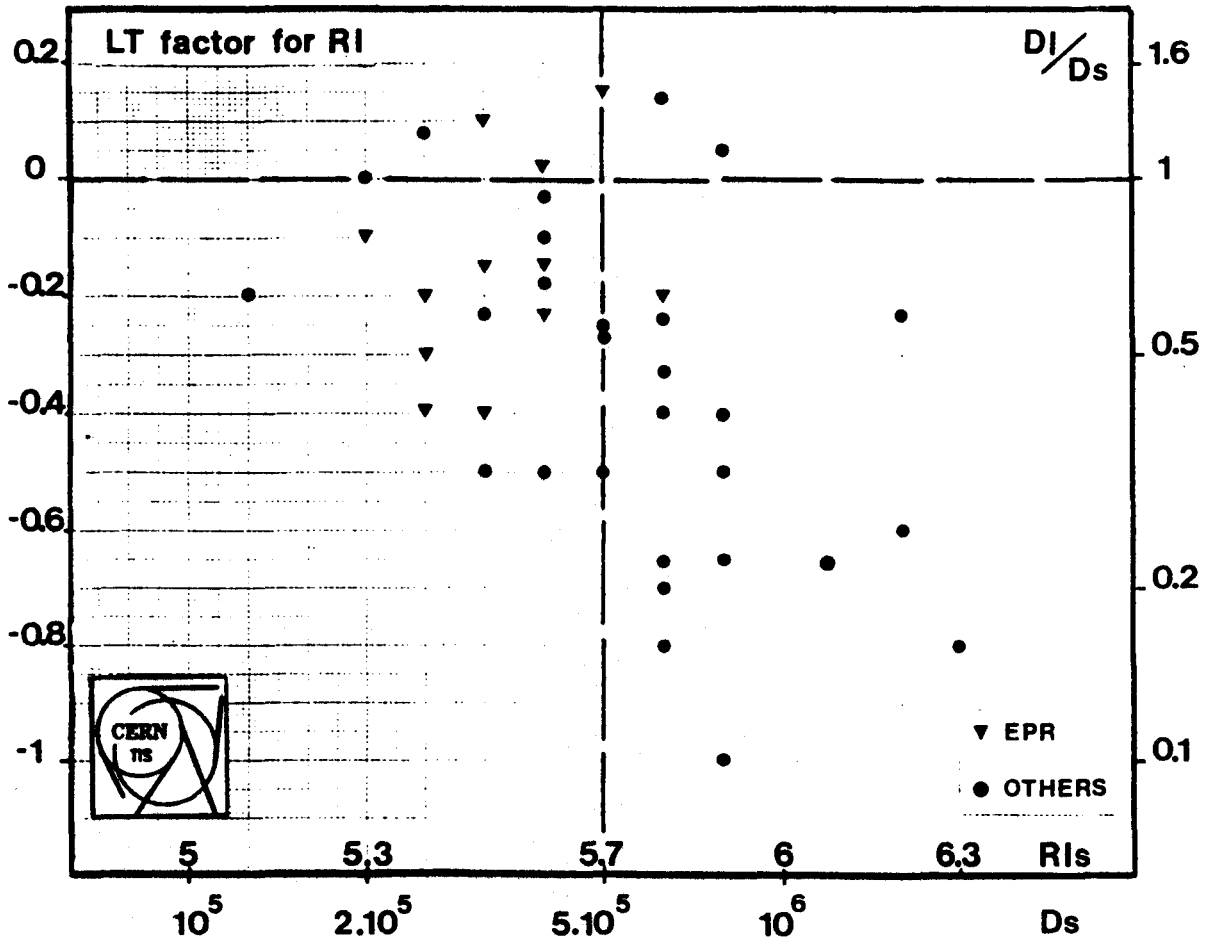

Fig. 2: Long Term factor (LT) for Radiation Indexe as a function of Radiation Index for short-term irradiations RI_s
End-point Criterion $E/E_0 = 0.5$
D_l = end-point dose for long-term irradiation
D_s = end-point dose for short-term irradiation
$RI_s = \log_{10} D_s$; $RI_l = \log_{10} D_l$
L.T.factor = $\log_{10} D_l/D_s = RI_l - RI_s$

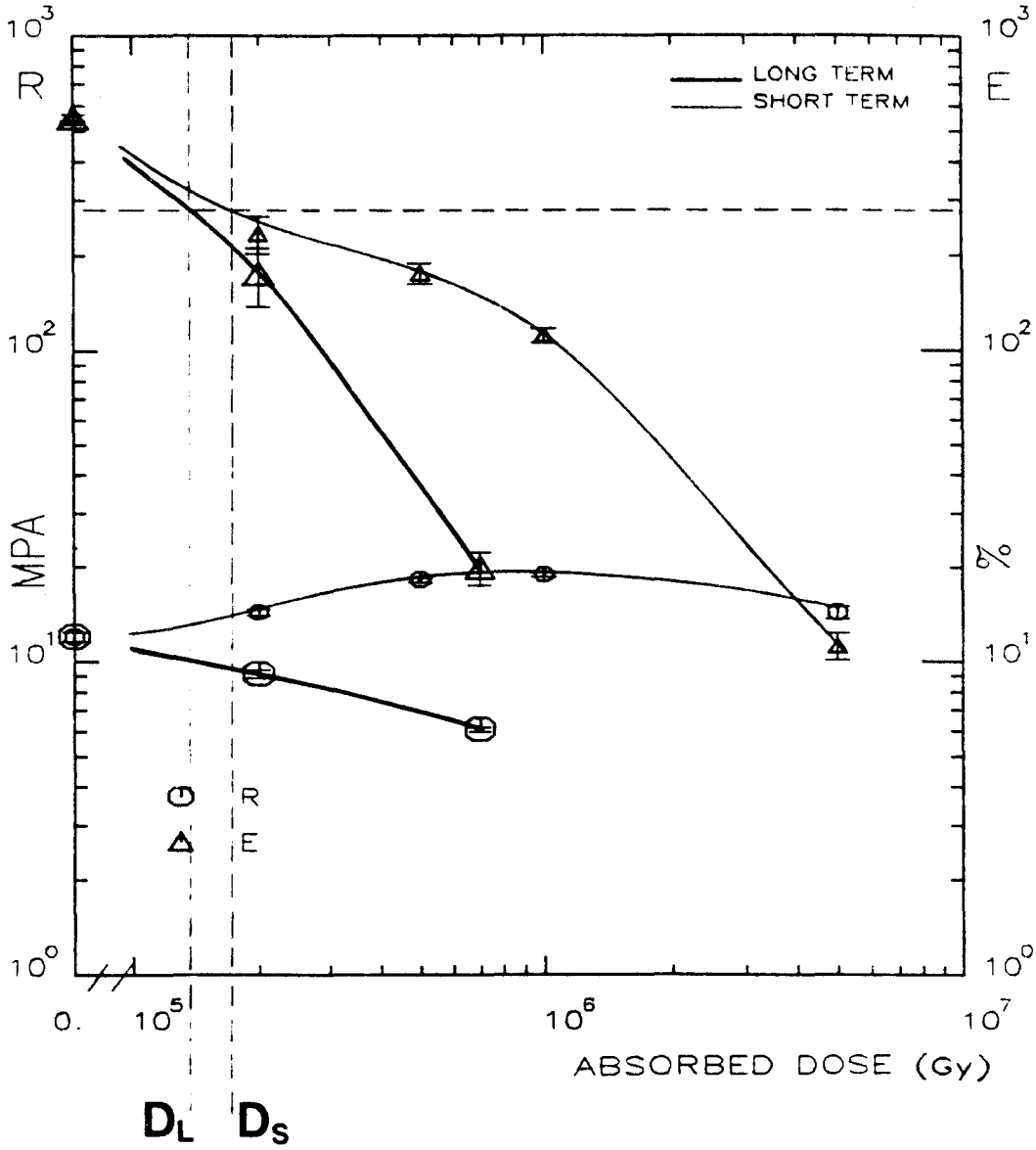

Fig. 3: Tensile properties (Elongation at break E and tensile strength R) versus absorbed dose for a cable sheath material.
D_S = end-point dose for short-term irradiation
D_L = end-point dose for long-term irradiation.

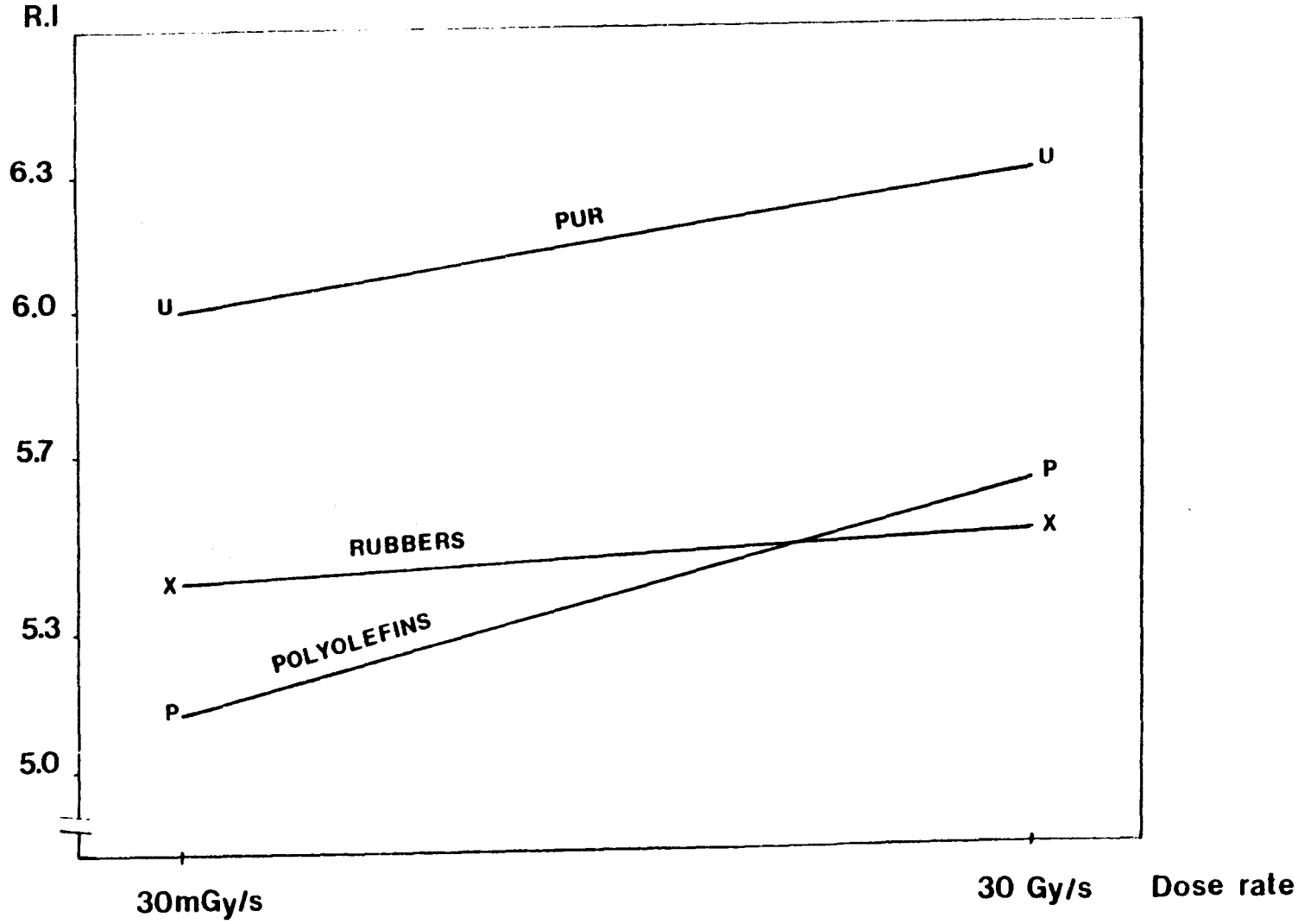

Fig. 4: General demonstration of Radiation Indexes (RI) and dose rate effect on EPR, Polyolefins and PUR. (the lines are drawn to guide the eye only).

APPENDIX 3

Radiation Sources for Material Testing in Europe

EUROPEAN ORGANIZATION FOR NUCLEAR RESEARCH

TIS-CFM/IR/90-02

INTERNAL REPORT
23.04.1990

RADIATION SOURCES FOR MATERIAL TESTING IN EUROPE

H. Schönbacher and M. Tavlet

The most radiation sensitive materials needed for future detectors around high-luminosity multi-TeV colliders are scintillators and semiconductors. Their damage depend on the radiation type and dose rate and environment during and after irradiation. To study the radiation damage in such devices, different radiation sources and on line measurements are needed.

This report summarizes the different sources used at present for CERN radiation tests: reactor, Cobalt, CERN target areas, X-rays, electron beams and small sources. Other European irradiation facilities are also presented.

1. INTRODUCTION

Radiation damage studies are carried out at CERN since many years in order to select suitable materials and components for the constructions of the accelerators.

Calculations and measurements in the existing accelerators show that, owing to their position, the materials may receive doses from 100 to 10^6 Gy per year.

To ensure, if possible, a service life of at least 10 years, the proper selection of materials and components is required. This implies preliminary tests after accelerated irradiation with strong radiation sources.

Several radiation sources were used at CERN: the ASTRA pool reactor for high-doses or neutron irradiations and different strong Cobalt sources. CERN target areas and accelerators were also used, in a parasitic way.

Up to now the studies of radiation damage have been concentrated on materials and components used in the primary beam areas of the accelerators. Very little consideration has been given so far to detector materials, because the radiation doses in present fixed target or collider experiments are in most cases far below any damage level.

Exactly the opposite will be the case for future high luminosity hadron colliders in the multi-TeV energy range where the accelerator will have to operate with low beam loses and hence low radiation doses, whereas in the collision region of the detector the doses will be in the order of 10^4 to 10^6 Gy (1 to 100 Mrad) per year and therefore similar or higher than normally accumulated in present primary beam areas in more than 10 years (Ref. 1).

The most radiation sensitive materials in the accelerators were the organic materials (mainly the cables and the coil insulations) for which the principle "equal dose - equal damage" is valid however with a dose rate effect for certain materials, which becomes to be well known and understood. Large experience has been gained on radiation effects on accelerator components and the data are published (Ref. 2). This is also of interest for future detectors, but information is missing on the most sensitive components: scintillating materials, semiconductor materials and electronics.

The radiation damage mechanisms may be different in different types of material, therefore the type of irradiation may be of importance on the damage level.

Further both scintillating and semiconductor materials are sensitive to dose rate effect but not always in the same way and scintillators and fibres may be very sensitive to the surrounding atmosphere, during and after irradiaton.

For electronic components radiation damage may be different when they are irradiated, biased or unbiased.

Considering all these parameters, it becomes evident that different radiation sources are needed to study radiation damage, and that one needs to be able to carry out irradiations under different environmental conditions and measurements during or soon after the irradiation.

In this report, we describe some available radiation sources, their main characteristics as well as the dosimetry methods. Some recommendation and projects for the future are also presented. The list of sources given is by no means exhaustive.

2. ASTRA REACTOR

2.1. Description of the reactor (Ref. 3)

The ASTRA reactor of the Oesterreichisches Forschungszentrum Seibersdorf (OFS) is a pool reactor with a thermal power output of 7 MW. The fuel elements are of the MTR type and contain 23 fuel plates. The fuel is uranium enriched to 93 % U 235. The reactor core consists of standard, control and irradiation elements; it stands on a grid plate with 9 x 6 positions and is surrounded on four sides by beryllium reflector elements. Located in the reactor core and in the reflector, as well as outside the reflector, are several irradiation channels and irradiation facilities for the production of radionuclides, activation analysis and testing of materials. Fig. 1 shows the reactor configuration and the irradiation positions.

2.2. Irradiation positions in plane 1 (Ebene 1)

The irradiation positions in plane 1 are located outside the reactor core at a distance of about 26 cm from the core edge. Plane 1 is equipped with fixed rails with uniformly spaced perforations. The rails provide fixed support and guidance for inserted racks into which, in turn, it is possible to insert irradiation containers of various sizes and shapes. The standard arrangement consists of 4 cylindrical containers (D = 62 mm, L = 200 mm) irradiated simultaneously. The exact dimensions, dose rate and neutron fluxes are given in table 1.

The dosimetry is ensured by three different ionization chambers to distinguish between γ-dose and neutron-dose. For plastic materials, the neutron dose is less than 5 % of the total dose. It is still less in silicon devices, but the presence of neutrons leads to induced radioactivity.

2.3. Irradiation position SNIF

SNIF (Standard Neutron Irradiation Facility is an irradiation facility for fast neutrons with the lowest possible contributions by gamma radiation and by thermal neutrons to the total dose. The unit constitutes a filter against gamma radiation and thermal neutrons and consists of two concentric cylindrical lead shields for the attenuation of the gamma dose rate, with a boron carbide layer attached to the outside of the inner lead shield for the attenuation of the flux density of thermal neutrons. Projecting over the irradiation space is a 2 m long tube with a funnel for rapidly bringing the irradiation container into

the irradiation position. The entire irradiation facility can be set up at a distance of 48 to 63 cm from the core depending on the required neutron dose rate. The irradiation container itself has dimensions D = 56 mm, L = 120 mm and consists of a 1 cm thick lateral lead shielding and a 5 cm thick lead cover for the attenuation of the scattered gamma radiation entering the irradiation container from above. The container is suspended on a steel rope and is rotated during irradiation by a motor in order to ensure a uniform dose distribution in the material being irradiated .

The dosimetry is also ensured by ionization chambers plus activation detectors if the neutron spectrum has to be precisely known. The gamma dose rate and the neutron fluxes as well as the available dimensions are given in table 1. The neutron to gamma dose ratio is 2 for CH materials and only 0.1 for silicon devices (4). Even if the displacement damage due to neutrons may be 100 times as large as the ionization damage due to gammas, the gamma dose in such irradiations may not be neglected.

2.4. Irradiation position 35

In order to be able to use also the periods of reactor shut down for material irradiations, a fuel element is removed from the middle of the core and a cylindrical irradiation container with the dimensions D = 61 mm, L = 500 mm is inserted into the vacant position. As the intensity of the radiation field varies considerably during the irradiation time, depending on the prior history of the reactor core, the gamma dose rate is monitored during the irradiation by means of ionisation chambers. The dose rates are given in table 1. This position is suitable for irradiation to high-doses when induced radioactivity by neutrons must be avoided.

2.5. Other positions

For very high-doses or neutron fluxes, materials may be irradiated in position 11 or inside the reactor core (see Ref. 3).

3. COBALT SOURCES

Both for radiation damage studies and dosimeter calibration the gamma rays (1.17 and 1.33 MeV) from cobalt sources are very frequently used. They are available at numerous places (see table 2), we list below only those which have been used so far for CERN.

3.1. Industrial sources at Conservatome (F)

The French company Conservatome in Dagneux-Montluel carries out sterilization of food and medical materials and treatment of plastics on an industrial basis. They operate three ^{60}Co irradiation facilities: two industrial ones with automatic handling of samples and one "experimental cell" with a 150.000 Ci Cobalt source, which is used for radiation damage tests.

In the "off" position, of the experimental cell the source is immersed in water in a well located in the centre of a shielded room (see Fig. 2). In the "on" position, the source is lifted above the lip of the well and irradiates the whole room. The sample could be placed anywhere in the room or inside the cobalt bars. The corresponding dose rates are given in table 1.

The irradiation position in the cell is a function of the required dose rate (which is calculated in terms of the source activity and the distance and sometimes the shielding). After irradiation, the exact dose (in CH materials) is read by means of Perspex dosimeters (the formation of color centers in this PMMA is a function of the dose).

The typical irradiation medium is air at ambient temperature, but the room is large enough to mount special sets with gases or a cryostat. Electronic components may be powered during irradiation.

3.2. Experimental source at OFZ Seibersdorf

The Oesterreichisches Forschungszentrum Seibersdorf operates a ^{60}Co source for sterilization, radiation testing and dosimetry.

The general configuration of the source and the irradiation room is similar to the one at Conservatome, but the source is weaker (20000 to 30000 Ci) and the room somewhat smaller.

Up to now, this source was mainly used for long-term irradiations of the insulating materials, at low dose rates of 100 Gy/h.

4. X-RAY SOURCE

An industrial analysis X-Ray set was made operational at CERN for material testing which allows high dose rates for long operation times. (Ref. 5). The generator is a 3 kW Philips PW1140. The X-ray tube is mounted in a shielded room (see Fig. 3a), its maximum tension is 80 kV. An antico cone is placed around the beam and supports the samples. The irradiation position is at 25 cm from the tube window and the available diameter of uniform beam is 14 cm (see Fig. 3b).

Three different filters may be used: two times 1 mm Cu and 1 mm Al. The mean energy and hence the penetration power of the filtered beam increases but the dose rate decreases. Two examples of the irradiation conditions are given in table 1. The dose-rate may of course be reduced by reducing the current and/or by increasing the distance from the tube. In the latter case, larger samples may be irradiated but they always must be thin e.g. electronic circuits or thin plastic samples.

In the unfiltered beam, dosimetry is very difficult; at 80 kV the mean energy is around 15 KeV, the penetration power is very low and the dose distribution is not homogeneous. This may not be used for irradiation of integrated circuits.

For routine irradiations, RPL dosimeters and silicon diodes are used for dosimetry of silicon devices and an alanine dosimeter is used for plastics. Intercalibrations have been made with a medical X-ray set with a maximum tension of 100 kV which was modified for calibration of radiation protection instruments. This set may exceptionally also be used for the irradiation of small items at low dose and dose rate.

5. HAHN MEITNER INSTITUTE (HMI)

HMI carries out on a routine basis irradiation and tests of electronic components and circuits for more than 10 years, mainly for the European Space Agency. They have a well equipped laboratory to make irradiations and on line measurements of characteristic parameters or immediately after irradiation.

They operate an X-ray irradiator (150 kV), an electron accelerator (2.5 MeV) and two cobalt sources. Details about their sources and procedures can be found in reference 6. The main characteristics of the sources are given in table 1.

Ionization chambers, TL dosimeters and solar cells are used for dosimetry.

6. CERN ACCELERATORS

6.1. Parasitic irradiations in SPS north targets area

When the CERN SPS operates in "fixed target" mode, it is possible to carry out material irradiations behind or near to the targets. Extensive dose measurements were carried out behind T6 in TCC2 (Ref. 7). The materials are irradiated in a radiation field which is representative of their life exposure during operation. The doses and irradiation times are evaluated before the materials are put in place, the real doses depend on the machine schedule and running mode. In this radiation field, the absorbed dose depends on the material composition; the dosimetry is ensured by RPL and alanine dosimeters.

Close to the beam line behind T6, the dose rate is in the order of 1000 to 3000 Gy/h. Only relatively small items can be irradiated in these conditions (see for example table 1). On the QNL magnets behind T6, the dose rate is of the order of 100 to 500 Gy/h with a more homogeneous distribution, bigger items may be irradiated there (see Figs 4 and 5).

6.2. Project in PS-ACOL target area

An irradiation facility for small items is under construction at PS-ACOL target area. Samples can be introduced through a hole from the top (9 m above the beam line) down between the target and the beam dump (see Fig 6 and Ref. 8). The position of the samples can be adjusted and the dose-rates and dose levels can be controlled during irradiation; we expect dose-rates between 10 and 1000 Gy/h in plastic materials (see table 1). Also measurements and powering of circuits could be made during or immediately after irradiation.

The dimension of the irradiation container will be of the order of 18 cm diameter and 20 cm height, but if an unhomogeneous irradiation is allowed, much longer samples could be irradiated.

The project is well advanced: the antico fixed tube is installed, the tightness of the area is ensured and the basis for a small surface building is ready. Also the mechanical devices to handle the samples are ready.

Whenever the antiproton target is in operation, samples can be irradiated in this facility independent from the operation schedule (which is not the case for T6 described above).

7. OTHER IRRADIATION FACILITIES

7.1. Small sources from TIS-RP group

At CERN, the TIS-RP group may provide small sources suitable for irradiation at low doses (< 100 Gy) of small items. Many types of α, β and gamma sources are available. Members of the group may ensure the dosimetry.

7.2. Outside firms or institutes

Several European firms or institutes may carry out irradiations with different types of sources, accelerators or reactors. A list is given in table 2, which of course is not exhaustive.

8. SUMMARY AND RECOMMENDATIONS

A number of facilities are available in Europe and offer various types of irradiation types and conditions (see tables 1 and 2).

The distances from CERN, the fact that we are not the only customers and the delay for the return of the samples are often an handicap for our radiation damage tests.

As stated above the presentation given here is by far not complete and further enquiries in the near future will allow to update this list. On the other hand many of these sources are not in the places where tests are carried out and are not dedicated for material testing. Long handling and delivery times may be the consequences.

It is recommended to make more use of the CERN accelerators and their target areas, where the irradiation facilities need to be increased and the irradiation conditions improved. On the other hand TIS-CFM should require a new powerful X-ray set (with a maximum tension of 200 or 300 kV, the price is of the order of 63 KCHF) and a gamma irradiator (type Gammacell, the price is of the order of 180 KCHF). It would be a considerable improvement of service to have this facilities available at CERN. This especially in view of the increasing requests from the high energy physics community for irradiation of materials to be

operated in future multi-TeV detectors. In these detector the main contribution of radiation dose will come from electromagnetic radiation and the measurements during or immediately after irradiation are of importance for many materials (scintillators and electronics); this supports the above recommendations to install powerful X-ray and gamma sources at CERN for material testing.

Adequate neutron sources need still to be found.

REFERENCES

1. H. Schönbacher, Radiation damage studies for detector materials. Proceedings of ECFA Study week on Instrumentation for High-Luminosity Hadron Colliders, Barcelona, 14-21.09.89, CERN 89-10 and ECFA 89-124 (129).

2. Compilation of radiation damage test data CERN Reports 89-12, 82-04, 79-08, 79-04.

3. H. Schönbacher et al., Study on radiation damage to high energy accelerators components by irradiation in a nuclear reactor, Kerntechnik, 17 Jg. 1975

4. H. Schönbacher and M. Tavlet, Doses to materials irradiated in SNIF, TIS-CFM/TM/89-01.

5. M. Tavlet, Adaptation d'une source de rayons X pour des tests de radiorésistance, TIS-CFM/TM/89-03.

6. D. Bräunig, F. Wulf, W. Gaebler, A. Boden, Irradiation Test Guidelines for Radiation Hardness of Electronic Components. HMI B 380, TN 53/10.

7. B. Baeyens, F. Coninckx, Dose measurements for material irradiations behind SPS target 6, TIS-RP/TM/85-49.

8. M. Tavlet, Project for an irradiation facility in the PS-ACOL target area, TIS-CFM/TM/89-08.

TABLE 1

IRRADIATION FACILITIES AND THEIR MAIN CHARACTERISTICS

Firm	Type of Source	Dose rates (or particles fluxes)	Available dimensions
O.F.S.	Astra/Ebene 1	$3x10^{11} n_{th} cm^{-2}s^{-1}$ + $3x10^{10}$ n(E>1MeV)$cm^{-2}s^{-1}$ + 1-3 x 10^5 Gy/h (g in CH)	Ø 60 cm x H 20 cm
	Astra/SNIF	$2x10^9$ $n_{th} cm^{-2}s^{-1}$ + $8x10^9$ n(E>0.1 MeV)$cm^{-2}s^{-1}$ + 300 Gy/h (g in CH)	Ø 5.6 cm x H 12 cm
	Astra, Pos. 35	10^4 - 10^5 Gy/h (g in CH)	Ø 6.1 cm X H 50 cm
CONSERVATOME	^{60}Co (cell D2)	"inside" of source: 3000 to 7000 Gy/h on the platform: 10 to 500 Gy/h	Ø 19.5 cm x H 50 cm > 1 m³ (maxi 50 kg)
O.F.S.	^{60}Co	1 - 200 Gy/h (CH) on the platform inside the source	> 1 m³
CERN	X-Ray 80 kV	maxi with 2 mm Cu = 2 Gy/h (CH) , 6 Gy/h (Si) maxi with 1 mm Al = 120 Gy/h (CH) , 600 Gy/h (Si)	Ø 14 cm, thin samples greather Ø available
H.M.I.	2.5 MeV e^- ^{60}Co (1) ^{60}Co (2) X-Ray 150 kV	10^8 - 10^{10} e^- cm^{-2} s^{-1} 10 - 100Gy/h (Si) 1300 Gy/h (Si) maxi 180 Gy/h (Si)	20 x 20 cm² Ø 20 cm x H 30 cm Ø 7 cm x H 14 cm 40 x 40 cm²
CERN	TCC2-T6	beside or above the magnets: 10 - 500 Gy/h close to the beam pipe: 500 - 3000 Gy/h	~ 50 x 50 x 50 (cm³) ~ 20 x 5 x 5 (cm³)
	PS-ACOL Target	10 - 1000 Gy/h (CH)	Ø 18 cm x H 20 cm

Table 2

IRRADIATION FACILITIES IN EUROPE

Institute	Place	Type of sources
OESTERREICHISCHES FORSCHUNGSZEBTRUM SEIBERSDORF (OFS)	A-2444-SEIBERSDORF	Reactor, γ, e–
SCK/CEN	B-2400 MOL	Reactor, γ
IRE-MEDIRIS	B-6220 FLEURUS	γ
RISØ National Laboratory	DK-4000 ROSKILDE	γ, e–
BGS Beta-Gamma-Service	D-5276 WIELL-BOMIG	γ, e–
CEA-CEN	F-13115 ST-PAUL-LES-DURANCE	γ
CEA-ORIS	F-91190 GIF-SUR-YVETTE	γ, e–
CEN	F-38041 GRENOBLE	γ
CERT-DERTS	F-31055 TOULOUSE	γ, β, e–
CONSERVATOME	F-01120 DAGNEUX-MONTLUEL	γ
A.E.R.E. HARWELL	GB-OXFORDSHIRE OX11 ORA	Reactor, γ, ^{252}Cf, e^-, p^+
GANIL	F-14021-CAEN	Heavy ions
CEA DEMOKRITOS	GR-ATTIKIS	γ
ENEA CASACCIA	I-00100 ROMA	γ
INSTITUTE OF ATOMENERGY	N-2007 KJELLER	Reactor
EURATOM C.E.C.	NL-1755 ZG PETTEN	Reactor
STUDSVIK ENERGITEKNIK AB	S-61182 NYKOPING	Reactor, γ
HAHN MEITNER INSTITUT (HMI)	D-1000 BERLIN 39	X-ray, γ, e^-

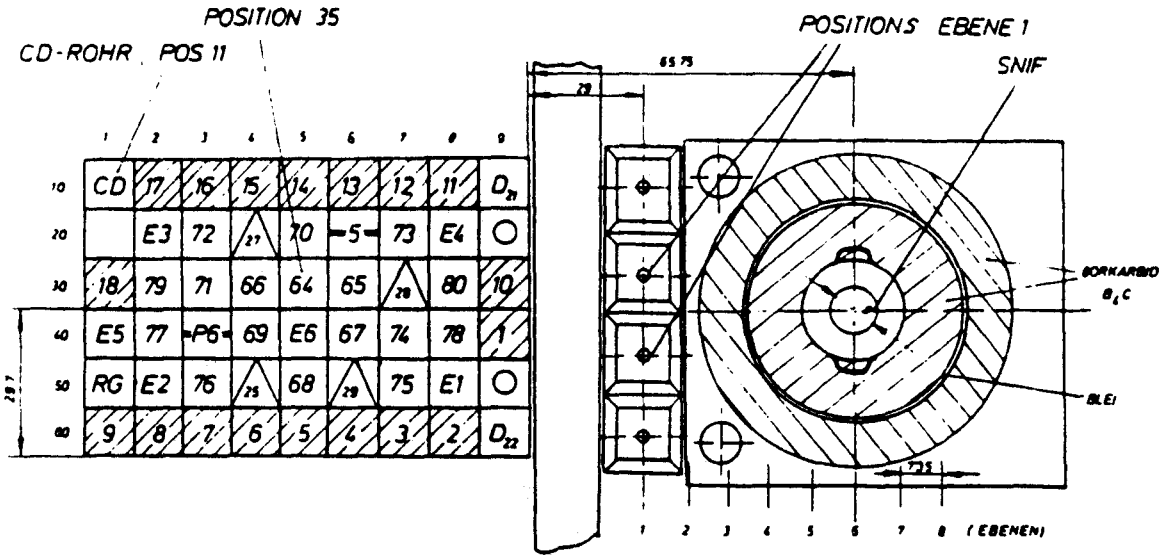

Fig. 1. Core configuration and radiation facilities in the 7 MW ASTRA pool reactor

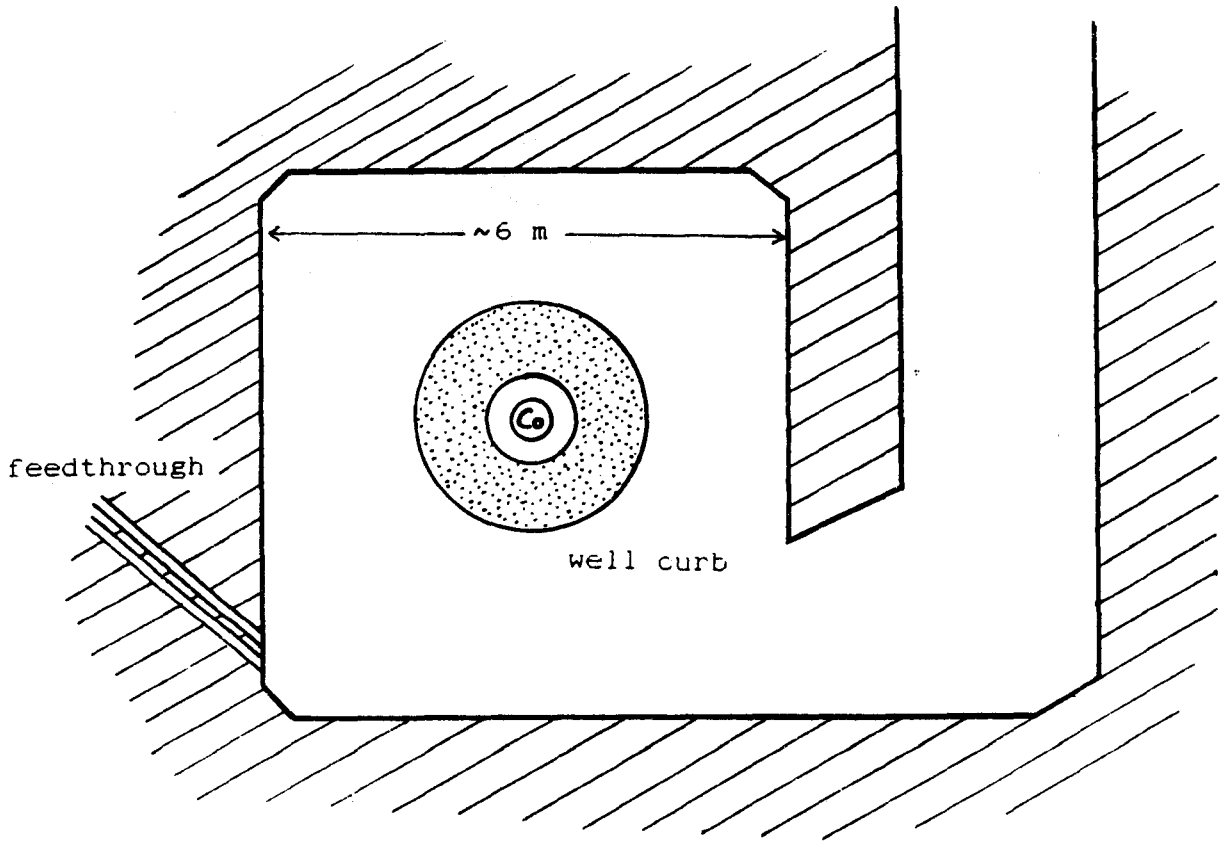

Fig.2 : Cobalt irradiation cell at Conservatome.

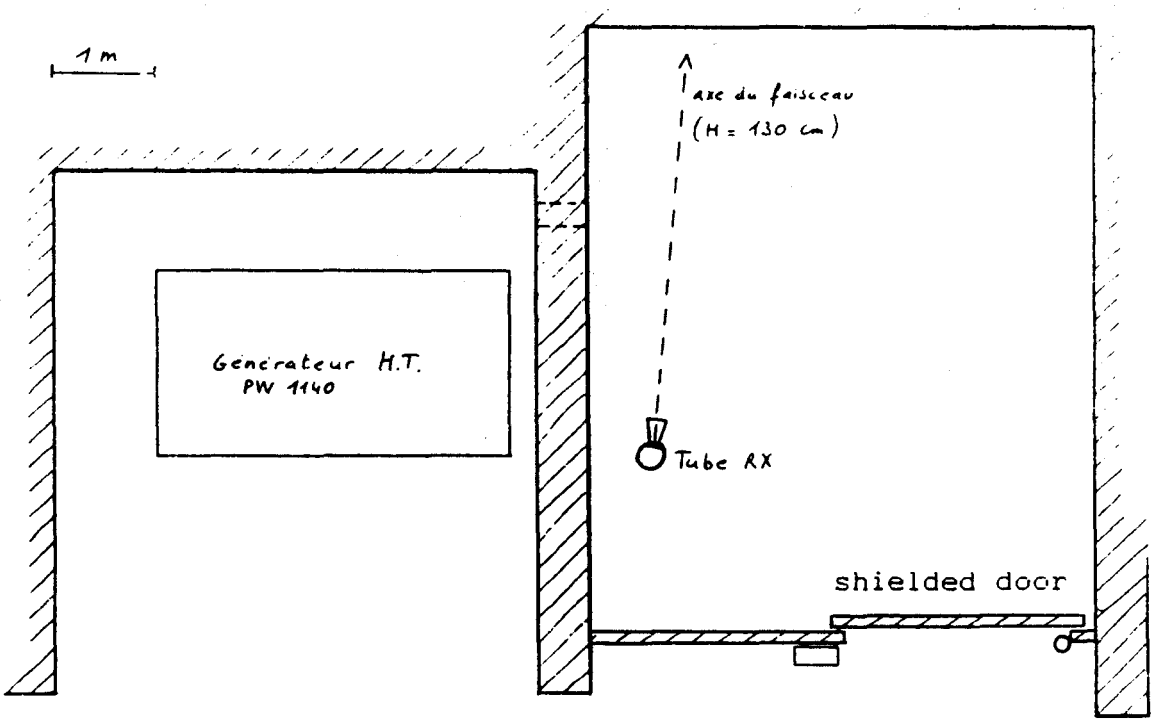

Fig.3a : X-ray irradiation cell at CERN.

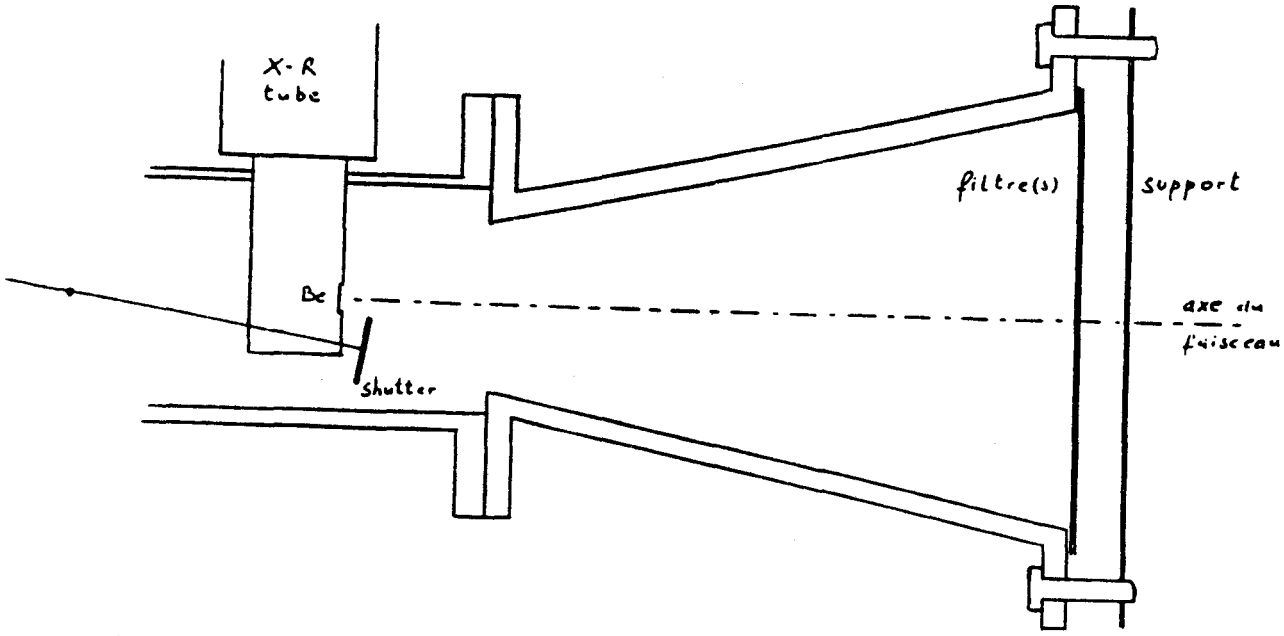

Fig.3b : X-ray tube head and irradiation cone.

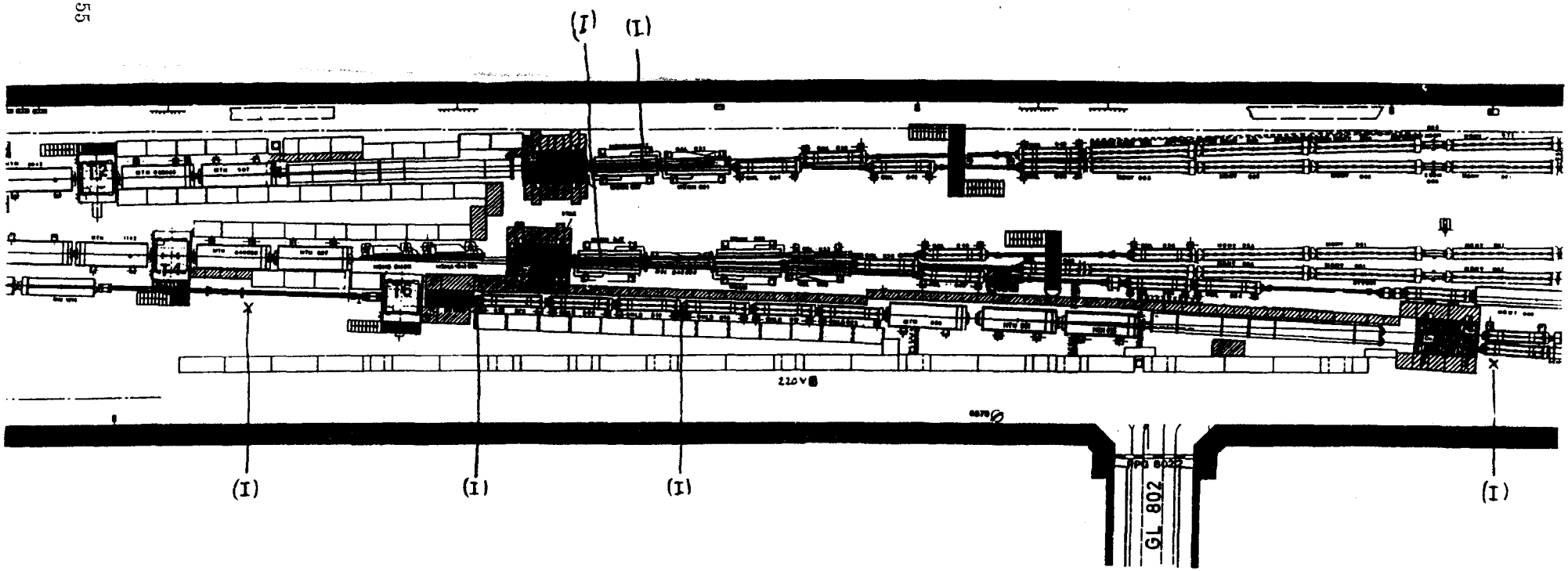

Fig.4 : CERN SPS target area TCC2 and irradiation positions(I)

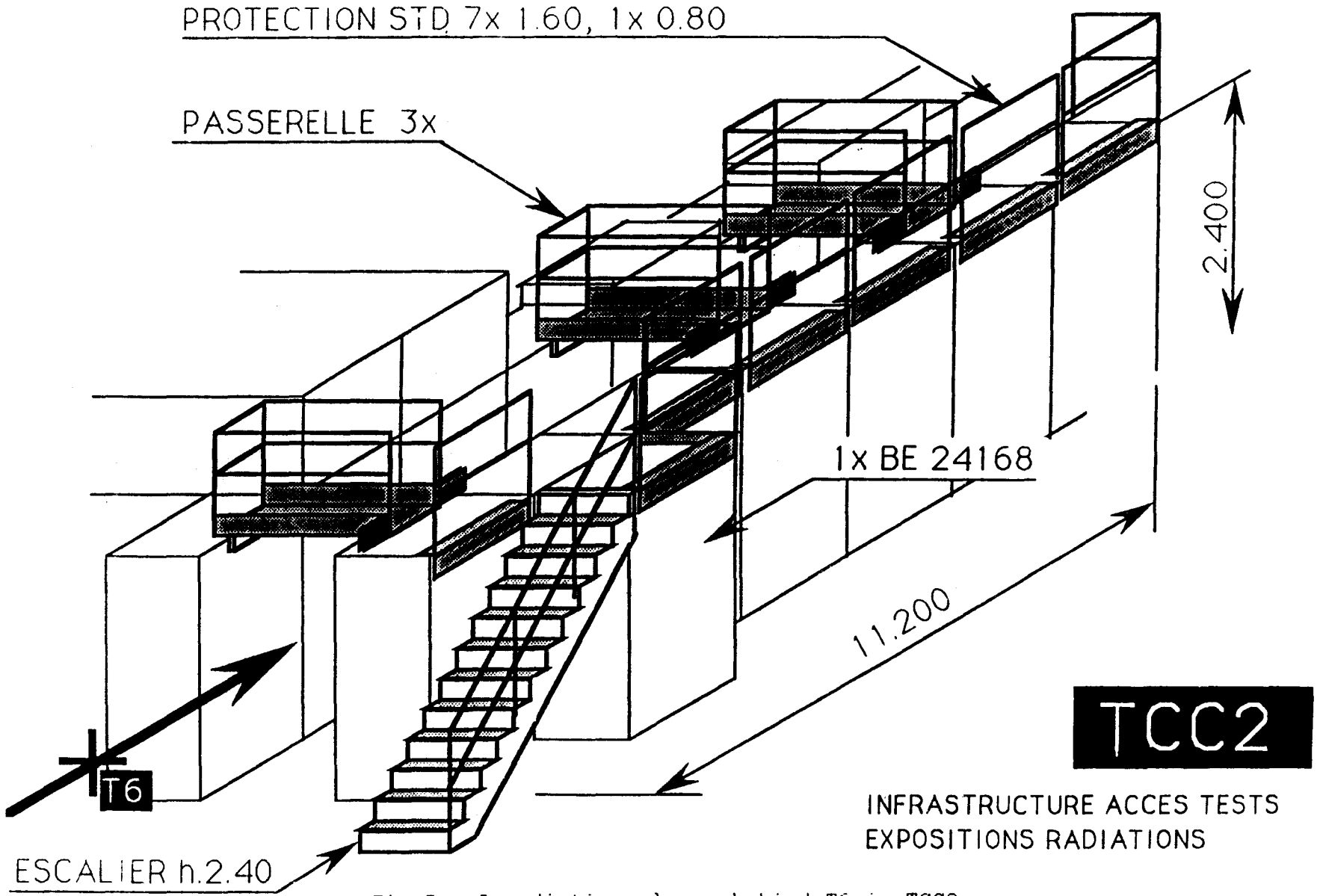

Fig.5 : Irradiation places behind T6 in TCC2.

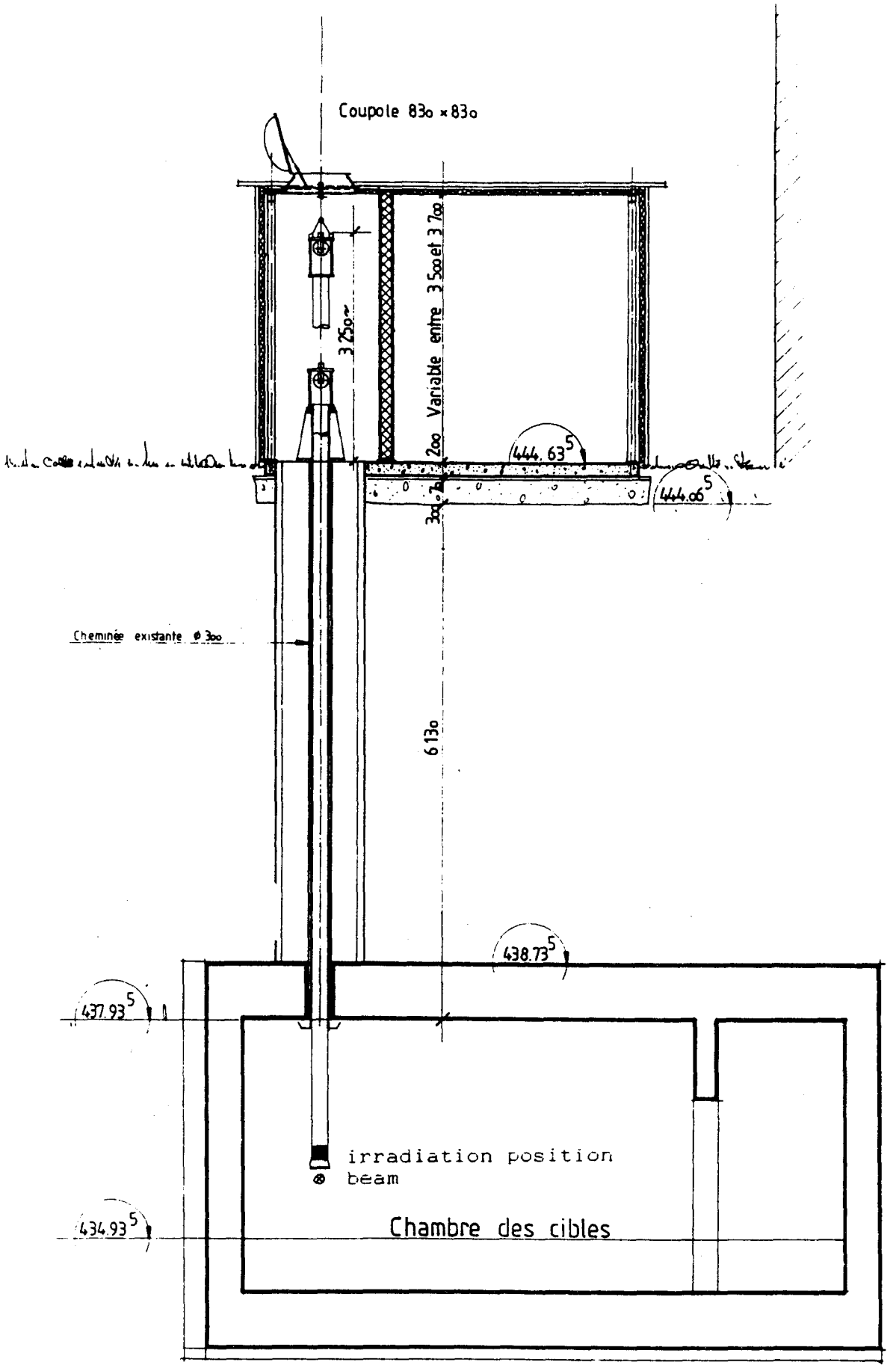

Fig.6 : Irradiation facility in ACOL target area at CERN.

APPENDIX 4

Overview of Radiation Effects on Polymers

OVERVIEW OF RADIATION EFFECTS ON POLYMERS

R. L. Clough and K. T. Gillen
Sandia National Laboratories
Albuquerque, New Mexico, 87185

GENERAL DISCUSSION OF RADIATION EFFECTS ON POLYMERS

Radiation effects in organic materials are initiated by ionization events as shown in Eqn. 1, below. Secondary electrons created in the initial event can lead to a series of additional events in a localized region of the polymer (Eqn. 2). Recombination of electrons and cationic sites leads to highly excited electronic states in the material (Eqn. 3). Excited states may also be formed directly in radiation events which lack sufficient energy to result in ionization (Eqn. 4). The excited states formed can undergo radiative or non-radiative decay back to the ground state, which results in no molecular structural change in the material. However, a portion of the excited states lead to dissociation of chemical bonds (Eqn. 5), generating reactive species called free radicals which are capable of undergoing further chemical reactions within the matrix. It is these processes of bond breaking and of subsequent free-radical-mediated chemical reactions which lead to changes in molecular structure and hence macroscopic properties of polymeric materials (1-5).

$$R \xrightarrow{\gamma} R^+ + e^- \quad (1)$$

$$e^- + R \longrightarrow R^+ + 2e^- \quad (2)$$

$$R^+ + e^- \longrightarrow R^* \quad (3)$$

$$R \longrightarrow R^* \quad (4)$$

$$RX^* \longrightarrow R\bullet + X\bullet \quad (5)$$

Radiation-induced changes in polymers can be contrasted to radiation effects in inorganic crystalline materials - for example in silicon devices. In crystals, damage primarily involves creation of defect sites resulting from displacements of nuclei; in polymers, damage results primarily from rearrangements of chemical bonds between atoms. Note that even in the case of bombardment of polymers by neutrons, although the initial event involves neutron capture by a nucleus, most of the damage results from secondary ionizations which again lead to excited states and to free radicals.

Organic polymers are macromolecules which consist of very long chains of carbon atoms and/or other elements. It is not unusual for individual molecules within the polymer matrix to consist of chains of 50,000 or more atoms. Side branches of various lengths, and chemical ties between chains (crosslinks) may also be present. The detailed molecular structures of macromolecules are primarily responsible for determining the physical properties of polymeric materials. When subjected to ionizing radiation, the molecular bonds which are broken to yield radicals can involve bonds between atoms along the chain backbone and/or bonds between atoms in side groups which are appendages to the chain. Overall, the most important molecular change which polymers undergo when irradiated involves either or both of the two processes illustrated in Fig. 1 (i.e., scission and crosslinking). Cleaving bonds between atoms which comprise the chain backbone ["scission"] results in chopping the macromolecule into smaller molecules. For polymers whose degradation is dominated by scission, the material generally becomes softer and weaker as it degrades; when taken to the extreme, the polymer is converted to a viscous liquid. The other primary degradation mode, crosslinking, occurs when free radicals generated by the irradiation engage in subsequent chemical reactions which result in formation of covalent bonds between adjacent macromolecular chains. For polymers dominated by crosslinking, the material

generally becomes harder and stiffer as it degrades, and eventually becomes highly embrittled. Table 1 shows the classification of major polymer types in terms of their primary degradation mode when irradiated in the absence of oxygen.

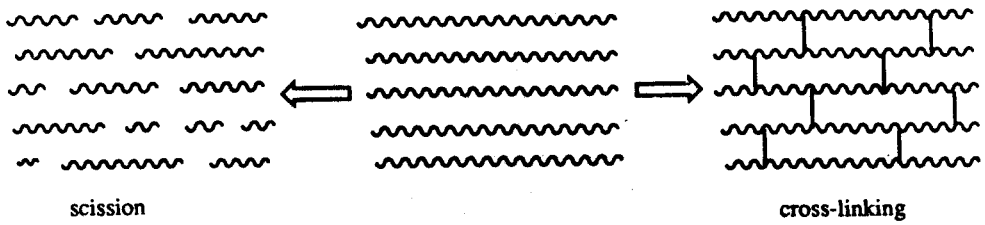

FIG. 1. Irradiation of a matrix of macromolecular chains (center) can result in chain scission (left) or in crosslinking between chains (right).

Due to diverse molecular structures and macroscopic properties, different types of polymers exhibit a wide range of different inherent resistance to ionizing radiation, spanning roughly 5 orders of magnitude in dose. Overall, elastomers (rubbers), which are lightly-crosslinked materials, are among the most sensitive to radiation. This is because the elastic nature of these materials, which is their unique property, is extremely sensitive to small changes in cross-link density or molecular weight (which is reduced by chain scission). In contrast, highly cross-linked, glassy resins such as epoxy or phenolic materials are among the most radiation resistant polymers. Their high strengths are not strongly affected by raising or lowering the number of interconnection points by crosslinking or scission except at very high doses, since the radiation-induced changes account for only a small change in molecular interconnections compared with the number which exist initially.

Polymers having aromatic groups (such as phenyl rings) incorporated in their molecular structure are much more resistant to radiation than aliphatic polymers. The aromatic group acts as a trap for excited state energy in the irradiated polymer. The excited-state aromatic group has a very low quantum yield for bond dissociation, and undergoes decay to the ground state with high efficiency. Several examples of radiation-resistant aromatic polymers are shown below.

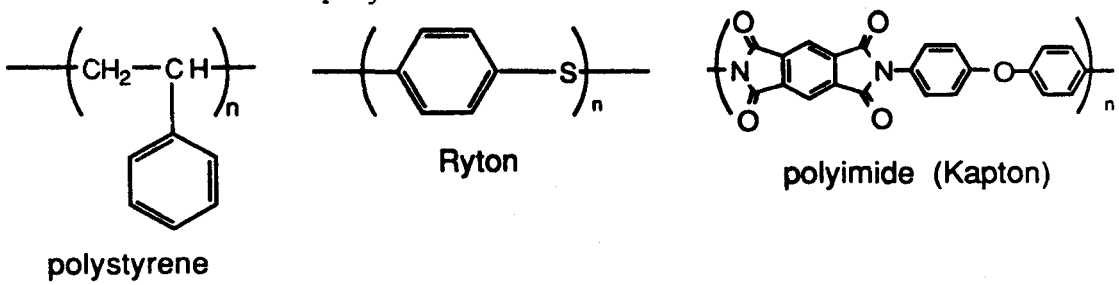

Radiation stability of polymeric materials does not necessarily correlate with thermal or chemical stability. A case in point is Teflon, which has outstanding stability with respect to elevated temperature environments, and which is probably the most resistant polymer known with respect to chemical attack. Despite this, Teflon is one of the least resistant polymers towards ionizing radiation.

Outgassing is another radiation degradation phenomenon which can be important. The composition of gaseous radiolysis products depends upon the molecular composition of the polymer. Hydrogen is the primary product for most polyolefins. For rigid, glassy polymers, which typically have low permeation coefficients for gas transport, bubbles may sometimes form within the polymer (particularly under high dose rate irradiation), resulting in dimensional deformation. In some cases, the outgassing

products themselves may be problematic, leading to pressure build-up inside closed containers, or causing corrosion of other materials. Of particular concern in this regard are chlorinated polymers such as polyvinylchloride (PVC), for which the primary radiolysis product is hydrochloric acid (HCl).

INFLUENCE OF OXYGEN

One environmental variable which is of extreme importance in the radiation-degradation of polymers is oxygen. If present, oxygen becomes involved in the free radical chemistry initiated by irradiation; in many cases this results in much more extensive degradation than in the absence of oxygen. Also the classification of polymers in terms of whether they undergo primarily scission or primarily crosslinking (as in Table 1) no longer applies; scission dominates for many more materials under oxidizing conditions. The importance of enhanced degradation under oxidizing conditions is illustrated in Fig. 2, which compares the decrease in ultimate strength of polystyrene as a function of absorbed dose for irradiations in the presence and absence of air (6).

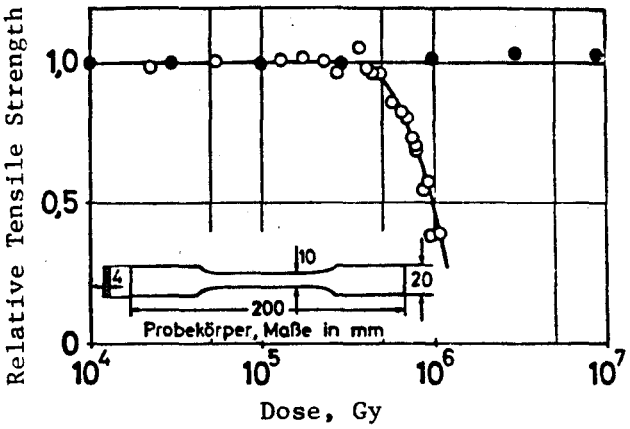

FIG. 2. Changes in relative tensile strength of polystyrene samples as a function of radiation dose: ● - irradiation under nitrogen (4.7×10^3 Gy/h), O - irradiation in air (13 Gy/h).

In addition to enhanced damage, complicated degradation behaviors involving time-temperature effects can arise when oxygen is present. As a result, the degradation may depend not only on the absorbed dose, but also upon the dose rate, the temperature, and the time period following the irradiation. The magnitude of such effects is material dependent. The occurrence of strong dose rate effects is illustrated in Fig. 3 for a PVC cable jacketing material (1). The data show the decrease in elongation at break versus dose for experiments run at five different dose rates. As is often the case, this material exhibits higher damage per equivalent dose at successively lower dose rates.

Figure 4 illustrates post-irradiation degradation (elongation-at-break) of polyethylene cable insulation material, for pre-irradiated and non-irradiated samples, as a function of aging time in air at 80° C in the absence of radiation (7). For the unirradiated material, negligible degradation takes place. For the pre-irradiated material, very marked deterioration in properties takes places over a period of about two months. The rate of post-irradiation oxidation is temperature dependent. Although the rate is higher at elevated temperatures, the effect can also be significant at room temperature, given longer time periods.

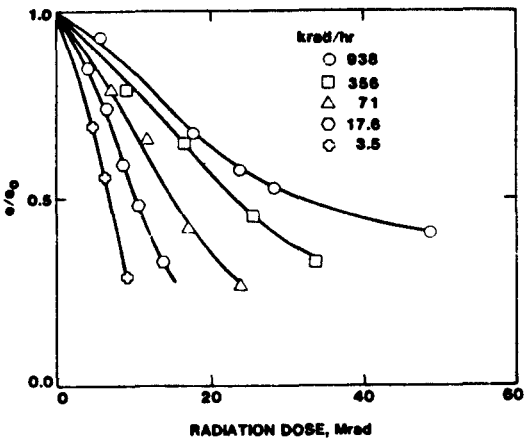

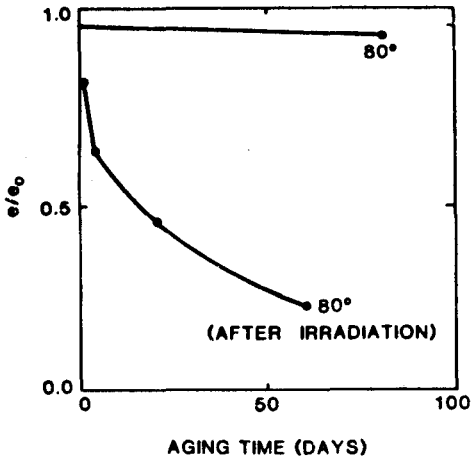

FIG. 3. (Left). Decrease in elongation at break for PVC cable jacket material irradiated at 60° C in air at five different dose rates as indicated. (100 rad = 1 Gy).

FIG. 4. (Right). Decrease in elongation at break of polyethylene cable insulation as a function of exposure time at 80° C in the absence of radiation. Upper curve: unirradiated material. Lower curve: material preirradiated at 50 Gy/h for 83 days at 25° C in air.

There are several causes of time-dependent effects (1). In many cases, free radicals trapped within crystalline regions of polymer matrices (which are inaccessible to oxygen) migrate slowly into amorphous regions where they can then react with oxygen. Also, peroxides formed in the course of radiation-oxidation undergo a time-temperature dependent decomposition, providing a chain branching step in the free radical mechanism. This results in more radicals than the number which arise directly from irradiation, and consequently leads to enhanced degradation. These mechanisms lead directly to post-irradiation oxidation effects, and also to dose-rate effects.

Another reason for dose rate effects is oxygen-diffusion-limited complications which can result at high dose rates. This is a common occurrence, and it results in strongly heterogeneous degradation. When free radicals are generated at very high rates (as occurs under high dose rate irradiation), oxygen may be consumed, by reaction with radicals, more rapidly than additional oxygen can be supplied from the surrounding atmosphere by diffusion through the matrix. In this case, strong oxidation takes place in the edge regions, whereas the sample interior may undergo radiation-degradation in the absence of oxygen, or under conditions of depleted oxygen availability. By comparison, in the case of irradiation of a sample of the same material at a lower dose rate, the rate of radical generation (and hence oxygen consumption) is much lower. Consequently, oxygen can permeate more deeply into the sample. At sufficiently low dose rate, homogeneous oxidation throughout the sample thickness will occur. As a consequence of oxygen diffusion effects, the overall degradation of a material under high dose rate conditions may be much less severe compared with a sample irradiated to the same dose at lower-dose-rate, more-highly-oxidizing conditions.

Several techniques have been developed to profile heterogeneous degradation across thin polymer samples (8-10). One versatile technique, developed by the authors, is modulus profiling (8,9). By this technique, degraded samples are cut in cross-section, and the depth of penetration of a tiny, weighted, paraboloidally-shaped tip into the sample is precisely determined as a function of position across the cross-sectional surface. The data obtained provide an edge-to-edge profile of modulus (or relative hardness) of the sample. Figure 5 illustrates heterogeneous oxidation

effects in 3-mm thick samples of EPR rubber that have been irradiated in air to a dose of 1.7 MGy at two different dose rates. At the higher dose rate (0.065 MGy/h), the edge regions undergo oxidation, whereas the interior portion degrades anaerobically; a distinct U-shaped profile results. At lower dose rate (0.011 MGy/h), the degradation approaches homogeneous oxidation.

Figure 6 illustrates another example of heterogeneous oxidation effects (8). In this case, 1.9-mm thick sheets of Viton o-ring material were irradiated at three different dose rates. The dotted line represents the flat modulus profile of an unirradiated sample. More extensive penetration of oxygen into the sample is clearly seen at successively lower dose rates. In the case of this Viton material, not only is degradation more severe at the lower dose rates, but the very nature of the degradation is fundamentally different in oxidized as opposed to unoxidized regions (9). In the edge regions, where oxidation occurs, the material becomes softer as it degrades (lower modulus), whereas in the interior, where degradation takes place in the absence of oxygen, the material becomes harder (higher modulus). The result is that when samples of the Viton material are irradiated at high dose rate, where oxidation is minimal, the overall sample characteristics are those corresponding to degradation in the absence of air (i.e., the sample becomes hard and brittle). In contrast, when samples are irradiated at very low dose rate, the overall sample characteristics are those of oxidative degradation (i.e., the sample becomes soft, more stretchable, and weak).

The occurrence of time-dependent effects has important implications. Because of dose rate effects, it is very difficult to carry out accelerated radiation aging tests on materials to determine what the degradation behaviors and rates will be under application conditions involving long time periods and low dose rates. Also, because of post-irradiation effects, there must be concerns that even for applications where irradiation may take place in the absence of oxygen, occasional exposure to air may lead to significantly enhanced degradation.

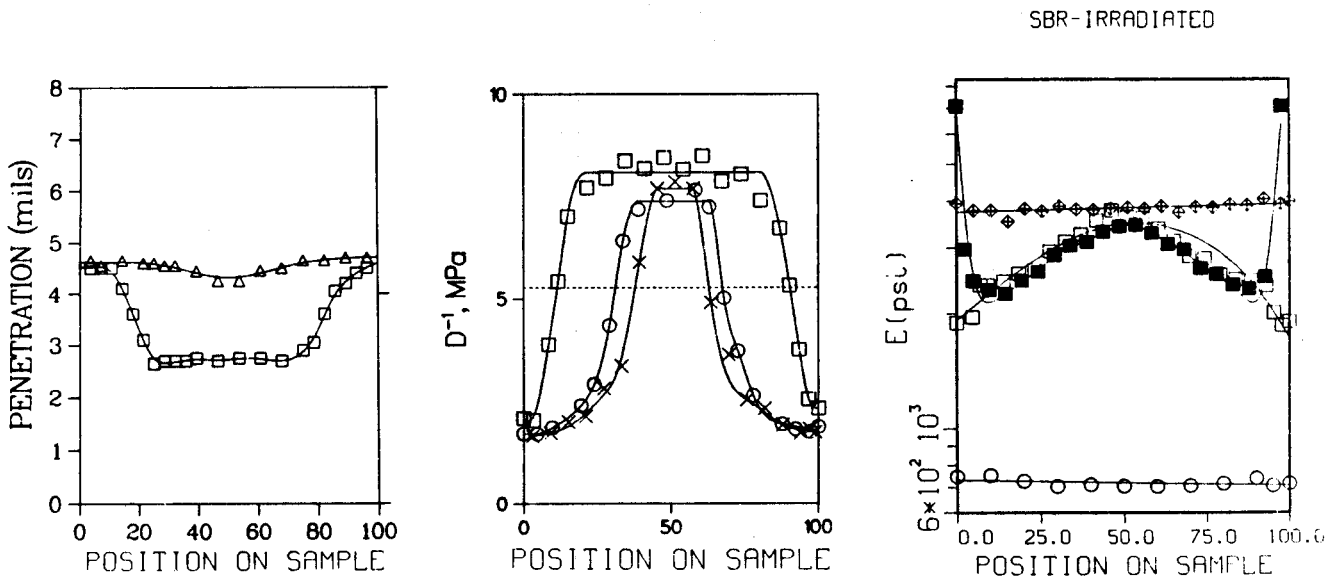

FIG. 5. (Left). Edge-to edge profiles of relative hardness in 3-mm thick samples of EPR (ethylene propylene rubber). □ = 6.7 x 10^3 Gy/h, △ = 1.1 x 10^3 Gy/h. Total dose in both samples was approximately 1.7 x 10^6 Gy. Greater probe penetration values correspond to relatively softer regions of the material.

FIG. 6. (Center). Edge-to-edge modulus profiles of of 1.9-mm thick samples of Viton material, after irradiation to a total dose of approximately 2.1 x 10^5 Gy, at three different dose rates. □ = 7.3 x 10^3 Gy/h, ○ = 6.1 x 10^2 Gy/h, × = 3.3 x 10^2 Gy/h. The dashed line represents the flat modulus of unaged material. Relatively higher modulus values correspond to relatively harder regions of the material.

FIG. 7. (Right). Edge-to-edge modulus profiles of 1.9-mm thick samples of styrene-butadiene rubber after gamma-irradiation at 5 x 10^3 Gy/h to a dose of 8.4 x 10^5 Gy. ○ = unirradiated material, ■ = following irradiation in air, □ = following irradiation in air for a sample surrounded with a 0.5-mm thick glass wool cocoon impregnated with KI, which filters out atmospheric ozone, ◇ = following irradiation under vacuum.

One other consideration involving the presence of air in the radiation degradation of polymers is the fact that irradiation of air can lead to the formation of ozone, and this ozone may attack polymeric materials. Certain rubbers are most susceptible to ozone attack, and this effect is enhanced if the rubber is under mechanical stress. Figure 7 (solid squares) illustrates radiation-degradation of styrene-butadiene rubber (SBR) under high dose rate conditions where both an oxygen-diffusion effect in the interior regions of the sample, and an ozone attack at edge of the sample, have occurred (11).

STABILIZERS FOR RADIATION ENVIRONMENTS

There has been some work on the development of stabilizer additives for polymers in radiation environments (1). Two main classes of stabilizers exist: energy deactivators and radical traps. Both can be effective in the presence or absence of oxygen. Energy deactivators are primarily polycyclic aromatic hydrocarbons which are incorporated into the polymer formulation. These molecules function analogously to aromatic polymers discussed earlier in this report, by acting as traps for excited state energy, and then decaying harmlessly to the ground state. Radical traps are antioxidant-type compounds such as hindered phenols or amines, which serve to capture free radicals and thereby interrupt the radical chain reactions which lead to degradation. Table 2 provides data illustrating the stabilization of polyethylene toward irradiation in the presence of air by inclusion of various additives at a concentration of 0.25%. In the best case, a factor of six times higher radiation resistance was achieved with this material.

TABLES OF RADIATION RESISTANCE

Tables of radiation resistance of various polymer types have been compiled (1,12); one such table is provided in this report (Table 3). This table provides data on the dose required for a significant change in mechanical properties (i.e., lowering the elongation at break or the bend strength to half of the initial value) under two different sets of conditions: 1) non-oxidizing conditions (inert atmosphere irradiation or high dose rate irradiation in air), and 2) oxidizing conditions in the dose rate range of 5-50 Gy/h in air. These tables are intended to be used as a rough guide in selection of materials. Note that because of differences in material formulation, and because of time-dependent effects which occur under conditions of radiation-oxidation, significant variances can be expected. In particular, under oxidizing conditions, the data represent only one range of dose rates and temperatures; lower radiation resistance could be expected for a number of the materials at still lower dose rates. Unfortunately, because of the long time periods involved, little data exist on radiation degradation rates at lower dose rates than those shown in the table. For predictions of material lifetimes in critical applications, the above considerations imply the need to perform and understand accelerated aging experiments on the material formulation of interest.

RADIATION AGING EXPERIMENTS

In the case of irradiation under non-oxidizing conditions, accelerated aging experiments which make the assumption of equal dose, equal damage, appear to suffice. However, as discussed above, predicting radiation degradation rates under oxidizing conditions can be very difficult due to dose rate effects, and other time/temperature-phenomena. In recent years, methods for performing meaningful accelerated aging experiments have been developed which can treat cases involving complicated aging effects such as dose rate effects. These methods depend upon an understanding of the mechanisms underlying the degradation, and use equations to manipulate data obtained under a series of different dose rate and temperature conditions. The procedure developed by the authors is basically similar to the Arrhenius method for extrapolating thermal degradation data obtained at a series of different temperatures (13). By this approach, a plot is prepared of the dose required to cause some chosen amount of damage, as a function of dose rate. Such a plot is illustrated in Fig. 8, which gives data for the dose required to reduce the elongation-at-break of a PVC cable jacketing material to 40% of the initial value, as a function of numerous dose rate and temperature conditions. By use of profiling methods, data corresponding to conditions which have resulted in heterogeneous oxidation are identified. Treatment of the data corresponding to homogeneous oxidation conditions with suitable equations shifts the data points to conditions of equivalent damage at some chosen reference temperature, yielding predictive information on degradation at lower dose rates. The shifted data from Fig. 8 are presented in Fig. 9, for a chosen reference temperature of 43° C (14). As can be seen, the data coalesce into a curve which predicts the dose required to reduce the elongation to 40% of initial at 43° C over a range of very low (experimentally inaccessible) dose rates. Predictive curves, such as this one, have been successfully correlated with results obtained under long-term application conditions (13,14).

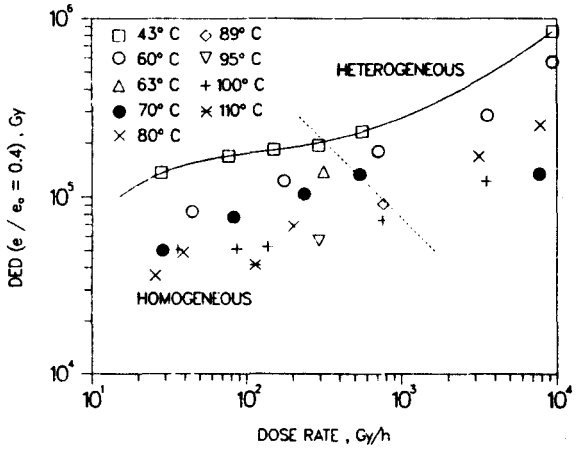

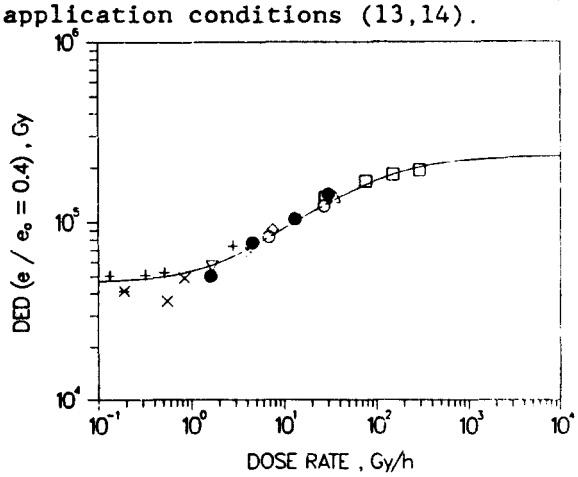

FIG. 8. (Left). Radiation dose required for the elongation-at-break of PVC to be reduced to 40% of the unaged value at various dose rates and temperatures. A solid curve is drawn through the 43° C data. The dashed curve separates the experiments which resulted in homogeneous oxidation from the experiments which resulted in heterogeneous oxidation.

FIG. 9. (Right). Elongation data of Fig. 8 (homogeneous oxidation data only) after shifting to a reference temperature of 43° C, yielding predictive curve of dose required to reduce elongation-at-break to 40% of unaged value at low dose rates.

COMPOSITE MATERIALS

Polymeric composites are composed of two different materials: a polymeric matrix resin, and a fiber or cloth (typically glass, carbon or another polymer) reinforcement. Inclusion of the fiber or cloth material can result in greatly enhanced strength, compared with that of the pure resin. Glass-epoxy composites have been proposed for use in SSC in several important applications, such as structural materials inside the superconducting magnets. Radiation effects on composites have not been extensively investigated compared with non-composite polymers, and there remain some conflicting findings. Major points concerning radiation degradation on composites are summarized in this section.

Although several studies indicate that the temperature of irradiation is generally unimportant, the temperature at which mechanical properties are measured can make a difference. Frequently, radiation-induced effects can be much more noticeable at very low temperatures (liquid nitrogen or liquid helium temperatures). Different mechanical properties are differentially affected by irradiation. For example, ultimate strength usually changes much more than Young's Modulus.

In general, non-organic reinforcements (glass or carbon) have comparatively high radiation resistance and are unaffected at doses leading to failure of the composite material. Radiation degradation of composites with non-organic reinforcement may be resin-dependent or interface-dependent. A wide range of different resins and curing agents have been evaluated. In the case of organic resins of relatively poor inherent radiation resistance, the radiation-degradation of the composite may closely track the degradation of the resin. For organic resins of very high radiation resistance, the degradation of the composite may result from failure at the resin-matrix interface at a dose below that at which the resin degrades. In such cases, radiation-induced debonding at the glass-resin interface can be observed experimentally. This would affect interface-sensitive properties such as transverse tensile strength. This debonding may be due to build-up of gaseous radiolysis products at the interface, or may result from radiation-degradation of the "coupling agent" used to covalently bond the fibers, such as glass, to the resin. When this debonding effect occurs, it gives rise to a very distinct breaking mode when samples are tested to failure. In such cases, delamination at the matrix-resin interface can be observed at the break site by scanning electron microscopy. As with non-composite polymeric materials discussed earlier in this report, aromatic structures are found to be more radiation resistant than aliphatics. This statement applies to the resins themselves, to the curing agents used to cross-link the resins, to the glass-resin coupling agents, and to the fiber (if an organic polymer fiber is used). It should also be noted that composites based on aromatic polyimide resins, rather than the more common epoxy resins, generally show considerably higher radiation resistance. Although the former are also considerably more expensive, use of such materials may be preferable in areas of especially high radiation dose. Figure 10 provides representative radiation-degradation data on several important composite materials (15).

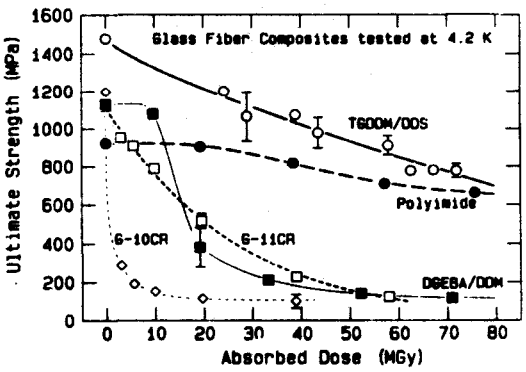

FIG. 10. Decrease in ultimate strength, at 4.2° K, of composite materials following irradiation at 1.8 x 10^4 Gy/h at room temperature. ● = glass-polyimide composite material, all others are glass-epoxy materials.

Although non-organic fiber reinforcement does not directly degrade, the nature of the reinforcement can still play a role in the composite degradation. For example, because of the neutron-absorbing property of boron present in glass fibers, the absorbed dose at the fiber-resin interface can be significantly higher compared with the bulk resin. This can enhance the rate of radiation degradation for materials in which the failure process is interface-dependent. Use of boron-free glass in such cases was shown to result in substantial improvement in radiation resistance of the composite.

REFERENCES

1. R. L. Clough and K. T. Gillen, "Gamma-Radiation-Induced Oxidation and Mechanisms of Its Inhibition." in P. Klemchuk and J. Pospicil, eds., Inhibition of Oxidation Processes in Organic Materials, CRC Press, Boca Raton (1988).
2. R. L. Clough, "Radiation-Resistant Polymers," in The Encyclopedia of Polymer Science and Engineering, John Wiley and Sons, New York (1988).
3. A. Chapiro, Radiation Chemistry of Polymeric Systems, Wiley, New York (1962).
4. M. Dole, Ed., The Radiation Chemistry of Macromolecules, Vol. I, Academic Press, New York (1972).
5. M. Dole, Ed., The Radiation Chemistry of Macromolecules, Vol. II, Academic Press, New York (1973).
6. H. Wilski, E. Duch, H. Leugering and S. Rosinger, Coll. and Poly. Sci., 259, 818 (1981).
7. R. L. Clough and K. T. Gillen, Nuclear Tech., 59, 334 (1982).
8. K. T. Gillen, R. L. Clough, and C. A. Quintana, Polym. Deg. and Stab., 17, 31 (1987).
9. R. L. Clough and K. T. Gillen, "Physical Techniques for Profiling Heterogeneous Polymer Degradation," in P. Klemchuk, ed., Polymer Stabilization and Degradation, (ACS Symposium Series No. 210), ACS, Washington D. C. (1985) Chap. 28.
10. K. T. Gillen and R. L. Clough, "Techniques for Monitoring Heterogeneous Oxidation of Polymers," in Encyclopedia of Engineering Materials, Marcel Dekker (1988).
11. R. L. Clough and K. T. Gillen, "Polymer Degradation Under Ionizing Radiation: The Role of Ozone," J. Polym. Sci., Part A: Polym. Chem., in press.
12. P. Beynell, P. Maier, and H. Schonbacher, Compilation of Radiation Damage Test Data -- Part III: Materials Used Around High-Energy Accelerators. CERN 82-10, European Organization for Nuclear Research, Geneva (1982).
13. K. T. Gillen and R. L. Clough, "Time-Temperature-Dose Rate Superposition: A Methodology for Extrapolating Accelerated Radiation Aging to Low Dose Rate Conditions," J. Polym. Sci., Part B: Polym. Phys. (submitted).
14. K. T. Gillen and R. L. Clough, J. Polym. Sci., Polym. Chem. Ed., 23, 2683 (1985).
15. S. Egusa, H. Nakajima, M. Oshikiri, M. Hagiwara and S. Shimamoto, J. Nucl. Materials, 137, 173 (1986).

TABLE 1.

CLASSIFICATION OF POLYMERS
ACCORDING TO THEIR PREDOMINANT DEGRADATION MODE
WHEN IRRADIATED UNDER INERT ATMOSPHERE CONDITIONS

Polymers Which Undergo Primarily Chain Scission	Polymers Which Undergo Primarily Crosslinking
polyisobutalene	polyethylene
poly-α-methylstyrene	polypropylene
polyvinylidenechloride	polystyrene
polyvinylfluoride	poly(vinylchloride)
polychlorotrifluoroethylene	poly(vinyl alcohol)
polytetrafluoroethylene	poly(vinyl acetate)
polyacrylonitrile	poly(vinylmethylether)
polyvinylformal	polybutadiene
polyvinylbutyral	polychloroprene
polymethylmethacrylate	poly(styrene-co-acrylonitrile)
polymethacrylamide	poly(styrene-co-butadiene)
polymethacrylonitrile	poly(butadiene-co-acrylonitrile)
polyoxymethylene	natural rubber
poly(propylene sulfide)	chlorinated polyethylene
poly(ethylene sulfide)	chlorosulfinated polyethylene
cellulose	polyamides
polyalanine	polyesters
polylysine	polyurethanes
DNA	polysulfones
	polyacrylates
	polyacrylamides
	polydimethylsiloxane
	polymethylphenyl siloxane
	phenol-formaldehyde
	urea-formaldehyde
	melamine-formaldehyde

TABLE 2.

Dose Required to Reduce Tensile Elongation to Half the Initial Value, for Polyethlene Containing Various Stabilizers at a Concentration of 0.25%*

Stabilizer	Dose (Gy, x 10^3)
Nothing	6
2-Mercaptobenimidazole	6
Trilaurylphosphite	6
Ionox 330**	8
2-Mercaptobenzothiazole	13
N,N'-Di-(β-Naphthyl-p-phenylenediamine) (DPPD)	15
Santonox R**	23
Santowhite Powder (refined)**	24
Phenothiazine: Ionol** 50:50	32
Phenothiazine: Ionol** 30:70	36

*For samples containing two stabilizers, the combined concentration equaled 0.25%.

**A hindered phenol derivative.

TABLE 3.

RELATIVE RADIATION STABILITIES* OF POLYMERS, UNDER TWO DIFFERENT SETS OF CONDITIONS, AS INDICATED BY THE DOSE (in rads) REQUIRED TO REDUCE MECHANICAL PROPERTIES TO 50% OF THEIR ORIGINAL VALUE.**

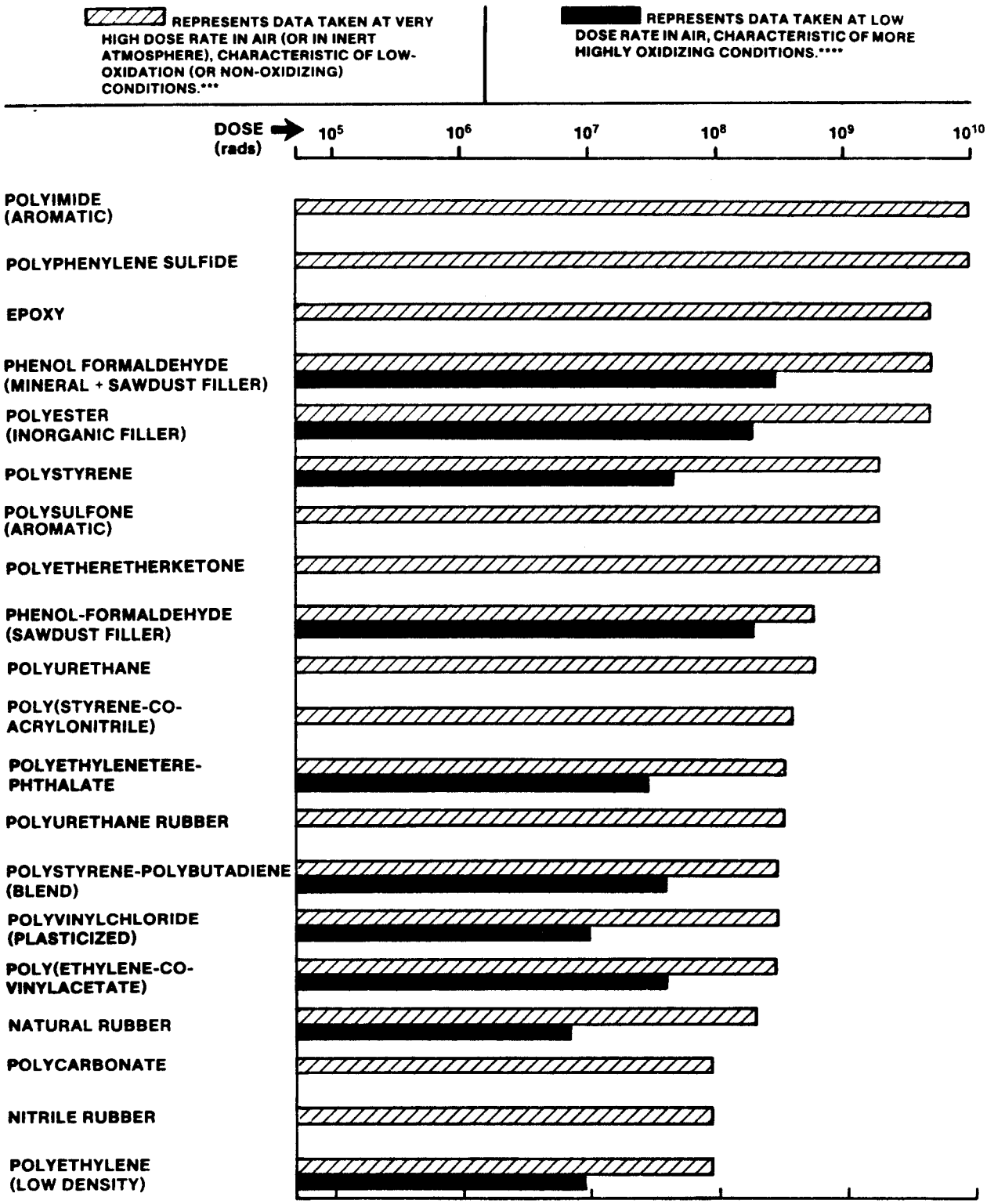

TABLE 3. (continued)

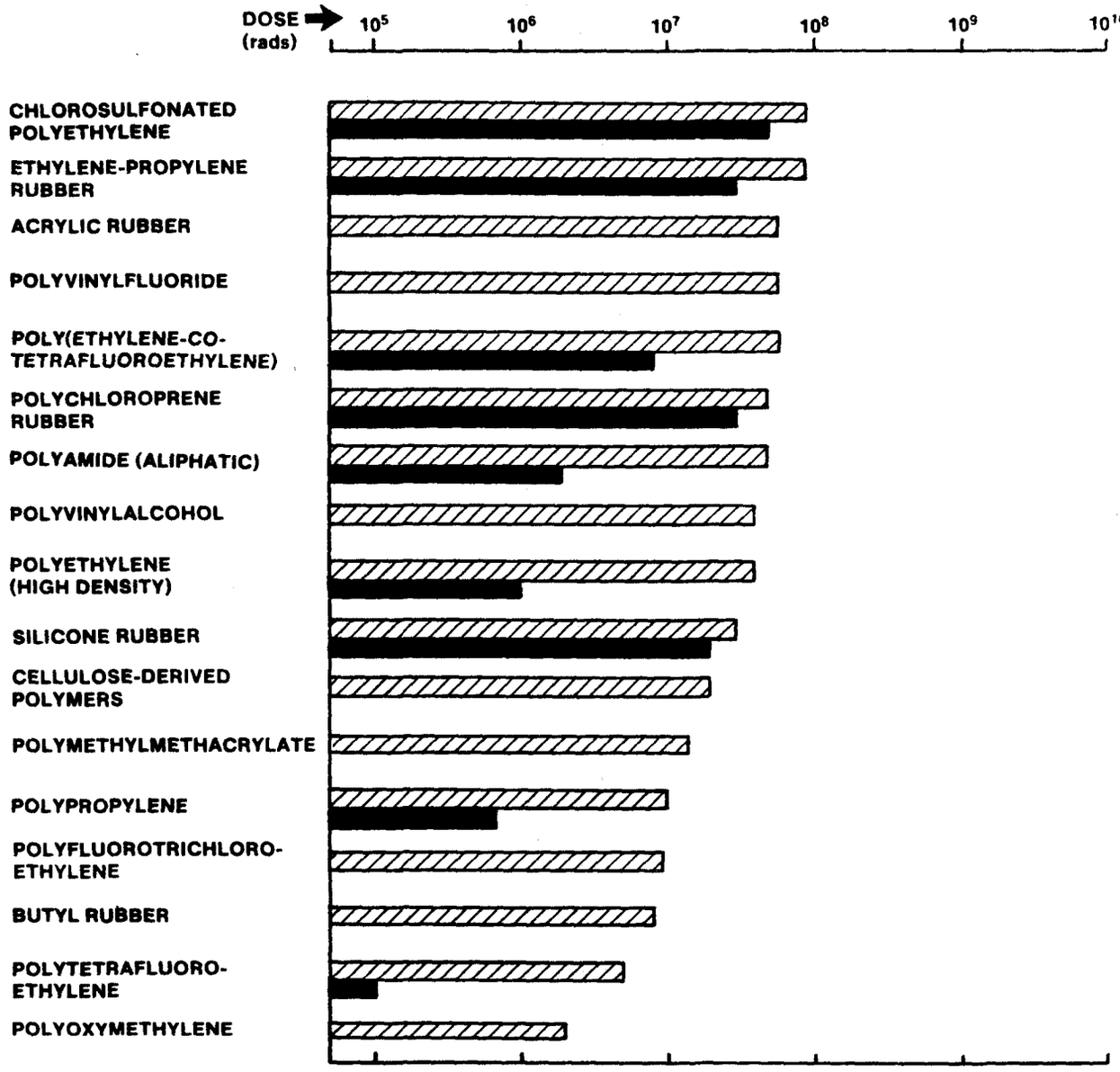

* This table is intended as a rough guide, to be used as an aid in selection of materials for further testing. The data were taken from numerous literature sources, and represent approximate radiation tolerances of individual polymeric materials under two specific environmental conditions. As discussed in the text, other factors not taken into account in the data will have a major influence on radiation resistance due to differing oxidation effects. These factors include: other dose rates, temperature, post-irradiation time, formulation and sample thickness.

** In most cases, the mechanical property considered was tensile elongation at break. Where elongation data were unavailable, some other important mechanical property, such as bend strength, was considered.

*** Data were taken at a variety of high dose rates, primarily in the range of 10^6 - 10^7 rads/h or above.

**** Data were taken within or near the dose rate range of 5×10^2 - 5×10^3 rad/h, in air. Sample thicknesses were primarily in the range of 0.4 - 1.5 mm. Samples were irradiated at or somewhat above room temperature. Mechanical properties were measured shortly after the irradiation was completed.

APPENDIX 5

Recommended Total-Dose Radiation Test
Guidelines for SSC Detector Applications

Recommended Total-Dose Radiation Test Guidelines for SSC Detector Applications

P. S. Winokur and D. M. Fleetwood
Sandia National Laboratories
Albuquerque, New Mexico 87185
(505) 846-2998

Abstract

Semiconductor detectors for high-energy physics applications offer the potential to obtain accurate particle spatial resolution and on-line data reduction. A significant disadvantage of semiconductor detectors and their associated circuitry however, is their sensitivity to radiation. This paper focuses on radiation-damage testing of the peripheral detector electronics to ensure their survival in the Superconducting Super Collider (SSC) radiation environment. Primary emphasis is on silicon-based integrated circuits (ICs) and on the degrading effects of "total-dose" ionizing radiation. The ionizing radiation effects problem for Complementary-Metal-Oxide-Semiconductor (CMOS) devices is reviewed, and it is shown that the survivability of detector electronics strongly depends on the dose rate of the incident radiation. A technical basis is then provided for using laboratory irradiations, followed by high-temperature anneals, to accurately predict survival levels of semiconductor components in the SSC environment.

Introduction

One goal of the Radiation Damage Testing Task Force is to predict the long-term radiation response of detector electronics used in the SSC from short-term, practical, and cost-effective laboratory measurements. For SSC applications, this task will prove extremely challenging for CMOS circuits and devices. This difficulty occurs because: (1) Typical laboratory radiation source (e.g. Co-60) dose rates commonly differ by orders of magnitude from dose rates in the SSC. The SSC radiation total-dose environment, expected to exceed 10^6 Gy(Si), will be delivered at moderate dose rates extended over several years; this radiation scenario provides for an effective time-averaged dose rate that is very low. Co-60 dose rates typically range from 50 to 300 rad(Si)/s. (2) CMOS "total-dose response" depends strongly on dose rate, bias, and postirradiation annealing time [1-7]. Problems in defining test methods to qualify CMOS devices for use in an SSC environment are due primarily to uncertainty about how time-dependent phenomena, such as trapped-hole annealing and interface-trap buildup, affect CMOS circuit and device performance. Based on previous work [1,4,6,7], this

* This work performed at Sandia National Laboratories was supported by the Defense Nuclear Agency under subtask X99QMXVA/00089 and by the U.S. Department of Energy under contract number DE-AC04-76DP00789.

paper outlines test guidelines that translate existing knowledge of radiation-induced defect growth and annealing processes into practical acceptance tests for CMOS devices.

Basic Mechanisms and Device Response

When metal-oxide-semiconductor (MOS) structures using SiO_2 gate insulators are exposed to ionizing radiation, electron-hole pairs are generated along the track of the incident particle. (Total-dose radiation effects are illustrated in Fig. 1 with the use of an MOS band diagram.) In general, some fraction of these electron-hole pairs will recombine, but that fraction is a complicated function of the material, the kind of radiation, and the applied field. Experimentally the "Yield" of hole-electron pairs that escape bimolecular recombination is determined from a threshold-voltage shift measured at liquid nitrogen temperature [8] and, in SiO_2, is consistent with an electron-hole pair-creation energy of ~ 17 eV. Following the initial creation process, the radiation-generated electrons and holes transport under the applied electric field. For positive bias, the electrons are swept to the gate and collected in picoseconds, while the holes undergo a "stochastic" transport to the SiO_2/Si interface [9]. "Stochastic" transport involves hole motion via polaron hopping between localized sites randomly distributed in the SiO_2. When the holes arrive at the SiO_2/Si interface a certain percentage are trapped. This percentage strongly depends on processing. In commercial oxides, it can be greater than 50 percent, while for oxides that receive special processing to decrease their sensitivity to radiation, it can be as low as several percent. Most of the positively-charged holes are trapped within 7.5 nm of the SiO_2/Si interface, although holes trapped within the first 1.5 nm probably recombine immediately with electrons that tunnel from the Si. In addition to hole trapping at the SiO_2/Si interface, there is buildup of radiation-induced interface states. Many models have been proposed to describe the origin and nature of these electronic states at the interface. Some models suggest that interface states result from: (1) hole trapping at the interface followed by electron injection [10], (2) hydrogen that is liberated in the bulk of the oxide during irradiation and interacts at the interface [11], and (3) stress [12]. Radiation-generated interface states can have either a positive or negative charge depending on whether they are donor or acceptor states, and their charge occupancy depends on the applied bias or band bending at the SiO_2/Si interface.

The total-dose response of n- and p-channel MOS transistors to ionizing radiation, illustrated in Fig. 2, is due to trapping of holes in the oxide and the buildup of interface traps. In general, the effect of radiation-generated charge, $\Delta\rho$, on the threshold-voltage shift, ΔV_{th}, of a transistor is given by

$$\Delta V_{th} = (-1/C_{ox})\int_0^{t_{ox}} \Delta\rho(x)(x/t_{ox})dx, \qquad (1)$$

where t_{ox} is the oxide thickness, C_{ox} is the oxide capacitance, and x is measured from the gate-SiO_2 interface. From Eq. (1) it can be seen that positive charge, i.e., trapped holes, will cause a negative shift in the threshold voltage of a device, while negative charge will cause a positive shift in the threshold voltage. In general, the initial response of an MOS transistor to radiation is a negative shift in the threshold voltage due to the buildup of trapped holes. At some later time (usually, but not always, at the end of the radiation exposure) the threshold voltage of an n-channel transistor will start to shift in the positive direction. This recovery can be attributed to either: (1) the anneal of the trapped holes or (2) for n-channel transistors, the buildup of negatively charged interface traps. It is possible for the threshold voltage of an n-channel transistor to increase above its preirradiation value following irradiation, a condition termed "rebound" [2,3]. This occurs when most of the trapped holes are annealed leaving mainly the negative charge contribution of the interface traps. "Rebound" has been observed to cause IC failure and is likely to occur in complex electronics used in research or industrial accelerators where semiconductor components can be exposed to long term, intermittent radiation in the beam environment. In addition, the buildup of radiation-induced interface traps can degrade transistor mobility and transconductance, and increase surface recombination velocities.

In the next series of figures (nos. 3-6), we investigate the dependence of CMOS device response on dose rate, and characterize the time-dependent nature of the relevant defect growth and annealing processes that govern CMOS device response. This discussion largely focuses on radiation-hardened devices, since their use will most likely be required for the high total-dose SSC application. To begin, in Fig. 3, threshold-voltage shifts (ΔV_{th}) for an n-channel transistors are shown following irradiations at varying dose rates. At a dose rate of 200 rad(Si)/s, the threshold-voltage shift steadily decreases with dose and is -0.4 V at 1 Mrad(Si). At 0.23 rad(Si)/s, the threshold-voltage shift steadily increases or "rebounds" with dose and is +0.7 V at 1 Mrad(Si). Data for the 0.05 rad(Si)/s irradiation is only available to 500 krad(Si), but indicates more "rebound" at equivalent doses than the 0.23 rad(Si)/s irradiation. The behavior of the threshold-voltage shift at dose rates of 20 and 2 rad(Si)/s is intermediate between what is observed at 200 and 0.23 rad(Si)/s.

At Sandia Laboratories, a technique has been developed [13] for splitting the net threshold-voltage shift into a contribution due to interface traps, ΔV_{it}, and a contribution due to oxide-trapped charge, ΔV_{ot}, i.e.,

$$\Delta V_{th} = \Delta V_{it} + \Delta V_{ot}. \qquad (2)$$

In Fig. 4, the contributions to the net-threshold-voltage shift due to oxide-trapped and interface-trap charge are shown for the devices of Fig. 3. The oxide-trapped charge component, ΔV_{ot}, steadily decreases as the dose rate decreases. This is

consistent with the fact that lower dose-rate irradiations are longer and consequently the oxide-trapped charge (i.e., trapped holes in the vicinity of the SiO /Si interface) has more time to anneal. This annealing of oxide-trapped charge may result from injection of electrons from the Si, from thermal detrapping, or some combination or injection and detrapping. The interface-trap charge component, ΔV_{it}, is steadily increasing as the dose rate is decreasing. This results from the longer times associated with lower dose-rate irradiations which supports a very long-term delayed buildup of interface states [6,11]. As the dose rate is lowered, there are fewer oxide-trapped charges and more interface traps. This results in the net threshold being more positive at any given total dose as the dose rate is lowered. Therefore, in a low-dose rate environment, the net threshold-voltage shift for these transistors would be positive and largely controlled by the component due to interface traps.

In Fig. 5, the threshold voltage shift due to interface traps, ΔV_{it}, is plotted as a function of postirradiation anneal time for n-channel transistors with 60 nm gate oxides. Irradiation and anneal bias is 6 V. "Zero" on the time axis is taken to be the beginning of each of the respective irradiation periods. Data are shown for LINAC, x-ray, and Cs-137 irradiations to a total dose of 100 krad(SiO_2), followed by biased anneal. Dose rates range from 6 x 10^9 to 0.05 rad(SiO_2)/s. It is most important to notice here is that the buildup of interface traps with postirradiation annealing time is independent of the radiation source employed and dose rate, and the results all fall on a common "defect- growth" curve. For example, whether devices were exposed to two LINAC pulses, each of 8 ms duration, and annealed for one week, or whether devices were exposed to the same total dose over the course of a week, the same number of interface traps are measured [6].

In Fig. 6, the threshold voltage shift due to oxide-trapped charge, ΔV_{ot}, is plotted as a function of postirradiation anneal time for the transistors of Fig. 5. Note that, with the exception of the small, "short-lived" tails (regions in which ΔV_{ot} falls slightly below the straight line, as shown most clearly for the LINAC data), the values of ΔV_{ot} all fall on a straight line that represents linear response with logarithmic time. The slight deviations from this response at short times after exposure are a result of the detailed impulse response of MOS devices, and are due simply to the fact that the total charge in each irradiation is not deposited at the same time. To be able to plot points on a single "transient-annealing" curve, one must be 1-2 decades beyond that time in which (at least the greatest fraction of) the dose is deposited so that differences in annealing time for different units of trapped charge are no longer significant. This impulse response for trapped-hole annealing has been characterized extensively in previous work via linear-response analysis [1], and does not represent a true dependence on radiation source or dose rate.

Taken together, the results of Figs. 5 and 6 strongly suggest that, over the wide range of dose rates and measuring times,

there are no true dose rate effects on MOS device postirradiation response. As long as the time is appropriately normalized, bias and temperature are maintained roughly constant, and corrections are made for dose-enhancement and electron- hole recombination effects, MOS postirradiation response at a given total dose can be described with simple defect-growth and transient-annealing curves. The same general trends are observed for p-, as well as n-channel transistors, and for irradiations in either the "on" or "off" state [6].

These changes in basic transistor properties described in Figs. 3-6 then result in parametric changes in the operation of silicon integrated circuits, e.g., increased timing, decreased speed and drive. In Fig. 7, where the change in "read" timing, Δt_{RD}, of a 2K SRAM (fabricated in the same technology as the transistors reported on above) is plotted versus dose at dose rates of 200 and 0.09 rad(Si)/s, we see the natural consequences of the mechanisms described above. At a given dose, the timing is larger ("degraded" more) due to an increased interface-trap growth and its resultant mobility degradation. This once again illustrates that the radiation response of CMOS devices depends strongly on dose rate. In addition, device response in low-dose-rate radiation environments can be dominated by interface-trap growth and resultant changes in timing.

Testing Recommendations

Having defined the basic mechanisms governing the response of CMOS devices to ionizing radiation, we are ready to focus on practical approaches toward predicting total-dose hardness of ICs in low-dose-rate radiation environments from laboratory measurements. Recent work has demonstrated that failure dose is a complicated function of dose rate, and that a peak in the failure-dose versus dose-rate curve generally results when there is a change in failure mode [4]. The dominant failure mechanisms, and total-dose hardness, of radiation-hardened SRAMs (no doubt required for SSC applications) in low-dose rate radiation environments were often found to be quite different than those observed at considerably higher laboratory dose rates. Based on the results shown in the previous section, it is very easy to imagine extrapolating interface trap and oxide trap densities, measured in a reasonable sequence of laboratory x-ray or Co-60 irradiations and anneals [6], to obtain very reasonable estimates of these quantities in low-dose-rate environments. For example, one could use the long time response (greater than 1000 s) to predict device response at low dose rates with very good probability of success. Coupling this type of information, obtained for all important gate oxide and parasitic transistors (at several biases) for each technology of interest, with detailed SPICE circuit simulations and detailed circuit testing may well be the most aesthetically appealing method by which to proceed with a hardness assurance program. In fact, we believe that, to minimize uncertainty about CMOS circuit performance in low-dose-rate environments, particularly as circuits become more complex and radiation environments become more challenging, this

method of approach should be vigorously pursued in the future. However, it is clear that hardness assurance involving such an extensive measurement and analysis program is years away from practical implementation. Better practical tests are available [6,7].

To achieve improved hardness assurance for low-dose-rate systems, we endorse previous suggestions [3,6] of using Co-60 exposure, followed by elevated temperature annealing. To illustrate this point, in Fig. 8 we plot the critical parameter ΔV_{it} as a function of postirradiation annealing time for n-channel transistors irradiated to 300 krad(SiO_2) with a Co-60 source. Devices are annealed either at room temperature (solid circles) or at 100°C (solid triangles). Note that 1) the value of ΔV_{it} obtained from room temperature annealing measurements agrees exactly with the value of ΔV_{it} obtained from a 3-week long Cs-137 exposure to the same total dose, and 2) that measurements of ΔV_{it} obtained for elevated temperature annealing saturate very quickly at a level that is slightly above that achieved at the end of 4 months of room temperature postirradiation measurements. Having demonstrated in Figs. 5 and 6 that there are no true dose rate effects over 11 decades in dose rate, we feel comfortable with extrapolating the remaining decade or two to space-like dose rates. Circuit parameters that depend strongly on ΔV_{it}, such as speed and timing [4,5], are expected to show a similar response to that observed in Fig. 8.

Based on the results and discussions above, we recommend the following total-dose testing guidelines for components to be used in the SSC. We recommend 1) that devices be exposed in a Co-60 cell to a total dose that is ~ 50 percent greater than that projected for the system lifetime, 2) that devices be annealed for one week at 100°C following irradiation, 3) that the same static bias be applied for both the irradiation and annealing period, and 4) that functionality and compatibility with intended system use be determined by functional and parametric testing performed after the annealing period [6,7]. We suggest ~ 50 percent overexposure as reasonable margin to compensate for uncertainties in defining true worst-case bias conditions [6,7]. We recommend Co-60 irradiation because it provides a better match to space radiation spectra than a 10-keV x-ray source, and because of practical difficulties associated with performing a one-week elevated temperature anneal on anything other than packaged parts. Static bias is similarly selected for its simplicity, and for ease of performing the postirradiation anneal. Finally, postirradiation anneal at 100°C provides a reasonable match to interface trap and oxide trapped charge densities under low-dose-rate conditions for most devices we have seen or measured, without the accompanying danger of significant interface trap annealing (leading to an underestimate of damage) often observed above 100°C [14]. The technical basis for this recommended test is discussed further in Refs. 6 and 7.

Conclusions

We recommend that radiation-hardened CMOS circuits intended for use in the SSC environment be exposed in a Co-60 cell to a total dose 50 percent greater than the system requirement, followed by a one week biased anneal at 100°C. While these tests do not, and should not, provide the final word on relating CMOS device response observed under laboratory test conditions to real use conditions, the tests we recommend are practical to implement, and should greatly improve confidence in CMOS performance in SSC applications.

References

1. P. S. Winokur, K. G. Kerris, and L. Harper, IEEE Trans. Nucl. Sci. NS-30, 4326 (1983).
2. A. H. Johnston, IEEE Trans. Nucl. Sci. NS-31, 1427 (1984).
3. J. R. Schwank, P. S. Winokur, P. J. McWhorter, F. W. Sexton, P. V. Dressendorfer, and D. C. Turpin, IEEE Trans. Nucl. Sci. NS-31, 1434 (1984).
4. P. S. Winokur, F. W. Sexton, J. R. Schwank, D. M. Fleetwood, P. V. Dressendorfer, T. F. Wrobel, and D. C. Turpin, IEEE Trans. Nucl. Sci. NS-33, 1343 (1986).
5. P. S. Winokur, F. W. Sexton, G. L. Hash, and D. C. Turpin, IEEE Trans. Nucl. Sci. NS-34, 1448 (1987).
6. D. M. Fleetwood, P. S. Winokur, and J. R. Schwank, IEEE Trans. Nucl. Sci. NS-35, 1497 (1988).
7. D. M. Fleetwood, P. S. Winokur, L. C. Riewe, and R. L. Pease, IEEE Trans. Nucl. Sci. NS-36, 1963 (1989).
8. G. A. Ausman, Jr. and F. B. McLean, Appl. Phys. Lett. 23 173 (1975).
9. F. B. McLean, H. E. Boesch, Jr., and J. M. McGarrity, IEEE Trans. Nucl. Sci NS-27, 1651 (1976).
10. S. K. Lai, Appl. Phys. Lett. 39 58 (1981).
11. F. B. McLean, IEEE Trans. Nucl. Sci NS-27 1651 (1980).
12. V. Zekeriya and T. P. Ma, IEEE Trans. Nucl. Sci. NS-31, 1261 (1984).
13. P. J. McWhorter and P. S. Winokur, Appl. Phys. Lett. 48, 133, (1986); P. S. Winokur, J. R. Schwank, P. J. McWhorter, P. V. Dressendorfer, and D. C. Turpin, IEEE Trans. Nucl. Sci. NS-31, 1453 (1984).
14. D. M. Fleetwood, F. V. Thome, S. S. Tsao, P. V. Dressendorfer, V. J. Dandini, and J. R. Schwank, IEEE Trans. Nucl. Sci. NS-35, 1099 (1988).

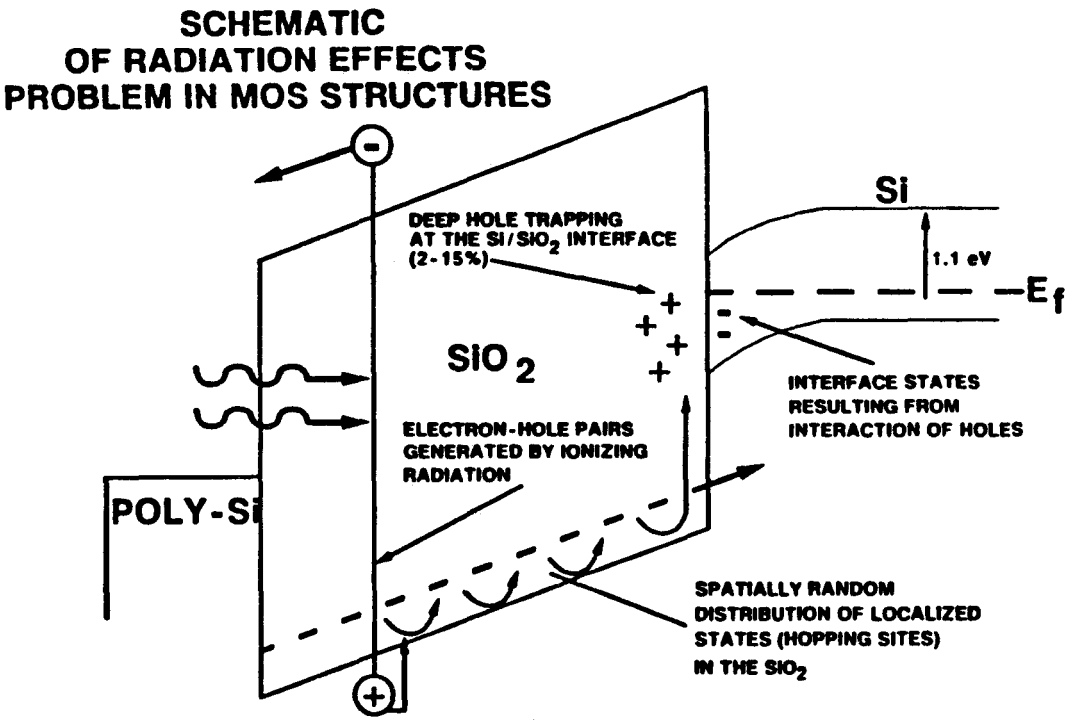

Fig. 1 Metal-oxide-semiconductor band diagram illustrating the physical mechanisms governing the total-dose response of CMOS devices to ionizing radiation.

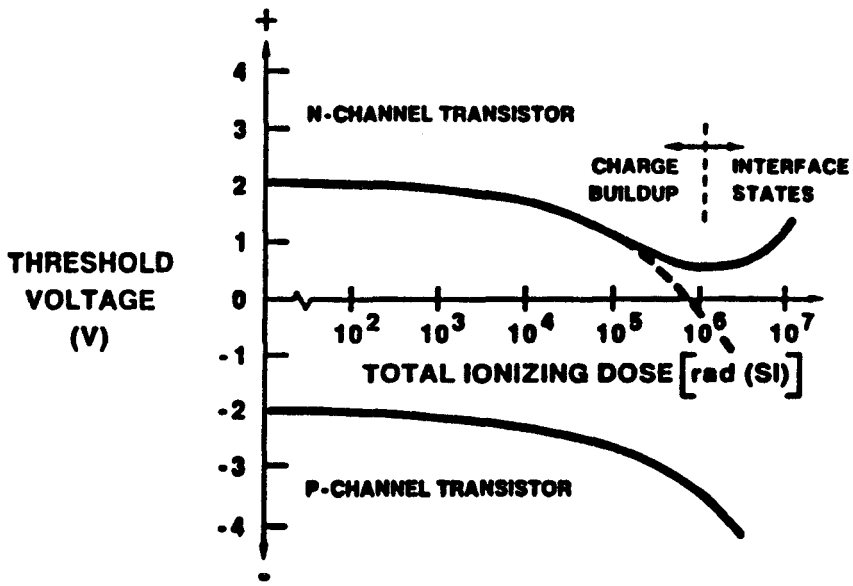

Fig. 2 Threshold-voltage of n- and p-channel transistors as a function of radiation dose.

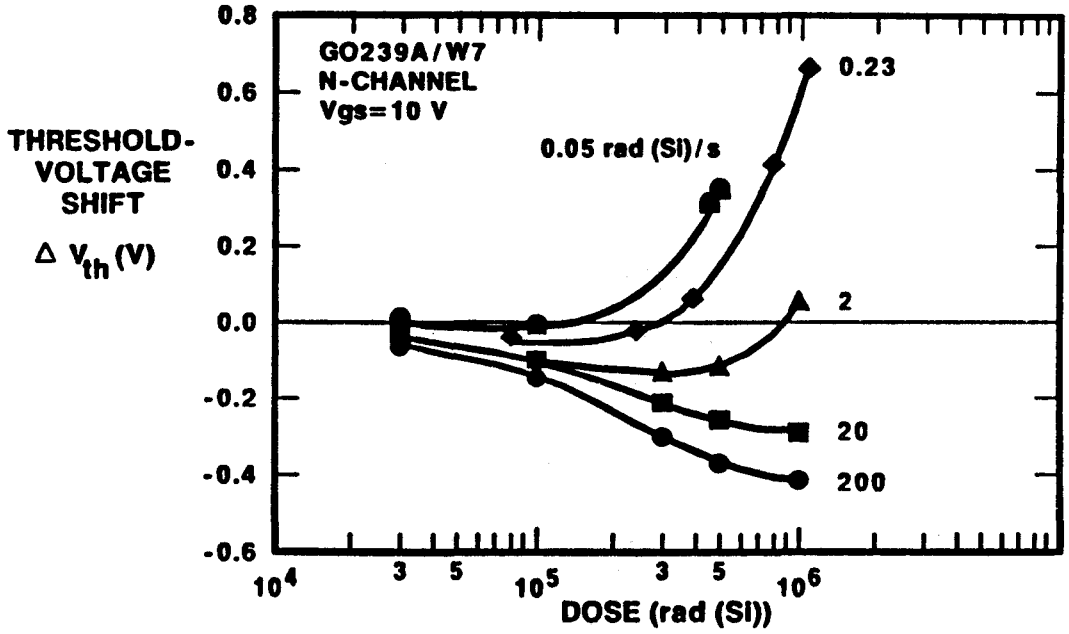

Fig. 3 Threshold-voltage shifts versus dose at varying dose rates for n-channel transistors irradiated with 10-V bias applied between gate and substrate.

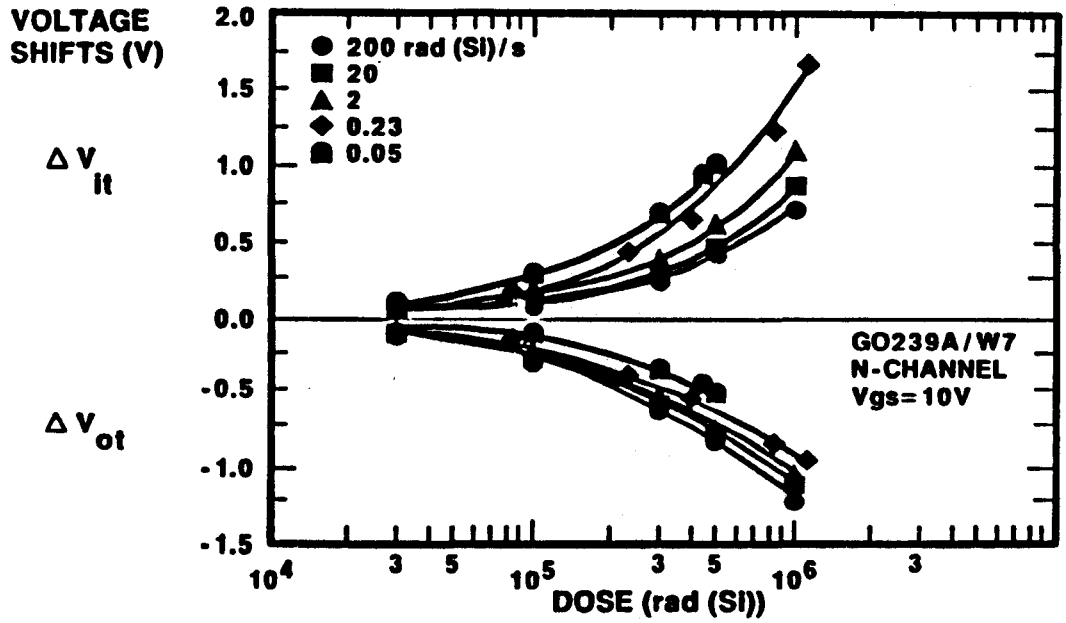

Fig. 4 Contributions to the net threshold-voltage shift from oxide-trapped, ΔV_{ot}, and interface-trap charge, ΔV_{it}, for the irradiations shown in Fig. 3.

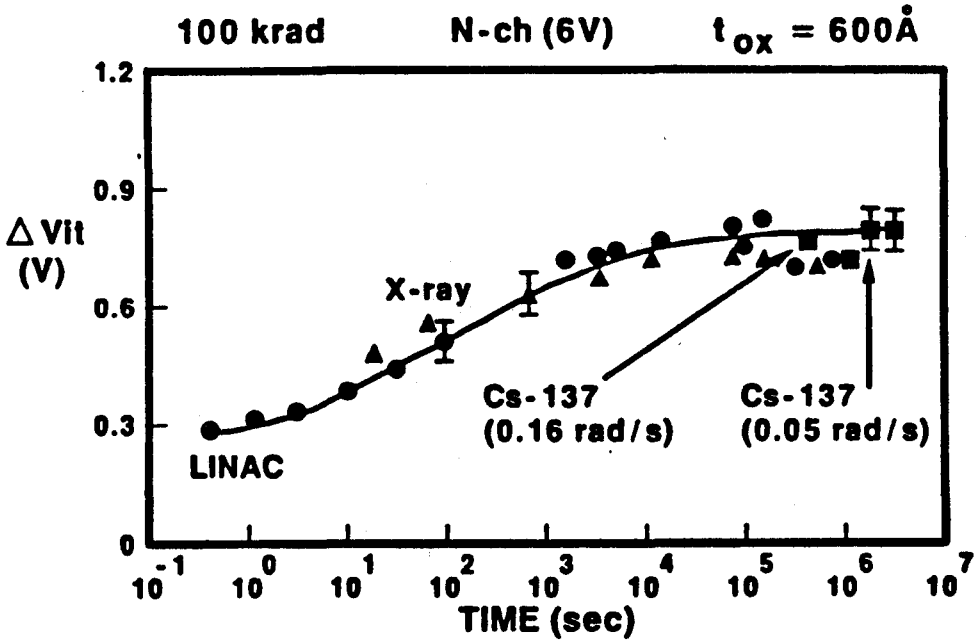

Fig. 5 Threshold-voltage shift due to interface traps for n-channel transistors with 60-nm gate oxides versus postirradiation annealing time for varying dose rate exposures to 100 krad(SiO_2). Irradiation and anneal bias was 6 V.

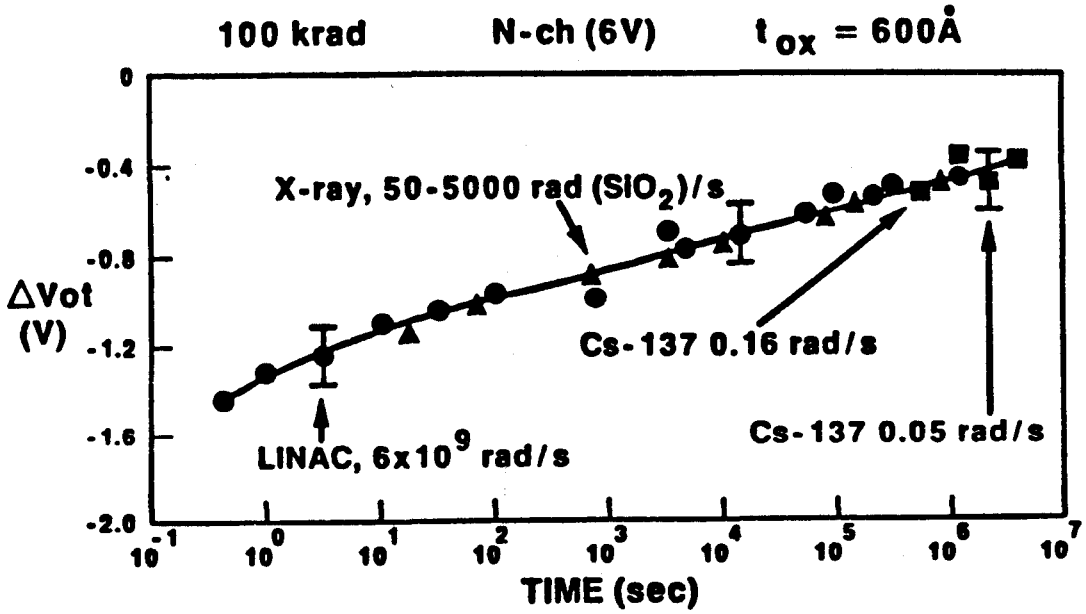

Fig. 6 Threshold-voltage shift due to oxide-trapped charge for n-channel transistors with 60-nm gate oxides versus postirradiation annealing time for varying dose rate exposures to 100 krad(SiO_2). Irradiation and anneal bias was 6 V.

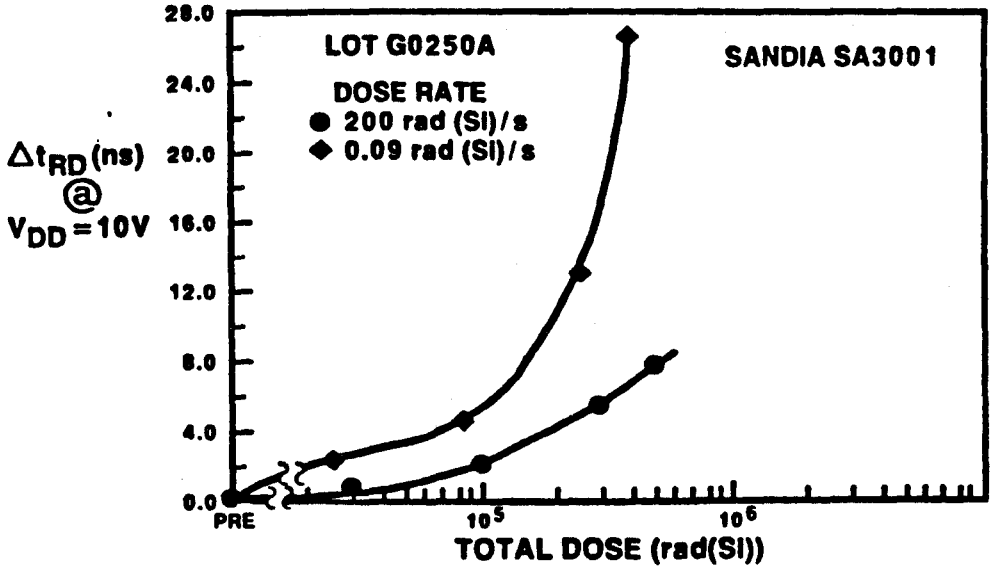

Fig. 7 Change in "read access" timing, Δt_{RD}, versus dose for Sandia SA3001 2K SRAMs irradiated with 10-bias at 200 and 0.09 rad(Si)/s.

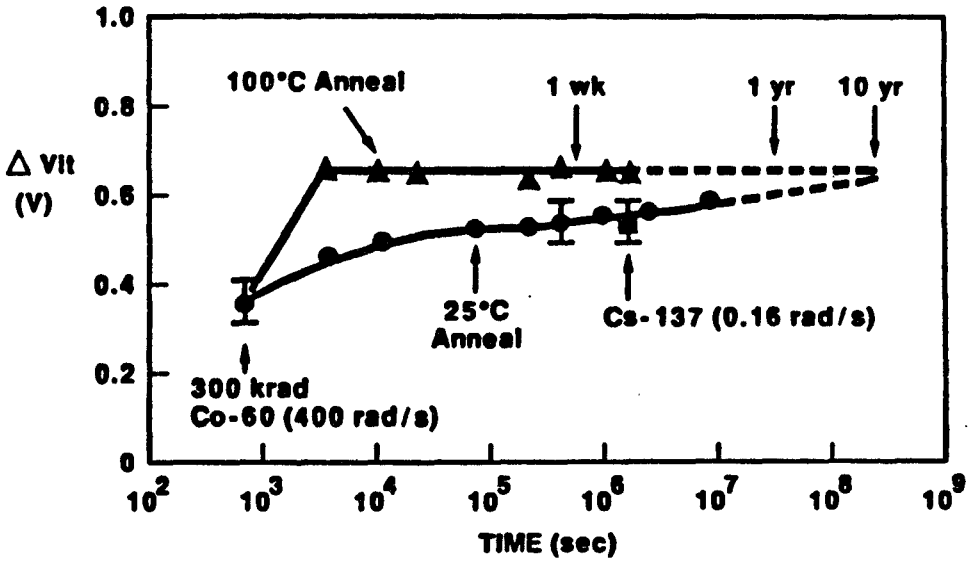

Fig.8 ΔV_{it} for n-channel transistors with 32-nm gate oxides versus postirradiation anneal time following Co-60 exposure to 300 krad(SiO_2) for room temperature and elevated temperature anneals. Irradiation and anneal bias was 6 V. Shown for comparison is a low-dose-rate Cs-137 exposure to 300 krad(SiO_2).

Sandia National Laboratories radiation facilities

Brochure prepared by:
G. A. Zawadzkas
STL Operations Division
P. A. Kuenstler
Experimental Systems Design Division
L. M. Choate
Simulation Operations Division
Sandia National Laboratories, TA-IV and TA-V
PO Box 5800
Albuquerque, New Mexico 87185

July 1977
July 1979 - Second Edition
Dec 1985 - Third Edition

SAND83-0598

Contents

Introduction 3
Annular Core Research Reactor 7
Sandia Pulse Reactor II 11
Sandia Pulse Reactor III 13
Gamma Irradiation Facility 17
HERMES II Facility 19
SPEED Facility 23
Hydramite II Facility 25
Simulation Technology Laboratory ..... [illegible]
Saturn Facility ..... [illegible]
HERMES III Facility ..... [illegible]
Gemini ..... [illegible]
Radiation Dosimetry Laboratory ..... [illegible]
Hot Cell Facility ..... [illegible]
Data Acquisition Systems ..... [illegible]

NOTES:

Sandia National Laboratories is a multiprogram laboratory operated for the United States Department of Energy by AT&T Technologies, Inc., a wholly-owned subsidiary of AT&T. It is one of the nation's largest engineering research and development facilities, with headquarters at Albuquerque, New Mexico; a laboratory at Livermore, California; and a test range near Tonopah, Nevada.

The primary responsibilities of the laboratory are research and development of nuclear weapon systems from concept to retirement. Additionally, the laboratory has extensive responsibilities in other areas of national importance. These include fusion energy, reactor safety, nuclear safeguards, energy research, and microelectronics.

This publication describes the radiation facilities utilized in the weapon systems development and Strategic Defense Initiative programs conducted for the Office of Military Application and in energy-related research and development programs. The radiation facilities are available to the Department of Energy, the Department of Defense, the Nuclear Regulatory Commission, and to their contractors. The facilities are also available to other federal agencies for reimbursable programs conducted without interference to Department of Energy programs.

Introduction

This brochure is a basic source of information for prospective users of Sandia National Laboratories Radiation Facilities. It contains a brief description of the various major radiation sources, a summary of their output characteristics, and additional information useful to experimenters. Radiation source development and source upgrading is an ongoing program with new source configurations and modes of operation continually being devised to satisfy the ever-changing radiation requirements of the users. For most cases, the information presented here should allow a potential user to assess the applicability of a particular radiation facility to a proposed experiment and to permit some preirradiation calculations and planning.

The Radiation Facilities

Sandia National Laboratories operates major research nuclear reactor and electron/ion accelerator facilities for the DOE Office of Military Application . At each facility research and development activities are conducted relating to nuclear weapon systems, non-nuclear weapon systems, advanced nuclear reactors, simulation source development, and other basic and applied research areas. Sandia also operates these facilities in support of DOD, NRC, multinational reactor safety, and university (public service) programs.

Sandia National Laboratories operates other radiation facilities not described in this brochure which are used in energy and simulation research. Examples of these are Febetrons, Van de Graaffs, etc., as well as other accelerators used in support of particle beam fusion research, such as the Particle Beam Fusion Accelerator II, Demon, and Decamite.

Neutron/Gamma Sources

Annular Core Research Reactor (ACRR)

The ACRR is a pool-type research reactor capable of both pulsed and steady-state operation. The facility was designed and constructed by Sandia National Laboratories under a program jointly funded by the DOE and NRC. It provides a 23-cm-diameter central irradiation cavity, a large (38-cm-diameter) external cavity, and a neutron radiography facility. It is used primarily for reactor safety research and for testing of electronics and materials.

Sandia Pulse Reactor II (SPR-II)

The SPR-II is a GODIVA-type, bare, fast-burst reactor capable of both pulsed and steady-state operation. Designed and constructed by Sandia National Laboratories, it incorporates a small (3.8-cm-diameter) central irradiation cavity. It is used primarily to meet narrow-pulse, high-dose-rate requirements in the testing of electronic devices.

Sandia Pulse Reactor III (SPR-III)

The SPR-III is a fast-burst reactor capable of both pulsed and steady-state operation. Designed and constructed by Sandia National Laboratories, it incorporates a large (17-cm-diameter) central irradiation cavity. It is used primarily to meet high-neutron-fluence or pulsed high-dose requirements in the testing of electronic subsystems and components.

Gamma Irradiation Facility (GIF)

The GIF is a gamma irradiation facility consisting of two adjoining irradiation cells. ^{60}Cobalt and ^{137}Cesium sources are available at the GIF. Designed and constructed by Sandia National Laboratories, it provides a variety of radioactive source geometries for irradiation of experiments.

Electron/Gamma-Ray/X-Ray Sources: Current Capability

The HERMES II Facility

The HERMES II is a high-energy, pulsed, field-emission electron-beam or bremsstrahlung gamma-ray (10-MeV-endpoint) generator. It was designed and constructed by Sandia National Laboratories to provide a radiation or impulse energy source for high-dose-rate radiation effects studies and materials response studies of rapid energy depositon. HERMES II has been in operation since 1968.

The SPEED Facility

SPEED is a high-energy, very short pulse, bremsstrahlung x-ray (1.0-MeV-endpoint) accelerator. It was designed and constructed by Sandia National Laboratories for simulation source development and high-dose-rate radiation effects studies. SPEED became operational in 1983.

The Hydramite II Facility

The Hydramite II Facility is a dual-line, high-energy, short-pulse source for electron-beam or bremsstrahlung x-ray (2.0-MeV-endpoint) generation. It was designed and constructed by Sandia National Laboratories for use in radiation effects and materials response studies. Hydramite II became operational in 1984.

Source Support Facilities

Radiation Dosimetry Laboratory

The Radiation Dosimetry Laboratory provides dosimetry services to the accelerator, reactor, and gamma-irradiation facilities in support of source development and radiation-effects experiments. Various measurement techniques are used to provide neutron fluence, neutron spectrum, and gamma absorbed-dose measurements in the test radiation environment.

Hot Cell Facility

The Hot Cell Facility provides means of handling and examining radioactive materials from the Sandia reactors and reactor experiments. The facility is comprised of three laboratories: the hot cell laboratory, the glove-box laboratory, and the analytical laboratory. The hot cell laboratory is a concrete shielded area containing three steel containment boxes and a staging area. The glove-box laboratory contains ten glove-boxes with high purity environments. The analytical laboratory provides for analysis of the metallurgical and elemental composition of radioactive material samples.

Data Acquisition Facilities

Data acquisition requirements for the nuclear reactors (ACRR, SPR-II, and SPR-III) and electron-beam weapon simulation facilities (HERMES II, SPEED, Hydramite II, and Proto II) are supported separately.

Photon Source Data Acquisition System

Data acquisition support for accelerator, diode, and experimental diagnostics from HERMES II, SPEED, Hydramite II, and Proto II is provided by the Photon Data Acquisition System. High-speed transient digitizers, oscilloscopes, computers, and printer/plotters are available for data recording, processing, and presentation. Isolated screen rooms for data acquisition equipment provided by users are also available.

Neutron Source Data Acquisition Systems

Data acquisition support is provided by separate systems for the SPR Facility and the ACRR Facility. The SPR Facility is supported by a series of high-speed transient digitizers with associated computer, software, and peripherals to record, process, and display data. The ACRR Facility is supported by two systems: one based on the DAASY II recording system, and the Data Acquisition and Display System (DADS). Both the DAASY II and the DADS are stand-alone systems for recording, processing, and displaying data.

Future Capability - Simulation Technology Laboratory (STL)

The Simulation Technology Laboratory (STL) project will include three new simulation facilities - HERMES III, Saturn and Gemini. These sources will provide major improvements over existing gamma-ray and x-ray laboratory sources. For example, the new radiation sources will possess larger exposure areas and, concurrently, better matches to the vulnerability requirements of dose, dose rate, pulsewidth, and risetime than are presently available. New exposure areas for testing will satisfy most DOE requirements. In addition to weapons effects testing, these sources will be available for use in future weapon system development and stockpile evaluation programs.

footnote:

All the facilities mentioned in this brochure are part of the radiation simulation facilities located at Sandia National Laboratories Technical Area IV (TA-IV) and Technical Area V (TA-V) on Kirtland Air Force Base, East, in Albuquerque, New Mexico. Experimenter's manuals containing detailed operational and performance information are provided upon request for each radiation facility.

General information regarding capabilities and utilization of the radiation facilities for weapons effects simulation may be obtained by contacting:

HERMES II, SPEED, Hydramite II, Proto II
Larry M. Choate
Simulation Operations
Division 1233
(505) 844-3131

STL, Gemini, Saturn, HERMES III
Jerry A. Zawadzkas
STL Operations
Division 1236
(505) 844-7483

Photon Data Acquisition System
Ken Mikkelson
Simulation Operations
Division 1233
(505) 844-3741

Simulation Theory, Calculations
Thomas P. Wright
Simulation Theory
Division 1231
(505) 844-4239

Simulation Fidelity, Radiation Effects Testing
Wendland Beezhold, Mark A. Hedemann
Simulation Technology Research
Division 1232
(505) 844-7830, -3154

ACRR, SPR-II, SPR-III
Ted F. Luera
Reactor Applications
Division 6451
(505) 844-0049

Radiation Dosimetry Laboratory
Dave W. Vehar or Ben B. Conklin
Experimental Systems Design
Division 6452
(505) 844-4820, -7567

Hot Cell Facility, GIF
Gilbert L. Cano
Radiation Physics & Diagnostics
Division 6454
(505) 844-2337

Neutron Source Data Acquisition Systems
SPR Facility and DAASY-II
Ben A. Garcia
Experimental Systems Design
Division 6452
(505) 844-3560

DADS
Arthur A. Key
Radiation Physics & Diagnostics
Division 6454
(505) 844-6896

Annular Core Research Reactor Facility

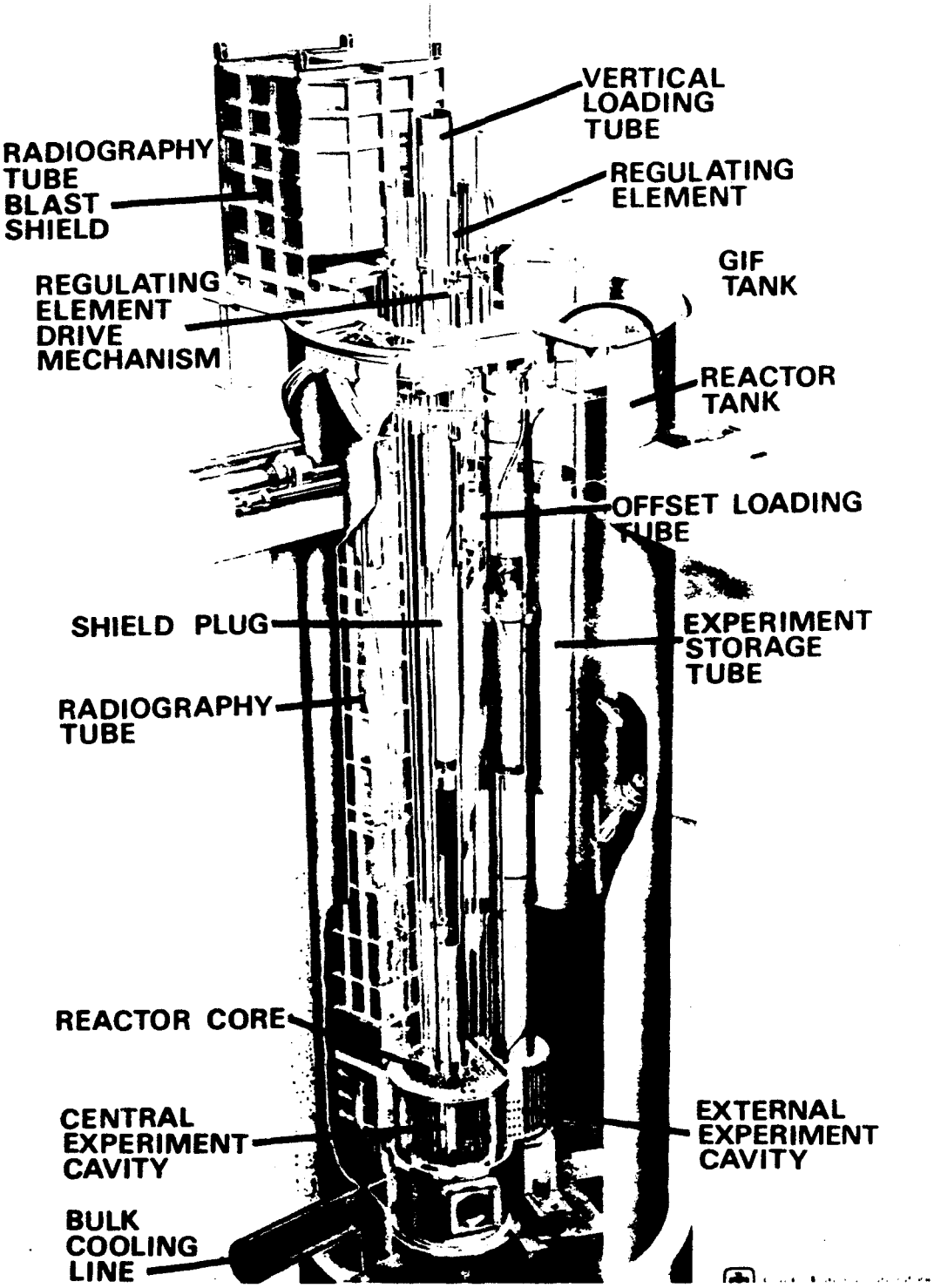

Annular Core Research Reactor (ACRR)

The ACRR is a research reactor capable of pulsed operation, steady-state operation, and tailored transient rod withdrawal operation. This facility provides a large (23-cm-diameter) central irradiation cavity, a neutron radiography facility, and a large (38-cm-diameter) external fueled irradiation cavity.

The ACRR is a pool-type reactor designed and constructed by Sandia National Laboratories and is operated for the DOE. The annular-shaped core is formed by 236 BeO fuel elements arranged in a hexagonal grid around the 23-cm-diameter, dry, central irradiation cavity. The reactor is controlled by two fuel-followed safety rods, three poison transient rods, and six fuel-followed control rods. The fuel-followed rods make up part of the 236 elements for the normal core configuration. Additionally, the external irradiation cavity is ringed with 80 U-ZrH fuel elements from the dismantled Annular Core Pulse Reactor (ACPR).

The cylindrical fuel elements contain a uniquely designed BeO-UO_2 fuel material held within niobium cups inside a stainless steel cladding. The fuel is uranium enriched to 35 percent ^{235}U, with 21.5-weight-percent UO_2 and 78.5-weight-percent BeO. The BeO fuel elements were designed to allow operation at fuel temperatures up to 1400°C in both the pulse and steady-state modes.

The core is located in an open pool, 3.1 m in diameter and 8.5 m deep, which contains 16,800 gallons of deionized water. The core is cooled by natural convection. The bulk water and the cooling-tower water systems are used to maintain the pool water near ambient temperature; additionally, a cleanup loop provides for removal of debris from the pool surface and maintains the required pH level of the pool water. *(cont.)*

Performance Characteristics

Maximum Nominal Operating Parameters

Pulse Operation	
Reactivity Insertion	$3.00
Peak Power	30,000 MW
Pulse Width	6.5 ms
Reactor Period	1.7 ms
Energy Release	300 MJ
Steady-State Operation	
Reactor Power (Continuous)	2.0 MW
(Intermittent)	4.0 MW[1]

Fluence per MJ (MW-s) of Reactor Operation[2]

Neutron Fluence (neutrons/cm²/MJ)	Central Cavity, Free Field	Central Cavity, Pb-B_4C Liner	External Cavity
All Energies	1.9×10^{13}	2.0×10^{13}	5.7×10^{12}
<1 eV	2.3×10^{12}	4.6×10^{11}	2.1×10^{12}
>10 keV	1.2×10^{13}	1.3×10^{13}	2.3×10^{12}
>3 MeV	1.0×10^{12}	7.5×10^{11}	2.6×10^{11}
1 MeV Si Equiv (95 MeV-mb)	8.9×10^{12}	8.7×10^{12}	1.8×10^{12}
Gamma Dose [rads(Si)/MJ]	1.0×10^{4}	1.6×10^{3}	5.8×10^{3}
Neutron Radiography (Top of Tube) (Thermal neutrons/cm²/MJ)			5.0×10^{6}

[1] *The ACRR has been operated at power levels up to 4.5 MW for reactor-behavior evaluation, and approval is being sought to operate at steady-state power levels up to 4.0 MW.*

[2] *Neutron-to-gamma ratios and neutron spectra are variable over a wide range through the use of attenuators and converters.*

ACRR NEUTRON SPECTRA[1]

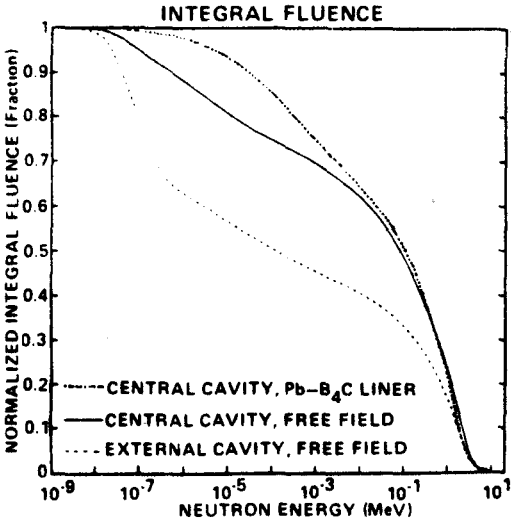

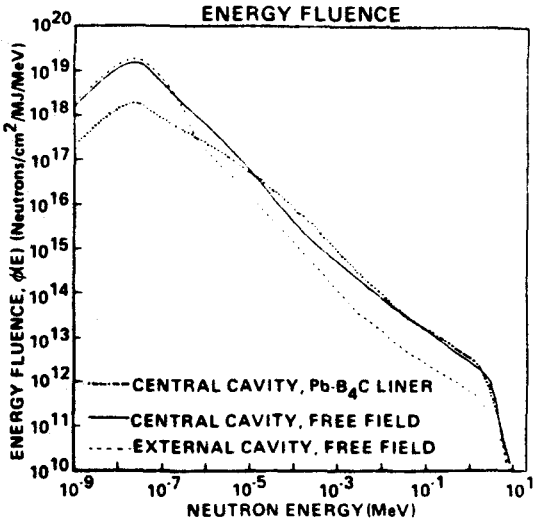

ACRR NEUTRON SPECTRA DATA

GROUP	LOWER LIMIT ENERGY OF GROUP	NORMALIZED ENERGY SPECTRA (FRACTION OF TOTAL FLUENCE)					
		CENTRAL CAVITY, FREE FIELD		CENTRAL CAVITY, Pb - B_4C LINER		EXTERNAL CAVITY, FREE FIELD	
		SCALAR FLUENCE	INTEGRAL FLUENCE	SCALAR FLUENCE	INTEGRAL FLUENCE	SCALAR FLUENCE	INTEGRAL FLUENCE
1	6.3 MeV	0.004	0.004	0.004	0.004	0.005	0.005
2	4.0	0.016	0.020	0.014	0.018	0.021	0.026
3	2.5	0.062	0.082	0.038	0.056	0.035	0.061
4	1.6	0.076	0.158	0.072	0.128	0.050	0.111
5	1.0 MeV	0.075	0.233	0.088	0.216	0.055	0.166
6	450 keV	0.105	0.338	0.128	0.344	0.075	0.241
7	210	0.082	0.420	0.096	0.440	0.053	0.294
8	100	0.067	0.487	0.069	0.509	0.038	0.332
9	34	0.075	0.562	0.073	0.582	0.041	0.373
10	10	0.059	0.621	0.063	0.645	0.033	0.406
11	3.4	0.039	0.660	0.049	0.694	0.024	0.430
12	1.0 keV	0.036	0.696	0.054	0.748	0.024	0.454
13	340 eV	0.026	0.722	0.051	0.799	0.023	0.477
14	100	0.026	0.748	0.056	0.855	0.028	0.505
15	34	0.025	0.773	0.042	0.897	0.029	0.534
16	10	0.034	0.807	0.038	0.935	0.031	0.565
17	3.4	0.035	0.842	0.024	0.959	0.030	0.595
18	1.0	0.039	0.881	0.018	0.977	0.033	0.628
19	.34	0.033	0.914	0.010	0.987	0.041	0.669
20	.10 eV	0.035	0.949	0.007	0.994	0.123	0.792
21	0	0.051	1.000	0.006	1.000	0.208	1.000
NORMALIZING FLUENCE (neutrons/cm^2/MJ)		1.9×10^{13}		1.9×10^{13}		5.7×10^{12}	

Based on best available measurements at time of publication.

PULSE OPERATION

The following graphs are power profiles of several single pulse operations. Examples are given of operations terminated by dropping the transient and safety rods (normal pulse), and of operations which are terminated by dropping the transient, safety, and control rods (reduced-tail pulse). Rod hold-up (RHU) values given are the delay times following pulse initiation before the rods are dropped.

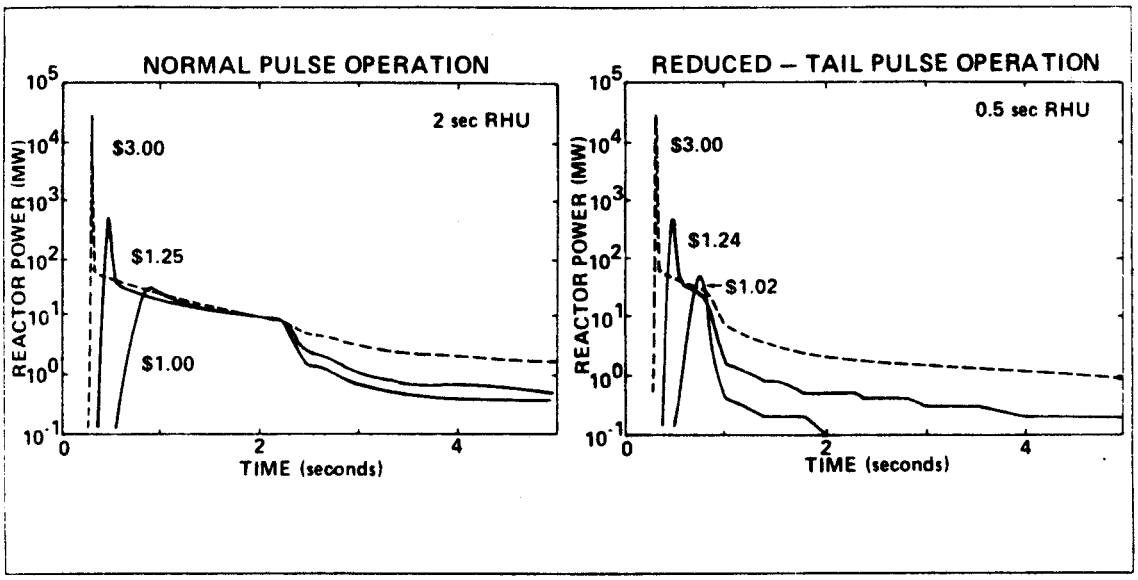

TAILORED TRANSIENT OPERATION

The ACRR can provide transient power profiles that are tailored to the needs of a particular experiment. Shown below are an example of a programmed mechanically driven transient rod withdrawal (TRW) operation and an example of a double pulse operation produced by pneumatically driving the transient rods.

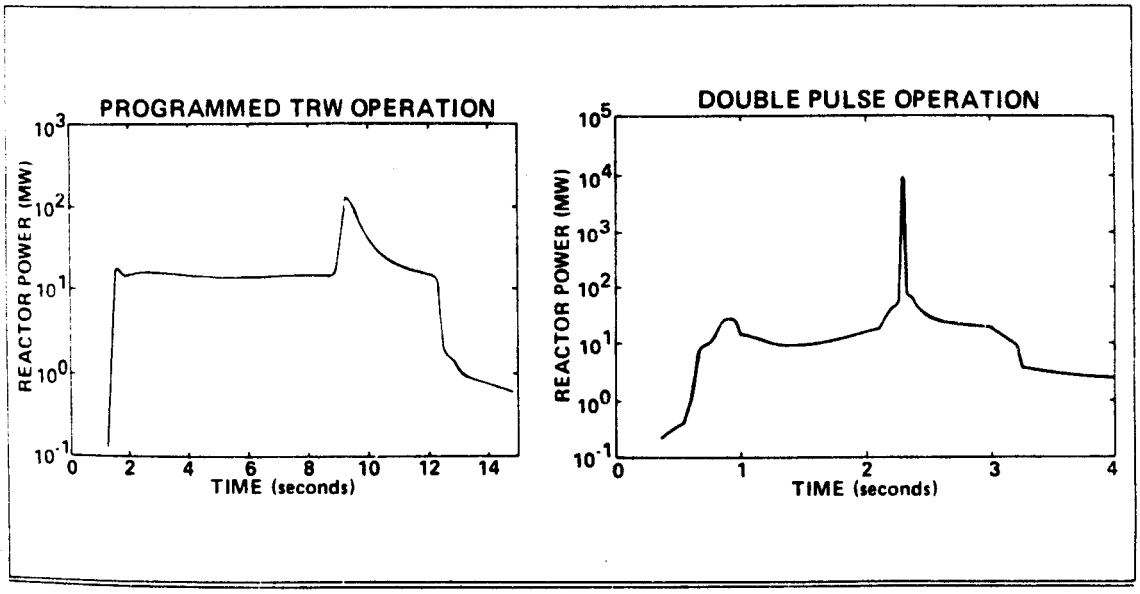

Sandia Pulse Reactor II (SPR-II)

The SPR-II is a fast-burst reactor designed and constructed by Sandia National Laboratories. It is an unreflected and unmoderated cylindrical assembly of uranium enriched to 93 percent ^{235}U. The uranium is alloyed with 10-weight-percent molybdenum to ensure phase stabilization of the fuel material. The operational core consists of six fuel plates divided into two assemblies of three plates each. The mass of the individual plates varies between 16.5 and 17.2 kg, and the total mass of the core (which includes fueled control rods and burst rod) is 106 kg. The three lower plates are attached to an electromechanical drive mechanism. Four holes through the core assembly accommodate three fuel control rods and one fuel burst rod. The burst rod is pneumatically driven to achieve the high rate of reactivity insertion required for pulse reproducibility. The control rods are used to establish a critical configuration of the core and to adjust pulse yield.

The primary shutdown mechanism in the pulse mode is the inherent negative temperature coefficient of reactivity caused by thermal expansion of the fuel.

The primary use of the reactor is for experiments mounted around the periphery. A central cavity, measuring 3.8 cm in diameter and extending vertically through the core, may also be used for small experiments. An aluminum shroud, covered with an adhesive mixture loaded with Boron, is placed over the reactor. This shroud provides a flow channel for nitrogen cooling gas, and it decouples the core from low-energy neutrons that are scattered back toward the core from experiments and the reactor room. The reactor stand is mounted on an elevator which can lower the reactor into a shielded pit, permitting access to the reactor room within 30 minutes of an operation

The SPR-II can be operated in a steady-state mode; however, the cooling capability of the nitrogen system and administrative restrictions effectively limit the time at power. Normally, steady-state power operations are limited to 5 kW.

Performance Characteristics (Central Cavity, Horizontal and Vertical Centerline, Free Field)

Maximum Nominal Operating Parameters

Pulse Operation	
Neutron Fluence	
>10 keV (≈ Total)	8.1×10^{14} neutrons·cm^{-2}
1 MeV Si Equiv. (95 MeV-mb)	7.3×10^{14} neutrons cm^{-2}
Peak Neutron Flux	2.0×10^{19} neutrons cm^{-2}, s
Gamma Dose[1]	1.65×10^{5} rads(Si)
Peak Gamma Dose Rate[1]	4.1×10^{9} rads(Si) s
Pulse Yield[2] (Fuel Temp Rise)	450 C
Pulse Width (FWHM)	40 μs

[1] *Neutron-to-gamma ratios are variable over a wide range through the use of attenuators or converters.*

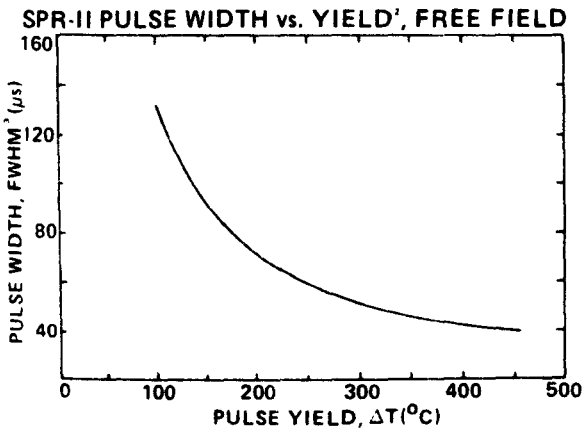

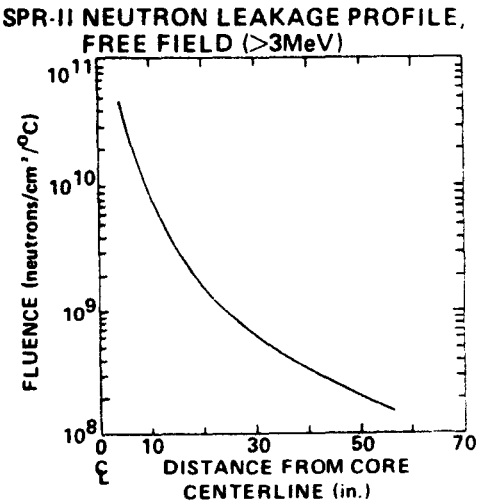

[2] *Neutron fluences are directly proportional to the temperature rise in the fuel during pulse operation.*
[3] *Pulse widths given are full width half maximum (FWHM) values.*

Sandia Pulse Reactor III (SPR-III)

The SPR-III is a fast-burst reactor designed and constructed by Sandia National Laboratories. It is an unmoderated cylindrical assembly of uranium enriched to 93 percent ^{235}U and alloyed with 10-weight-percent molybdenum to ensure phase stabilization. The core consists of eighteen fuel plates mechanically fastened into two halves of nine plates each. The mass of the individual plates varies between 6.8 and 15.4 kg, and the total mass of the core is about 258 kg. The nine upper plates are held stationary by the core support structure; the nine lower plates are attached to an electromechanical drive mechanism. Four reflector-type control devices are used: three are used for control, and the fourth is the burst element. The burst element is electromagnetically driven to achieve the high rates of reactivity insertion required for pulse reproducibility. The control elements are used to establish a critical configuration of the core and to adjust pulse yields.

The primary shutdown mechanism in the pulse mode is the inherent negative temperature coefficient of reactivity caused by the thermal expansion of the fuel.

A central cavity, measuring 17 cm in diameter and extending through the core, is the primary experiment facility. In addition, experiments may be mounted around the periphery of the reactor.

The leakage fluence provide by SPR-III in the reactor kiva is shown below. The neutron spectra at SPR are quite hard so that activation of parts is minimized. The kiva is provided with beam ports so that experiments can be irradiated at greater distances from the reactor. These ports have also been used to provide optical paths for laser beams.

The SPR-III can be operated in a steady-state mode; however, the cooling capability of the nitrogen system and administrative restrictions effectively limit the time at power. Normally, steady-state power operations are limited to a maximum of 9 kW.

(cont.)

Performance Characteristics (Central Cavity, Horizontal and Vertical Centerline, Free-Field)

Maximum Nominal Operating Parameters

Pulse Operation	
Neutron Fluence	
>10 keV (≈ Total)	6.5×10^{14} neutrons/cm^2
1 MeV Si Equiv. (95 MeV-mb)	5.5×10^{14} neutrons/cm^2
Axial Peak-to-Average Flux Ratio	1.2
Peak Neutron Flux	1.1×10^{19} neutrons/cm^2/s
Gamma Dose[1]	1.2×10^5 rads(Si)
Peak Gamma Dose Rate[1]	1.6×10^9 rads(Si)/s
Pulse Yield[2] (Fuel Temp Rise)	450°C
Pulse Width (FWHM)	76 μs
Steady-State Operation	
Power	9 kW
Neutron Flux	
>10 keV (≈ Total)	4.5×10^{11} neutrons/cm^2/s
1 MeV Si Equiv. (95 MeV-mb)	4.1×10^{11} neutrons/cm^2/s
Gamma Dose Rate[1]	9.0×10^1 rads(Si)/s

[1] *Neutron-to-gamma ratios are variable over a wide range through the use of attenuators or converters.*

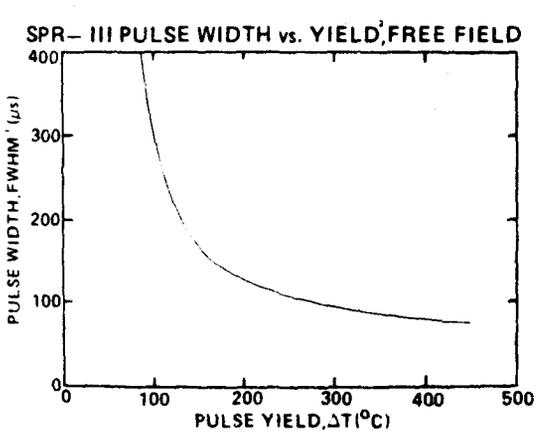

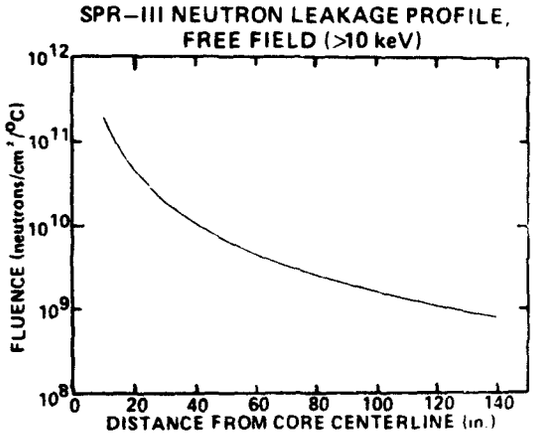

[1] *Neutron fluences are directly proportional to the temperature rise in the fuel during pulse operation.*
[2] *Pulse widths given are full width half maximum (FWHM) values.*

SPR-III Cont.

An aluminum shroud, covered with an adhesive mixture loaded with ^{10}Boron, is placed over the reactor. This shroud decouples the core from low-energy neutrons that are scattered back toward the core from experiments and the reactor room. The reactor stand is mounted on an elevator which can lower the reactor into a shielded pit, permitting access to the reactor room within 30 minutes of an operation.

The remotely controlled experiment retrieval device is used to place experiments in the reactor and retrieve them after irradiation. The experiments are loaded and unloaded into the experiment stand tube in a room adjacent to the reactor kiva.

To load the tube, the cart is remotely driven into position adjacent to the reactor pit, and the reactor is raised lifting the experiment stand off the cart. The cart is then withdrawn from the room to avoid activation. To remove the tube, the following operations are performed remotely: (i) the kiva door is opened, (ii) the cart is driven into position, (iii) the reactor is lowered to position the experiment stand on the cart, (iv) the cart is withdrawn from the kiva, and (v) the kiva door is closed.

SPR-III NEUTRON SPECTRA[1]

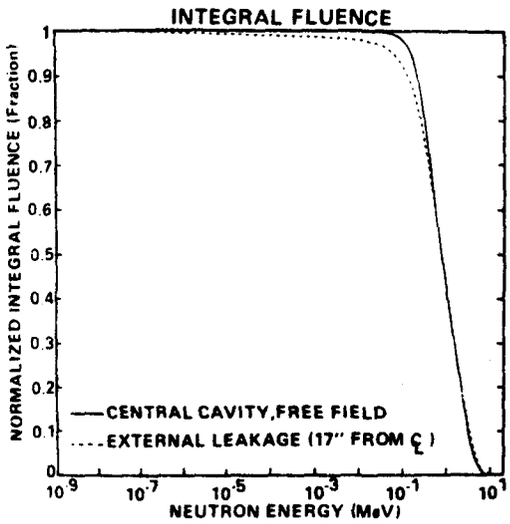

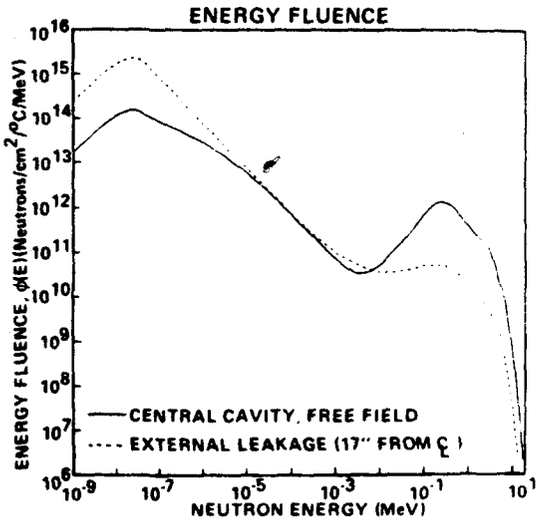

SPR–III NEUTRON SPECTRA DATA

GROUP	LOWER LIMIT ENERGY OF GROUP	NORMALIZED ENERGY SPECTRA (FRACTION OF TOTAL FLUENCE)			
		CENTRAL CAVITY, FREE FIELD		EXTERNAL LEAKAGE (17" FROM ℄)	
		SCALAR FLUENCE	INTEGRAL FLUENCE	SCALAR FLUENCE	INTEGRAL FLUENCE
1	10 MeV	0.001	0.001	0.001	0.001
2	6.3	0.010	0.011	0.011	0.012
3	4.0	0.041	0.052	0.058	0.070
4	2.5	0.114	0.166	0.104	0.174
5	1.6	0.126	0.292	0.121	0.295
6	1.0 MeV	0.132	0.424	0.136	0.431
7	450 keV	0.261	0.685	0.234	0.665
8	210	0.213	0.898	0.172	0.837
9	100	0.080	0.978	0.084	0.921
10	34	0.019	0.997	0.045	0.966
11	10 keV	0.002	0.999	0.013	0.979
12	0	0.001	1.000	0.021	1.000
NORMALIZING FLUENCE (neutrons/cm²/°C)		1.4×10^{12}		6.6×10^{10}	

[1] Based on best available measurements at time of publication.

Gamma Irradiation Facility (GIF)

The GIF, a gamma irradiation facility, consists of two adjoining radiation cells situated over a 6-m-deep pool of demineralized water. When not in use, the sources are stored in the base of the pool so that the water in the pool serves as a biological shield for personnel when entry into the cells is necessary. Entry is gained into either cell through movable concrete doors. The sources are mounted on elevators and are raised into the cells to mate with the experiment configuration.

Lead-glass windows permit observation of the sources and/or experiments in the cells. Located near the windows are switches that operate the source elevators so that raising and lowering of the sources may be observed by experimenters. The source in each cell of the GIF is completely independent of the other source and has its own electric elevator, unique geometry, and control switches.

North Cell: the north cell contains a ^{60}Cobalt source array with a strength of about 49 kilocuries and a Cesium source with a strength of approximately 163 kilocuries. A stainless-steel experiment-positioning plate runs on the north-south axis of the cell, with the source occupying a corner of the cell. Dosimetry is available for measuring doses.

South Cell: the south cell contains the High-Intensity Adjustable Cobalt Array (HIACA) and the steam test facility.

The HIACA is designed for large volume irradiation tests. HIACA contains about 150 kilocuries of ^{60}Cobalt, in 32 rods about 2 feet long and 5/8 inch in diameter; these in turn are located in 32 pneumatic-telescoping tubes The number of rods (four at a time for symmetry) can be selected and are positioned to surround the experiment. The number of rods determines the dose rate for the experiment (or, for example, it can be changed during the experiment to observe dose-rate effects.)

The steam facility is specifically designed for use in simultaneous reactor accident tests in conjunction with the HIACA facility. It has a working pressure of 200 psig using a 6 HP boiler, and two-35 ft^3 accumulators as steam-storage systems. A transient superheater has recently been installed.

Performance Characteristics

NOMINAL OPERATING PARAMETERS:

	NORTH CELL
^{60}Co Source	
Source Strength	49 kilocuries (Aug. 1985)
(To be Upgraded to 100 kilocuries 1986)	
Half-Life	5.27 years
Gamma Energy	1.17, 1.33 MeV
Doses	*
Maximum Dose Rate at Source Array Center	2.63 x 10^3 k rads(Si)/hr
^{137}Cs Source	
Source Strength	163 kilocuries (Aug 1985)
Half-Life	30.17 years
Gamma Energy	0.66 MeV
Doses	*

**Doses are dependent upon source configuration and experiment location.*

Performance Characteristics

NOMINAL OPERATING PARAMETERS: SOUTH CELL

HIACA Features

Irradiation Volumes:	Heights:	25 or 50 inches
	Diameters:	12 to 22 inches in several discrete diameters
Dose Rates	Maximum Volume:	up to 600 krad/hr in 9 discrete steps
	Minimum Volume:	up to 5 Mrad/hr in 9 discrete steps
Design		Sized to accept large stainless steel test chamber for simultaneous accident environment testing

Note: Values given are based on a 150 kilocurie source; to be upgraded to 300 kilocuries in late 1985.

Steam Features

Design:

Pressure:	200 psig
Temperature:	750°F

Saturated-Steam Ramps (12,000 lb/hr peak)	16 ft^3 chambers 1 chamber	2 chambers
0 - 70 psig (314°F Sat):	5 sec	10 sec
0 - 110 psig (343°F Sat):	9 sec	15 sec

Superheat-Steam Ramps

Ramp:	to 750°F in 10 sec
Continuous:	2000 lb/hr at 750°F for 5 min, then 200 lb/hr at 750°F and 200 psig

◁ HERMES II

The HERMES II (High Energy Radiation Megavolt Electron Source II) is a high-energy, pulsed, field-emission electron-beam or bremsstrahlung x-ray source. It was designed and constructed by Sandia National Laboratories to provide a source for high-dose-rate radiation effects studies and material response studies of rapid energy deposition. The principal components of HERMES II are a Marx generator, a Blumlein transmission line, and an output tube. Stored low-voltage energy is converted to high-voltage energy by the Marx generator and then transferred to the Blumlein transmission line, which serves as a fast-discharge, pulse-forming, low-inductance energy source for the output.

The Marx generator consists basically of a bank of capacitors that are charged in parallel and discharged in series by means of spark-gap switches. The negative-voltage output of the Marx generator is placed on the coaxial Blumlein transmission line consisting of three concentric cylinders. The voltage pulse formed by the Blumlein is impressed across the tube diode, which consists of an insulating and vacuum-holding structure, a field-emission cathode, and an anode.

The anode used for the electron-beam mode of operation is a thin, low-Z target that allows passage of the electrons with minimal energy loss. For the x-ray mode of operation, the anode used is a thick, high-Z target selected for maximum efficiency in converting electron-beam energy into bremsstrahlung x-radiation.

Accelerator Parameters

Peak Diode Voltage	10 MV
Peak Diode Current	100 kA
Total Beam Energy	70 kJ
Power Pulsewidth	100 ns
Repetition Rate	3 pulses/hr

GAMMA-RAY ENVIRONMENT

HERMES II can operate in either of three bremsstrahlung modes. The standard mode is most commonly used and utilizes a 60-mil tantalum plate as a converter. In the pinched-beam mode, the electron beam passes through the anode and self-pinches onto a tungsten-carbide composite, yielding higher dose but smaller exposure area. In the outdoor mode, the electron beam is drifted beyond the test cell to a point outdoors where it can be converted to bremsstrahlung radiation with either a standard or pinched-beam converter.

Standard Mode Performance

Peak Dose	70 krads(Si)
Peak Dose Rate	1×10^{12} rads(Si)/s
Radiation Pulsewidth	65 ns
Risetime (10 - 90)	40 ns
Exposure Area (10% uniformity)	400 cm^2 (30 krads average)

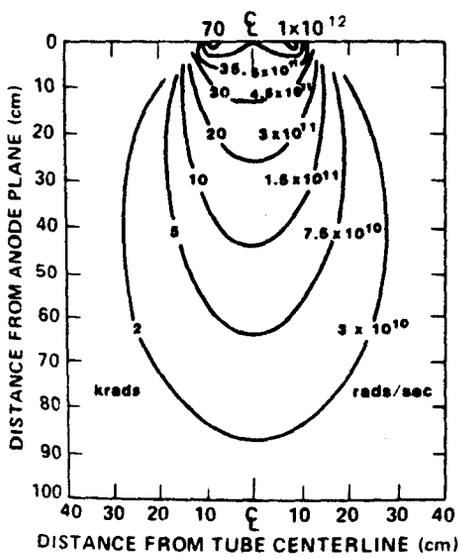

Isodose Contours for Standard Mode

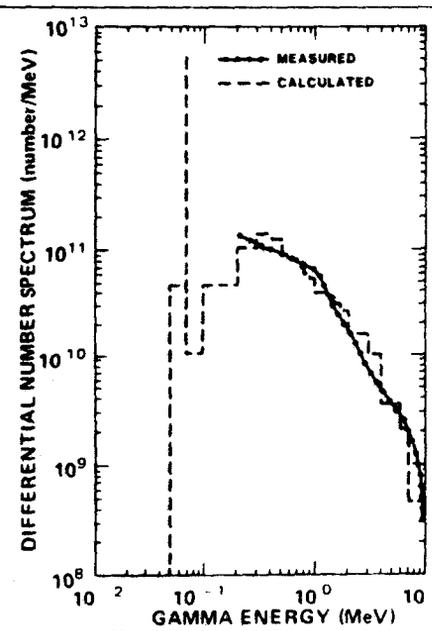

HERMES II Photon Spectrum

(cont.)

Pinched-Beam Mode Performance

Peak Dose	300 krads(Si)
Peak Dose Rate	6×10^{12} rads(Si)/s
Radiation Pulsewidth	60 ns
Risetime (10 - 90)	35 ns
Exposure Area	(see isodose contours)

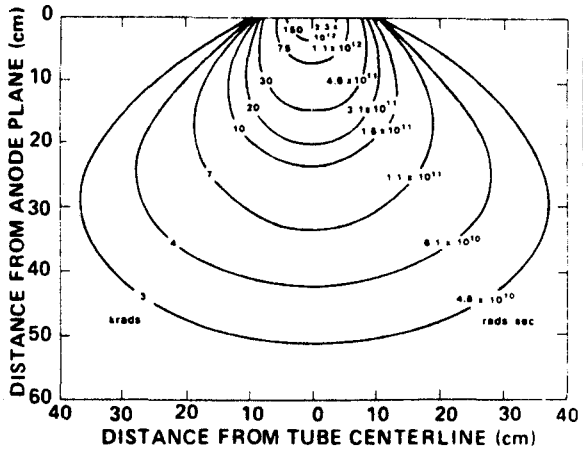

Isodose Contours for Pinched-Beam Mode

Outdoor Mode Contours

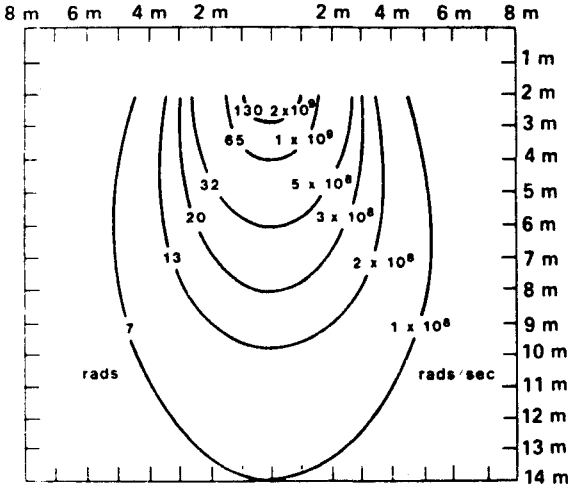

Isodose Contours for Outdoor Mode (Standard Configuration)

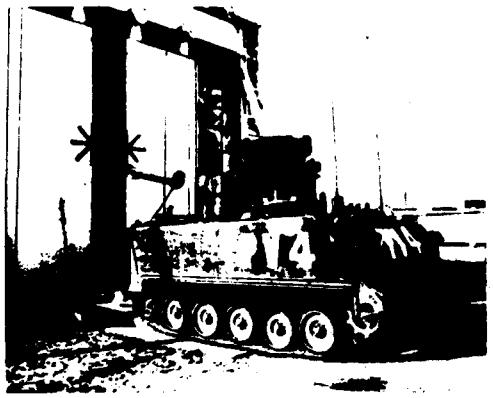

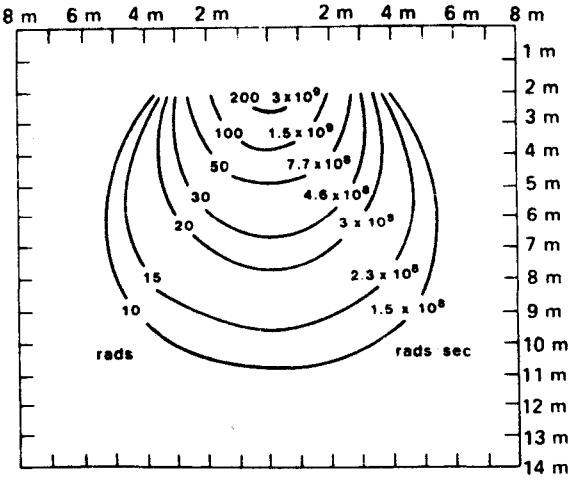

Isodose Contours for Outdoor Mode (Pinched-Beam Configuration)

HERMES II cont.

ELECTRON-BEAM ENVIRONMENT

By replacing the bremsstrahlung converter with a 5-mil titanium foil, the HERMES II electron beam can pass through the anode plane and be used for rapid energy deposition, source-region EMP, or propagation experiments. Drift chambers of various sizes are available for both atmospheric and vacuum environments. The range of values listed below reflect performance for different configurations. As in the bremsstrahlung case, the HERMES II electron beam can be drifted beyond the confines of the building and injected into the atmosphere outdoors.

Electron-Beam Mode Performance

Transported-Beam Energy	60 kJ
Peak Beam Fluence	300 - 400 cal/cm^2
Exposure Area (50% falloff)	25 cm^2
Pulsewidth (FWHM)	55 - 65 ns

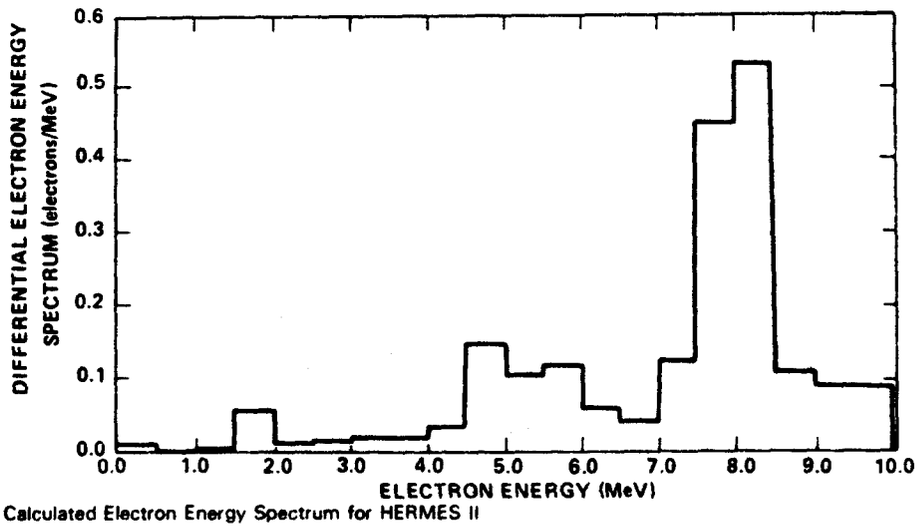

Calculated Electron Energy Spectrum for HERMES II

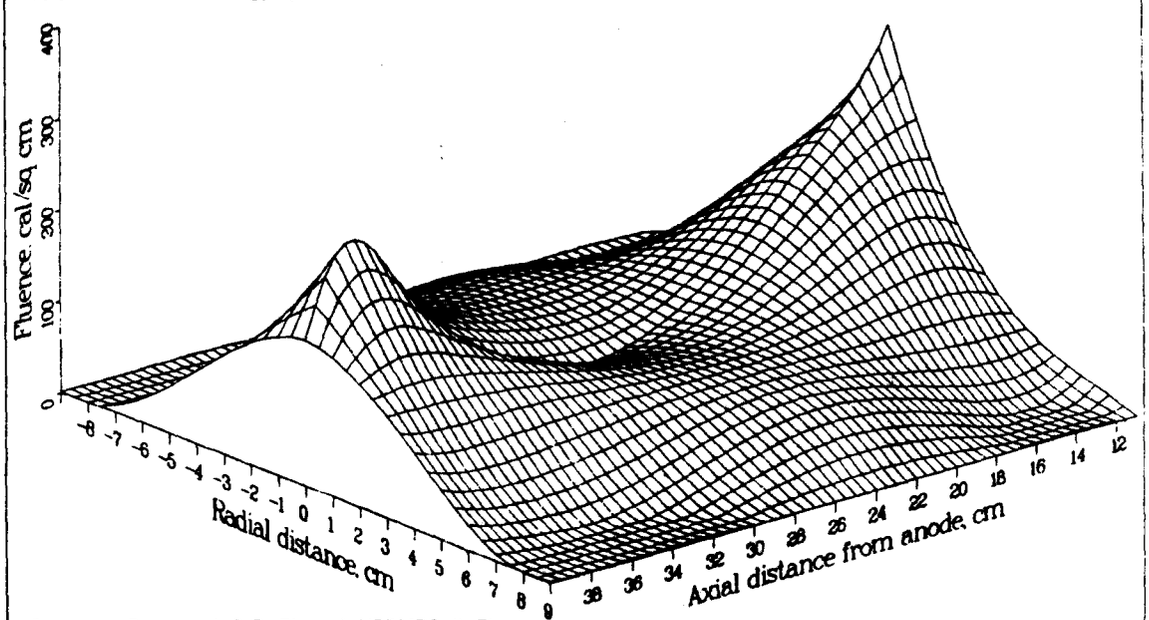

Computer-Generated 3-D Plot of HERMES II Electron Beam Profile at Atmospheric Pressure Based on Measured Values

◁ SPEED

SPEED (Short Pulse Experimental Electron Device) is a 1-MV-peak, very-short-pulse, high-energy bremsstrahlung source constructed in 1982 to enhance Sandia's simulation capabilities. This x-ray simulator incorporates several innovations over previous Sandia simulation accelerators and features a radiation pulse width (FWHM) in the range of 10-20 ns. The new technologies include a 3-MV multistaged, self-breakdown switch; a donut-shaped, pulse-charged intermediate storage capacitor; a triaxial pulse-forming network; a cylindrical, 60-point water switch; and a triaxial, low-impedance (0.4 ohm) transmission line.

Accelerator Parameters

Peak Diode Voltage	1.0 MV
Diode Current at Peak Voltage	1.2 MA
Total Beam Energy	25 kJ
Power Pulsewidth (FWHM)	20 ns
Repetition Rate	3 Pulses/Day

A triplate vacuum transmission line is used to feed either a double-pinched-beam diode in the AKA configuration or a triaxial diode. These provide small and large area sources, respectively. A vacuum convolute to a five-plate transmission line feeding two nested triaxial diodes also provides a small area source.

X-Ray Environment

	Small Area Source
Peak Dose	20-40 krads (CaF_2 TLD) [approx. 2.5 cal/g (1 mil Au)]
Peak Dose Rate	$1.5-2 \times 10^{12}$ rads (CaF_2)/s
Exposure Area (50% falloff)	20 cm^2
Radiation Pulsewidth (FWHM)	10-20 ns
	Large Area Source
Peak Dose	8-15 krads (CaF_2 TLD) [approx. 1.0 cal/g (1 mil Au)]
Peak Dose Rate	$6-7 \times 10^{11}$ rads (CaF_2)/s
Exposure Area (50% falloff)	180 cm^2
Radiation Pulsewidth (FWHM)	10-20 ns*

** Typical pulse is 12 - 14 ns (FWHM) with a peak dose rate of 7×10^{11} rads (CaF_2)/s*

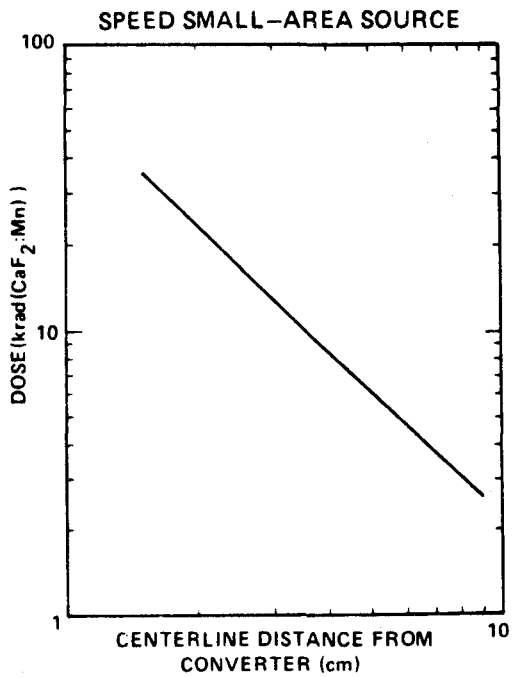

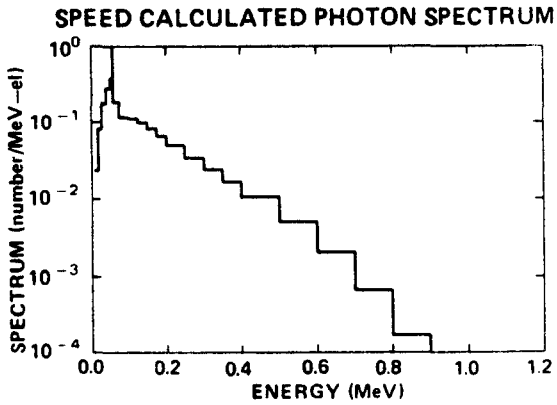

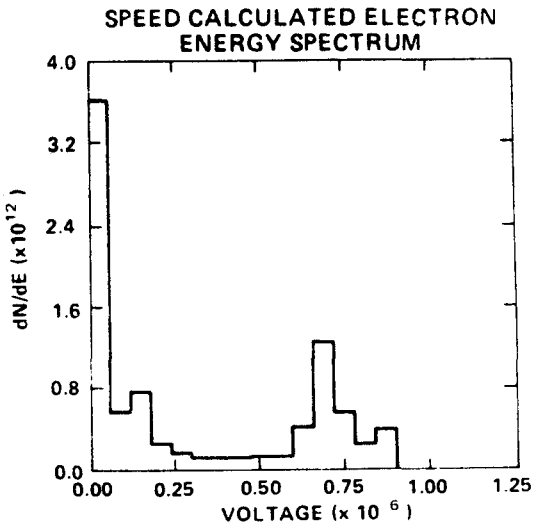

◁ Hydramite II

The Hydramite II accelerator is a 2-MV-peak, short-pulse, high-energy bremsstrahlung or electron beam source. It is based on technology developed for Sandia's Inertial Confinement Fusion Energy program. Hydramite II is very similar to two modules of the 36 module PBFA-I (Particle Beam Fusion Accelerator), differing in that the Marx generator contains 1.3-μF capacitors and that magnetically-insulated transmission lines (MITLs) are not used. Each Hydramite II line operates independently of the other or they may be fired in unison.

Accelerator Parameters

Peak Diode Voltage	2.0 MV
Peak Diode Current	350 kA
Power Pulsewidth (FWHM)	40 ns
Total Beam Energy	25 kJ
Repetition Rate	3 Pulses/Day/Line

A bremsstrahlung source has been developed on Hydramite II using a pinched-beam parapotential diode with a split converter. Further bremsstrahlung diode development is continuing. Development is also in progress for providing electron beam exposure capability using Bz transport.

X-Ray Environment

Peak Dose	60 krads (CaF_2 TLD) [approx. 2.4 cal/g(Au)]
Peak Dose Rate	1.5×10^{12} rads(CaF_2)/s
Exposure Area (50% falloff)	30 cm^2
Radiation Pulsewidth (FWHM)	35 ns

E-Beam Environment

Peak Fluence	100 cal/cm^2
Exposure Area (10% uniformity)	120 cm^2

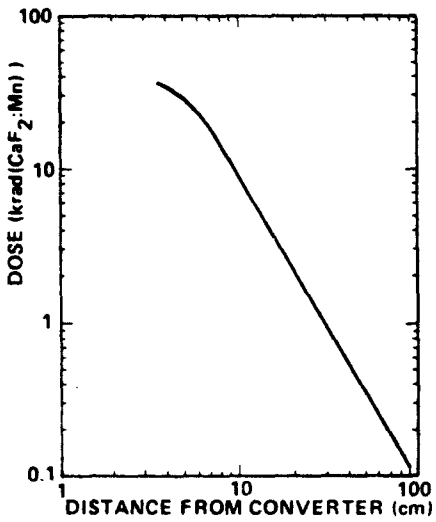

Hydramite Dose on Center Line as Function of Distance

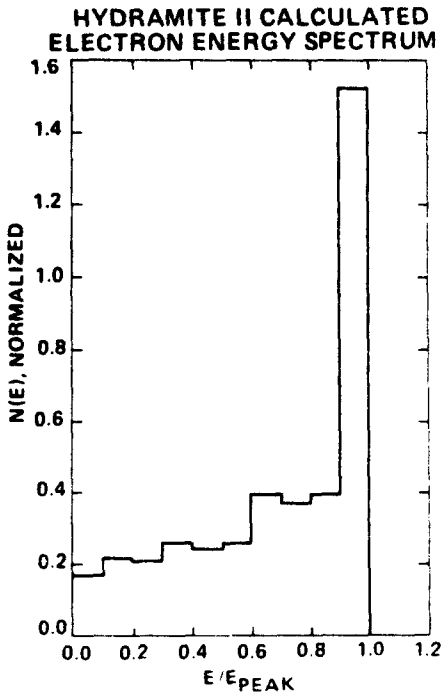

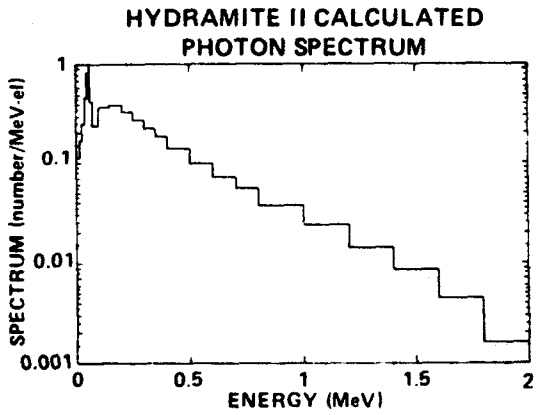

Simulation Technology Laboratory (STL)

The Simulation Technology Laboratory (STL) project includes two new simulation facilities - HERMES III and Saturn. These sources will provide major improvements over existing gamma-ray and x-ray laboratory sources. For example, the new radiation sources will possess larger exposure areas and, concurrently, better matches to the vulnerability requirements of dose, dose rate, pulsewidth, and risetime than are presently available. Larger exposure areas for testing will satisfy most DOE requirements. In addition to weapons effects testing, these sources will be available for use in future weapon system development and stockpile evaluation programs.

HERMES III will be housed in a new building which will be ready for occupancy in early 1986. This 55,000 sq. ft. facility will include light lab and office space, high-bay space, and an advanced pulsed power laboratory. The layout of the high-bay and adjacent low-bay is shown below. In addition to HERMES III, the high-bay will house Proto II, SPEED, Hydramite II, and a HERMES III Subsystem Test Facility (STF). The low bay will contain areas for facility users and operations personnel. Two of these areas, the Dosimetry Laboratory and the User Data Analysis Room, will be housed in a RF-shielded screen room. The Dosimetry Laboratory will be equipped with two computer-driven TLD readers and operated by personnel from Sandia's Reactor Development and Applications Department. The User Data Analysis Room will be equipped with several computer terminals and a laser printer which will be linked to STL's Main Screen Room, located directly above the low bay. Via these links, users will have access to all data acquired in the Screen Room for processing and analysis.

User Test Preparation bays will be equipped with basic test equipment and will provide users with dedicated space for preparing their packages for testing in the various test cells. A conference room in the low bay is also available to users for group discussion and meetings.

A General Maintenance area will provide space both for users who need more room than available in the Test Prep Areas and for operations personnel to conduct general maintenance and repair work. This area will be furnished with workbenches, tools, nuts and bolts, etc. It will be serviced by a two-ton bridge crane.

A fully equipped Machine Shop will also be available to both users and operations personnel for quick turn-around jobs required by tests or repair needs. The Component Test Area will contain equipment for high-pot testing, monitor calibration, vacuum leak checking, and pressure testing. The Spark Gap and Switch Rebuild Area and the Resistor Fabrication Area will be used by operations personnel for accelerator component maintenance.

The bulk of data acquisition will be handled by the Main Screen Room which will operate several subsystems dedicated to the various accelerators. The equipment will be comprised mostly of fast and slow transient digitizers driven by mini-computers, and scopes. A VAX 780 will be used primarily for data processing and analysis. Local screen rooms on the high bay floor will also be available for experimenters using custom test equipment.

The Advanced Pulsed Power Lab will house development-type accelerators for conducting advanced research in pulsed power technology.

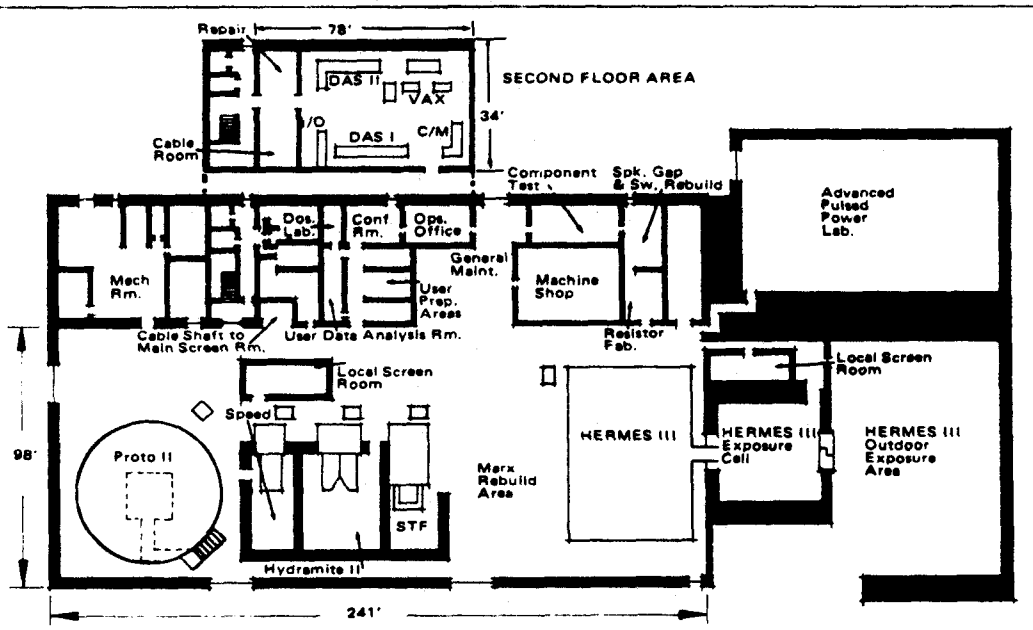

Saturn

By 1986, the Particle Beam Fusion Accelerator-I (PBFA-I) will have completed its program of fundamental research on inertial confinement fusion. The X-Ray Simulation Program will take advantage of the numerous advances in pulsed power technology made by the ICF program by converting PBFA-I into the large-area x-ray source for the Simulation Technology Laboratory (STL). Renamed Saturn, for its unique multiple-ring diode design, the facility will be ready for x-ray effects testing in 1987.

Saturn will include significant upgrades in the energy storage and pulse forming sections of PBFA-I. The 36 magnetically insulated transmission lines (MITL) that provide power flow to the ion diode on PBFA-I will be replaced by 36 vertical, parallel plate, water transmission lines. These lines will be connected to three horizontal triplate disks in a water convolute section. Power will flow through an insulator stack into radial MITLs that drive the diode.

Each diode element will be a triaxial diode. The three triaxial diodes will be nested concentrically, forming a multiple-ring diode. The accelerator current will be divided so that 17% flows to the inner ring, 33% to the middle ring, and 50% to the outer ring. This current division will provide a very uniform radiation profile a short distance behind the converter, enhancing the efficiency of the x-ray source. Saturn will be a unique facility for subsystem and system testing and will represent a significant advance in above-ground testing technology. Projected output parameters are given below.

Accelerator Parameters

Peak Diode Voltage	2.0 MV
Peak Diode Current	12.5 MA
Total Beam Energy	750 kJ
Power Pulsewidth (FWHM)	30 ns
Repetition Rate	3 Shots/Day

X-Ray Environment

Peak Dose (30-ns pulsewidth)	150 krads (Si) [approx. 5 cal/g (Au)]
Peak Dose Rate (30-ns pulsewidth)	5.0×10^{12} rads(Si)/s
Exposure Area (50% falloff)	500 cm^2*
Radiation Pulsewidth (FWHM)	15–30 ns

**A large area (10,000 cm^2) mode at lower fluence levels will also be available*

HERMES III

New technology developed in the joint DNA/DOE High Energy Linear Induction Accelerator (HELIA) program will be used to build HERMES III. The HELIA concept uses modular pulsed power components to drive ferromagnetically isolated induction cavities. The outputs of these cavities are added on a magnetically insulated transmission line (MITL) and an electron beam is generated in a single anode-cathode gap diode at the end of this MITL. A bremsstrahlung gamma-ray converter on the anode side of the diode generates the gamma-ray output. HERMES III will be ready for gamma-ray effects testing in 1987.

The HERMES III energy storage section consists of 10 2.4 MV, 156 kJ Marx generators. Each of the Marx generators charges two water dielectric intermediate storage capacitors. The 20 intermediate storage capacitors are switched with laser triggered gas switches and each charges four water dielectric pulse-forming lines. Each cavity is driven by four pulse-forming lines. Azimuthal transmission lines in each cavity further symmetrize the four-point feed to provide azimuthal symmetry of the power feed to the MITL. Metglas cores are used for ferromagnetic isolation. The MITL is tapered to satisfy the minimum current condition for magnetic insulation as the voltage is increased through the adder. A constant impedance MITL transports the power from the adder to the diode/converter in the exposure cell.

The accelerator will be 21-m wide, 11-m long, and 5-m high. A 5-m long constant impedance MITL transports the power to the diode/converter in the exposure cell. HERMES III is a state-of-the-art accelerator which takes advantage of short pulse, low inductance pulsed power technology to provide dose-rate area products which have not been previously available. Projected output parameters are given below.

Accelerator Parameters

Peak Diode Voltage	20 MeV
Peak Diode Current	800 kA
Total Beam Energy	640 kJ
Power Pulsewidth (FWHM)	40 ns
Repetition Rate	4 Shots/Day

Gamma-Ray Environment

Peak Dose	100 krads (Si)
Peak Dose Rate	5.0×10^{12} rads(Si)/s
Exposure Area (50% falloff)	500 cm^2
Radiation Pulsewidth (FWHM)	20 ns

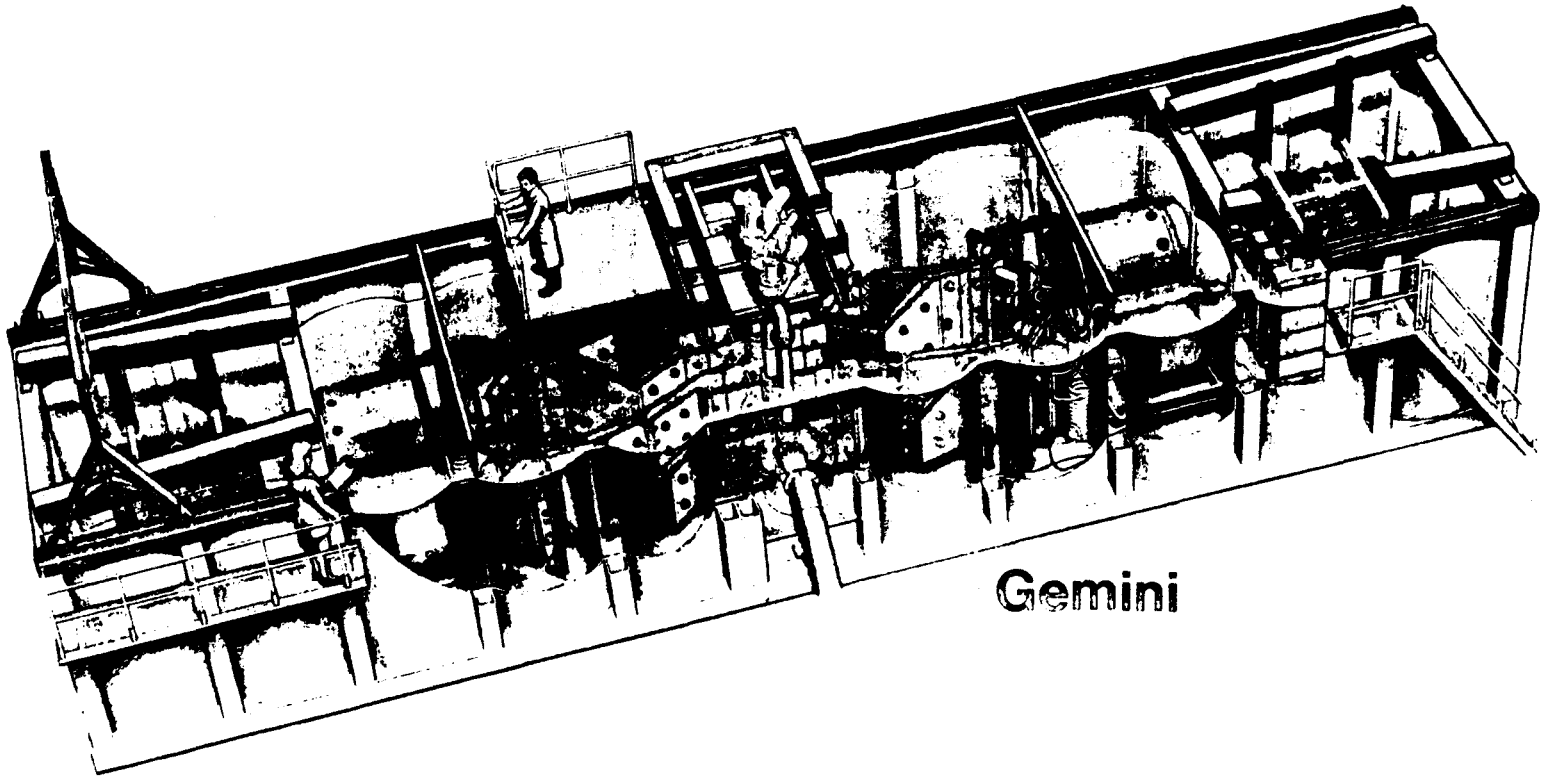

Gemini

Gemini

Built in 1981, the Megamp Accelerator and Beam Experiment (MABE) was the technology development testbed for the multiple-beam, linear induction accelerator approach for HERMES III. With the completion of that program, MABE will be reconfigured, during 1986, into a two-beam linear induction accelerator for use as a gamma-ray simulator, and renamed Gemini.

This accelerator combines the technology of the high-current radial pulse line induction accelerator (RADLAC) program with the modular water stripline technology from the Particle Beam Fusion Accelerator (PBFA) program. In order to produce the required gamma-ray dose at photon energies which would not cause excessive neutron activation, it was necessary to achieve very high current. Because space charge limitations precluded accelerating such high currents through a linear induction accelerator in a single beam, the concept of simultaneously accelerating multiple beams was conceived. The two-beam accelerator is designed for two 10-MeV, 80-kA beams which will produce a dose rate of 2.3×10^{12} Rad/sec over a 100-cm^2 area, in a 20-ns pulsewidth.

The pulsed power system consists of two Marx generators, four intermediate storage capacitors (IS), triggered gas switches, pulse-forming lines (PFL), sets of multiple point water switches, and triplate transfer lines, which feed eight parallel plate transmission lines. Each Marx generator charges two IS, and each IS charges a single PFL, which drives a transfer line and two transmission lines. Half of the pulsed power system is on each side of the beam transport/accelerating section to provide a symmetric power feed. Two of the parallel plate transmission lines on each side of the beam line are convoluted to apply the correct polarity pulse to the diodes for accelerating electrons. Each set of two opposing transmission lines drive a water-vacuum interface. There are four of these interfaces which house a two-beam injector and three sets of two accelerating gaps.

Projected Accelerator Parameters

Peak Output Voltage	10 MV
Peak Output Current	160 kA
Power Pulsewidth	40 ns
Total Beam Energy	64 kJ
Repetition Rate	10 Pulses/Day

Projected X-Ray Environment

Peak Dose	45 krads (CaF$_2$ TLD)
Peak Dose Rate	2.3×10^{12} rads(CaF$_2$)/s
Exposure Area (50% falloff)	100 cm^2
Radiation Pulsewidth (FWHM)	20 ns

Gemini and Saturn will be housed in Building 981, Technical Area IV. A layout of the building is illustrated below. In general, user activity pertaining to Gemini will occur in the north end of the building, and activity related to Saturn will take place in the southern part of the building. A fusion research accelerator, SuperMite, is also located in the high bay. The bulk of the data acquisition will be handled in a common screen room, although separate screen rooms for custom equipment will be available. DAS equipment will consist primarily of fast and slow transient digitizers.

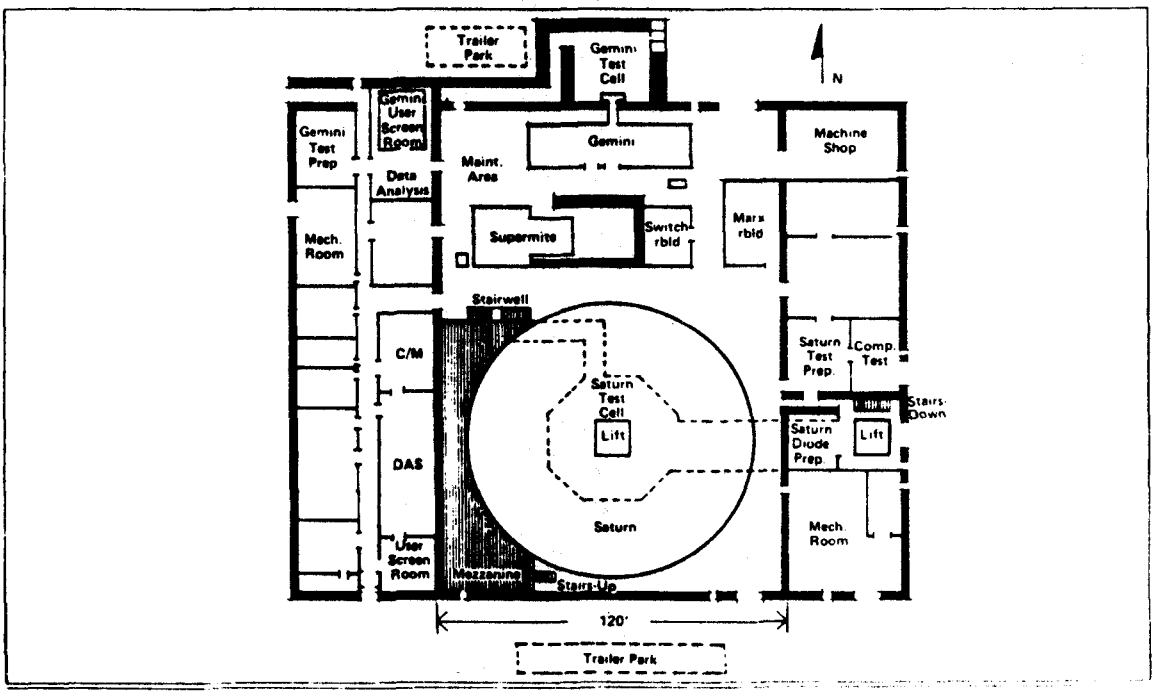

Radiation Dosimetry Laboratory

The Radiation Dosimetry Laboratory provides dosimetry services to the accelerator, reactor, and radioactive-source facilities. It supports development and characterization of the irradiation facilities, and radiation exposure data for experiments. Several forms of gamma and neutron dosimetry are available, and the laboratory is computer automated to insure reliable processing and quick response. System calibrations are traceable to NBS.

Available Gamma Dosimetry includes

- CaF_2:Mn Thermoluminescence Dosimetry (TLD) for doses from 1 to 10^5 rads
- Radiochromic Dye Film Dosimetry for doses greater than 10^5 rads
- Fricke Chemical Dosimetry and ionization chambers for calibration purposes

Available Neutron Dosimetry includes

- Sulfur activation analysis with gas-flow proportional counting for neutron fluence monitoring
- Nickel activation analysis with high-resolution gamma spectroscopy for neutron fluence monitoring
- Fission and activation-foil analysis with high-resolution gamma spectroscopy for fission rate and spectrum measurements
- Fission chamber measurements

Hot Cell Facility

The Hot Cell Facility is comprised of three laboratories located on-site: the hot cell laboratory, the glove-box laboratory, and the analytical support laboratory. The hot cell laboratory is a concrete shielded area containing three steel containment boxes (SCBs) and an experimental staging area, each remotely operated by means of master-slave manipulators (MSM). Each SCB and the staging area can contain up to 6000 curies of fission products (nominal 1 MeV γ's) and/or 500 curies of plutonium. SCBs 1 and 3 are 4.57-m long, 1.67-m wide, and 2.44-m high. The SCBs are interconnected with 38-cm-diameter pass-throughs. SCB 1 is set up primarily for assembly/disassembly of experiments, SCB 2 is devoted to metallurgical sample preparation (potting, grinding, and polishing), and SCB 3 is for wet chemistry. The staging area has a re-entry well equipped with a remotely operated elevator to accommodate experiment packages up to 4.57-m long and 76 cm in diameter. Also, such packages can be assembled/disassembled in the staging area.

The glove-box laboratory consists of eight interconnected glove boxes which may be operated with controlled high purity inert atmosphere. Two of the boxes are shielded and fitted with MSM for remote operations. Up to 300 curies of fission products can be handled in these two boxes. Complete metallurgical capabilities exist in the box line for low-level radioactive materials that are sensitive to moisture and/or oxygen. One of the inert boxes has a Wild M400 macroscope with photographic capability at magnifications up to 64X. Two other boxes are available for work with activated non-special nuclear materials.

The analytical laboratory includes: (1) metallurgical sample preparation capability which incorporates ion milling and etching, metal and carbon coating, and a Leitz remote metallographic microscope; (2) optical microscopy by means of free standing Wild M400 macroscope, and a Zeiss Ultraphot 11; (3) scanning electron microscope with both wavelength and energy-dispersive analytical capabilities; (4) gas analysis via gas chromatography and quadrupole mass spectrometry; and (5) limited wet chemical analysis.

Photon Source Data Acquisition Facilities

The primary Photon Simulation Data Acquisition System is housed in a centrally located instrumentation trailer. The system supports HERMES II, SPEED, and Hydramite II and is operated by the Simulation Operations Division 1233.

The equipment available for users includes

- Twenty-four Tektronix R7912 Transient Digitizers (350 MHz) with associated computer, software, and peripherals to record, process, and plot data
- Eighteen HP 183 Oscilloscopes (350 MHz)
- One HP 3456A/3497A voltmeter/scanner system capable of taking 40 channels of calorimetery data with associated computer, software, and peripherals to record, process, and plot data
- One Biomation 1015 capable of recording 4096 samples at 10 μs - 1 s/sample rates

Typically, the processed data is available within 15 minutes after the test. Programs are available for extensive data analysis.

At the Simulation Technology Laboratory, which will house HERMES III and other accelerators, the Data Acquisition System (DAS) will be located in the 2600-ft² Main Screen Room. Several sub-systems will support the various accelerators, and will be networked to a VAX 11/780, located in the screen room, for interactive data analysis. Instrumentation will consist primarily of fast transient digitizers, such as Tektronix 7912 series, and slow digitizers such as Tecktronix 7D20's

Saturn and Gemini, in Building 981, will be supported by a common DAS which utilizes Tektronix 7912AD's and 2430's to cover the wide range of bandwidth requirements in weapon-effects testing. Interactive data analysis is provided by an HP-1000 computer and Tektronix high-resolution graphic terminals.

Neutron Source Data Acquisition Systems

Data acquisition for the neutron source facilities is provided by three systems; one that is primarily dedicated to the SPR Facility, and two that are primarily dedicated to the ACRR Facility.

Users of the SPR Facility have the following equipment available to record, process, and display data:

- Twenty-two Tektronix R-7612D Transient Digitizers (80 MHz)
- Eight Tektronix R-7603 Oscilloscopes (100 MHz) with 7D20 Plug-in Digitizers (15 MHz)
- Five Tektronix R-7844 Oscilloscopes (400 MHz)
- DEC 11/73 computer with software and peripherals

The ACRR Facility is supported by

- The DAASY-II digital recording system (70 channels, 100 kHz), with associated computer, software, and peripherals to record, process, and display data
- The Data Acquisition and Display System (DADS), with an HP1000 computer system, software, and peripherals to record, process, and display data. HP9845 computer-controlled terminals perform data acquisition and processing functions, as well as interfacing with the HP1000

APPENDIX 6

Standards for Electronics Radiation Testing and
Remarks about SSC Displacement Damage Testing

Standards for Electronics Radiation Testing and Remarks about SSC Displacement Damage Testing

E. L. Petersen
P. W. Marshall*

Naval Research Laboratory
Washington D.C. 20375

Introduction

The main goal of this paper is to present the radiation testing standards that have been developed by the radiation effects community over a number of years. We will also present the compilations of available radiation sources that have been assembled for the Defense Nuclear Agency. Before presenting this information, we want to summarize some testing approaches and results pertinent to the SSC that are not yet in the standards literature.

Displacement damage presents the major damage mechanism for many types of electronic and non-electronic devices. For mixed environments, such as at the SSC, it is important to understand the energy and particle dependence of the damage. This has not been addressed in any standards to date. It is only recently that this information has become available. The first section will summarize this recent work.

The possible use of CCDs and other small area type detectors as particle detectors brings up questions about their damage susceptibilities. They have long been known to be susceptible to total dose damage, but as total dose hard devices have been developed, it has become clear that permanent bulk damage effects are also very important. The second section will summarize recent observations in this area.

Traditional radiation effects measurements have been aimed at a single type of radiation environment. The SSC will not necessarily have only a single type of radiation environment, so it is necessary to consider device susceptibility in mixed radiation fields. Section three will introduce a method of comparing the various effects.

A large number of the traditional radiation damage problems in device testing and dosimetry have been addressed by the radiation and hardness assurance communities. The results have been assembled as testing standards. These are available primarily from the ASTM, with a few of them available as military standards. Dosimetry standards have also been developed by the ICRU and NBS (now NIST). The fourth section of the paper will introduce these standards.

*Sachs/Freeman-Associates

There are a large number of facilities in the country that are used for electronics radiation testing. The Defense Nuclear Agency (DNA) periodically assembles lists of representative sources that are commonly used. The last section presents some data from these reports.

Energy and Particle Dependence of Displacement Damage

Radiation effect analysis for many of the electronic devices and technologies proposed for the SSC can draw heavily on the body of information which has been developed through DoD funded efforts over the past decades. In particular the work addressing displacement damage effects will be applicable to the solid state detector technologies under consideration. These effects will be expected to dominate detector degradation for both neutron and charged particle environments. Many of the salient points describing displacement damage have already been identified by the SSC Central Design Group [1], however there are some very recent and potentially very useful developments which will be outlined in this and the following section. This material will illustrate how accurate prediction of detector degradation in a specified radiation environment can be accomplished with minimal testing.

The central premise underlying the predictive approach is that the displacement damage effects in a device for a given particle with a given energy can be correlated to the effects of other energies and other particles. Once the the response to a single test environment has been determined for the detector in question, the correlation, which has been shown to be independent of device and material, can be used to predict the degradation expected in the given detector from the spectrum of particles and energies anticipated in the SSC application.

The correlation is based on the concept of nonionizing energy loss (NIEL), which is the energy a particle imparts to a solid through means other than ionization. Nonionizing energy deposition plays the same role in displacement damage effects that ionizing energy deposition (i.e., dose) plays in ionizing effects. First proposed by Burke [2], NIEL is calculated from first principles based on differential cross sections and interaction kinematics. NIEL is that part of the energy introduced via both Coulomb (elastic), and nuclear elastic and inelastic interactions, which produces vacancy-interstitial pairs and phonons. Its units, ($kev*cm^2/g$), are the same as for stopping power produced by ionization phenomena, thus offering a convenient means for calculating cumulative effects from a variety of particles and energies.

Burke has calculated NIEL in silicon for electrons, protons, neutrons, deuterons, and helium ions over a broad energy range. Figure 1 shows the NIEL energy dependence for these particles as well as the results of recent work by Van Ginneken [3] which extends the calculations to higher energies and includes photons, muons and pions. The figure contains the information necessary for a quantitative assessment of damage from a mixed particle environment and enables trends to be readily identified.

For example, highly relativistic particles all have similar displacement producing characteristics whereas with lower energies the inverse energy dependence of the Coulomb interaction dominates for charged particles, and the more massive charged particles are seen to be the most damaging of all.

Figure 2 offers an energy dependent comparison between experimental displacement damage data and the calculated NIEL for protons, deuterons, helium ions, and 1 MeV equivalent neutrons [4]. The NIEL for 1 MeV equiv. neutrons is 2.04 kev-cm^2/gm [4]. Summers, et.al. measured damage factors for gain reduction in several bipolar Si transistors. Here the damage follows from a reduction in the minority carrier lifetime through the particle induced introduction of recombination sites in the base region. Each charged particle damage factor was normalized to its corresponding neutron damage factor measured under the same conditions. The two ordinates in the figure plot the measured damage factor ratios and the calculated NIEL ratios against particle energy. Measured ratios from five transistor types (both n- and p-type Si) fall on common curves though the absolute damage factors varied significantly among the transistor types. More importantly, there is a one-to-one correspondence with no fitted parameters between the measured ratios and the NIEL ratios based on first principle calculations.

The implication of the correspondence shown in figure 2 is that a direct proportionality exists between the measured damage factors and the calculated NIEL. This is illustrated in figure 3 [4] where the absolute damage factors from one transistor type and each particle and energy tested are plotted against the calculated NIEL. The solid line has a slope of one, and the excellent agreement confirms that the linear relationship exists even though the microscopic distribution of the damage is thought to be quite different for the range of particles considered. Several studies have explored and extended this basic result. In silicon the correlation has been extended to electrons with energies from 5 to 60 MeV for minority carrier lifetime effects [5]. More importantly for the SSC, by measurement of the leakage current in a Si sensor array, Dale et.al. [6] have shown that carrier generation displacement effects can also be correlated on the basis of NIEL. Calculations of NIEL and comparisons with experimental data have been reported now in several materials including Ge [7], GaAs [8], and in high temperature superconductor materials [9].

Permanent Damage in Small Volume Detector Elements

Nonionizing energy loss, as described above, is an average quantity just as stopping power is an average quantity. For ionization damage the departure from the average dose delivered in a uniform medium is insignificant down to dimensions measured in tens of cubic angstroms, however this is not the case with NIEL. For Si detector arrays with elements measured in tens or hundreds of cubic microns the displacement damage sustained by adjacent pixels can vary considerably even though the identical elements are exposed to identical environments.

Figure 4 illustrates the variance associated with displacement damage processes for the case of the dark or leakage current induced in a Si sensor array damaged incrementally by fission neutron exposure [6]. Here the increase over the pre-irradiation dark current is determined for each pixel and the four histograms are formed from the 61,504 pixel population following each exposure. The width of the distribution continues to increase with increasing damage. It is the average dark current that is correlated and predicted based on the NIEL, and the variance is determined by the dimensions of the detector element and the radiation in question. In [6] a quantitative approach, again based on interaction cross sections and reaction kinematics, is demonstrated for determining the fluctuations associated with a given radiation environment and detector geometry. Comparisons of fluctuations associated with fission neutron damage and monoenergetic proton damage at several energies are then used to illustrate salient points governing the inherent fluctuations in NIEL. The example sited here is for leakage current, however other displacement damage effects such as charge trapping would be expected to reflect the same fluctuations if small volumes are involved.

Another recent finding which may affect the SSC detector designs involves leakage currents associated with high electric fields within depletion regions. When radiation damage occurs in field regions exceeding 10^5 volts/cm there is an enhanced emission of carriers and the localized leakage currents can be extremely high. Electric field enhanced emission has been shown to be responsible for the largest leakage currents measured in some radiation damaged detector arrays [10,11], and it may well be an important consideration for minimizing the leakage current in large area detectors as well. Figure 5 demonstrates the striking effect as fields exceed 10^5 volts/cm [11].

Damage in Mixed Environment

The traditional nuclear weapons radiation effects community ordinarily considers various effects separately. Dose rate upset and latchup occur near weapon bursts in space. Single event upset and latchup occur in the natural space environment. Neutron effects are important near nuclear weapons on the ground. High level total dose effects occur in space after weapon bursts. Dose rate effects should not be important at the SSC. Single event upset and latchup may occur, leading to loss of data or of individual devices, but will not be discussed here [12]. However the SSC is likely to have both total dose and displacement damage effects occurring simultaneously.

The susceptibility data banks ordinarily contain neutron and ionizing dose susceptibilities in separate data banks. When one goes to these banks, one finds a range of values for even one electronics technology. Therefore summaries are often presented using bar charts for each device technology. A schematic representation can be presented in two dimensions for simultaneous viewing of both neutron and ionizing dose susceptibilities. The presentation uses boxes where one dimension corresponds to representative ionizing dose susceptibilities and the other dimension corresponds to the range of neutron susceptibilities [13]. Figure 6 shows this generalized representation of microcircuit susceptibility. A particular device would be represented as a single point at

the intersection of its two types of susceptibility.

The new insight on energy and particle dependence of displacement damage effects that was presented in section 1 laid the groundwork for a schematic approach to radiation effects in combined fields or in proton environments for which both types of effects occur simultaneously [13]. For example, at a given proton energy, it is possible to calculate the total dose and the equivalent 1 MeV neutron flux that occur for a given particle flux. A single line can then be superimposed on figure 6 that shows the increasing equivalent neutron flux as a function of the total ionizing dose delivered. This is shown in figure 7 for 90 MeV protons. If a particular device falls on the left side of the line, it will fail to ionizing dose effects before it fails for displacement damage. Similar lines could be drawn for other charged particles using the information presented in section 1.

Operation in a given mixed field can also be represented in figure 7. For example, a reactor will often present both gamma and neutron environments. If the ratio of the two fields is known, then a corresponding line can be drawn as shown. Again, the devices on the left will fail first due to ionizing dose while those on the right will fail due to displacement effects. In this situation, prior assumptions about the dominant damage mechanism are often wrong.

The schematic approach presented here can in general be applied to any mixed field environment and so is very appropriate for use while estimating radiation effects around the SSC. It is necessary to estimate the failure levels for both mechanisms and it is necessary to understand the working environment.

ASTM and Mil Standards for radiation testing

The nuclear radiation effects community initially was involved with the basic measurement of radiation effects and then with the development of parts that would work in the radiation environment. It was soon recognized that the radiation response of a specific semiconductor device could vary among manufacturers and often also among a given manufacturers production lots. The variations made part selection and system design for nuclear hardening difficult. This in turn led to diverse testing methods and test results.

In response to these needs, the Defense Nuclear Agency (DNA), in 1975 under the leadership of E. A. Wolicki, started a formal Hardness Assurance Program for Electronic Parts. It was recognized that the way to procure radiation-hardness-assured electronic parts was to use standard test methods -- both for measuring the radiation response of the parts and for measuring the radiation dose. Since such standard test and dosimetry methods did not exist at the time, their development became one of the first objectives of the Hardness Assurance Program [14].

The program was joined by a large number of government agencies, and the final

standards are now published by the American Society for Testing and Materials (ASTM) and by the Military Standards establishment. The dosimetry efforts were done in collaboration with the National Bureau of Standards which established a dosimetry calibration service [15]. Total dose measurements should be done only at locations where the dosimetry or source calibrations can be traced back to NBS.

There very early arose questions about the equivalence of irradiations performed at various reactors, due to different neutron spectra. This led to the establishment of a 1-MeV silicon-damage-equivalent standard, and organized comparisons of various neutron sources. Neutron damage measurements should be carried out using sources that are well calibrated in terms of the 1 MeV standard, such as the one at White Sands.

There are now a number of published ASTM and Mil standards applicable to electronics and dosimetry. Table I presents a summary as assembled by Floyd Coppage and Harvey Eisen [16]. The International Commission on Radiation Units and Measurements (ICRU) has also assembled standards for radiation dosimetry. These are available in references 17-19.

The standards are necessary if you are to avoid a number of simple but not obvious pitfalls, primarily in dosimetry. Some of the problem areas in total ionizing dose testing with Co-60 are:

1. non uniform dose across large areas,
2. shielding effects due to orientation in water or room sources,
3. low energy scattering from a wall near the device or source,
4. effect 3 exacerbated by high z materials such as gold and kovar lids,
5. other high z materials near the device.

These effects can produce orders of magnitude differences in results, and make apparently simple experiments completely non-reproducible.

Sources Normally used for Hardness Assurance Testing

As DNA supports a large amount of radiation testing both by its own contractors, and indirectly that of contractors for other government programs, it periodically assembles summaries of the available test sites. Two recent publications are one on Co-60 facilities by Humphreys and Dozier [20] and one on general weapon simulation facilities, including Co-60, by K. E. Gould and coworkers [21]. Table II summarizes some of the information available in the list of Co-60 facilities, while Table III lists some of the other facilities from ref 21.

The lists are not complete, but do include all of the facilities with extensive experience with electronics testing. The lists do attempt to have a good geographical coverage, so that all parts of the country are covered.

The complete references [20 and 21] also include data on the maximum dose rate, the usable irradiation volume, temperature rises, costs, and other comments. One

or two of the sources may require security clearances to be on file. The facilities vary on source operators, equipment operators, support for testing, and who does the dosimetry. It is always necessary to call and visit the facility before arriving there for testing. Few things are more frustrating than arriving at a facility with 8 ft cables, and finding that you need 10 foot cables, while paying $1000/day.

Very little electronics radiation effects work has been done using proton accelerators. The two facilities in current use are the U.C. Davis cyclotron and the 200 MeV linac Radiation Effects Facility (REF) at Brookhaven. In these cases there was extensive dosimetry comparisons between the two machines and with Co-60 sources at NRL and HDL, and with the NRL electron linac [4, 22].

Concluding Remarks

1. Know your device susceptibilities. You should identify the type of susceptibility that your devices will have. If you don't know, look at the radiation effects literature. If you can't find any information, then make some rough measurements. In mixed environments, such as at the SSC, it is often the unplanned-for susceptibility that ruins an experiment. Generalities about one or another type of damage dominating should not be trusted without careful consideration.

2. Know your target environment. You need to know what the operating environment is; the types of particles and their energy spectra. Is it primarily a gamma or total dose environment, or primarily a neutron environment (therefore displacement damage dominates) or is it mixed neutrons and gammas or high energy charged particles, so that you have both types of damage. It is not necessary to do careful neutron damage measurements when your components are very total dose susceptible and will operate in a low or medium dose environment.

3. Know your test environment. Dosimetry problems have ruined more device radiation tests than any other single type of problem. Even if the dosimetry is being furnished by the facility, check it carefully yourself. Occasionally an experienced operator will do dosimetry for one type of test, while you are doing a different type of test. And you are often assigned the inexperienced operator.

4. Know your test procedures. The standard test procedures often appear overly complicated and detailed. You can't afford to ignore a section because you don't understand it or it appears unnecessary. The test procedures are the results of a large number of people making a large number of mistakes. Skip a sub-procedure only if you thoroughly understand what you are doing.

References:

1. M.G.D.Gilchriese, Editor, "Radiation Effects at the SSC". SSC Central Design Group Report SSC-SR-1035, June 1988.

2. E.A.Burke, "Energy Dependence of Proton-Induced Displacement Damage in Silicon". IEEE Trans. on Nucl. Sci., Vol. NS-33, No.6, pg. 1276, Dec. 1986.

3. A.Van Ginneken, "Non Ionizing Energy Deposition in Silicon for Radiation Damage Studies". Fermi National Accelerator Laboratory Report FN-522, Oct. 1989.

4. G.P.Summers, E.A.Burke, C.J.Dale, E.A.Wolicki, P.W.Marshall, and M.A.Gehlhausen, "Correlation of Particle-Induced Displacement Damage in Silicon". IEEE Trans. on Nucl. Sci., Vol. NS-34, No.6, pg.1134, Dec. 1987.

5. C.J.Dale, P.W.Marshall, G.P. Summers, E.A.Wolicki, and E.A.Burke, "Displacement Damage Equivalence to Dose in Silicon Devices". Appl. Phys. Lett., 54(5), pg. 451, 30 Jan. 1989.

6. C.J.Dale, P.W.Marshall, E.A.Burke, G.P.Summers, and G.E.Bender. "The Generation Lifetime Damage Factor and its Variance in Silicon". IEEE Trans. on Nucl. Sci., Vol. NS-36, No.6, pg. 1872, Dec. 1989.

7. P.W.Marshall, C.J.Dale, G.P.Summers, E.A.Wolicki, and E.A.Burke. "Proton, Neutron and Electron-Induced Displacement Damage in Germanium". IEEE Trans. on Nucl. Sci., Vol. NS-36, No.6, pg. 1882, Dec. 1989.

8. G.P.Summers, E.A.Burke, M.A.Xapsos, C.J.Dale, P.W.Marshall, and E.L.Petersen, "Displacement Damage in GaAs Structures". IEEE Trans. on Nucl. Sci., Vol. NS-35, No.6, pg. 1221, Dec. 1988.

9. G.P.Summers, D.B.Chrisey, W.G.Maisch, G.H.Stauss, E.A.Burke, M.Nastasi, and J.R. Tesmer, "Electron and Proton Radiation Effects in the High Temperature Superconductor $YBa_2Cu_3O_{(7-d)}$". IEEE Trans. on Nucl. Sci., Vol. NS-36, No.6, pg. 1840, Dec. 1989.

10. J.R.Srour and R.A.Hartmann, "Enhanced Displacement Damage Effectiveness in Irradiated Silicon Devices". IEEE Trans. on Nucl. Sci., Vol. NS-36, No.6, pg 1825, Dec. 1989.

11. P.W.Marshall, C.J.Dale, E.A.Burke, G.P.Summers, and G.E.Bender. "Displacement Damage Extremes in Silicon Depletion Regions". IEEE Trans. on Nucl. Sci., Vol. NS-

36, No.6, pg. 1831, Dec. 1989.

12. E. L. Petersen and P. W. Marshall, "Single Event Phenomena in the Space and SDI Arenas," Journal of Radiation Effects Research and Engineering, Vol 6, No. 2, pg 1, Sept 1988.

13. J. P. Raymond and E. L. Petersen, "Comparison of Neutron, Proton, and Gamma Ray Effects in Semiconductor Devices," IEEE Trans. on Nuc. Sci., Vol NS-34, No. 6, Pg 1622, Dec 1987.

14. E. A. Wolicki, I. Arimura, A. J. Carlan, H. A. Eisen, and J. I. Halpin, "Radiation Hardness Assurance for Electronic Parts: Accomplishments and Plans". IEEE Trans. on Nuc. Sci., Vol. NS-32, No.6, pg 4230, Dec 1985.

15. J. C. Humphreys, D. Hocken, and W. L. McLaughlin, "NBS Measurement Services: Dosimetry for high Dose Applications." NBS spec. Pub. 250-11, March 1988.

16. F. Coppage and H. Eisen, "Documentation Available for Radiation Hardness Assurance Programs," unpublished.

17. ICRU Report 14, "Radiation Dosimetry: x Rays and Gamma Rays with Maximum Photon Energies Between 0.6 and 50 MeV." Sept 1969.

18. ICRU Report 21, "Radiation dosimetry: Electrons with Initial Energies Between 1 and 50 MeV." May 1972.

19. ICRU Report 34, "The Dosimetry of Pulsed Radiation," August 1982.

20. J. C. Humphreys and C. M. Dozier, "Cobalt-60 Facilities Available for Hardness Assurance Testing," NBSIR 86-3480, Nov 1986.

21. K. E. Gould, et. al., "Program Manager's Guide to Simulation Facilities for Nuclear Hardness Validation - 1987 Edition," Dasiac SR-219, Oct 1987.

22. M. A. Xapsos, et. al., "Single-Event, Enhanced Single Event, and Dose-Rate Effects with Pulsed Proton Beams," IEEE Trans. Nucl. Sci, NS-34, Pg 1419, Dec 1987.

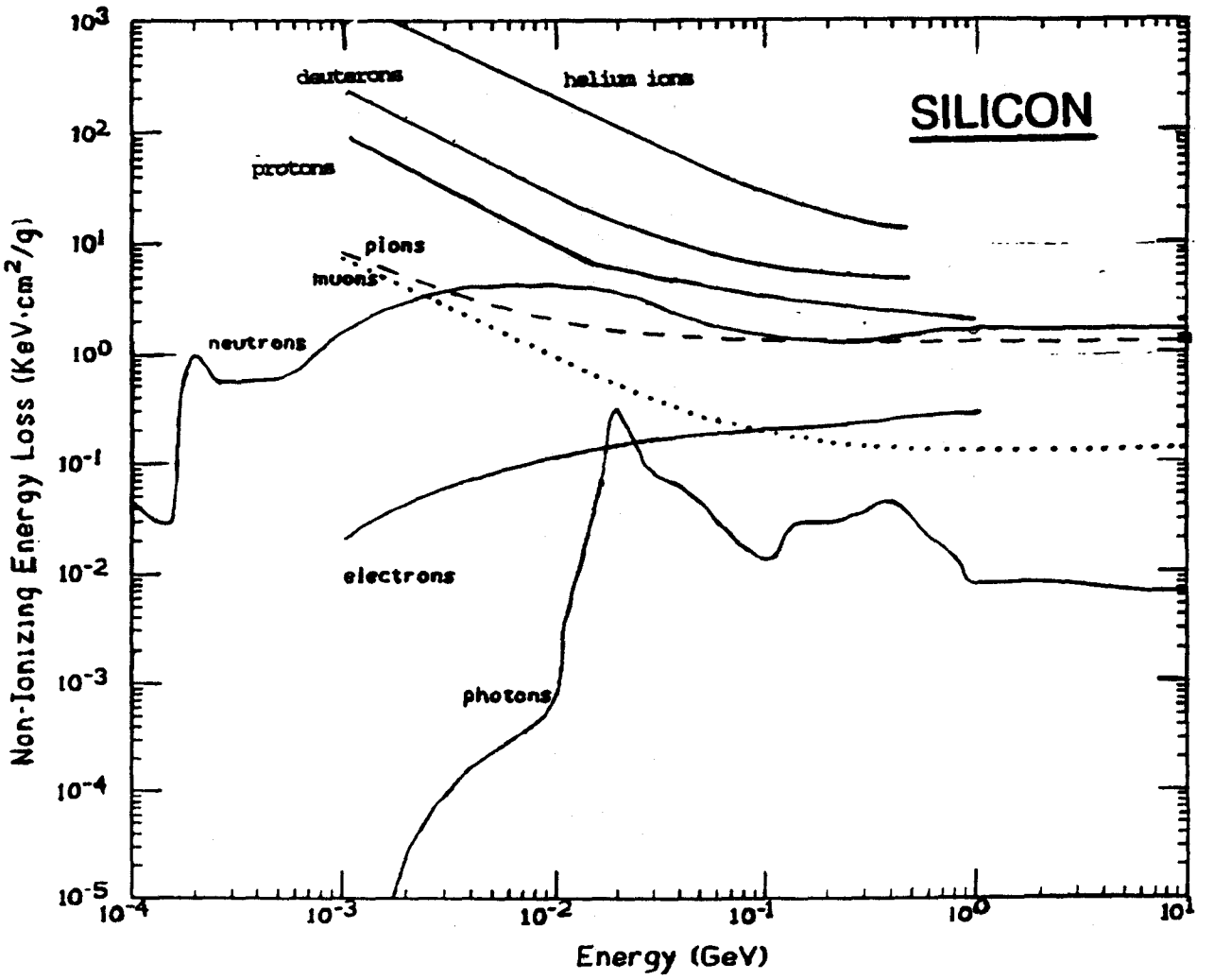

Figure 1. Nonionizing energy loss (NIEL) as calculated by Burke [2] and Van Ginneken [3] plotted versus energy for photons and seven particles. NIEL quantifies displacement damage for a given radiation in exactly the manner that stopping powers determine dose for ionizing radiations.

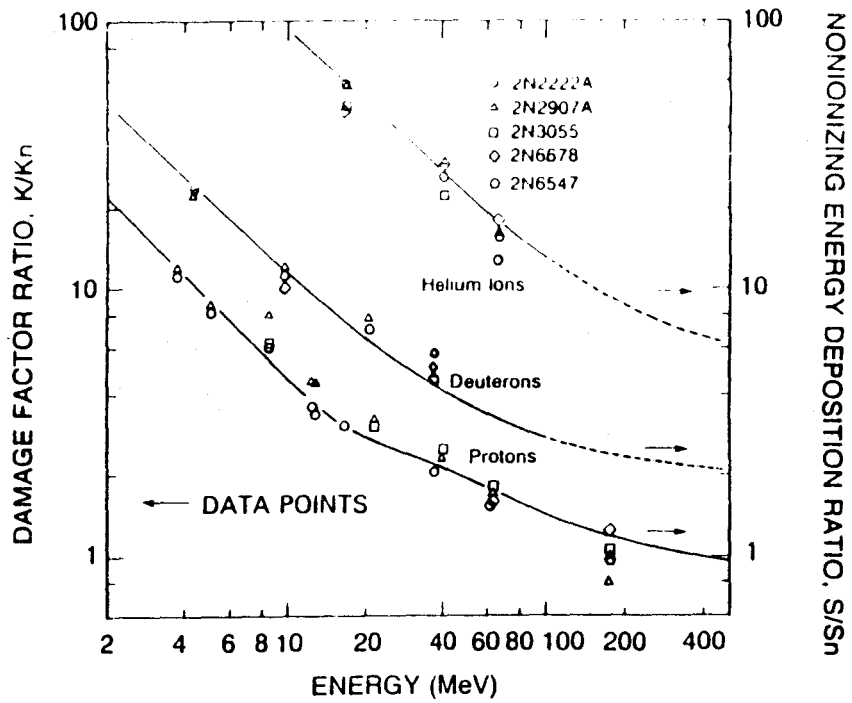

Figure 2. Bipolar transistor damage factors for protons, deuterons, and helium ions are normalized to the 1 MeV equivalent (Si) neutron damage factor and plotted versus particle energy. The continuous lines are calculations of the corresponding ratios of the nonionizing energy loss in Si as a function of energy. Note that the left hand ordinate corresponds to data and the other to calculation.

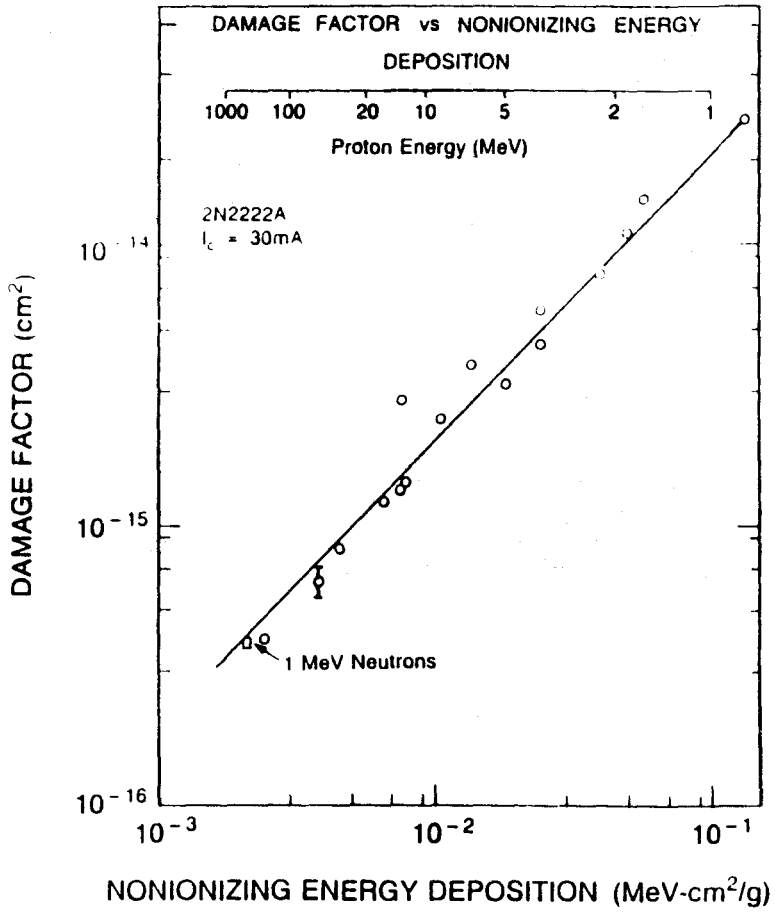

Figure 3. Measured damage factors for 2N2222A transistors are shown to be directly proportional to the calculated nonionizing energy loss for protons, deuterons, helium ions and 1 MeV equivalent (Si) neutrons. For convenience the corresponding proton energy is shown at the top of the figure, although the figure also contains data for deuterons and helium ions. The solid line defines linearity on the log-log plot.

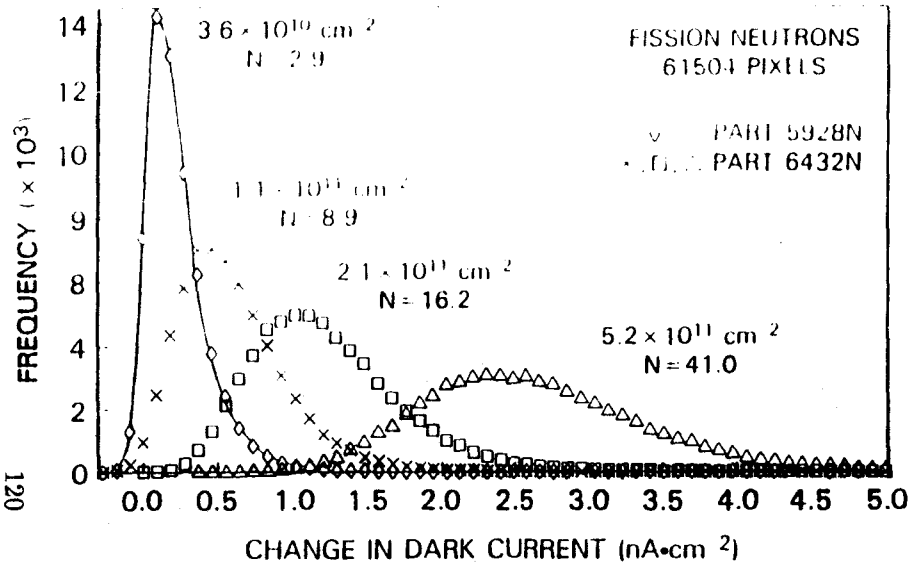

Figure 4. Silicon charge injection device (CID) dark current histograms were formed from 61,504 pixels following four levels of neutron exposure. N, the average number of primary knock-on atoms within each pixel is noted below each fluence. Fluctuatiuons in damage within the 20 micron square pixels are inherent to displacement damage processes.

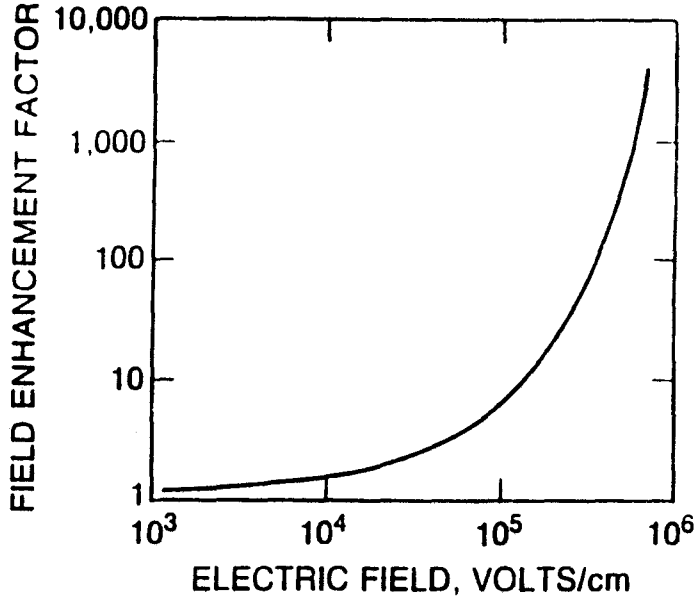

Figure 5. Calculated carrier generation enhancement factor due to electric field enhanced emission. Note the dramatic increasing trend above 0.1 megavolts/cm. Radiation damage in high field regions leads to very high leakage currents.

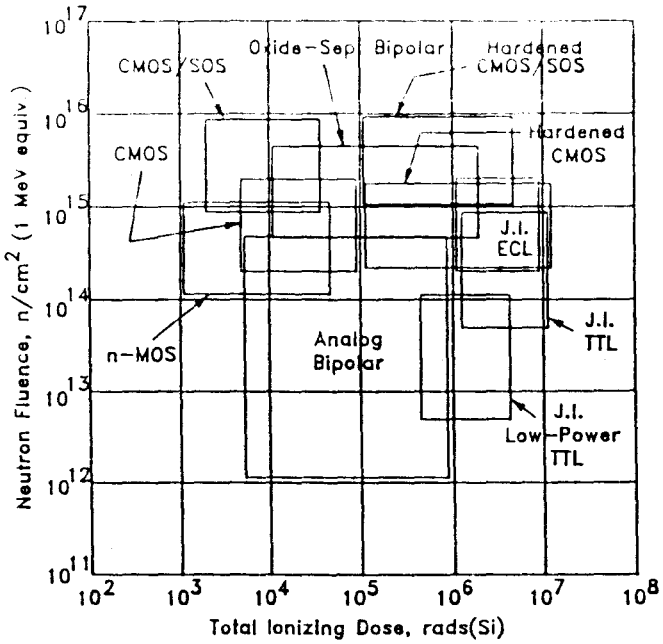

Figure 6. Regions of microcircuit susceptability are shown for several device technologies. Susceptability ranges in each case reflect independent characterizations of neutron displacement damage shown along the ordinate and ionization radiation damage shown along the abcissa. Plots such as this can help in the selection of devices to be used in mixed particle environments.

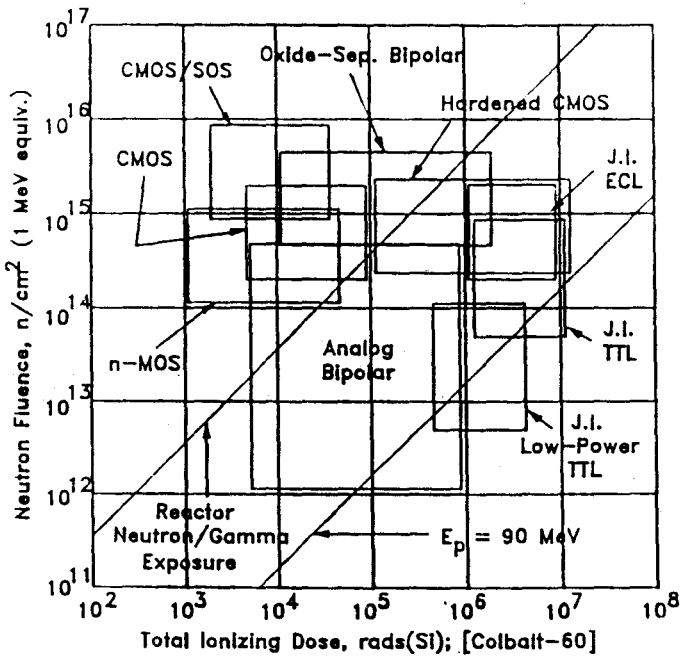

Figure 7. Combined ionization and displacement damage failure susceptabilities are presented in the two lines overlayed on the figure 6 schematic. The reactor neutron/ gamma line indicates failure by ionization damage from gammas accompanying nuclear fission, and the 90 MeV proton line indicates displacement damage failure as determined by the nonionizing energy loss associated with a given dose of 90 MeV protons..

TABLE I. Radiation Effects Testing Standards

Data from Coppage and Eisen

1. ASTM E720-86, Guide for SELECTION OF A SET OF NEUTRON-ACTIVATION FOILS FOR DETERMINING NEUTRON SPECTRA USED IN RADIATION-HARDNESS TESTING OF ELECTRONICS.

2. ASTM E721-85, Method for DETERMINING NEUTRON ENERGY SPECTRA WITH NEUTRON-ACTIVATION FOILS FOR RADIATION HARDNESS TESTING OF ELECTRONICS.

3. ASTM E722-85, Practice for CHARACTERIZING NEUTRON ENERGY FLUENCE SPECTRA IN TERMS OF AN EQUIVALENT MONOENERGETIC NEUTRON FLUEN FOR RADIATION HARDNESS TESTING OF ELECTRONICS.

4. ASTM E763-85, Method for CALCULATION OF ABSORBED DOSE FROM NEUTRON IRRADIATION BY APPLICATION OF THRESHOLD-FOIL MEASUREMENT DATA.

5. ASTM E82O-8A, Practice for DETERMINING ABSOLUTE ABSORBED DOSE RATES FOR ELECTRON BEAMS.

6. ASTM E845-81, Methods for CALIBRATION OF DOSIMETERS AGAINST AN ADIABATIC CALORIMETER FOR USE IN FLASH X-RAY FIELDS.

7. E1026-84, Method for USING THE FRICKE DOSIMETER TO MEASURE ABSORBED DOSE IN WATER.

8. E1027-84, Practice for EXPOSURE OF POLYMERIC MATERIALS TO IONIZING RADIATION.

9. E1205-88, Method for USING THE CERIC-CEROUS SULFATE DOSIMETER TO MEASURE ABSORBED DOSE IN WATER.

TABLE I. Radiation Effects Testing Standards (continued)

10. E1249-88, Practice for MINIMIZING DOSIMETRY ERRORS IN RADIATION HARDNESS TESTING OF SILICON ELECTRONIC DEVICES.

11. E1250-88, Test Method for APPLICATION OF IONIZATION CHAMBERS TO ASSESS THE LOW ENERGY GAMMA COMPONENT OF CO-60 IRRADIATORS IN THE RADIATION HARDNESS TESTING OF SILICON ELECTRONIC DEVICES.

12. ASTM F617-86, Method for MEASURING MOSFET LINEAR THRESHOLD VOLTAGE.

13. ASTM F618-79, Method for MEASURING MOSFET SATURATED THRESHOLD VOLTAGE.

14. ASTM F632-86, Method for MEASURING SMALL-SIGNAL COMMON EMITTER CURRENT GAIN OF TRANSISTORS AT HIGH FREQUENCIES.

15. ASTM F675-80, Method for MEASURING NONEQUILIBRIUM TRANSIENT PHOTOCURRENTS IN p-n JUNCTIONS.

16. ASTM F676-83, Method for MEASURING UNSATURATED TTL SINK CURRENT.

17. ASTM F744-81, Method for MEASUREMENT OF DOSE RATE THRESHOLD FOR UPSET OF DIGITAL INTEGRATED CIRCUITS.

18. ASTM F769-87, Method for MEASUREMENT OF TRANSISTOR AND DIODE LEAKAGE CURRENTS.

19. ASTM F773-87, Method for MEASURING DOSE RATE RESPONSE OF LINEAR INTEGRATED CIRCUITS.

20. ASTM F774-82, Guide for ANALYSIS OF LATCHUP SUSCEPTIBILITY IN BIPOLAR INTEGRATED CIRCUITS.

21. F867-87, GUIDE FOR TOTAL DOSE RADIATION TESTING OF SEMICONDUCTOR DEVICES.

22. F980-86, GUIDE FOR THE MEASUREMENT OF RAPID ANNEALING OF NEUTRON-INDUCED DISPLACEMENT-DAMAGE IN SEMICONDUCTOR DEVICES.

23. F1032-86, GUIDE FOR MEASURING TIME-DEPENDENT TOTAL-DOSE EFFECTS IN SEMICONDUCTOR DEVICES EXPOSED TO PULSED IONIZING RADIATION.

TABLE I. Radiation Effects Testing Standards (continued)

24. F1096-87, MOSFET SATURATION THRESHOLD VOLTAGE.

25. F1190-88, PRACTICE FOR NEUTRON IRRADIATION OF UNBIASED ELECTRONIC COMPONENTS.

26. F1191-88, GUIDE FOR THE RADIATION TESTING OF SEMICONDUCTOR MEMORIES.

MILITARY HANDBOOKS

1. MIL HANDBOOK 279; TOTAL DOSE HARDNESS ASSURANCE GUIDELINES FOR SEMICONDUCTOR DEVICES AND MICROCIRCUITS; February 1985.

2. MIL HANDBOOK 280; NEUTRON HARDNESS ASSURANCE GUIDELINES FOR SEMICONDUCTOR DEVICES AND MICROCIRCUITS; February 1985.

3. MIL HANDBOOK XXX; DOSE RATE HARDNESS ASSURANCE (submitted to DESC; now available as DNA-TR-86-29, November 1988).

4. MIL HANDBOOK 339 APPENDIX; CUSTOM LARGE SCALE INTEGRATED CIRCUIT DEVELOPMENT AND ACQUISITION FOR SPACE VEHICLES; January 1986.

5. MIL HANDBOOK XXX; TOTAL DOSE AND NEUTRON HARDNESS ASSURANCE GUIDELINES FOR SEMICONDUCTOR DEVICES AND MICROCIRCUITS (in draft form).

GUIDELINE DOCUMENTS

1. SUBTHRESHOLD TECHNIQUE FOR CHARGE SEPARATION IN IRRADIATED MOSFETS, E. Enlow, MRC.

2. TEST STRUCTURES FOR RADIATION HARDENING AND HARDNESS ASSURANCE, D. Alexander, MRC.

TABLE I. Radiation Effects Testing Standards (continued)

MILITARY STANDARD TEST METHODS

1. Method 1015, STEADY STATE PRIMARY PHOTOCURRENT, MIL-STD 750C.

2. Method 1017, NEUTRON IRRADIATION, MIL-STD-750C.

3. Method 1017.2, NEUTRON IRRADIATION, MIL-STD-883C.

4. Method 1019, STEADY STATE TOTAL DOSE IRRADIATION PROCEDURE, MIL-STD 750C.

ASTM Documents may be obtained by sending your request to:

ASTM
1916 Race Street
Philadelphia, PA 19103-1187
(215) 299-5400
FAX: (215) 977-9679

Additional information may be obtained from the chairpersons of the committees on Electronics and Dosimetry. They are:

Committee Fl.11 on Electronics, Quality and Hardness Assurance
Chairman: W. A. Alfonte
Kaman Tempo
2560 Huntington Ave. Suite 500
Alexandria, VA 22303 (703) 960-4774

Committee E10.07 on Dosimetry
Chairman: David W. Vehar
Sandia National Laboratories Division 6452
Albuquerque, NM 87185 (505) 844-4820

Copies of Military Specifications or Military Standards may be obtained by sending requests to:

Naval Publications and Forms Center
5801 Tabor Avenue
Philadelphia, PA 19120 (215) 697-2179

Use DD Form 1425 if available.

Table II. Cobalt-60 Sources for Radiation Testing

Excerpted from J. C. Humphreys and C. M. Dozier, "Cobalt-60 Facilities Available for Hardness Assurance Testing," NBSIR 86-3480, Nov 1986. (note that in many cases the name of the contact is no longer applicable.)

1. ORGANIZATION: Armed Forces Radiological Research Institute
   Bethesda, MD

CONTACT: Capt. Leonard Alt
Armed Forces Radiological Research Institute NMC-NCR
Bethesda, MD 20814 Telephone: (202) 295-1096

TYPE OF SOURCE: H_20 pool, 33' by 33' by 33'.
Samples can be placed in interior of source region.

2. ORGANIZATION: Battelle Memorial Institute
   Columbus, OH

CONTACT: Dr. V. Pasupathi
Battele Columbus Laboratories
505 King Avenue Columbus, OH 43201 Telephone: (614) 879-5140

TYPE OF SOURCE: Room source, 3300 Curies (acquiring 50 kCuries in near future). Sources are cylindrical rods which are arranged for test.

3. ORGANIZATION: Boeing Aerospace Company
   Seattle, WA

CONTACT: Mr. Dennis Russell
Boeing Aerospace Company P.O. Box 3999 Seattle,
WA 98124 Mail Stop 2R-00 Telephone: (206) 655-6712

TYPE OF SOURCE: (1) Gammacell 220
(2) Gammacell 220 (3) Gammacell 200 (4) Gamma Lab (room)

Table II. Cobalt-60 Sources for Radiation Testing (continued)

4. ORGANIZATION: Brookhaven Gamma-Irradiation Facilities
Brookhaven National Laboratory
Upton, New York

CONTACT: Mr. Walter Becker
Brookhaven National Laboratory
Bldg. 830
Upton, NY 11973
Telephone: (516) 282-4533 or 4526

TYPE OF SOURCE: Water Pool

5. ORGANIZATION: General Electric Company Utica, NY

CONTACT: Mr. Charles M. Hewison
General Electric Company Aerospace Electronic
Products Dept. French Road Utica, NY 13502 Telephone: (315) 793-5375

TYPE OF SOURCE: AECL Gammacell 220

6. ORGANIZATION: General Electric Company
Space Division, Valley Forge, Pennsylvania

CONTACT: Mr. Larry C. Jeffers
P.O. Box 8555
Philadelphia, PA 19101
Telephone: (215) 962-3811 x3196

TYPE OF SOURCE: Gammacell 220

7. ORGANIZATION: Georgia Institute of Technology
Atlanta, Georgia

CONTACT: Mr. Jerry Taylor
Georgia Institute of Technology Frank H. Neely Nuclear Research Center
900 Atlantic Drive, NW Atlanta, GA 30332 Telephone: (404) 894-3608

TYPE OF SOURCE: Room source - stored in H_2O pool. Have 8 source frames and 5 cylindrical sources. 30 ports for 1" cables.

Table II. Cobalt-60 Sources for Radiation Testing (continued)

8. ORGANIZATION: Harry Diamond Laboratories, Adelphi, MD

CONTACT: David Davis
Harry Diamond Laboratories 2800 Powder Mill Road
Adelphi, MD 20783 Phone: (202)394-2238

TYPE OF SOURCE: POOL

9. ORGANIZATION: Hughes Aircraft Company
El Segundo, CA

CONTACT: Mr. Joe Zeleck
Hughes Aircraft Company
P.O. Box 902
Bldg. E-2 MS-SlO7
El Segundo, CA 90245, Telephone: (213) 616 -0277

TYPE OF SOURCE: (1) Gammacell 220
(2) GR9 (3) GR9

10. ORGANIZATION: International Nutronics
Irvine, CA

CONTACT: Mr. Charles Dorthalina, Mgr/RSO
International Nutronics, 1962 Barranca Rd.
Irving, CA 92714
Telephone: (714) 863-9361

TYPE OF SOURCE: 1.6 MCuries in 195 cylindrical rods.
Source also used for medical and food irradiations

11. ORGANIZATION: International Nutronics
Palo Alto, CA

CONTACT: Mr. Tom Rensel
International Nutronics
1237 N. San Antonio Road
Palo Alto, CA
Telephone: 415-968-5257

TYPE OF SOURCE: 250 Curies in 48 cylindrical rods
Source also used for medical and food irradiations.

Table II. Cobalt-60 Sources for Radiation Testing (continued)

12. ORGANIZATION: IRT Corporation
San Diego, CA

CONTACT: Mr. John Harrity
IRT Corporation
3030 Callan Rd. San Diego, CA 92121
Telephone (619) 450-4343

TYPE OF SOURCE: Gammacell 220

13. ORGANIZATION: Jet Propulsion Laboratory
Pasadena, CA

CONTACT: Mr. Michael Gauthier
Jet Propulsion Laboratory MS-TI180
4800 Oak Grove Drive Pasadena, CA 91109, Telephone: (818) 354-2126

TYPE OF SOURCE: Room source. Two Co-60 sources on rails.

14. ORGANIZATION: Martin Marietta Aerospace
Orlando, FL

CONTACT: Mr. Jim Simmons
Martin Marietta Aerospace
P.O. Box 5837
MS - 163
Orlando, FL 32855, Telephone: (305) 356-4458

TYPE OF SOURCE: J.L. Shepard Model 109 -- 6 rods in Pb shielding container. H20 cooled.

15. ORGANIZATION: National Bureau of Standards
Gaithersburg, MD

CONTACT: Mr. J. C. Humphreys
National Bureau of Standards
C216 Radiation Physics Building
Gaithersburg, MD 20899, Telephone: (301) 921-2201

TYPE OF SOURCE: (1) AECL Gammacell 220 (2) Pool source: 12 source pencils in cylindrical array (3) Teletherapy collimated beam source

Table II. Cobalt-60 Sources for Radiation Testing (continued)

16. ORGANIZATION: Naval Research Laboratory
Washington, DC

CONTACT: Mr. Ken Gage
Radiation Facilities Section Code 4614
Naval Research Laboratory
Washington, DC 20375 Telephone: (202) 767-3938

17. ORGANIZATION: Rockwell International
Anaheim, CA

CONTACT: Mr. Larry Green or Rick Halverson
Rockwell International Defense Electronics Operations
3370 Miroloma Ave., P.O. Box
3105 Anaheim, CA 92803 Telephone: (714) 632-0775

TYPE OF SOURCE: (1) AECL Gammacell 200 (2) J.L. Shepard Model 109 (3) J.L. Shepard Model 81 (semicollimated source in shielded room)

18. ORGANIZATION: Rome Air Development Center (RADC)
Hanscom AFB, MA

CONTACT: Mr. John Schott
RADC/ESR
Hanscom AFB, MA 01731
Telephone: (617) 861-3445

TYPE OF SOURCE: Room source - 20 rods approximately
12' long arranged in 5" diameter cylindrical array.

19. ORGANIZATION: Sandia National Laboratories
Albuquerque, NM

CONTACT: Dr. David Vehar
Sandia National Laboratories
Org 6452
P.O. Box 5800
Albuquerque, NM 87185, Telephone: (505) 844-4820

TYPE OF SOURCE: Gamma Irradiation Facility.
Room source with sources in one corner of
room.

Table II. Cobalt-60 Sources for Radiation Testing (continued)

20. ORGANIZATION: Southwest Research Institute Gamma Facility
Southwest Research Institute
San Antonio, TX

CONTACT: Mr. David G. Cadena, Jr., Senior Research Physicist
Department of Fuels and Lubricant Technology
Southwest Research Institute 6220 Culebra Road
San Antonio, TX 78238
Telephone: (512) 684-5111

TYPE OF SOURCE: Two hot cells.
Multiple configurations possible.

21. ORGANIZATION: TRW, Inc.
Redondo Beach, CA

CONTACT: Mr. Paul Guilfoyle
TRW, Inc. MS 84/1002 One Space Park
Redondo Beach, CA 90278 Telephone: (213) 535-0056

TYPE OF SOURCE: (1) Gammacell 220
(2) Gammacell 220

22. ORGANIZATION: University of Maryland
College Park, MD

CONTACT: Dr. Walter J. Chappas
University of Maryland
Chemical Engineering Building
College Park, MD 20742, Telephone: (301) 454-8757

TYPE OF SOURCE: Room source. 10 source pencils in cylindrical array 3.251 in diameter. Sources stored in water, raised to irradiate position 30 inches above floor.

23. ORGANIZATION: USAF School of Aerospace Medicine Isotopic Facilities

CONTACT: USAF School of Aerospace Medicine Radiation Sciences Division (RZ)
Brooks AFB, TX 78235-5301 Phone: (512) 536-3416

TYPE OF SOURCE: AECL Eldorado 78 Teletherapy unit

Table II. Cobalt-60 Sources for Radiation Testing (continued)

24. ORGANIZATION: University of Lowell
Lowell, MA

CONTACT: Mr. Tom Wallace
University of Lowell Radiation Laboratory
1 University Ave.
Lowell, MA 01854 Telephone: (617) 452-5000

TYPE OF SOURCE: Approximately 1 MCi plaque array of sources in H_2O Pool- Moved to 1/2' Al window for irradiations. 4 plugs and 4 electrical conduits for access to experiment.

25. ORGANIZATION: White Sands Missile Range White Sands, NM

CONTACT: Mr. Roland Penny
White Sands Nuclear Effects Facility Gamma
Radiation Facility
White Sands Missile Range NM 88002 Telephone: (505) 678-1161

TYPE OF SOURCE: Room source. 1 to 10 cylindrical source capsules are transferred pneumatically from storage to head assembly. Samples can be placed in cavity in head assembly for maximum absorbed dose rate.

Table III. Radiation Test Facilities from: "Programs Manager's Guide to Simulation Facilities for Nuclear Hardness Validation - 1987 Edition," K. E. Gould, et. al. DASIAC SR-219, Oct. 1987.

PULSE REACTOR	STATE	PULSE PEAK POWER (MW)	REMARKS
AFRRI Triga	MD	2.5×10^3	also steady state, biomedical
LLNL Super Kukla	NV	4.0×10^5	deactivated, in standby
WSMR FBR	NM	6.5×10^4	
SNLA ACRR	NM	3.0×10^4	
SNLA SPR-II	NM	2.0×10^5	
SNLA SPR-III	NM	2.0×10^5	

ACCELERATOR	STATE	MAX ENERGY (MeV)	X-RAY MODE DOSE	REMARKS
AFRRI Linac	MD	50.5	5 R/pulse	biomedical
Boeing Dynamitron ion capable	WA	2.8		positive
LLNL Linac	CA	50		
NRL Linac	DC	65	50 krad (Si)	
WSMR Linac rad(Si)/sec	NM			5×10^9

BREMMSSTRAHLUNG	STATE	MEAN DOSE RATE (Rads (Si)/s)	TARGET AREA (m^2)	REMARKS
Maxwell MBS	CA	1.2 x 10 10	0.3	
PI MBS	CA	2.6 x 10 11	3	
PI MBS II	CA	3.3 x 10 9	2.25	in storage

Table III. Radiation Test Facilities (continued)

FLASH X-RAY	STATE	MEAN DOSE RATE (rads(Si)/s)	TARGET AREA (m^2)	FLUENCE (cal/cm^2)
Boeing	WA	3.3×10^{11}	0.0176	
GE FX-25	PA			
NRL Gamble II	DC	4.7×10^{10}	0.1	0.1 USN
Postgrad School	CA	5.0×10^{10}	0.005	
NSWC TAGS	MD	1.0×10^{11}	0.196	

MULTI-MODE RADIATION SIMULATORS	STATE	---BREMSSTRAHLUNG MODE---- Mean Dose Rate (Rads (Si)/s)	Fluence (cal/cm^2)	Target Area (M2)	---X-RAYMODE--- Mean Dose Rate (rads(Si)/s)	Target Area (M^2)
DNA/NSWC Casino	MD				1.7×10^{10}	0.1
DNA/NSWC Phoenix	MD	3.0×10^{10}		1		
HDL Aurora 6	MD	2.5×10^{11}		1		
Maxwl Blackjack 3	CA	5.0×10^{10}		0.1		
Maxwell Blackjack 5	CA		0.1	1		
PI Double Eagle	CA	4.0×10^{10}	0.08	1		0.1
PI Owl (dismantled)	CA	5.0×10^{10}	0.08	0.1		
PI Pithon	CA	3.0×10^{11}	0.7	0.1		0.1
PI Pulserad 1150	CA	8.0×10^{10}		0.1		
SNLA HERMES II	NM				1.0×10^{12}	0.04
SNLA HERMES ITI	NM	5.0×10^{12}		0.05		
SNLA Saturn	NM	5.0×10^{12}	9.0	0.05		
TRW Vulcan	CA				1.0×10^{12}	
WSMR REBA	NM				2.6×10^{11}	

APPENDIX 7

Radiation Studies in Iron Calorimeter Structures

RADIATION STUDIES IN IRON CALORIMETER STRUCTURES

J.S. Russ
Carnegie Mellon University, Pittsburgh, PA 15213 USA

ABSTRACT

Hadronic calorimetry is a vital element of an SSC detector, but it is a major source of low energy neutrons which may damage other detector elements. Experimental data on neutron fluences are presented and compared to simulations. Implications for detectors at hadron colliders are explored.

I. Introduction

In this paper I shall be concerned with the problems of measuring and predicting the radiation environment of the LHC or SSC. As is widely appreciated, the high luminosity of these machines means that the major source of radiation damage in detector systems will be luminosity-driven, either charged particles produced directly in the collisions or neutrons generated by hadronic cascades in calorimeters or structural elements. Tracking elements placed close to the beam will be damaged chiefly by the charged- particle flux of hadrons produced directly in the collision. Calorimeter sampling elements will see low energy hadrons, electrons, or neutrons as the most damaging radiation in their environment. Because charged particle damage in detectors is well-understood experimentally [1], this paper will concentrate on the problems of calorimetry. For detectors and electronics inside the calorimeter volume, the radiation field will consist of the direct ionizing dose from the beam-beam collisions plus the displacement damage due to albedo neutrons, a calorimeter-dependent problem.

II. Radiation Environment for Calorimetry

One of the first concerns raised about detector subsystems and electronics in a high luminosity environment is about neutron damage. It is well-known that MeV-scale neutrons cause defects in silicon by elastic scatters and ensuing lattice displacements due to the recoiling Si nucleus. Neutrons also scatter in hydrogenous media, producing heavily ionizing stubs. This can perturb chamber operation, accelerate aging, and disrupt calorimetry. In order to evaluate the severity of this problem, it is necessary to predict accurately the neutron energy and spatial distributions from high energy hadron collisions. A number of elaborate neutron transport codes have been created by the neutron physics community for reactor problems.[2] Several large programs to couple these low energy neutron codes with high energy particle production models have been written by physicists concerned with shielding and radiation

protection problems.[3] It is important to provide experimental checks of these codes, to ensure that the distributions predicted in some testable cases actually are observed. This is the purpose of the ROSTI experiment to be discussed in the next section.

It has been known for years that the development of hadronic cascades in heavy absorbers, e.g., calorimetric detectors, involves nuclear processes of spallation and evaporation. After the first or second collision the number of pions and electromagnetic quanta in the cascade will be attenuated by absorption. However, the number of neutrons will continue to grow much deeper into the material because the neutrons originate primarily from evaporation processes in nuclei excited by collisions with higher energy spallation products. More recently, the crucial role of hydrogen-bearing compounds within the calorimeter volume in moderating the neutron spectrum and reducing the efficiency of the evaporation processes has been recognized, as part of the study of "compensation", i.e., equalization of the calorimetric response to electrons and hadrons of the same (large) incident energy.[4] Any measurement of the neutron flux within a calorimeter structure must not introduce low-Z elements which would modify the neutron flux. Also, the measurement should be done in a structure that accurately models the composition and layout of the real detector, since geometric and material distributions will affect tertiary neutron production probabilities. A project to use the classic neutron activation method long applied in radiation safety situations was advanced at the CERN La Thuile workshop by Russ, Stevenson and Rancoita.[5] This section discusses its implementation to study the neutron spectrum in an iron-aluminium dump, modelling an iron/silicon calorimeter. The work was done by A. Fassò, C. Furetta, P.-G. Rancoita, J.S. Russ, G. R. Stevenson, and L. Vismara, with the support of the CERN TIS division, INFN, and SSC Generic Detector program.

In measuring the neutron flux one wants to determine the neutron energy distribution at a set of points covering the solid angle around the entering particle's direction. For a dump measurement, using a parallel beam of particles of spot size small compared to the transverse attenuation length of the neutron flux, one can do this by integrating the neutron flux over many incident beam particles and doing a neutron-activation experiment. In this case the spatial distribution is determined by using activation foils of small cross section distributed throughout the transverse area illuminated by the hadronic cascade. The energy profile can be done by a subtraction method, using activation reactions with different energy thresholds. The key to the technique is to find activation reactions which are neutron-specific, so that no other component of the hadronic cascade can excite them, and which have sharp excitation thresholds. The unknown source spectrum is then found by an interative unfolding procedure, assuming initially that thresholds are sharp and that there is no energy-dependence of the cross section after turn-on.

III. ROSTI - Activation Measurement of Neutron Flux in Fe

The activation reactions chosen for the ROSTI experiment are listed in table

1. The high-energy spallation reaction producing F^{18} is not neutron-specific. It serves to measure the spallation processes and test high-energy production models which track particles down to cutoff energies of 30-35 MeV, sensitive to spallation but not evaporation. The remaining three reactions are neutron-specific with relatively sharp thresholds, as can be seen from the energy-dependence of the activation cross sections shown in figures 1(a)-1(c). This helps in the source function iteration referred to in section II. The activation foils themselves were cut into circular disks of known area and thickness, so that the number of target atoms could be determined accurately. The profile of the cascade was measured by inserting these disks into an Al carrier plate, so that the disks sampled the cascade development symmetrically about the entering beam axis. The sampling geometry is shown in figure 2. The Fe dump had 5 cm thick plates with 0.7 cm gaps. The Al carrier plates were 0.4 cm thick, and each gap contributed 0.3 cm of air. This allowed some additional shower spreading but it was not included in any detailed analysis. The overall dump thickness was 100 cm of Fe, or 5.95 interaction lengths. [measured density $\rho = 7.86\ g/cm^3$]. The dump transverse dimensions were 30 cm $\times$ 30 cm, not large in number of attenuation lengths available but adequate to see the main features of the relevant hadronic processes.

The experiment was carried out in the H6 beamline at CERN. The incident beam was 200 GeV positive, composed of 66% protons, 34% mesons.[6] Because the dump dimensions were not generous, we took care to locate the dump on the beam axis, using survey marks engraved on the front face, rear face, and top. The symmetry of the activation in the four arms of the activation foil assemblies confirmed that the surveying was good. The only deviation from symmetry was a 20% increase in the flux seen by the outer disks in the lower arm. These were adjacent to the iron table on which the dump was supported and the increased flux is interpreted as backscatter of the radially leakage from the additional iron in the 5-cm thick table top. These disks were not included in the analysis and the effects were ignored.

In order to determine the total number of interactions, the beam flux was monitored by an additional Al activation foil (0.5 mm thick) placed 60 cm upstream of the dump to avoid backsplash. The measured Na^{24} activation in this foil gave the overall integrated beam flux and hence the number of interactions. Radiography of an X-ray plate exposed to this foil determined the beam profile, elliptical with σ_x [horizontal] = 1.2 cm and $\sigma_y = 0.9$ cm.

Because of the relatively short lifetimes of the activation isotopes, one must know not only the integrated flux but also the time structure of the exposure in order to correct for decay losses and saturation. The ROSTI exposure lasted 1177 minutes, with an average intensity during the period of 1.32 x 10^7 particles/sec. The SPS cycle was a 2.2 sec spill with a 14.4 sec period. The nominal beam flux was 2×10^8 particles/spill. Instantaneous intensity was monitored by beam PWCs, which saturated under these conditions. An additional PWC monitored the transmitted flux downstream of the dump, and an ionization chamber (18 atm, argon) was set 2 meters to the side of the dump. The charge output from the ion chamber was integrated (100 s time constant) and sent to a ratemeter. These secondary monitors did not

saturate and were used to cross-check the direct beam monitors for exposure time profile information. The cross checks of all 4 monitors were very consistent, and the error on the integrated flux is no more than 10%, including the uncertainty in the Na^{24} cross section and all systematic effects. This kind of monitoring is important to obtain reliable exposure information, clearly.

Because the expected shower profile falls exponentially from the beam axis, the disk areas increased as the radius. The central disks were 1 cm in diameter; the outer disks were 3 cm diameter at 13.5 cm off axis. By this means the total activation of each disk was kept constant to roughly a factor of two, and the systematics of counting errors in the activation measurements were kept to a minimum. The Al activations were measured in a shielded, calibrated NaI counting system. The counting efficiency was measured using known sources. The Geiger counter for the P^{32} decay was calibrated with a β standard, and the In^{115m} decays were measured in a GeLi detector system again calibrated against an X-ray standard. The backgrounds in these decay measurements were reduced by counting each activation foil 3 times and fitting to the known lifetime curve to determine the true activation level extrapolated to the time of the exposure. Errors due to counting statistics were a few percent in all but the extreme radial points on the measurements.

The major source of uncertainty in the activation analysis is not counting-related, but stems rather from the cross section assumptions in modelling the energy dependence and in assuming that reactions are solely neutron- produced. Due to these uncertainties, we estimate that the overall normalization is good to a systematic uncertainty of $\pm$ 50%. The relative normalization within a single element is much better, of order $\pm$ 10%.

Because the measured activation rates were symmetric about the beam axis, measurements at equal radii were combined to determine the transverse profile of the cascade. There was substantial transverse leakage of shower particles. A factor of 1.8 correction to the total flux was determined from transverse integrals of the observed activation at all energies. As shown in figure 3(a)-3(c) the transverse attenuation of the shower at all energy regions was roughly exponential. The lowest energy component of the cascade, measured by the Indium foils, has a noticeably shallower slope than the higher energy components. This is consistent with the expected combination of spallation and evaporation as the source of the neutrons within the hadron cascade.

The transverse samples at each layer can be integrated and corrected for the sampling fraction to give the total number of neutrons crossing a given sampling layer. The resulting longitudinal shower profile for the four different energy bands is shown in figure 4. The energy leakage after six interaction lengths was estimated from the longitudinal cascade development to be 15% at 200 GeV. This is the same as the albedo leakage. In both cases the flux is dominated by the lowest energy components of the cascade, neutrons below 2 MeV. Again, one notes that the higher energy neutrons, especially the spallation neutrons, originate earlier in the shower

than the lowest energy neutrons. The distribution again supports the picture of a multi-step production process, with high energy particles produced by spallation and exciting other nuclei to emit evaporation neutrons. Figure 5 shows the success of a high-energy production model(FLUKA, ref. 3) in fitting the observed spallation-product distributions, both in shape and in normalization.

The success of the FLUKA model in representing both normalization and depth distribution of the spallation products from fig. 5 led us to push the idea of spallation followed by evaporation as the source of all low energy neutrons. G. Stevenson took the FLUKA spallation points and generated 10 isotropically- distributed evaporation neutrons with a 10 cm attenuation length. All evaporation neutrons were assumed to lie in the energy range unique to In^{115}. The neutron fluence as a function of depth and transverse position for the ROSTI data sample was then calculated. Note that this is an absolute comparison; every beam particle is accounted for. Figure 6 compares the model output to the In^{115} data. The agreement, with no free parameters, is excellent everywhere. This not only illustrates the underlying physics, but also gives a computational algorithm for modelling neutron fluxes for damage calculations. This code is much simpler and hence much faster than the elaborate reactor codes (MORSE) used in full simulations to handle the low energy neutron production. These same ideas will soon be checked against the 24 GeV data to verify the range of applicability.

One can combine the information in these measurements to estimate the total number of neutrons generated per 200 GeV hadronic interaction, as well as compute the energy flux carried by neutrons of different energies. At 200 GeV at the maximum of the hadronic cascade we observe 540 $\pm$ 270 neutrons, of which 80% lie between 0.8 and 2.0 MeV, the indium band. [The quoted error is systematic. Statistical error is negligible.] The albedo flux is 45 $\pm$ 22 neutrons, again with 80% in the indium band.

In order to generalize this measurement to the overall hadronic cascade problem, some ansatz must be made about the energy dependence. Existing data favor a power-law relationship between the number of secondaries and the energy of the hadron which initiates the cascade:

$$N_{sec} = k\left(\frac{E_{inc}}{E_o}\right)^{0.85}$$

This produces a scaled neutron flux at shower maximum of

$$N_o\ (cascade\ maximum) = 7.8\ neutrons/GeV^{0.85}$$

and an albedo flux of

$$n_o\ (albedo)\ =\ 0.7\ neutrons/GeV^{0.85}$$

One can compare these results to calculations using a full high energy production code plus neutron cascade Monte Carlo, e.g., the CALOR code from ORNL.[3] Calculations were done for an iron/silicon calorimeter at 20 GeV.[7] The comparison of the spectra predicted for the same depth in the stack are shown in figure 7. The agreement in normalization and spectral distribution is excellent, using the central values of the measurement. The model predicts a very large flux of soft neutrons which fall below the measurement threshold of the ROSTI foils. An improved version of the apparatus using Rhodium was exposed to the 24 GeV proton beam from the CERN PS machine. Analysis of those data are nearing completion. They will provide a direct test of the energy scaling law assumed in the Monte Carlo comparison. From just these data, along with the simulations, one concludes that the neutron flux between 0.2 and 2.0 MeV is the most serious source of damage in silicon, and that neutrons in the spallation energy range, above 30 MeV, are the most important for energy transport. Therefore, neutron detection in calorimeters needed to achieve compensation may focus either on efficient sampling of low-energy neutrons (scintillation calorimeters) or in good sampling of high energy neutrons.

IV. FUTURE WORK

The ROSTI group has been joined by members of the SICAPO collaboration at CERN to continue the study to other materials and other energies. As mentioned we are just finishing a study of the ROSTI dump exposed to 24 GeV protons from the PS. These results will test the energy scaling mentioned above in the Monte Carlo comparison. That run also introduced Rhodium foils, sensitive to neutrons down below 0.5 MeV. Results from that run will be given in Como this June, giving a comparison of neutron spectra from 200 GeV and 24 GeV incident hadrons in Fe.

The ROSTI group will then turn PLUMB SILLY, exposing a Pb dump with Al plates to simulate a Pb/silicon calorimeter stack. This dump is now ready at CERN, and we expect to install it in the H6 beam again in April. Later in the summer we hope to take it to the PS again for another 200 GeV and 24 GeV comparison.

V. CONCLUSIONS

The neutron energy and spatial distributions have been measured for an iron dump exposed to a 200 GeV positive hadron beam at the CERN SPS. The data agree well with a picture of evaporation-dominance of neutron generation in the hadronic cascade. The neutrons below 2 MeV consititute 80% of all neutrons and dominate the albedo and leakage neutron fluxes. The transverse attenuation of the neutrons is exponential at all energies, with a transverse attenuation length of 7.5 cm for the higher energies and about 10 cm for the lowest (1 MeV) part of the flux. The longitudinal shower development peaks near 2 interaction lengths, somewhat deeper

for the lowest energy band. The albedo flux is about 10% of the neutron flux at the cascade maximum.

To see the implications of these data for the LHC or SSC, consider the fluxes expected on the basis of high energy interaction models like DTUjet or ISAJET. Take an operating year to be 10^{15} interactions. For a calorimeter of inner radius of 0.8 m, the annual dose at cascade maximum will be about 6×10^{11} neutrons/cm^2 at $\eta = 0$ and 6×10^{12} neutrons/cm^2 at η=2.5, chosing a distance from crossing point to the start of the EM section of the calorimeter to be 3.8 m and taking the cascade maximum to be at 3 Λ_{int} for the 1 MeV neutrons. [Note: The neutron flux at $\eta = 0$ is overestimated in this extrapolation. This incident spectrum in the central ± 1 unit of rapidity is soft enough that many of the charged hadrons will stop by ionization loss before they interact. This phenomenon is not included in the energy scaling law used here.]

LIST OF REFERENCES

1) H. Dietl, P. Gooch, R. Klanner, M. Pepé, and F. Wickens, Nucl. Instr. & Meth. A253(1987)460 for silicon detectors

   Conference on Aging in Wire chambers and J. Vavra, Nuc. Instr. & Meth. A252(1986)547 for gaseous detectors

2) MORSE, Neutron and Gamma-ray Transport Code, Oak Ridge National Laboratory CCC-474 (1987)

3) CALOR: J. Brau and T.A. Gabriel, Nucl. Instr. & Meth. A238(1985)489 see also T.A. Gabriel, ORNL/TM-9727(1985)

   FLUKA: P.A. Aarnio, A. Fassò, H.J. Möhring, J. Ranft, and G.R. Stevenson, CERN TIS-RP/168 (1986)

4) H. Brueckmann, et al., Nucl. Inst. & Meth. A263(1988)136 J.E. Brau and T.A. Gabriel, Nucl. Inst. & Meth. A279(1989)40 R. Wigmans, Nucl. Instr. & Meth. A259(1987)389

5) T. Akesson, M. Albrow, P.N. Burrows, T. Cox, J.P. deBrion, C. Fabjan, M. Holder, G. Ingelman, G. Jarlskog, K. Meier, P.G. Rancoita, J. Russ, J. Schukraft, G. Stevenson, A. Weidberg, and R. Wigmans, "Detection of Jets Future Accelerators" in Proc. of the Workshop on Physics at Future Accelerators, CERN 87-07, p. 182 (1987)

6) H.W. Atherton, C. Bovet, N. Doble, G. von Holtey, L. Piemontese, A. Placci, M. Placidi, D.E. Plane, M. Reinharz, and E. Rossa, CERN 80-07 (1980)

7) J.E. Brau and T.A. Gabriel, "Calculations of Neutron Flux in Iron and Uranium Calorimeters" in SSC-SR-1033, D.E. Groom, ed. (1988)p. 217 Note that the ordinate in figs. 7-10 of appendix 15 is too large by a factor of 2, due to a scaling error. (J. Brau, private communication)

LIST OF FIGURES

Figure 1 Energy dependence of neutron-specific activation cross sections
(a) $In^{115}(n,n')In^{115m}$
(b) $S^{32}(n,p)P^{32}$
(c) $Al^{27}(n,\alpha)Na^{24}$

Figure 2 Iron Dump design for ROSTI, showing sampling element layout

Figure 3 Transverse variation of neutron fluence for different neutron energy bands:
(a) Na^{24} (6-20 MeV)
(b) P^{32} (2.5-15 MeV)
(c) In^{115m} (0.8-14 MeV)

Figure 4 Radially-integrated fluence versus depth, uncorrected for transverse leakage. [Factor of 1.8 in normalization; see text]

Figure 5 Comparison of FLUKA model predictions for spallation product depth profile with F^{18} excitation measurements.

Figure 6 Transverse distribution on neutron fluence measured by the IN^{115} foils at different depths, compared with the evaporation model described in the text. This comparison is absolube.

Figure 7 ROSTI 200 GeV data scaled to 20 GeV by $E^{0.85}$ scaling compared to CALOR Monte Carlo calculations from ref. 7. The Monte Carlo spectrum is folded with the activation cross sections from figure 1 to predict the number of neutrons in each energy interval. The ROSTI data are subtracted to give the number of neutrons in the energy region covered by each material uniquely, i.e., 0.8-2.4 for In^{115m}, 2.4-6.0 for P^{32}, and 6.0-12.0 for Na^{24}

Table I

Neutron Activation Reactions

Reaction	Energy	Range	Effective Cross Section
Al^{27} (h,x)F^{18}	35 -	MeV	7 mb
Al^{27} (n, α)Na^{24}	6.5 - 25	MeV	85 mb
S^{32}(n, p)P^{32}	2.0 - 25	MeV	280 mb
In^{115}(n, n')In^{115m}	0.8 - 12	MeV	210 mb

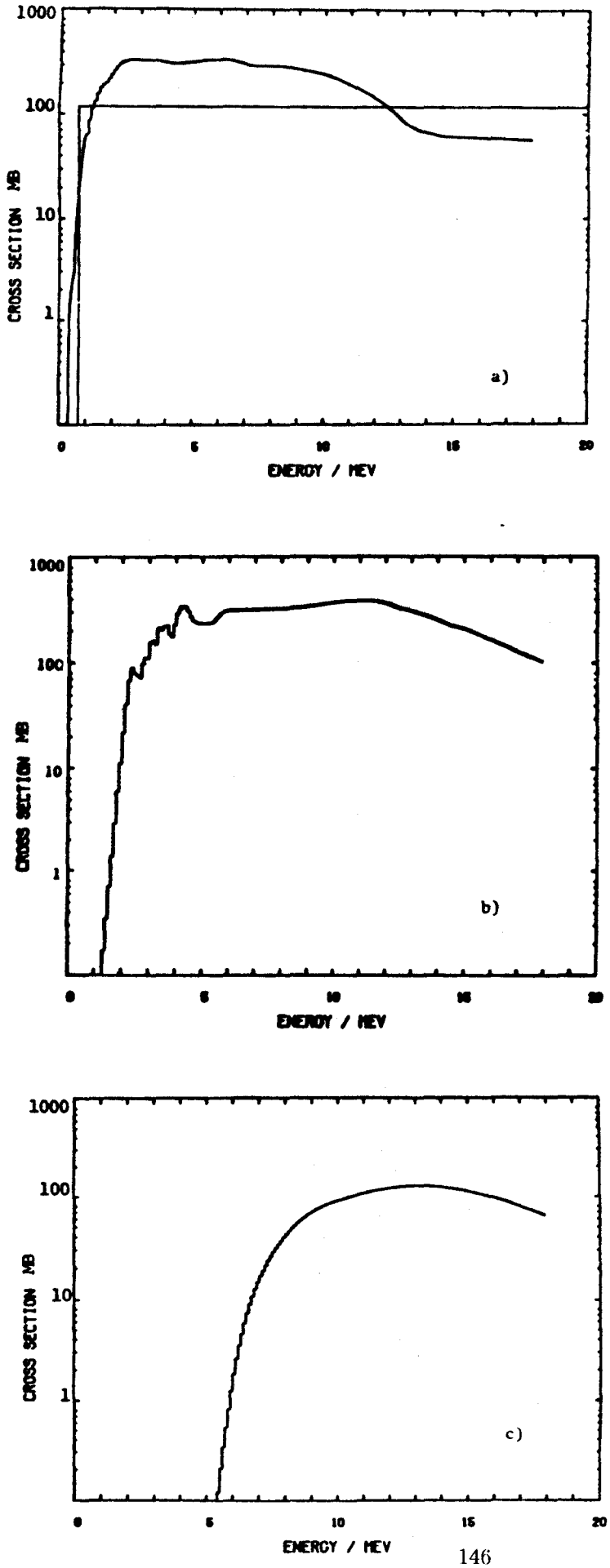
1000
100
10
1
CROSS SECTION MB
a)
0
5
10
15
20
ENERGY / MEV
1000
100
10
1
CROSS SECTION MB
b)
0
5
10
15
20
ENERGY / MEV
1000
100
10
1
CROSS SECTION MB
c)
0
5
10
15
20
ENERGY / MEV

Figure 1

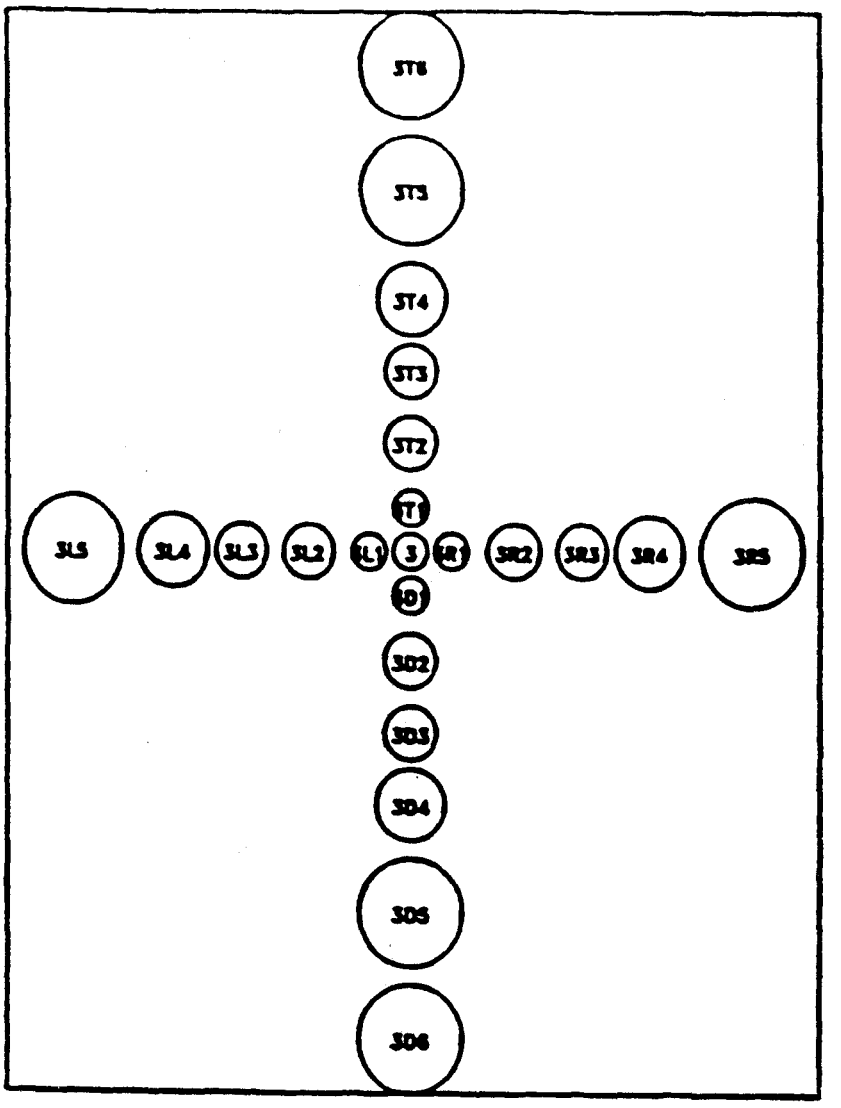
ST6
ST5
ST4
ST3
ST2
ST1
SL5
SL4
SL3
SL2
SL1
S
SR1
SR2
SR3
SR4
SR5
SD1
SD2
SD3
SD4
SD5
SD6

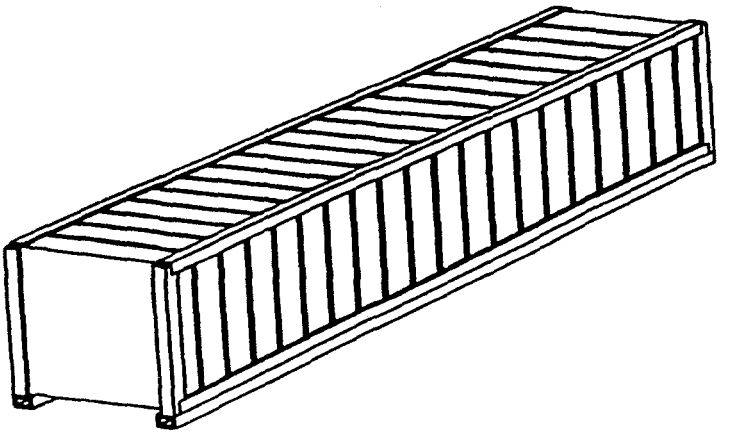

Figure 2

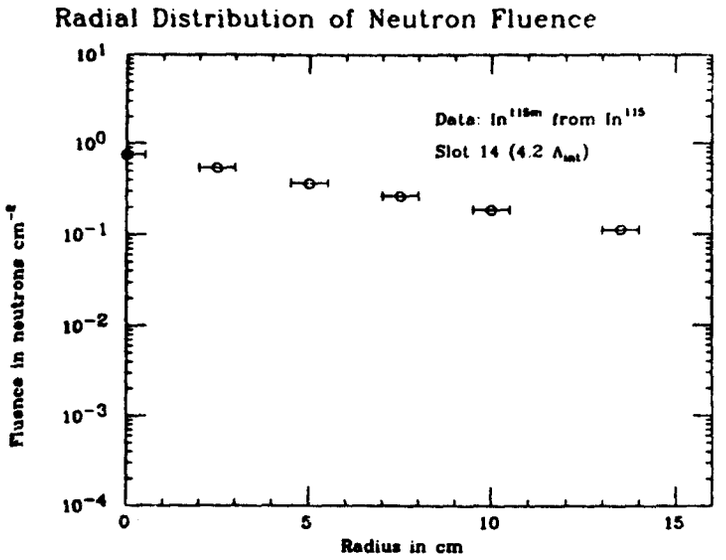
Radial Distribution of Neutron Fluence
Data: In115m from In115
Slot 14 (4.2 Λint)
Fluence in neutrons cm-2
Radius in cm

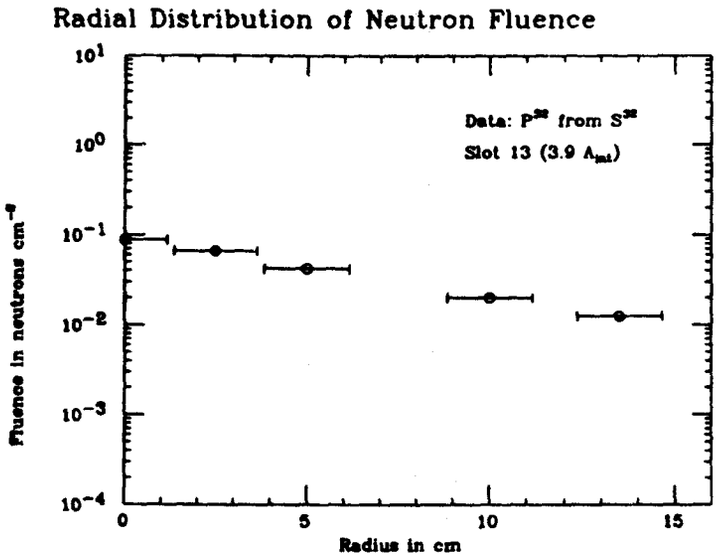
Radial Distribution of Neutron Fluence
Data: P32 from S32
Slot 13 (3.9 Λint)
Fluence in neutrons cm-2
Radius in cm

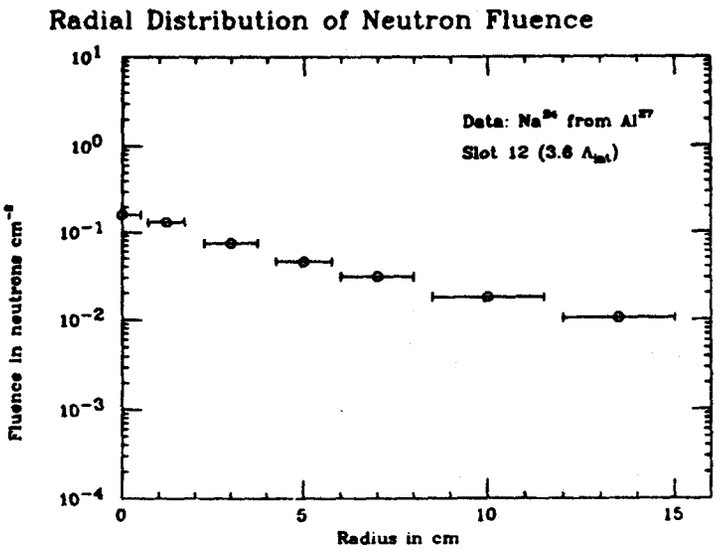
Radial Distribution of Neutron Fluence
Data: Na24 from Al27
Slot 12 (3.6 Λint)
Fluence in neutrons cm-2
Radius in cm

Figure 3

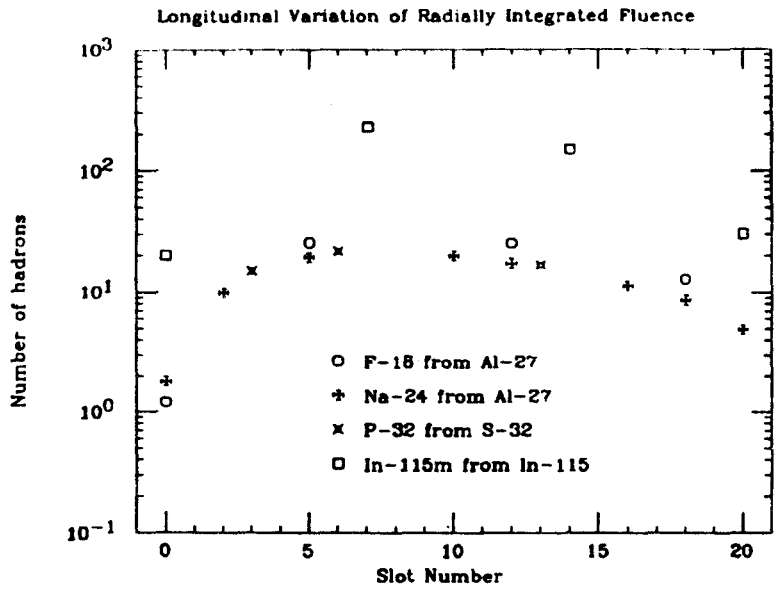

Figure 4

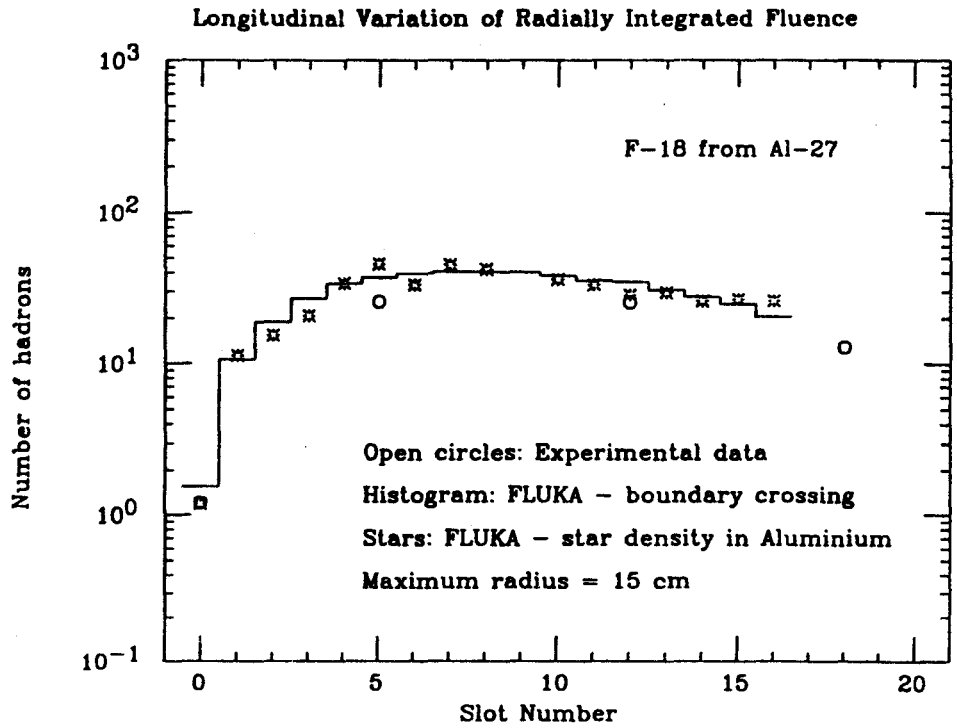

Figure 5

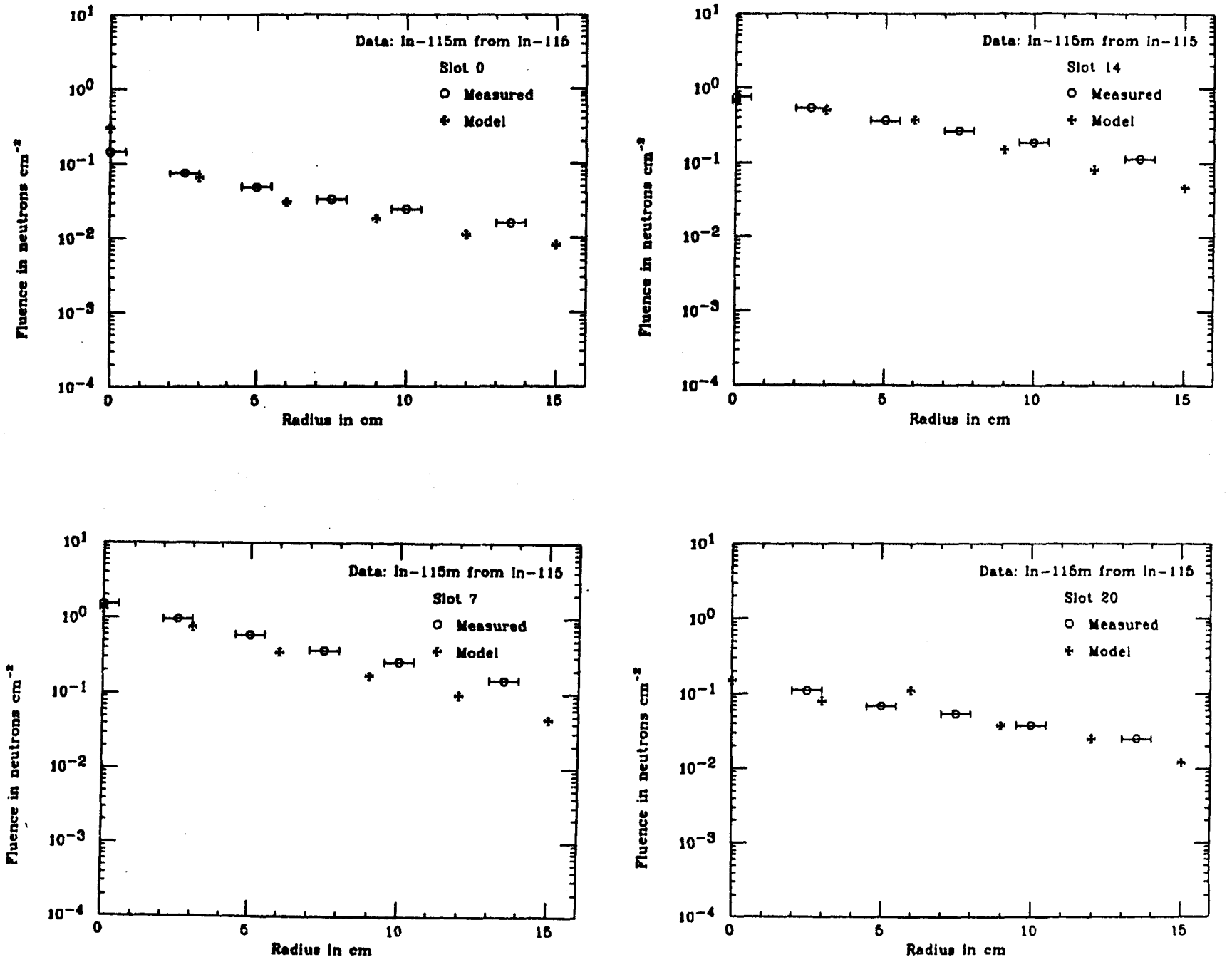
Data: In-115m from In-115
Slot 0
Measured
Model
Slot 14
Slot 7
Slot 20
Fluence in neutrons cm^{-2}
Radius in cm
10^{1}
10^{0}
10^{-1}
10^{-2}
10^{-3}
10^{-4}
0
5
10
15

Figure 6

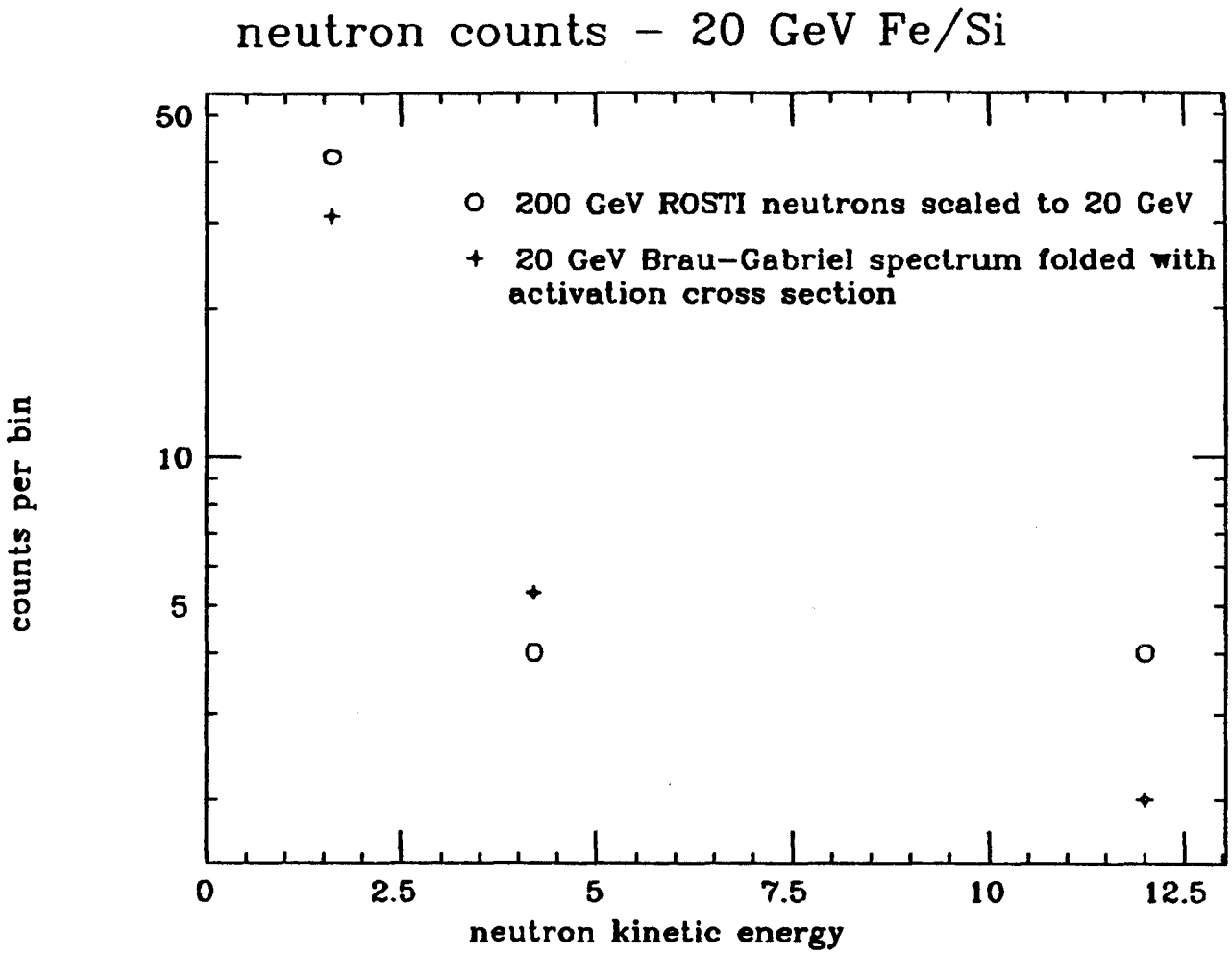
neutron counts – 20 GeV Fe/Si
50
10
5
counts per bin
O 200 GeV ROSTI neutrons scaled to 20 GeV
+ 20 GeV Brau–Gabriel spectrum folded with activation cross section
0
2.5
5
7.5
10
12.5
neutron kinetic energy

Figure 7

APPENDIX 8

Comments on Radiation Damage Tests with Neutron Sources and Other Available Sources

COMMENTS ON RADIATION DAMAGE TESTS WITH NEUTRON SOURCES AND OTHER AVAILABLE SOURCES

H. W. Kraner
Instrumentation Division
BNL

We have irradiated a variety of germanium and silicon detectors at accelerators and fixed, radioactive neutron sources. The following is an anecdotal description of some of this experience. It is not meant to be an exhaustive or highly researched compendium of the options for irradiations. Many nuclear physics texts and review volumes contain basic information on which these facilities are based; one to recommend is Experimental Nuclear Physics (1). Fast neutrons are produced in generally three types of sources:

1. A sealed, shielded radioactive source containing a mix of an alpha emitter and beryllium giving neutrons from the Be(a,n) reaction.

2. Particle accelerators producing neutrons from a given nuclear (low energy particles) or spallation reaction from high energy particles (protons)

3. Reactors, continuous power or pulsed.

There is some predisposition away from reactors (3) as the neutron spectrum can be relatively unknown and variable from reactor to reactor; we have had no direct experience with irradiations from reactors and they will not be listed. Table I lists a number of fast neutron producing facilities of experience and others which have some application to SSC problems. Table II lists other facilities which will also be of some interest to device qualification in general.

This table contains a heading: "Dosimetry/Availability" which is also marked in some cases with an asterisk(*) indicating a "USER FACILITY". This distinction is thought to be important and is perhaps best operationally defined: "a facility to which samples may be brought for irradiation that is managed by a knowledgeable operator, is in good repair and requires virtually only sample placement to set up for use". For these amenities one is usually charged a daily or hourly fee. For example, the University of Lowell Van de Graaff charges $1200 for an 8 hour shift of beam on target; following shifts are available at a lesser rate. One can also expect information about the faciltiy to be readily available and the facility will provide verifiable dosimetry and a concise report of the irradiation. Other help during the irradiation will be available in most case, computer facilities, scopes, meters, etc.

The following discussion will amplify some of the information given in the Table.

NEUTRON ENERGY SPECTRUM

A 3.5 MV Research Van de Graaff at BNL has been used to provide mostly monoenergetic fast neutrons from the D(D,n)3He (Q=3.1 MeV, En=2.5 MeV+Ed), D(T,n)4He (Q=18 MeV, En=14 MeV+ Ed) and 7Li(p,n)7Be (Q=-1.6 MeV, En=-1.88 MeV+Ep) reactions using "thin targets"--thicknesses of a few mg/cm2. At the present time this machine is not running routinely and is mentioned here to introduce the subject from direct experience. There are quite probably many such machines available in nuclear physics laboratories with the capability of producing useful neutron beams with these reactions that are not listed in the Table. Given the cross sections and the use of thin targets to preserve a narrow energy distribution of the neutrons and the low beam currents of barely 10 uA from an aging machine, neutron fluxes of 10E6/cm2-sec a few cm from the target in the forward direction were available. For studying charge collection effects in germanium detectors, upwards of 10E10 n/cm2 were required and this flux was adequate. Some information about the energy dependence was desired, hence the use of those reactions and thin targets.

From the table of sources, a higher current DD and DT machine is available at the Nevis Lab of Columbia University, the "RARAF". This is a well cared-for 4 MV Van de Graaff that started life as the injector for the BNL Cosmotron. Beam currents to 140 uA are available on this machine; they still use essentially thin targets. Most of their applications are biological. A typical irradiation protocol is included as Figure 1. A fluence of 1.4x10E12 neutrons/cm2 can be obtained in 8 hours at 10 cm from the target (or 5.6x10E12/cm2, 5 cm from the target) and these are quite monoenergetic 6 MeV (+/- 6%) neutrons. Higher yields can be achieved if somewhat thicker targets are used. Higher yields can also be derived with the DT reaction, producing higher energy neutrons, perhaps less equivalent to SSC applications.

We have recently used the Van de Graaff at the University of Lowell, MA, which is available to routinely produce large fluences of fast neutrons using the 7Li(p,n) reaction in a thick target (2). This is a type C, relatively new single-ended vertical Van de Graaff, that runs comfortably at 20 uA, 4 MV. Using a thick, pressed lithium metal target water cooled, 10E13 n/cm2-8 hour shift can be obtained at 5 cm from the target in the forward direction. In this case the monenergetic spectrum is sacrificed to achieve yield. A calculated neutron spectrum from 2.2 Mev to 10 KeV

is available. No thermal neutrons are produced as verified by no discernable activation of irradiated parts, etc. Because the cross section is well known over the proton energy range, calculated spectra and kerma values for displacement damage are regarded as reliable (+/-20% is reasonable).

Radioactive sources have been used for many years as neutron sources through the Be(a,n) reaction with the alphas provided by intermixed Ra, Po, Pu, Cm or Am. AmBe sources are now more common as PuBe sources have been suppressed because of the use of the "special nuclear" Pu, even 238Pu. RaBe, the historic source, emits an intolerable background of gamma rays. PoBe sources are short lived. PuBe sources once had the attractive feature that sources would be more identical from source to source than earlier sources because the Pu was alloyed with the Be and all sources were more or less PuBe/13 in intimate contact. They did not rely on intermixed grains for their characteristic spectrum.

The spectrum of all (a,n) sources is similar as they all use the same reaction on Be, having Q= 5.7 MeV to the ground state: the highest energy neutron group is centered between 6 and 10 MeV and is the ground state transition from the excited 12C+n compound nucleus; a mid energy group from transitions to the 4.4 MeV first excited state of 12C and a lower energy group from transitions to the 7.5 MeV excited state. A calculated spectrum (3) is shown in Figure 2 and it agrees well with measured spectra (4). Very little thermal flux is expected or observed.

Fluxes of neutrons in the 10E7/sec (into 4pi) are achieved with sources having in the range of 10Ci or more of contained alpha activity. These are useful, then, for studies needing up to 10E11n/cm2. With the lesser availablity of PuBe sources which may (or may not) be alloyed, suppliers suggest AmBe sources which are, they say, well mixed and can be certified source to source. CmBe sources may provide higher specific activities than AmBe sources.

252Cf is also a common source of neutrons emitting a fission spectrum through spontaneous fission. We have had no direct experience with this source, however it is routinely available and used by others.

NEUTRON FLUENCE DETERMINATION

Both Van de Graaff facilities used were equipped with an ancient "long counter" (5) which is placed several meters from the target in the same direction as the samples to be irradiated. The long counter is a barrel of paraffin with a BF3 counter along its axis and has a remarkably flat

efficiency versus neutron energy response. It is calibrated with a neutron source (eg PuBe) whose emission rate is known and traceable to NBS certification. Because of the flat energy response, this calibration serves for whatever energy neutrons are generated by the machine. Some correction to the response may be included for 14 MeV neutrons or above. Other such flat response counters include the well-known "Bonner Ball", a sphere of hydrogenous material with a scintillation detector in the middle.

The Lowell Van de Graaff uses an interesting method in addition to the long counter to estimate fluence. From the 7Li(p,n)7Be reaction, one produces the daughter, 7Be, which is radioactive and emits in its decay a 477 keV gamma ray. The target is demounted after a day of running and after a convenient time for it to decay somewhat is counted by a calibrated GeHP detector to determine the amount of 7Be formed during the run. This is a direct measure of the neutrons produced and is usually in good agreement with the long counter measurement.

It is customary and prudent to do neutron irradiations in an area which is not confined by concrete walls or floors or other scattering media. The target should be several meters from walls--the scattering room should not be a "cave". As much as 20% albedo may be expected from closely adjacent shielding.

NEUTRON PRODUCING TARGETS

Targets for the particle beams must dissipate considerable energy: 4 MeV and 20 uA is about 100 watts, not an untypical situation. Therefore they are generally water-cooled. A copper tube target was developed at BNL and is still in use at the RARAF. A 1/2" diameter copper tube is flattened in a jig but not so much to restrict water flow. The flat can be vacuum held to the end of the beam pipe. In the spot inside the beam pipe-usually about 3/8" diameter-is deposited the target material. For DD and DT targets, 1-5 mg/cm2 Ti is evaporated and reheated in a deuterium (or tritium) atmosphere. On cooling, the Ti becomes largely hydrated with deuterium and a rugged, thin target is formed. The target thickness and deuteration is noted in the RARAF protocol, Figure 1. The target as noted is 740 keV thick and with 140 ua of beam, one has again 100 watts in the target material to dissipate.

For the Li target used at Lowell, a slug of Li metal is quickly pressed into a planchet that receives the water cooling tube on the back. Barely 100 watts can be dissipated and it was suggested that the target may well be molten-or at least plastic-under irradiation. These comments are inserted to emphasize that the high current target technology must be

considered and respected.

OTHER USER FACILITIES

There are several user-type facilities that provide high energy protons, which may have some relevance for the SSC. They are listed in Table II. High energy proton facilities include the Radiation Effects Facility at BNL, the Indiana U. Cyclotron and the UC Davis Cycltron. A separate presentation describing LAMPF is given in this report. The former three facilities present themselves as USER facilities and would like to receive customers. Each machine provides copious doses of protons at 20 to 200 MeV

Perhaps less germane to the SSC requirements, but a well used accelerator facility that should be mentioned is the Single Event Upset Faciltiy at BNL which uses one or both of the MP tandems ("two or three staqe operation") to deliver ions from hydrogen to uranium from a few MeV to over 350 MeV for uranium. A dedicated beam line with large area sample positioning, beam spread and energy control is provided and is shown schematically in Figure 3.

In a separate presentation, Ed Petersen has listed a variety of 60Co irradiation facilities in the US. We add to this list the BNL facility which is available to users and will soon contain a 20 KCi source in place of the present 500 Ci source. Experiment specific dosimetry is available and convenient operation is assured.

REFERENCES

1. Experimental Nuclear Physics, Vol.II, E. Segre', ed., John Wiley, NY (1953).
   Properties of Neutron Sources, IAEA-TECDOC-410 (1987)

2. G. H. R. Kegel, Nucl. Inst. and Meth. in Phys. Res., B 40/41, 1165 (1989).

   G. H. R. Kegel, Comp. Phys. Comm. 36, 321 (1985).

3. K. W. Geiger and L. van der Zwan, Nucl. Inst. and Meth. 131, 315 (1975).

4. A. D. Vijaya and A. Kumar, Nucl. Inst. and Meth. 111, 435 (1973).

5. A. O. Hanson and J. L. McKibben, Phys. Rev. 76, 577 (1949).

TABLE I

FAST NEUTRON SOURCES FOR SAMPLE IRRADIATION

* = USER FACILITY

SOURCE	ENERGY	FLUX	DOSIMETRY AVAILABILITY	INSTITUTION -CONTACT
Neutron Source Be(α,n)	0.5-8 MeV	10^7-10^8 n/sec	yes/yes	Various - BNL PuBe,AmBe
Van de Graaff D,(D,n)^{3}He E_n=2.5MeV+E_D	6 MeV ± 6% Thin Target	$5x10^7$/cm^2 @ 10 cm $1.4x10^{12}$/cm^2 - 8 hrs.	yes/yes* $1200/day	Columbia U. "RARAF" Steve Marino 914-591-9244
Tandem Dynamitron Be(d,n) Q= +4.3 MeV	.2-6 MeV (7MeV D) Thick target	$3x10^9$n/sr-μC @ 10μA, 5cm from target $4x10^{13}$n/cm^2 - 8 hrs.	yes/yes	D.L. Smith et al., ANL 708-972-6021
IPNS-ANL Spallation Neutrons U(p,xn...)		> 10^{14}/shift	yes/	c.f. John Dawson ANL, this report 708-972-6541
Van de Graaff ^{7}Li(p,n)^7 Be E_n = -1.88 MeV+E_p	10 keV- 2.2 MeV Thick Target	10^{13}n/cm^2 - 8 hrs. @ 20μa - 4 MeV 5cm from target	yes/yes* (^{7}Be) $1200/8hrs .	U. Lowell MA Prof. G. Kegel 508-934-3280

Generally:
-others
D,D 2.5 MeV+
D,T 14 MeV+

TABLE II

OTHER IRRADIATION USER FACILITIES AVAILABLE FOR SSC QUALIFICATION

* = USER FACILITY

SOURCE	ENERGY	FLUX	DOSIMETRY AVAILABILITY	INSTITUTION -CONTACT
Protons- BNL REF AGS Linac	100-200 MeV	10^{14}p/pulse single pulse→ 5 pulse/sec 2 cm dia. spot→	yes/yes*	BNL - C.L. Snead 516-282-3502
Protons- Indiana Cyclotron	p to 200 MeV d to 100 MeV also n's liq. D_2O (p,n)	10^6p/cm^2-sec from 5 mm^2 - 25 cm^2	yes/yes*	Indiana U. Dennis Friesel 812-855-2944
Protons- Davis Cyclotron	p to 100 MeV			Contact: Ken Murray, UC Davis, CA or E.L. Petersen, NRL
Heavy Ions BNL Tandems	^{1}H→U 35 MeV→ 350 MeV	10^2/cm^2 - 10^{12}/cm^2	yes/yes* ~ $500/hr.	BNL - Single Event Upset Facility P. Thieberger 516-282-4581
Gamma Rays - ^{60}Co irradiators (typical)	1.2 MeVγ	Soon to be 200 KRad/hr.	yes/yes*	BNL - Paul Levy, H. Kraner 516-282 3170;4238

PROGRAM TTANY 01-MAR-90

TEST

2H (D ,N) 3HE BOMBARDING ENERGY 3.100 MEV

TARGET NO.	2H D-9	
REFERENCE KERMA RATE	0.00	MRAD/UA-H
FOR 1.000 MEV, 0.0 DEG . 0.0 CM		
ACTIVE TARGET THICKNESS RELATIVE TO INITIAL	100.0	PER CENT
OBJECT SIZE FOR ENERGY SPREAD CALCULATION	1.00	CM
BEAM SPOT DIAMETER	0.60	CM
CURRENT LIMIT DUE TO TARGET TEMPERATURE RISE	116.7	UA
CURRENT LIMIT DUE TO ACCELERATOR	177.0	UA
TOTAL TARGET THICKNESS	5.87	MG/CM2
2H/TI = 1.58		
TARGET THICKNESS USED	5.87	MG/CM2
INCIDENT PARTICLE ENERGY UPON LEAVING TARGET	2.359	MEV
ENERGY LOSS IN TARGET	0.741	MEV
EFFECTIVE HALF-ANGLE	4.57	DEGREES

NEUTRON EMISSION ANGLE (DEGREES)	DISTANCE TO OBJECT FRONT (CM)	NEUTRON ENERGY (MEV)	ENERGY SPREAD (%)	KERMA RATE (MRAD/UA-H)	KERMA SPREAD (%)	NEUTRON FLUX (NO/UA-S-CM2)	FLUX SPREAD (%)
0.00	10.00	6.015	+ 5.9 - 6.8	5804.82	+ 0.6 - 0.9	3.464E+05	+ 0.[illegible] - 0.[illegible]

$3.5 \times 10^{5}/\mu A\text{-}s\text{-}cm^2 \rightarrow 5 \times 10^{7}/cm^2\text{-}s$ at $140\ \mu A$

or $1.8 \times 10^{11}/cm^2\text{-}hr$ — $1.4 \times 10^{12}/cm^2\text{-}shift$

FIGURE 1. RARAF FACILITY RUN DATA SHEET

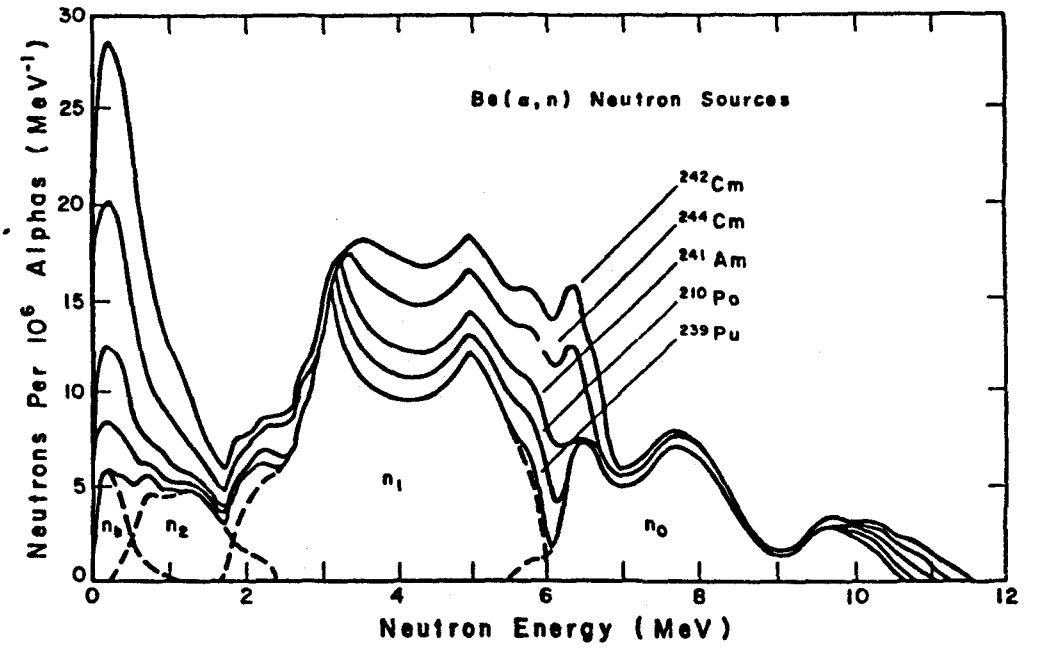

The calculated energy spectra of several Be(α, n) neutron sources. From K. W. Geiger and L. van der Zwan, Nucl. Inst. and Meth., 131(1975),315.

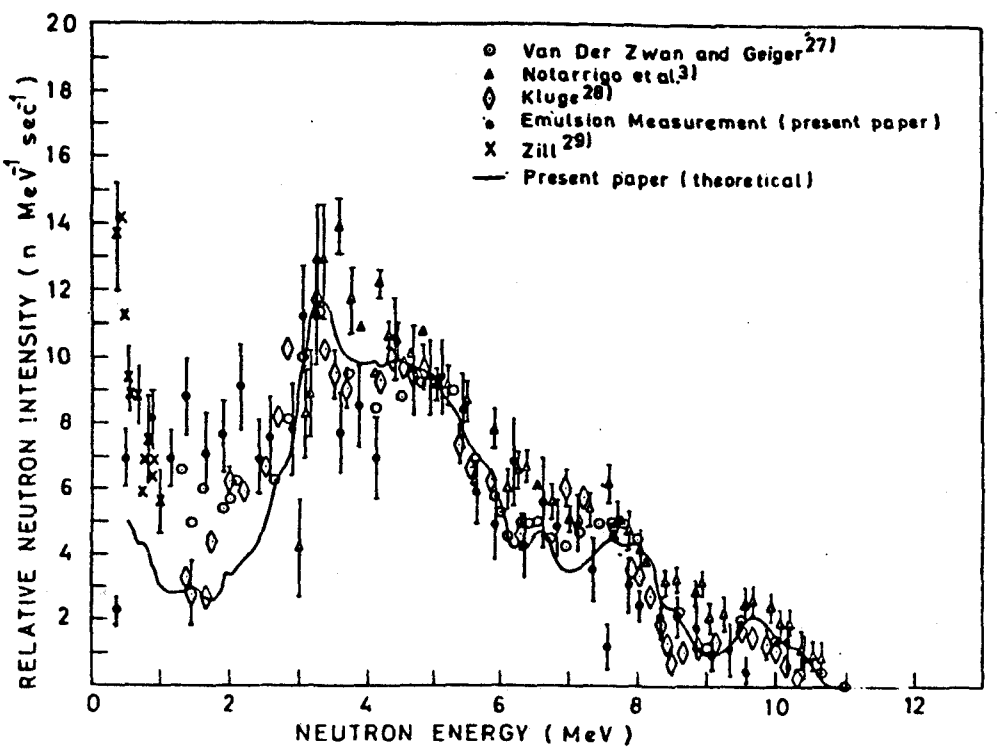

The comparison of measrements of the ^{241}AmBe Neutron energy spectrum with calculated spectra. From A. D. Vijaya and A. Kumar, Nucl Inst, and Meth. 111(1973),435.

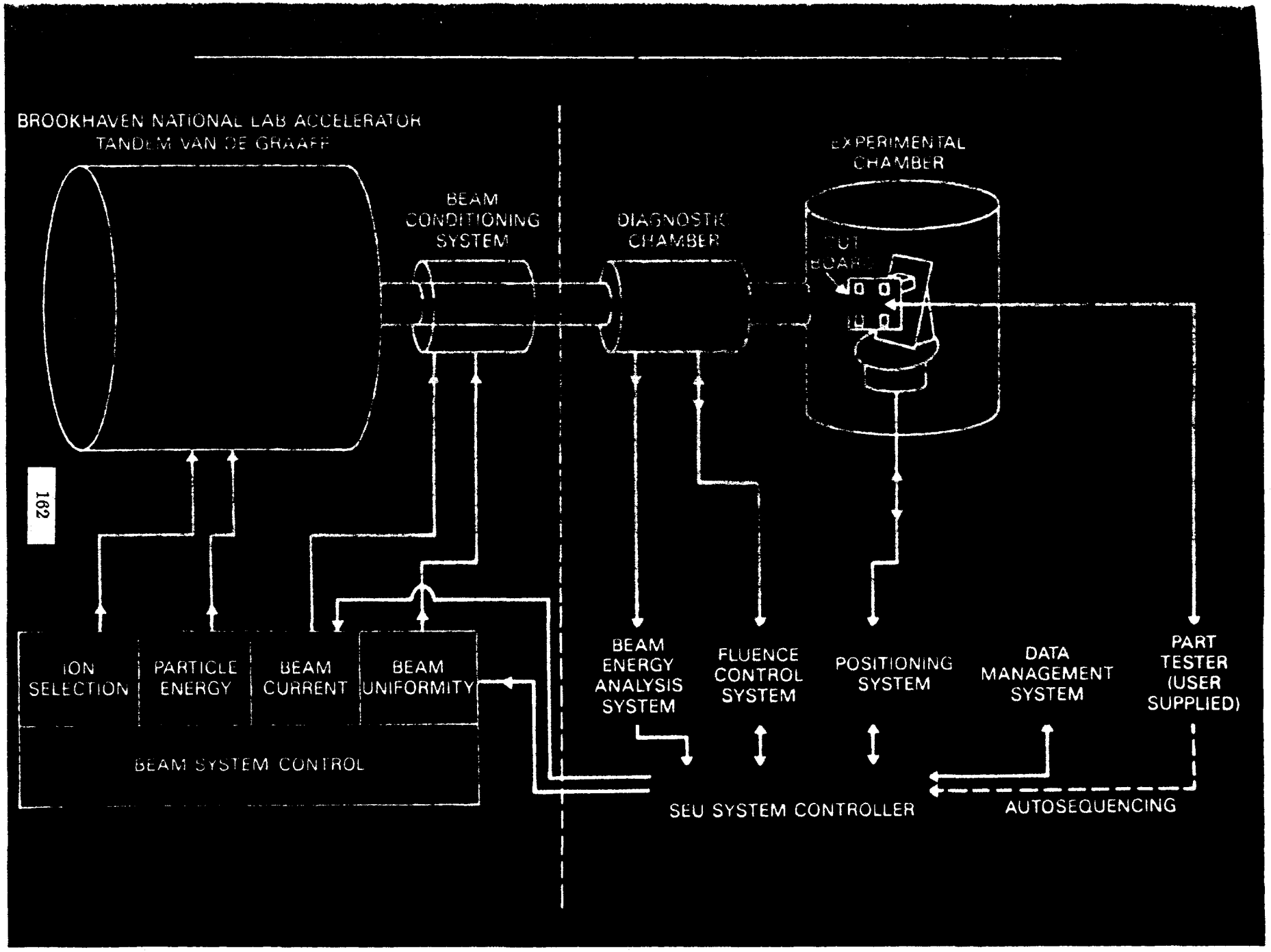
BROOKHAVEN NATIONAL LAB ACCELERATOR
TANDEM VAN DE GRAAFF
BEAM CONDITIONING SYSTEM
DIAGNOSTIC CHAMBER
EXPERIMENTAL CHAMBER
ION SELECTION
PARTICLE ENERGY
BEAM CURRENT
BEAM UNIFORMITY
BEAM SYSTEM CONTROL
BEAM ENERGY ANALYSIS SYSTEM
FLUENCE CONTROL SYSTEM
POSITIONING SYSTEM
DATA MANAGEMENT SYSTEM
PART TESTER (USER SUPPLIED)
SEU SYSTEM CONTROLLER
AUTOSEQUENCING

APPENDIX 9

Rad-Hard Electronics Development
Program for SSC Liquid-Argon Calorimeters

The submitted manuscript has been authored by a contractor of the U. S. Government under contract No. W-31-109-ENG-38. Accordingly, the U. S. Government retains a nonexclusive, royalty-free license to publish or reproduce the published form of this contribution, or allow others to do so, for U. S. Government purposes.

ANL-HEP-CP-90-33

RAD-HARD ELECTRONICS DEVELOPMENT PROGRAM FOR SSC LIQUID-ARGON CALORIMETERS

A. Stevens, J. Dawson

Argonne National Laboratory
High Energy Physics Division
Argonne, IL 60439

H. Kraner, V. Radeka, S. Rescia

Brookhaven National Laboratory
Instrumentation Division
Upton, NY 11973

ABSTRACT

The development program for radiation-hard low-noise low-power front-end electronics for SSC calorimetry is described. Radiation doses of up to 20 MRad and neutron fluences of 10^{14} neutrons/cm^2 are expected over ten years of operation. These effects are simulated by exposing JFETs to neutrons and ionizing radiation and measuring the resulting bias, leakage current and noise variations. In the case of liquid-argon calorimeters, a large part of the front-end circuitry may be located directly within the low-temperature environment (90 K), placing additional constraints on the choice of components and on the design. This approach minimizes the noise and the response time. The radiation damage test facilities at Argonne will also be described. These include sources of neutrons, electrons, and gamma radiation.

INTRODUCTION

The high energy and luminosity at SSC will generate a severe radiation environment for the detector materials. Estimates indicate that the radiation caused by the normal beam/beam interactions and subsequent particle/detector-material interactions will be equivalent to an accidental beam loss into the detector every six days. The expected radiation environment of a generic detector has been well described in [1]. The size and complexity of the proposed detectors as well as the high event rate for the collider dictate that the instrumentation be placed near or inside the detectors. This places a particularly harsh constraint on the electronics, which must remain operational for the projected ten-year lifetime of the detector.

A block diagram of a possible SSC detector is shown in Fig. 1 [2]. In this figure, the predicted radiation doses for neutrons and ionizing radiation are shown for several positions inside the calorimeter. It should be noted that these numbers are only rough estimates, as more accurate calculations of the radiation will depend largely on the actual geometry and materials used in construction. As shown in Fig. 1, the calorimeter is split into barrel and forward sections, with the most severe doses being close to the beamline in the forward section.

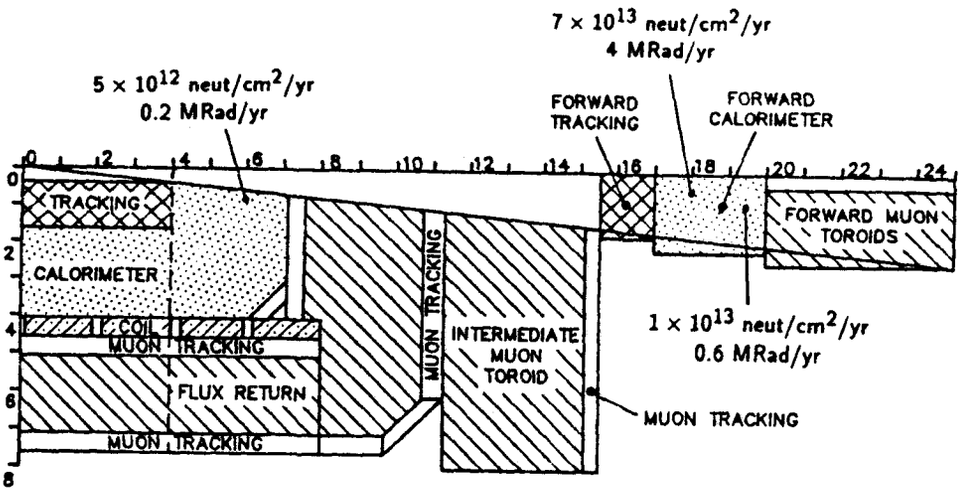

Figure 1: A possible detector implementation for SSC. The total radiation dose is shown for several locations within the calorimeter [2].

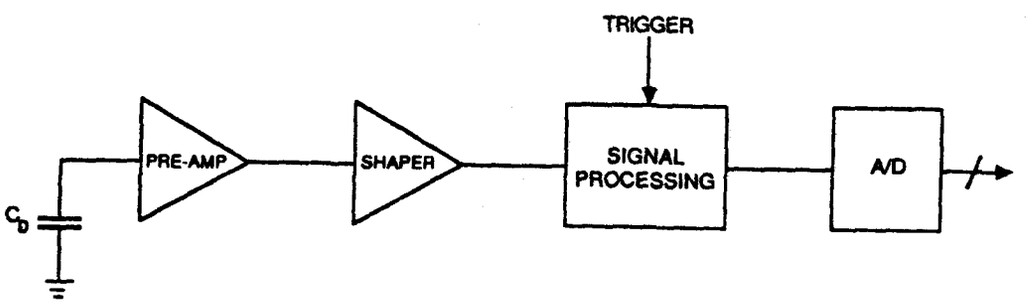

Figure 2: Detector front-end electronics.

A liquid-argon ionization chamber is one type of calorimeter which has been proposed for use in SSC detectors. It consists of plates of a heavy absorber material (typically iron, lead, or uranium) which sit in a cryostat filled with liquid argon. The designed segmentation of the detector will determine the number of plates and therefore the number of readout channels; quantities upward of 200,000 channels have been estimated for SSC. This places several constraints on the electronics associated with the calorimeter:

- They must be reliable over a large temperature range (90 K to room temperature).
- They must be low power, both due to the large number of channels, and due to thermal dissipation constraints inside the liquid-argon cryostat.
- They must be fast due to the high event rate (60 MHz).
- They must be low noise in order to maximize the energy resolution of the calorimeter.
- They must be radiation resistant to the levels described above.

A schematic of the detector front-end electronics is shown in Fig. 2. In this configuration, a charge pre-amplifier is connected directly to the detector plates in order to measure the charge generated by particles traveling through the calorimeter. A shaping amplifier is used to maximize the signal-to-noise ratio with optimal or near-optimal filtering. An analog signal processor follows the shaper and contains the waveform sampler, analog pipeline, trigger amplifiers, and event storage. Finally, an analog-to-digital converter is necessary to store the information in a computer.

The requirements and location of each section will determine the semiconductor technology to be used. In the case of the pre-amplifier, the low noise, temperature, and radiation-susceptibility requirements make JFETs the technology of choice. This is due to:

- Inherent radiation hardness due to the fact that the JFET is a majority carrier device and does not rely on oxides for charge control.
- Excellent noise performance of JFETs due to extremely low leakage currents and $1/f$ noise.
- The JFET noise performance is optimum at low temperatures, typically near 120 K.

The radiation hardness of JFETs will be discussed in this paper. We will give a qualitative account of the damage mechanisms due to radiation as well as test results on device performance at fluences up to 10^{15} neutrons/cm^2. Previous pre-amp designs have used commercially available JFETs with excellent results [3]. For example, at the HELIOS experiment at CERN, JFET pre-amps are used inside the liquid-argon cryostat and have shown 99.8% reliability. Although these pre-amps were not specifically designed for radiation immunity, we have also tested their radiation behavior with neutrons and gamma radiation. The balance of the electronics (shaper, signal processing, A/D) is currently under development. We are evaluating several rad-hard full-custom processes for this purpose, including CMOS, BiCMOS, SOS, and monolithic JFET.

Radiation damage testing will be necessary for all potential materials used in SSC detectors. Thus, the accessibility and availability of radiation sources will be key for any successful rad-hard design. Argonne National Laboratory has complete facilities for irradiation of materials with neutrons and ionizing radiation. These facilities are available to outside users and are currently used for evaluation of semiconductors and scintillators.

RADIATION DAMAGE MECHANISM IN JFETS

Radiation damage in JFETs has been well characterized with respect to DC and small-signal parameters [4,5,6]. However, to our knowledge, no comprehensive study has been made on the behavior of the device noise with respect to radiation. A JFET is pictured in Fig. 3 and consists of a conducting channel between source and drain whose dimensions are modulated by a variable width depletion region. The depletion width is controlled by varying the voltage on the gate terminal with respect to the source. Sources of noise in the JFET are as follows:

- Leakage current between the gate and source due to generation in the depletion region.
- $1/f$ noise due to generation-recombination centers in the depletion region [7].
- Thermal noise due to the finite resistance of the conducting channel between source and drain.

Upon exposure to neutrons, the JFET will experience damage to the crystal lattice due to collisions between the neutrons and the silicon atoms (Fig. 4). The resulting kinematic displacements, or vacancies, will have a finite mobility and will tend to accumulate around donor atoms. In addition, within a short range of a given collision, a cascade of silicon recoils will cause larger defect "clusters." Displacements and clusters will cause intermediate energy states, or traps, to exist in the bandgap. These mid-band states will make it easier for a carrier to jump to the conduction band. This translates into an increased leakage current ΔI_G in the device, which will be proportional to the density of the traps,

$$\Delta I_G = \alpha \phi V \tag{1}$$

where V is the volume of the depletion region, ϕ is the neutron fluence, and α is a leakage current damage constant which relates the neutron fluence to the displacement density and

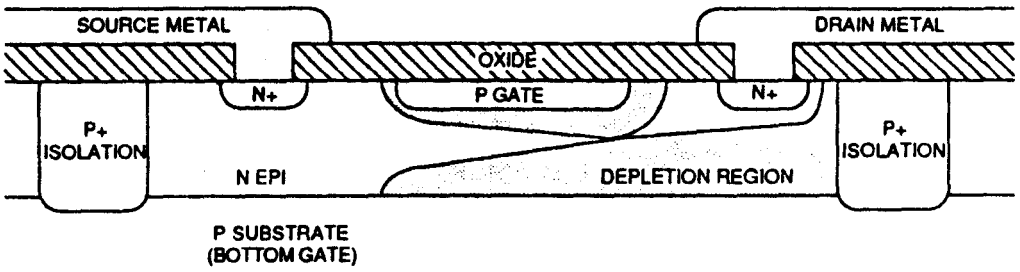

Figure 3: Cross-section of junction field-effect transistor.

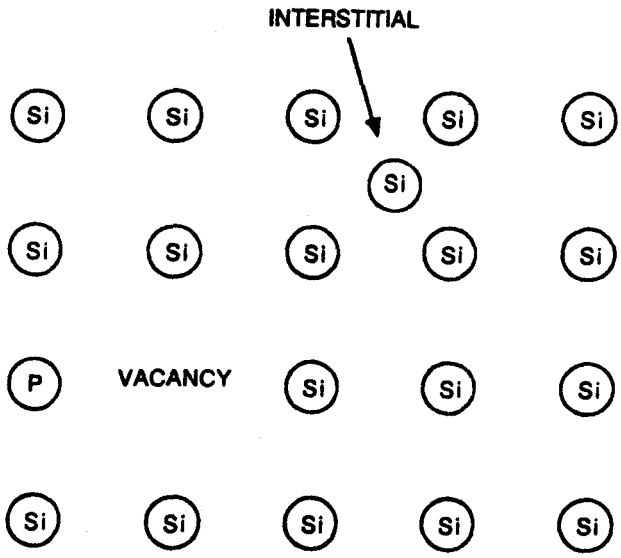

Figure 4: Neutron damage mechanism in silicon. Fast neutrons will damage the crystal and cause vacancies in the lattice, which will increase leakage currents [5].

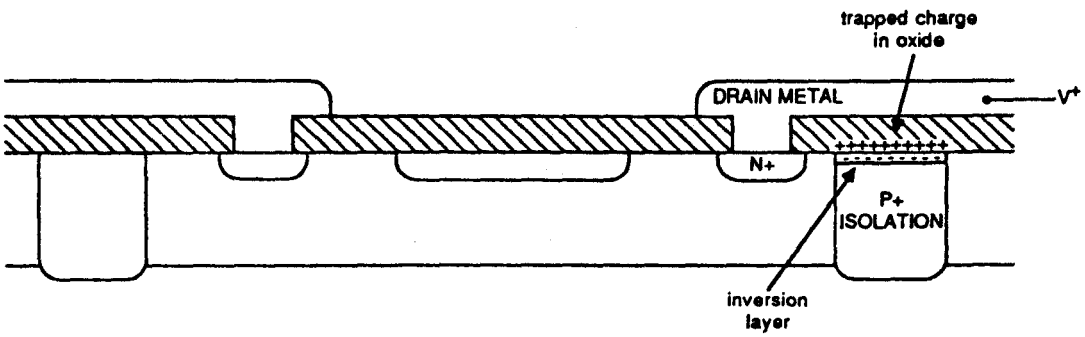

Figure 5: Ionizing radiation damage mechanism in the JFET. Charge build-up in the oxide can cause inversion in the p-type isolation region [3].

will depend on processing, temperature, and neutron energy [8]. Thus, the leakage current is strictly a volume effect in the silicon, and may be minimized by using smaller devices.

Ionizing radiation will cause carrier generation in all of the transistor materials, including the metal, silicon crystal, and silicon dioxide. As shown in Fig. 3, the oxide is used to insulate the metallization from the top of the die. In the case of the metal and silicon, the excess generated charge will be conducted away with little effect. However, in the case of the oxide, the charge will become trapped, causing a net charge to build up in the oxide. Enough of this built-up charge, together with a positive voltage on the metal, can cause a surface inversion in the p-type isolation region (Fig. 5). The mechanism is similar to that of an MOS transistor, where the threshold voltage V_t is given by

$$V_t = \Phi_{ms} + 2\Phi_f + \frac{Q_b}{C_{ox}} - \frac{Q_{ss}}{C_{ox}} \tag{2}$$

where Φ_{ms} is the metal-silicon work potential, Φ_f is the Fermi potential, Q_b is the channel charge, C_{ox} is the oxide capacitance, and Q_{ss} is the trapped charge in the oxide. The net result of the inversion is an increased leakage current due to the increased area of the p-n junction [4]. This effect can be minimized by heavily doping the p-type isolation (increasing Q_b), which will increase the threshold voltage and make it harder to cause inversion.

Ambient temperature will have an effect on the radiation damage, both with respect to neutrons and ionizing radiation [4,6]. Annealing effects occur because at higher temperatures (e.g. room temperature), the displacements and trapped charges caused by the radiation will tend to dissipate due to thermal motion. The result will be a decrease in the radiation damage. At SSC, annealing will generally not occur because the devices will always be held at liquid-argon temperature. However, annealing is an issue in the damage testing environment where the devices may be tested at room temperature. Thus, care must be taken when comparing tests done at low temperature (where noise is lower but there is no annealing), and at room temperature (where noise is higher but may be lessened due to annealing).

NEUTRON DAMAGE TESTING

Neutron damage testing was conducted at the IPNS facility at Argonne with the neutron spectrum shown in Fig. 6. The JFETs were irradiated at room temperature while under typical bias conditions. Measurements were performed approximately one week after the actual irradiation, which allowed the neutron activation of the devices to subside. All annealing effects should stabilize during such time. Fig. 7 shows measurements of I-V curves and gate leakage current before and after the irradiation. In the case of the I-V curves, ~5% variations were observed after exposure to 10^{14} neut/cm^2 (typical 10-year dose at SSC). Measurements of transconductance showed <2% variation. Thus, these JFETs could be used successfully at SSC with little or no loss in gain or bandwidth.

The gate leakage current (Fig. 7b) increased by one order of magnitude after the irradiation at room temperature. However, between room temperature and liquid-argon temperature, the leakage can be expected to drop by about six orders of magnitude. By extrapolating from the post-irradiated room-temperature measurement, the leakage current at 90° K will be on the order of 0.1 fA, which will not adversely affect the noise of the pre-amplifier.

Fig. 8 shows the room-temperature series noise for neutron fluences ranging from 10^{13} to 10^{15} neut/cm^2. The main effect of the neutrons is to increase the $1/f$ noise due to the displacement damage. Due to the limitations of our test equipment, we have not been able to directly measure the noise at the high frequencies which are of most interest. However, we can get an estimate of the high-frequency behavior by linearly extrapolating the $1/f$ noise and assuming the thermal noise to be constant (dashed lines in Fig. 8). This assumption should be valid because the thermal noise is proportional to the transconductance, which,

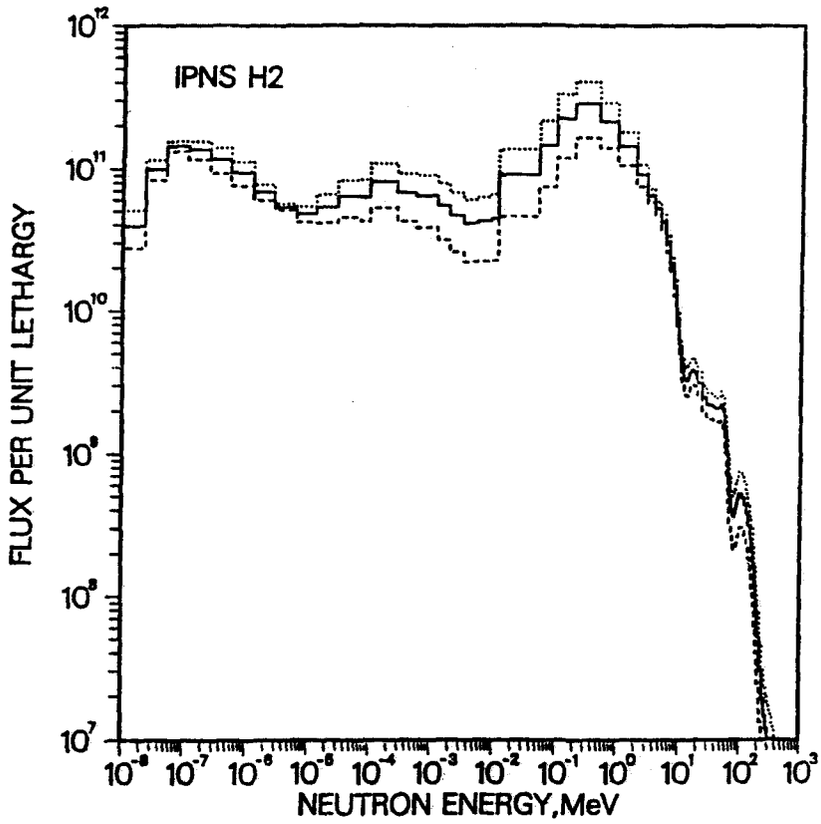

Figure 6: Neutron spectrum at Intense Pulsed Neutron Source.

as mentioned above, remains essentially unchanged by the neutrons. Assuming a bipolar shaping function of 100 ns peaking time, the noise will be bandlimited to the high-frequency region shown in the figure. After 10^{14} neut/cm^2, the noise increase, though measurable, is far less dramatic than the increase of the equivalent noise voltage at lower frequencies. This was confirmed by using one of the irradiated JFETs as the input transistor to an un-irradiated HELIOS pre-amp. An increase of 25% in the equivalent noise charge (ENC) was measured with 100 ns bipolar shaping at room temperature. This increase will be smaller at true operating conditions, i.e. at liquid-argon temperature and at faster shaping times.

IONIZING RADIATION DAMAGE TESTING

Several of the HELIOS JFET pre-amplifiers were subjected to 12 MRad(Si) of Cobalt-60 gamma radiation at Brookhaven at the rate of 5 kRad(Si)/hr. The devices were irradiated with power applied while kept at their normal operating temperature of ~120 K, and were kept cold for the duration of testing. The resulting change in the amplifier noise is shown in the noise spectrum of Fig. 9, which shows the ENC with respect to the shaping time constant for unipolar shaping. The ENC worsens, especially at longer shaping time constants. This corresponds to an increase of leakage current as the positive charges in the oxide drift to the oxide/silicon interface and cause inversion in the silicon. However, long shaping times are not of interest for SSC applications, therefore making this behavior unimportant. At the shorter shaping times (<100 ns), the noise increase is less than 20%.

RADIATION TEST FACILITIES

Because Argonne National Laboratory was for a number of years the site of one of the world's major high energy physics accelerators (ZGS), experienced groups were developed to supervise radiation safety, dosimetry, etc. After the ZGS was closed, these facilities continued to serve the needs of the various accelerators which continued to operate at Argonne. The

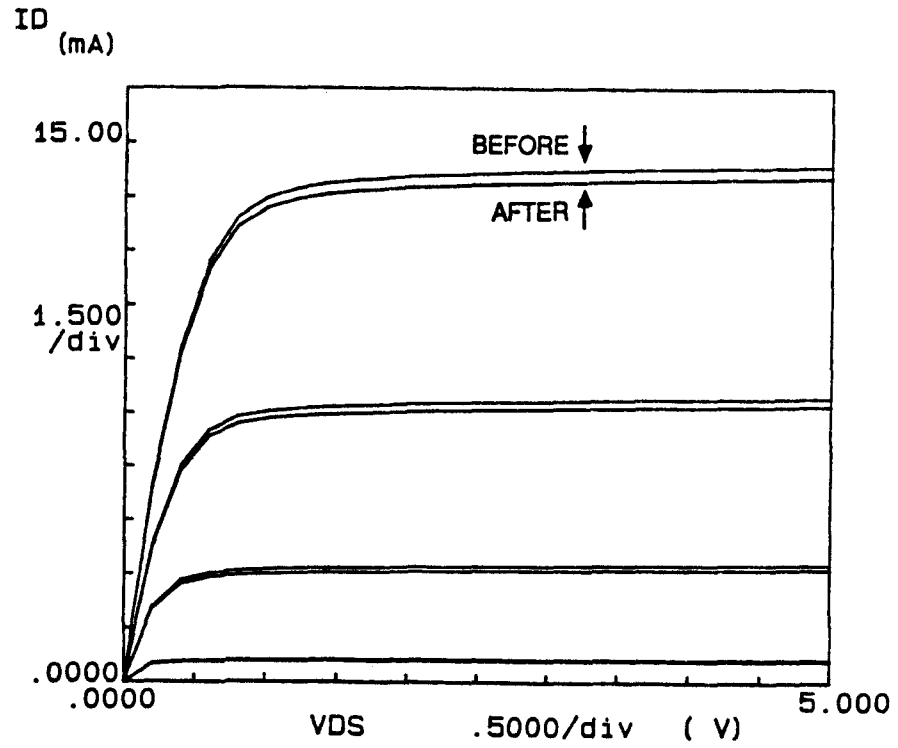

(a)

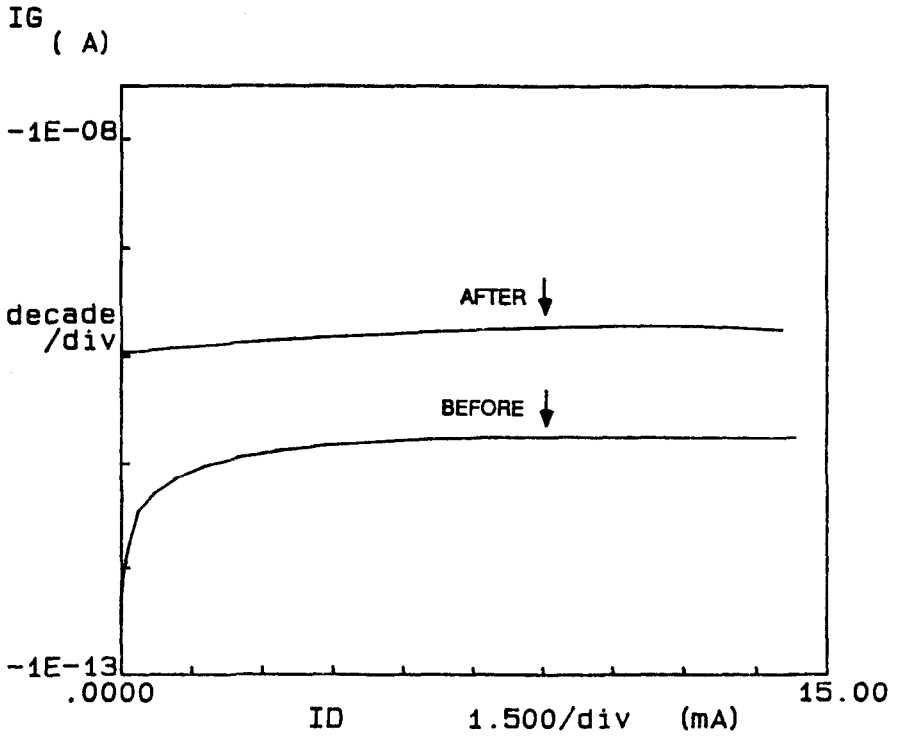

(b)

Figure 7: DC characteristics for SNJ132L JFET, before and after exposure to 10^{14} neutrons/cm^2. (a) I-V curves. (b) Gate leakage current.

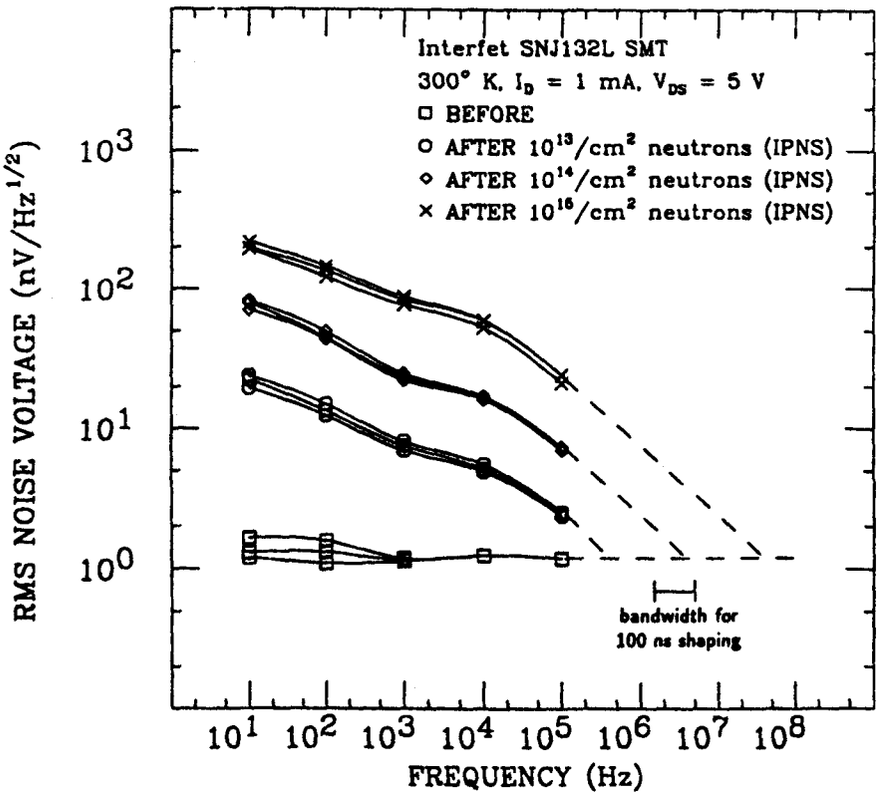

Figure 8: Input series noise for SNJ132L JFET, before and after exposure to neutrons.

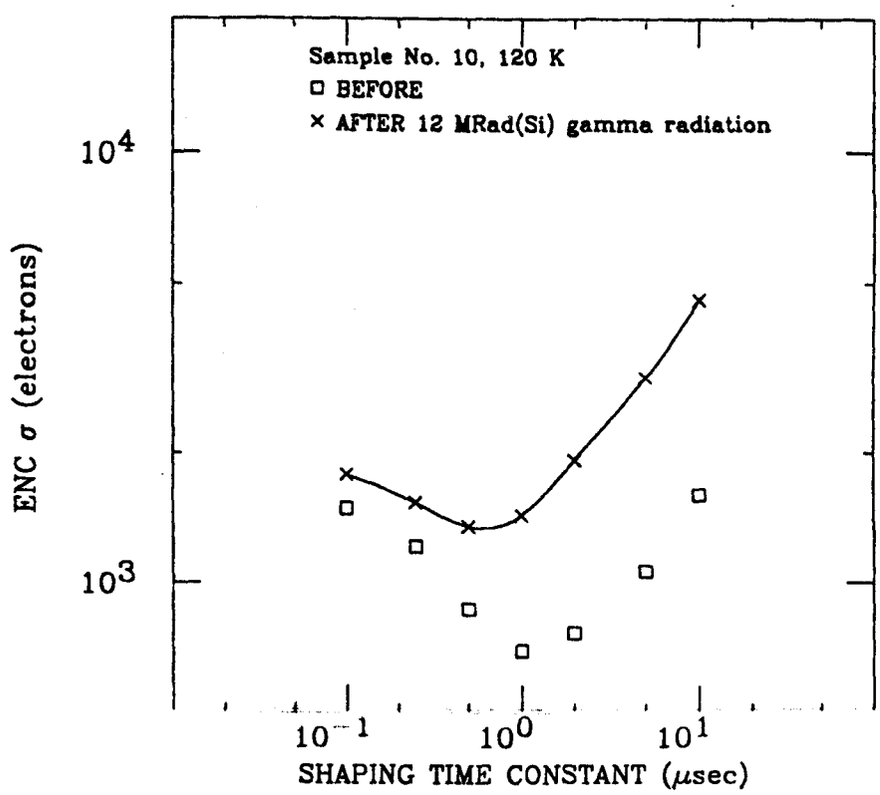

Figure 9: Equivalent noise charge spectrum for HELIOS pre-amplifier, before and after exposure to 12 MRad (Si) gamma radiation.

availability of these services makes the performance of radiation damage studies at Argonne particularly straightforward and efficient from the experimenter's point of view.

Intense Pulsed Neutron Source (IPNS):

The Intense Pulsed Neutron Source at Argonne is used routinely in an on-going program of material science research. It is a large well-staffed facility which runs a well defined schedule on average of two weeks per month throughout the year. This device is unique in that it can give in minutes or hours neutron fluences characteristic of several years of operation in the SSC environment at very forward pseudorapidities. Additionally, the IPNS offers the advantage over a reactor in that there is virtually no gamma contamination of the neutron flux. This is particularly valuable in semiconductor radiation damage testing because it allows the effects of displacement damage to be distinguished from the effects of ionization damage.

The IPNS uses a 50 MeV Linac and 500 MeV Rapid Cycling Synchrotron to produce a 500 MeV proton beam which is transported to a spallation target in a large experimental hall. The shielding in this facility has a number of ports which are used for material science experiments, and two test ports which are used parasitically for such things as radiation damage studies. One port is approximately 1 cm (3/8") diameter and the other is approximately 5 cm (2") in diameter. The neutron flux at either port is approximately 10^{12} neut/cm^2/sec, and the neutron energy is shown in the spectrum of Fig. 6. Fortunately, the neutron spectrum is roughly similar to the spectrum of the albedo neutrons in an SSC detector, peaking at approximately 1 MeV.

We have done a large number of neutron damage exposures using the test ports at fluences ranging from 10^{12} to 10^{17} neut/cm^2. These exposures have involved MOS, JFET, and bipolar semiconductors, and plastic scintillator.

Cobalt-60 Source:

Within the Biology Division, Argonne has a large Co-60 source which is used routinely in life science research. This source is capable of producing up to 2 MRad(Si)/hr. The source is periodically calibrated with an ion chamber which is calibrated by NIST, and subsequently only half-life corrections are made in dose calculations. This source has been used in tests of radiation damage in CMOS devices at room and cryogenic temperatures.

22-MeV Electron Linac:

The Chemistry Division at Argonne has a 22-MeV electron linac which is available for radiation damage research. The nominal beam current of the linac is 50 microamps, however this number may be reduced by as much as three orders of magnitude at the user's discretion. Typically, the beam is focused to a spot 0.6 cm (1/4") in diameter, however the user can de-focus the beam so that it fills the beampipe. Accordingly, the flux of 22 MeV electrons can be varied to fit the users requirements over a very large magnitude. This is particularly useful in semiconductor radiation damage research.

Fast Neutron Generator:

The Fast Neutron Generator in the Engineering Physics Division at Argonne is is capable of producing neutrons for radiation damage research through the Be(d,n) reaction, and is used currently for neutron physics. It consists of a dynamitron, which is similar to a large Cockroft-Walton accelerator, and can accelerate 7 MeV deuterons onto a thick beryllium target to yield 2.5 MeV neutrons and produce a flux of up to 10^{10} neut/cm^2/sec. The spatial constraints at the dynamitron are much more relaxed than at IPNS, allowing much easier installation of a cryostat for neutron damage research at cryogenic temperatures.

CONCLUSIONS

The radiation environment at the SSC interaction regions will place additional restrictions on the already conflicting requirements of high speed and low power for the electronics. However, we have shown that JFET technology is particularly well suited for use in this environment. The main source of damage due to neutrons is an increase in the $1/f$ noise of the devices. Our measurements show that after exposure to 10^{14} neut/cm^2, the pre-amplifier noise will increase by 25% for a bipolar shaper with 100 ns peaking time at room temperature. This figure should improve at faster shaping times and lower temperatures. For the case of ionizing radiation, the damage will be due to increased leakage currents. For 12 MRad(Si) of gamma radiation, the pre-amp noise increased by 20% for a unipolar shaper with 100 ns shaping time constant at 120 K. However, this figure will also decrease at faster shaping times.

Radiation sources will be necessary for damage testing of all detector materials. Argonne has complete facilities, including sources and dosimetry, for damage testing of total dose and dose rate effects with neutrons, electrons, and gamma radiation.

ACKNOWLEDGMENTS

The authors would like to thank T. Scott and G. Schulke of IPNS for help with the neutron irradiations.

Work supported by the U.S. Department of Energy, Division of High Energy Physics, under contract W-31-109-ENG-38.

REFERENCES

[1] D.E. Groom, ed., "Radiation Levels in the SSC Interaction Regions," *SSC-SR-1033*, June 10, 1988.

[2] J.W. Dawson, L.J. Nodulman, "Development of Radhard VLSI Electronics for SSC Calorimeters," in *Supercollider 1*, M. McAshan, ed., Plenum Press, New York, 1989, pp. 203-216.

[3] HELIOS Collaboration, unpublished report.

[4] D.J. Allen, et al., "Gamma-Induced Leakage in Junction Field-Effect Transistors," *IEEE Trans. on Nucl. Sci.*, Vol. NS-31, No. 6, Dec. 1984, pp. 1487-1491.

[5] S.S. Naik, W.G. Oldham, "Neutron Radiation Effects in Junction Field-Effect Transistors," *IEEE Trans. on Nucl. Sci.*, Vol. NS-18, No. 5, Oct. 1971, pp. 9-17.

[6] G.C. Messenger, M.S. Ash, *The Effects of Radiation on Electronics Systems*, Van Nostrand Reinhold Co., New York, 1986.

[7] M.B. Das, J.M. Moore, "Measurements and Interpretation of Low-Frequency Noise in FET's," *IEEE Trans. on Electron Devices*, Vol. ED-21, No. 4, April 1974, pp. 247-257.

[8] H.W. Kraner, Z. Li, K.U. Posnecker, "Fast Neutron Damage in Silicon Detectors," *Nucl. Instr. and Meth.*, A279 (1989), pp. 266-271.

APPENDIX 10

Radiation Damage Tests with Neutron and Proton Sources

SCIPP 89/06
E

Radiation Damage Tests with Neutron and Proton Sources*

HARTMUT F.-W. SADROZINSKI
Santa Cruz Institute for Particle Physics
University of California, Santa Cruz, CA 95064

Abstract

The radiation levels at the SSC require that both electronics and detectors are radiation hard. We describe an ongoing program to study radiation resistance of silicon μ strip detectors and read-out electronics for a high precision tracking system for the SSC .

* Work supported in part by the U.S. Department of Energy.

MOTIVATION

The large Hadron Colliders of the future (SSC, LHC) will require high luminosity to achieve their physics goals. This fact, together with the large hadronic cross-section, will result in very high radiation dosage from charged particles and albedo neutrons to detector elements close to the beampipe and the calorimeters. Because of the large multiplicities and particle densities, the number of channels of the read-out will be very large and the electronics have to be integrated and placed close to the detectors, thus exposing the VLSI read-out to the radiation. Hence, one of the main requirements for SSC/LHC front-end electronics is that it is radiation-hard. The SSC Workshop on Radiation Levels in the SSC[1] found that, for example, a silicon tracking device at a radius of 8cm has to survive about 1 MRad and 10^{13} neutrons/cm^2 per year. Note that the expected neutron fluence will be the same for all tracking devices situated in the calorimeter cavity, independent of radius, because the neutrons are from the calorimeter albedo. Similar radiation levels are expected for the Leading Proton Spectrometer (LPS) in ZEUS at HERA.

We would like to point out that although the physics processes leading to the high radiation levels are well understood,[2] the location of the detectors and the geometry of the calorimeter lay-out influence the radiation levels very strongly. In part, these effects have been discussed in Ref. 3. The charged particle flux

$$\frac{dN}{d\eta} = 7.5 \text{ per interaction}$$

has a distribution which varies as $r_\perp^{-2}$. Thus placing the detector far away from the interaction region helps. For fixed radius the magnetic field strength determines the role looping tracks are playing. In general, the lower magnetic field is better. The length of the detector is also important for the severity of the "looper" problem: a short detector—which for good η coverage has to be close to the beams—will not have the same looper problem as a long detector.

The geometrical layout of the calorimeter and its composition is important because it determines the albedo neutron flux. In the center of the detector a spherical calorimeter with radius r gives rise to a neutron flux[1]

$$\phi = \frac{dN}{dA} = \frac{N}{\pi r^2}(1+a)$$

where N is the number of albedo neutrons in the η interval considered and a is the number of reflections (about 1).

For a more realistic detector configuration, a cylinder of half-length L and radius r, the flux is

$$\phi = \frac{N}{\pi L^2}\left(1+\frac{aL}{r}\right),$$

which for $r = 2$m, $L = 5$m, and a Pb/LA calorimeter gives $\phi = 10^{12}\text{cm}^{-2}$ per year. This is a factor $\frac{1}{4}$ smaller than for a spherical calorimeter with the same radius $r = 2$m. Moreover, most of the neutron flux is generated in the endcaps and lining the endcaps with polyethylene could reduce the neutron flux by more than a factor 10.[4]

We propose to build a silicon micro-strip tracking device for a solenoidal general purpose detector at the SSC.[5] In order to benefit from the superior spatial and two-track resolution of the detector, we would like to place the detector as close to the proton beams as possible. The yearly radiation doses for the design luminosity are then about 10^{12} neutrons/cm^2 (without special liner) and 0.5 MRad. Any increased luminosity will increase these levels accordingly. The damage to detectors and associated VLSI circuits due to neutron and ionizing radiation is quite well known.[6] The detectors are subject to bulk damage due to neutrons ("displacement") which generates increased leakage currents and noise and changes the doping (from n to p type). The electronics (CMOS) is mainly damaged by ionizing radiation. These statements are only partially correct because double-sided silicon detectors might show surface damage in addition to the bulk damage[7] and the increase in noise in bipolar transistors due to neutron irradiation is not known. So the damage

TABLE 1: EXPOSURES AT LAMPF

a) neutrons (1 MeV)	
1st run ('88) ($\sim 10^{15} n/\mathrm{cm}^2$)	use diodes to determine fluence; use DVM's and write i–V curves down.
2nd run ('89) ($\sim 10^{17} n/\mathrm{cm}^2$)	very good fluence determination with a combination of foils; use HP4145B transistor tester to record data; monitor total ionizing dose.
b) protons (800 MeV)	
HRS beam line ('89) ($\sim 10^{14} p/\mathrm{cm}^2 = 3$ MRads)	fluence determination with Al activation; good beam control, need beam line operator.

So the damage to the complete detector system (double-sided detectors + analog front-end in bipolar technology + digital data storage in CMOS) has to be investigated both for neutrons and for ionizing particles.

EXPOSURES AT LAMPF

In collaboration with Los Alamos National Laboratory and University of Torino, we had several exposures at LAMPF in the spallation neutron source in the LAMPF beam stop and the 800 MeV proton beam. These sources are described in detail by Vern Sandberg.[8] Table 1 summarizes the exposures and our special experiences. In order to avoid very large extrapolation in the damage due to flux dependent annealing as described by P. Winokur[9] we tried to run at the lowest flux possible to accumulate the SSC 10 year dose. We also ran at two different fluxes to measure rate dependence. The devices were biased to realistic values and we monitored the important parameters (temperature, leakage currents for diodes,

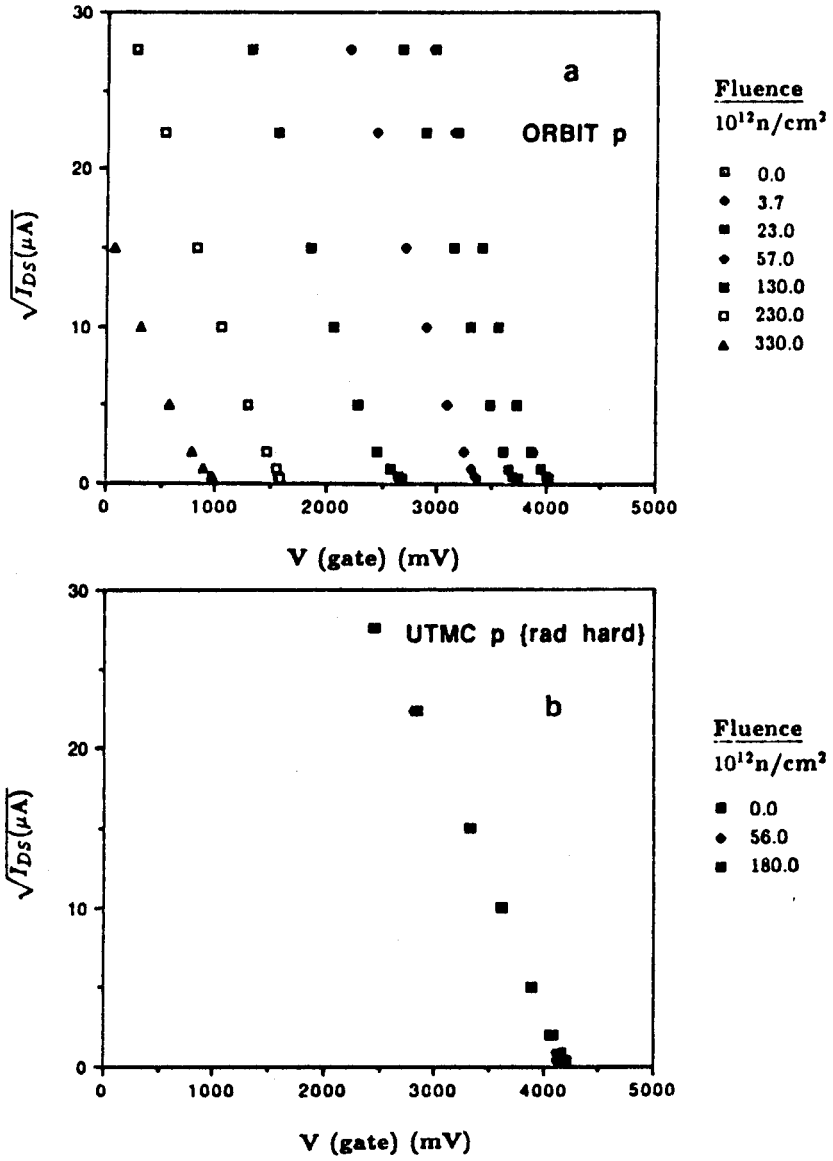

Fig. 1. (a) Square root of the drain-source current I_{DS} as a function of the gate voltage for the non-radiation hard p transitor #2 manufactured by ORBIT for different accumulated neutron fluences. (b) Square root of the drain-source current I_{DS} as a function of the gate voltage for the radiation hard p transistor #7 manufactured by UTMC for different accumulated neutron fluences.

threshold shifts for CMOS transistors) at regular intervals during irradiation. An example of the i-V curves of a rad-hard and non-rad-hard CMOS transistor from our 1988 neutron exposure is shown in Fig. 1 with the resulting threshold shift in

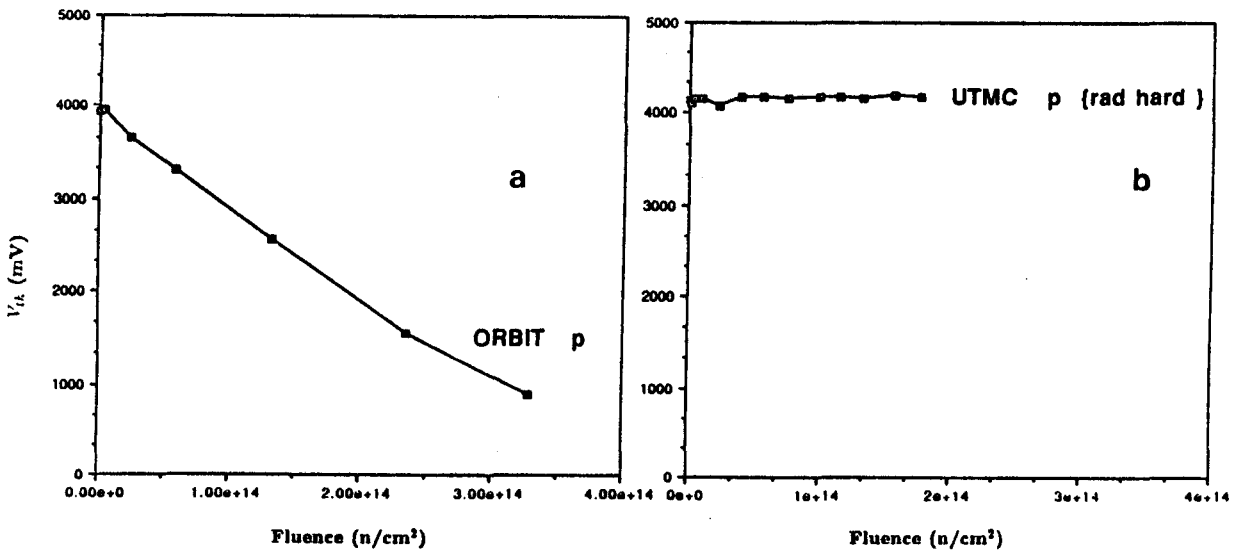

Fig. 2. (a) Threshold voltage V_{th} versus neutron fluence for the non-radiation hard p transistor #2 manufactured by ORBIT. (b) Threshold voltage V_{th} versus neutron fluence for the radiation hard p transistor #7 manufactured by UTMC.

Fig. 2.[10] This constant monitoring is important to ensure that the data are correct.

The main results of our investigation are the following:

a) Identify rad-hard processes with neutron and proton beams: the threshold voltage shifts of the rad-hard UTMC process are more than 100 times smaller than the ones of non-rad-hard chips (ORBIT).[10] (See Figs. 1 and 2.)

b) Measure radiation damage of UTMC transistors in a proton beam for different bias conditions and determine annealing.[11] The threshold voltage shift for transistors of various sizes were measured as shown in Fig. 3: to first order, the damage is independent of size, as one would naively expect, but there is evidence of short channel effects. Fig. 4 shows the threshold shifts as function of fluence and annealing times. The rebound is much less strong than in Ref. 12 due to our much lower dose rate where annealing sets in during irradiation. The whole question of annealing is discussed in P. Winokur's contribution to these Proceedings.[9]

c) An increase in noise in radiation damaged diodes was observed.

d) Measurements of leakage currents in diodes as function of flux and bias[11]

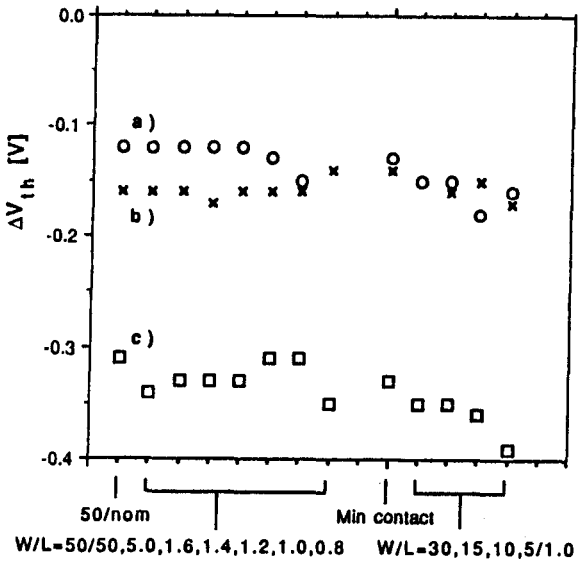

Fig. 3a. Threshold voltage shift ΔV_{th} for UTMC p transistors of various sizes (W/L = width/ length in μm) after a dose of 10^{14} protons/ cm^2 and unbiased room temperature annealing of 22 days for different biasing conditions during exposure: a) unbiased, b) $V_{Gate} - V_{Substrate} = -5$ V. c) $V_{Gate} - V_{Substrate} = 5$V.

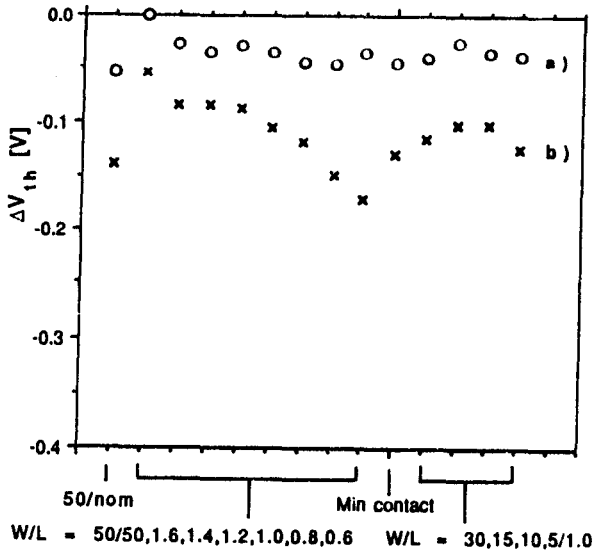

Fig. 3b. Threshold voltage shift ΔV_{th} for UTMC n transistors of various sizes (W/L = width/length in μm) after a dose of 10^{14} protons/ cm^2 and unbiased room temperature annealing of 22 days for different biasing conditions during exposure: a) unbiased, b) $V_{Gate} - V_{substrate} = 5$V.

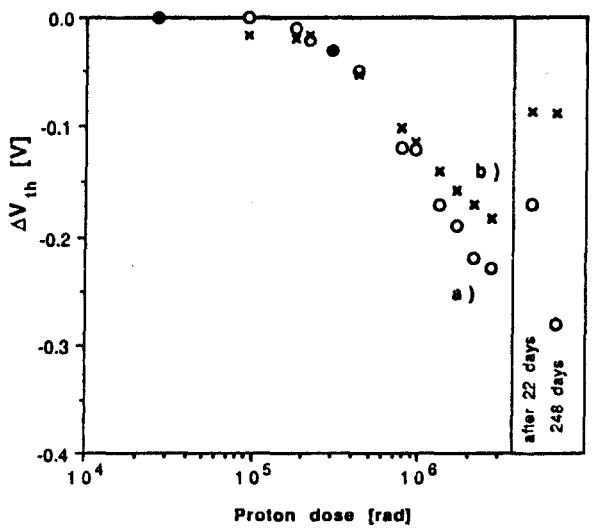

Fig. 4. Threshold voltage shift ΔV_{th} for UTMC transistors as function of fluence and after unbiased room temperature annealing of 22 and 248 days. a) p transistor (W/L = 50/1.6μm) [Bias: $V_{Gate} - V_{Substrate} = -5$ V]. b) n transistor (W/L = 50/1.4μm) [Bias: $V_{Gate} - V_{Substrate} = 5$ V].

TABLE 2: EXPERIENCE WITH LAMPF BEAMS

	Neutrons (1 MeV)	Protons (800 MeV)	Required Support
Environment (temperature)	−	+	
Control of beam	+	−	need operator for p beam line
Fluence calculation during/after	(−)	+	need 1 FTE
Adjust flux	(+)	+	
Uniformity of exposure	+	−	
Access	−	+	need Lab support
Correct energy spectrum	+	(−)	need M.C. calculation + measurement
Beam composition	−	+	need M.C. calculation + measurement
Monitoring of devices	+	+	
Separation of displacement and ionization	+	−	need π beams?

show that the bulk damage is independent of flux and bias.

In the near future, in the framework of the SSC and ZEUS Collaborations with European institutions, we will test the resolution of single- and double-sided strip detectors after irradiation, the radiation resistance of special bipolar processes in terms of gain and noise and the functionality of rad-hard SRAM chips during and after irradiation.

Our experience with neutron and proton beams are compared in Table 2, where a '+' indicates a favorable characteristic of the source and a '−' a negative one. Ref. 13 in these Proceedings makes it very clear that irradiation with protons gives about the right mixture of displacement and ionizing damage as expected at the

SSC. Because the conditions are much better controlled at the proton beams, we will do our most sensitive exposures of detectors and functional chips in the proton beams.

During our runs, we identified the following needs:

a) Good characterization of the neutron source

1. composition, spectrum
2. calibration of the neutron flux ϕ_n at location $\vec{x}$ in terms of accelerator current

$$\text{Flux } \phi_n(\vec{x}) = \alpha_n(\vec{x}) \cdot i_{\text{accelerator}}$$

b) Instrumentation

Basic semi-conductor and switching equipment should be present at the source: transistor tester, LCR meter, switching matrix, digitizing scope, DVM's, voltage sources.

c) Collaborators

1 FTE for fluence determination

1 FTE for beam control (protons)

1 technician for sample preparation.

REFERENCES

1. Radiation in the SSC Interaction Regions: Task Force Report, D. Groom ed., (SSC Central Design Group) SSC-SR-1033 (1988).
2. D. Groom, these Proceedings.
3. H.F.-W. Sadrozinski *et al.*, International Conference on Advanced Technology and Particle Physics, June 1988, Como, Italy (1989), *Nucl. Instrum. & Methods* **A279**, 223 (1989)
4. T.A. Gabriel and R.A.Lille, SSC-N-545, Sept 1988;
   B. Hubbard, private communication.
5. A.J. Weinstein *et al.*, SSC Subsystem R and D Proposal to Develop a Silicon Tracking System, SCIPP 89/39.
6. P. Winokur, these Proceedings;
   E. Petersen, these Proceedings;
   G. Soli, these Proceedings;
   T.P. Ma and P.V. Dressendorfer, *Ionizing Radiation Effects in MOS Devices and Circuits,* (Wiley, New York, N.Y., 1989);
   W.R. Dawes, Jr. *et al.*, *Hardening Semiconductor Components against Radiation and Temperature,* (Noyes Data Corp., Park Ridge, N.J.,1989);
   T. Ohsugi *et al.*, *Nucl. Instrum. & Methods* **A265**, 105 (1988).
7. H. Dijkstra *et al.*, *IEEE Transactions on Nuclear Science,* **36,** (Feb 1989).
8. V. Sandberg, these Proceedings.
9. P. Winokur, these Proceedings.
10. H.F.-W. Sadrozinski *et al.*, *Nucl. Instrum. & Methods* **A288**, 76 (1990).
11. H. Ziock *et al.*, *IEEE Transactions on Nuclear Science,* San Francisco, Jan 1990.
12. D.M. Fleetwood *et al.*, *IEEE Transactions on Nuclear Science,* **NS-34,**1178 (1987).
13. E. Petersen, these Proceedings.

APPENDIX 11

Irradiation Facilities at the Los Alamos Meson Physics Facility

Irradiation Facilities at the Los Alamos Meson Physics Facility

Vern Sandberg
Los Alamos National Laboratory
Los Alamos, New Mexico
87545

ABSTRACT

The irradiation facilities for testing SSC components and detector systems are described. Very high intensity proton, neutron, and pion fluxes are available with beam kinetic energies of up to 800 MeV.

Presented to the Task Force on Radiation Damage Testing at the SSC
March 5, 1990
SSC Laboratory
Dallas, Texas

Los Alamos National Laboratory, Los Alamos, New Mexico 87545

Los Alamos National Laboratory is operated by the University of California for the United States Department of Energy under contract W-7405-ENG-36.

By acceptance of this article, the publisher recognizes that the U. S. Government retains a nonexclusive, royalty-free license to publish or reproduce the published form of this contribution, or to allow others to do so, for U. S. Government purposes.

Los Alamos National Laboratory requests that the publisher identify this article as work performed under the auspices of the U. S. Department of Energy.

IRRADIATION FACILITIES AT LAMPF

INTRODUCTION

This report describes and surveys the irradiation exposure facilities available at the Clinton P. Anderson Meson Physics Facility (LAMPF). The heart of LAMPF is a proton linac that accelerates greater than 6 x 10^{15} protons per second to 800 MeV of kinetic energy. The primary beam of 1 mA of protons is delivered to Experimental Area A , which contains the pion-production targets A-1 and A-2, and the A-6 beam stop, which contains the neutrino source and the Radiation Effects Facility. An H^--ion beam of approximately 70 μA is also accelerated in the linac, concurrently with the proton beam, and delivered to external-proton-beam Experimental Areas B and C, to the Proton Storage Ring (PSR), to a group of spallation neutron sources (WNR), and to the Manuel Lujan, Jr. Neutron Scattering Center (LANSCE). The beam lines and the experimental areas are shown in Fig. 1. The areas of most interest for radiation damage studies are the Radiation Effects Facility at the A-6 beam stop, the HRS-external-proton-beam facility, the WNR-spallation neutron sources, and PSR-LANSCE. The Experimental-Area-A Test Channel and P^3 Channel may be of interest for the testing of components and detector elements in high intensity pion beams.

The LAMPF and WNR-LANSCE management are anxious to be involved in helping the community take full advantage of these facilities. The beams and facilities already exist and suitable program committees are in place to receive and review proposals. The facilities can be used "as is" or may be modified, subject to cost recovery for the total incrementally incurred costs. Interested persons are encouraged to contact LAMPF.

The following paragraphs describe the LAMPF accelerator, its beams, time structures, and beam delivery systems. The HRS external proton beam facility and the Area A channels are describe. Next the PSR and the WNR-LANSCE complex are discussed. Finally the A-6 beam-stop Radiation Effects Facility is summarized. Appendices describing each of these facilities in much greater detail are included at the end of this report.

ACCELERATOR AND BEAM TIME STRUCTURE

The LAMPF accelerator is a three stage design. Ion sources, located in the domes of three Cockcroft-Walton generators, provide proton and H^- beams and an optically pumped source supplies a polarized H^- beam. These beams are accelerated to 750 keV by the Cockcroft-Walton generators and are multiplexed, bunched, injected into an Alverez-drift-tube linac (operating at 201.25 MHz) and accelerated to 100 MeV. The bunches, protons and H^- in 180° RF phase buckets, are then transfered into a side-coupled linac operating at the fourth harmonic of the drift-tube linac (805 MHZ) and accelerated to 800 MeV of kinetic energy.

The beams are separated magnetically, with field strengths and gradients kept small enough so as not to strip off the electrons on the H^- beam and to preserve polarization, and transported to the experimental areas through good quality beam optics so as to preserve the beam phase space and minimize activation. Care in the beam transport systems is necessary in view of the relative low energy and high intensity of the beams. The beam delivery and experimental areas are shown in Fig. 1.

The proton beam and H^- beams each have a time micro-structure consisting of a pulse of particles less than 300 ps wide separated by 4.969 ns. There are approximately 10^8 protons per micro-pulse in the H^- beams and 5 x 10^8 protons per micro-pulse in the primary proton beam. The micro-structure is modulated by a macro-structure consisting of a 500 to 800 μsec long spill repeated at a 120 Hz rate. This is shown in Fig. 2.

The average current for the primary proton beam is 1 mA, which corresponds to 6.2 x 10^{15} protons per second. The peak current is approximately 17 mA, which correspond to macro-pulses of 10^{17} protons per second, or 5.2 x 10^{12} protons per macro-pulse. This beam is degraded in energy from 800

MeV to 760 MeV and reduced in current by approximately 150 μA in passing through the A-1 and A-2 pion-production targets, so that the A-6 beam-stop area receives approximately 850 μA of protons. It should be noted that what limits the operating current in the primary proton beam is the thermal power that can be dissipated by the A-1 and A-2 targets, not the capabilities of the A-6 beam stop or linac.

EXPERIMENTAL AREA A & HRS EXTERNAL PROTON BEAM AREA C

Experimental Area A is the main LAMPF experiment hall and houses the main experiment channels. Two graphite production targets, A-1 and A-2, receive the full primary proton beam. The surrounding beam optics collect the pion and muon beams and channel them into experiment caves. The A-1 target supplies a "test channel" with pions, muons, electrons, and gamma rays and is shown in Fig. 3. The test channel is intended to be used for quick set-up tests of simple detector systems. The A-2 target supplies pions for the high intensity P^3 channel. This channel is described in detail in Appendix 1, in particular Table II of Appendix 1 lists the pion rates as a function of energy. Typical values are of order $10^9\ \pi^+\ sec^{-1}$ for momenta of order 500 MeV/c.

Beam currents in hundreds of nanoamps are delivered to the external proton beam areas B and C. Although lower in intensity, these areas allow direct access to the proton beam through carefully designed transport optics and are more suitable for high precision experiments. Beam Area C is illustrated in Fig. 4. The high resolution spectrometer (HRS) facility has been used in a radiation damage study of protons on silicon strip detectors (LAMPF experiment E1139 [1]). Proton fluences for these exposures are shown in Table 1 (from P. D. Ferguson, "H^+ Fluence Determination for the SSC Silicon Strip Detector Irradiation" [2]).

WNR-PSR-LANSCE SPALLATION NEUTRON SOURCES

The major portion of the 70 μA H^- beam is transported to the WNR-spallation neutron sources and to the PSR-LANSCE complex. These facilities are summarized in this section. The WNR facility (shown in Fig. 5) is a source of high average neutron flux of well defined energy and beam quality. The PSR-LANSCE neutron sources are very high in peak intensity and well defined in time. Both sources are well characterized and offer well instrumented beam channels and flight paths.

The WNR area has two tungsten spallation targets, T2 and T4, water and liquid hydrogen moderators, and a variety of beam flight paths. There is a bare target exposure channel for fast neutrons in the energy range 100 keV to 800 MeV. Targets and flight paths are limited in the current they can receive by shielding requirements. Target T2 has shielding for up to 100 nA of 800 MeV protons. Target T4 has shielding for up to 20 μA of protons and is intended to be an intense white source of neutrons, with energies from 0.1 eV to greater than 750 MeV. The energy spectra from the spallation sources as functions of angle to the proton beam and target material are shown in Figs. 6 and 7.

The PSR is an accumulator-buncher ring that collects approximately 450 μs of the 800 MeV H^- beam, bunches the stored beam, and extracts it in a 250 ns burst. The burst is then delivered to several experimental areas in the LANSCE complex. The PSR is presently operating at an average value of 60 μA at a 20 Hz repetition rate. Work is under way to reduce the losses of the transport lines and ring to bring the facility to the design goal of 100 μA.

The LANSCE spallation source has several high intensity water and liquid hydrogen moderators. The neutron flux from the LANSCE white neutron source has been measured [3] and found to be well described by a thermal spectrum for energies less than 0.02 eV and by the function

$$\phi = \frac{2.3 \times 10^6}{E} + \frac{5.3 \times 10^4}{E^{0.69}} \text{ neutrons cm}^{-2}\text{ sec}^{-1}\text{ eV}^{-1},$$

for $0.02 < E < 100$ keV. These values were for a PSR current of 57 μA. This spectrum is shown in Fig. 8.

RADIATION EFFECTS FACILITY

This facility is located at the A-6 beam stop and receives the major portion of the primary proton beam, approximately 850 μA. Irradiations by both protons and neutrons are available at fluxes exceeding the radiation levels expected in the SSC. The facility is described in detail in Appendix 2. An illustration of the A-6 target station is shown in Fig. 9, with elevation and plan views in Figs. 10 and 11, respectively. The neutron flux as measured in an A-6 irradiation port is shown in Fig. 12. For comparison, a fission spectrum is also shown in Fig. 12 to illustrate the high energy ($E_n > 10$ MeV) flux available at the A-6 facility.

The neutron irradiation facility is located adjacent to and along the copper beam stop. The irradiation volume is segmented into 12 independent ports, each of which is 12 cm x 25 cm x 50 cm. The flux in these ports varies from a high of 6×10^{13} neutrons cm^{-2} sec^{-1} in the port nearest the beam stop to 6×10^{12} neutrons cm^{-2} sec^{-1} in the ports down stream. Smaller fluxes can be obtained by moving to a set of irradiation cells located in a porch above the beam stop shielding. Foil dosimetry measurements for the SSC irradiation described in Ref. 1 by Sadrozinski *et al.* have been carried out by Ferguson[4] and are summarized in Table 2.

For proton irradiations there are three independent ports of volume 150 cm^3. The proton beam has a gaussian intensity profile in the transverse directions, with a peak flux of 1.2×10^{14} protons cm^{-2} sec^{-1} and a $2\sigma = 5$ cm.

Closed-loop water and helium cooling services are available, as are monitor and control cabling (mineral insulated to withstand the radiation environment). Remote handling services are available and access may be obtained within a 4 to 6 hour period after the beam is turned off.

ACKNOWLEDGEMENT

The assembly of this brief review of the LAMPF and PSR-LANSCE facilities could not have been done without the help of Lou Agnew, Jim Bradbury, Phil Ferguson, Gerry Garvey, Paul Koehler, Dave Lee, Paul Lisowski, Bob MacFarlaine, Walt Sommer, and Dan Strottman.

REFERENCES

[1] H. F. W. Sadrozinski *et al.*, "Tests of Radiation Hardness of CMOS Transistors Under Neutron Irradiation", LA-UR-89-295 (1989),
H. F. W. Sadrozinski *et al.*, "Tests of Radiation Hardness of CMOS Test Structures in Neutron and Proton Beams", Santa Cruz Institute for Particle Physics SCIPP 89/49.

[2] Table 1 is taken from P. D. Ferguson, "H^+ Fluence Determination for the SSC Silicon Strip Detector Irradiation", Los Alamos internal memorandum dated Feb. 25, 1989.

[3] P. E. Koehler, "Measurement of the LANSCE Neutron Flux from 0.025 eV to 100 keV", LA-UR-90-XXXX (1990) (submitted to Nuclear Instruments and Methods).

[4] P. D. Ferguson, "Neutron Dosimetry for the A-6 SSC Irradiation", Los Alamos internal memorandum dated Feb. 23, 1990.

Table 1. Chip Irradiation Data

Foil ID	mass (g)	Fluence 10^{12} H^+/cm^2 Na-22	Be-7	ct time (min)	irr time (hrs)
V1	.0858	0.417 ± 0.170	0.681 ± 0.102	900	77.5
V2	.0837	32.78 ± 2.156	32.61 ± 1.807	120	77.5
V3	.0870	368.4 ± 19.92	345.8 ± 17.72	45	77.5
V4	.0845	226.4 ± 12.40	210.5 ± 10.85	60	77.5
H1	.0843	314.0 ± 16.80	300.2 ± 15.34	60	77.5
H2	.0859	439.2 ± 22.57	415.2 ± 20.94	120	77.5
H3	.0867	34.53 ± 2.069	30.78 ± 1.651	180	77.5
H4	.0855	5.554 ± 0.303	5.380 ± 0.277	3900	77.5

Table 1 is taken from P. D. Ferguson, "H^+ Fluence Determination for the SSC Silicon Strip Detector Irradiation", Los Alamos internal memorandum dated Feb. 25, 1989.

Table 2

Neutron Flux and Fluence for SSC Chip Irradiations
(from P. D. Ferguson, "Neutron Dosimetry Foil Calibrations at the A-6 Radiation Effects Facility" [1])

	Position 1	Position 2
E = 4.906 eV (gold foil: $^{197}Au(n,\gamma)^{198}Au$, σ(4.906 eV)= 1565 barns)		
flux (n cm^{-2} sec^{-1})	1.97×10^{6}	1.38×10^{8}
fluence (n cm^{-2})	6.92×10^{12}	4.86×10^{14}
E = 5 keV scandium foil: $^{45}Sc(n,\gamma)^{46}Sc$, σ(5 keV)= 11.3 barns)		
flux (n cm^{-2} sec^{-1})	2.43×10^{7}	1.21×10^{9}
fluence (n cm^{-2})	8.54×10^{13}	4.25×10^{15}
E = 3.1 MeV (iron foil: $^{54}Fe(n,p)^{54}Mn$, σ(3.1 MeV)= 78 millibarns)		
flux (n cm^{-2} sec^{-1})	1.86×10^{5}	2.00×10^{9}
fluence (n cm^{-2})	6.54×10^{11}	7.01×10^{15}

(At Position 1 an exposure of 3×10^{4} rad of γ were measured by means of TLDs.)

[1] P. D. Ferguson, "Neutron Dosimetry for the A-6 SSC Irradiation", Los Alamos internal memorandum dated Feb. 23, 1990.

FIGURE CAPTIONS

Fig. 1. Beam delivery and layout of the LAMPF, WNR, and PSR-LANSCE experimental areas.

Fig. 2. The LAMPF linac's time structure.

Fig. 3. Layout and beam optics of the Target Station A-1 Test Channel.

Fig. 4. Layout and beam optics of the Beam Area C HRS External Proton Beam.

Fig. 5. The WNR and PSR-LANSCE complex.

Fig. 6. Calculate neutron spectra as a function of angle. The spallation target is a 3 cm diameter x 7.5 cm long tungsten target. The calculation includes the effect of the stainless steel cooling jacket and the water cooling channels. (Fig. 9 of Appendix 2)

Fig. 7. Calculated neutron yield for WNR targets of berylium, copper, tungsten, and depleted uranium. The target has the same geometry as described in Fig. 7. (Fig. 10 of Appendix 2)

Fig. 8. The measured neutron flux for the LANSCE white neutron source. The realtive uncertainties are smaller than the size of the data points.

Fig. 9. A prespective view of LAMPF Target Station A-6, which houses the Radiation Effects Facility.

Fig. 10. Elevation view of Target Station A-6.

Fig. 11. Plan view of Target Station A-6 and the Radiation Effects Facility irradiation ports.

Fig. 12. Neutron flux spectra at the Target Station A-6 irradiation ports. For comparison, a fission spectrum is also shown ito illustrate the high energy (E_n > 10 MeV) flux available at the A-6 facility.

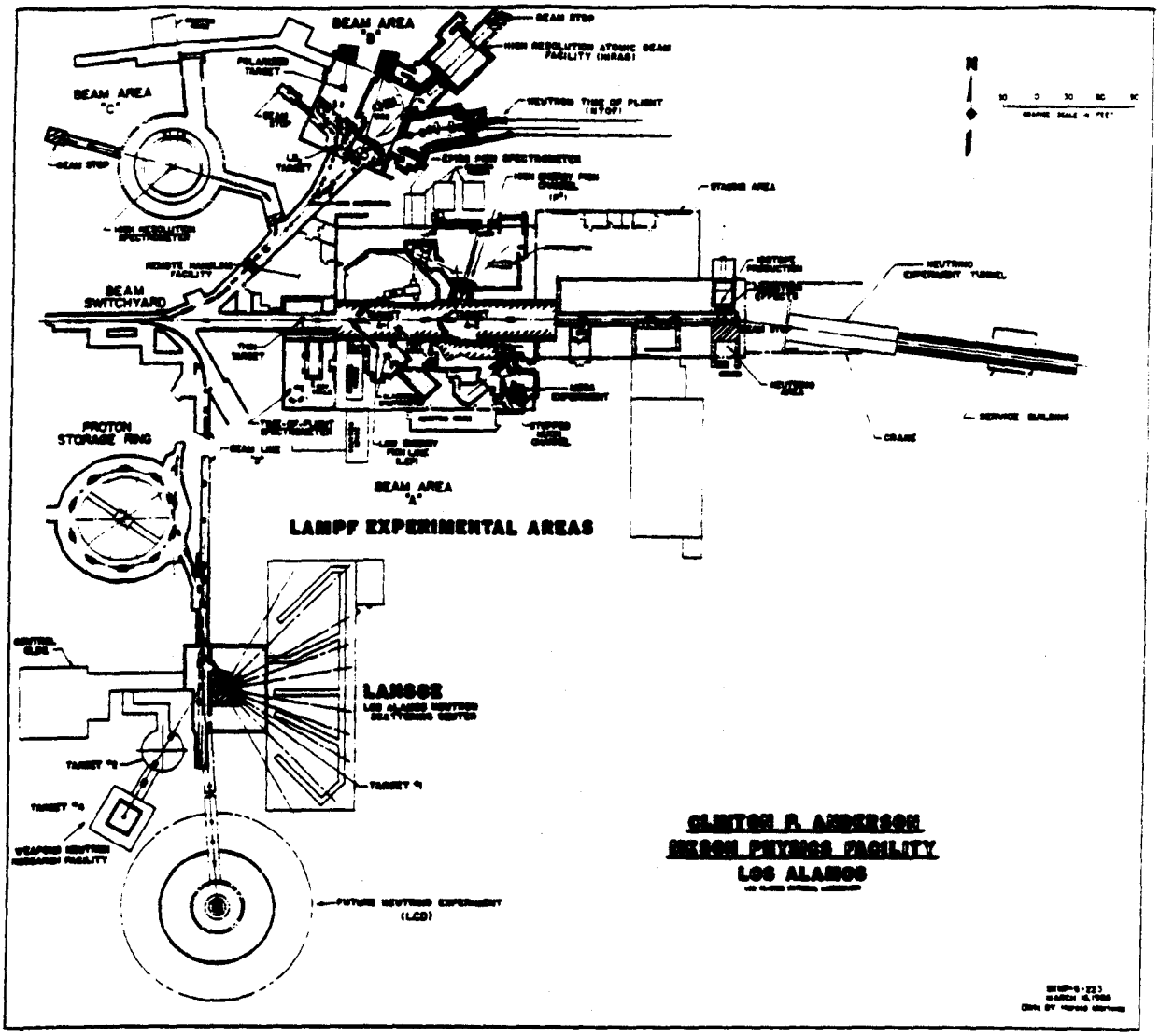

Fig. 1. Beam delivery and layout of the LAMPF, WNR, and PSR-LANSCE experimental areas.

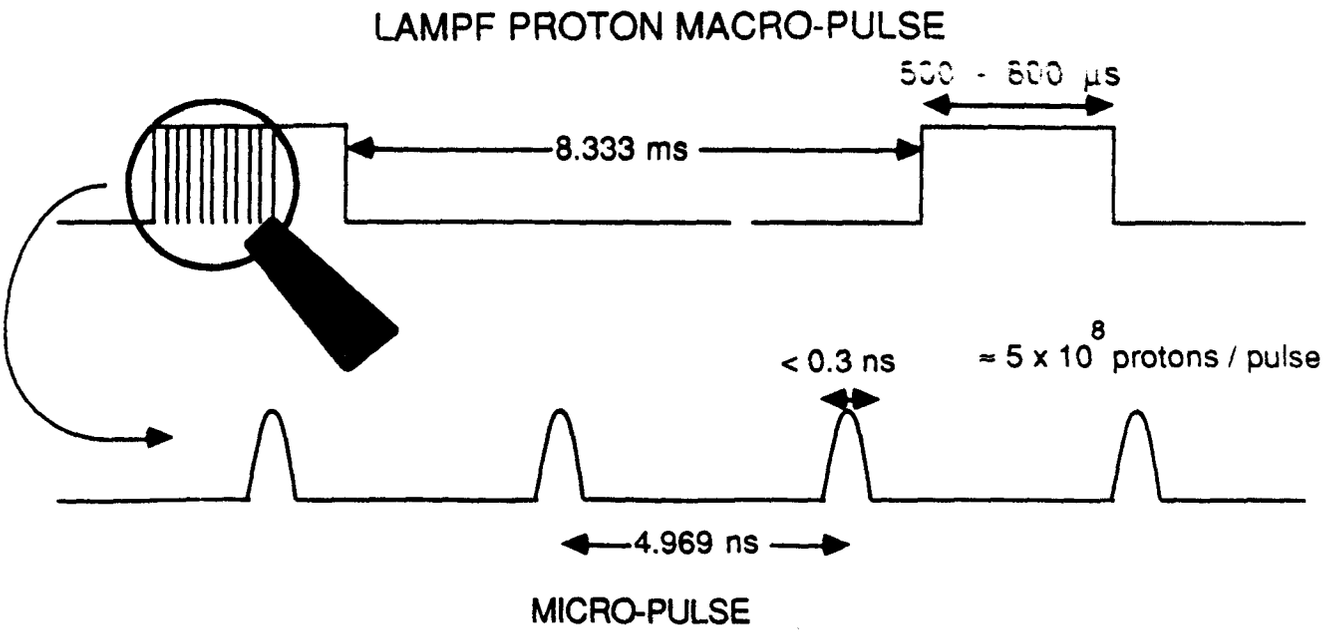

Fig. 2. The LAMPF linac's time structure.

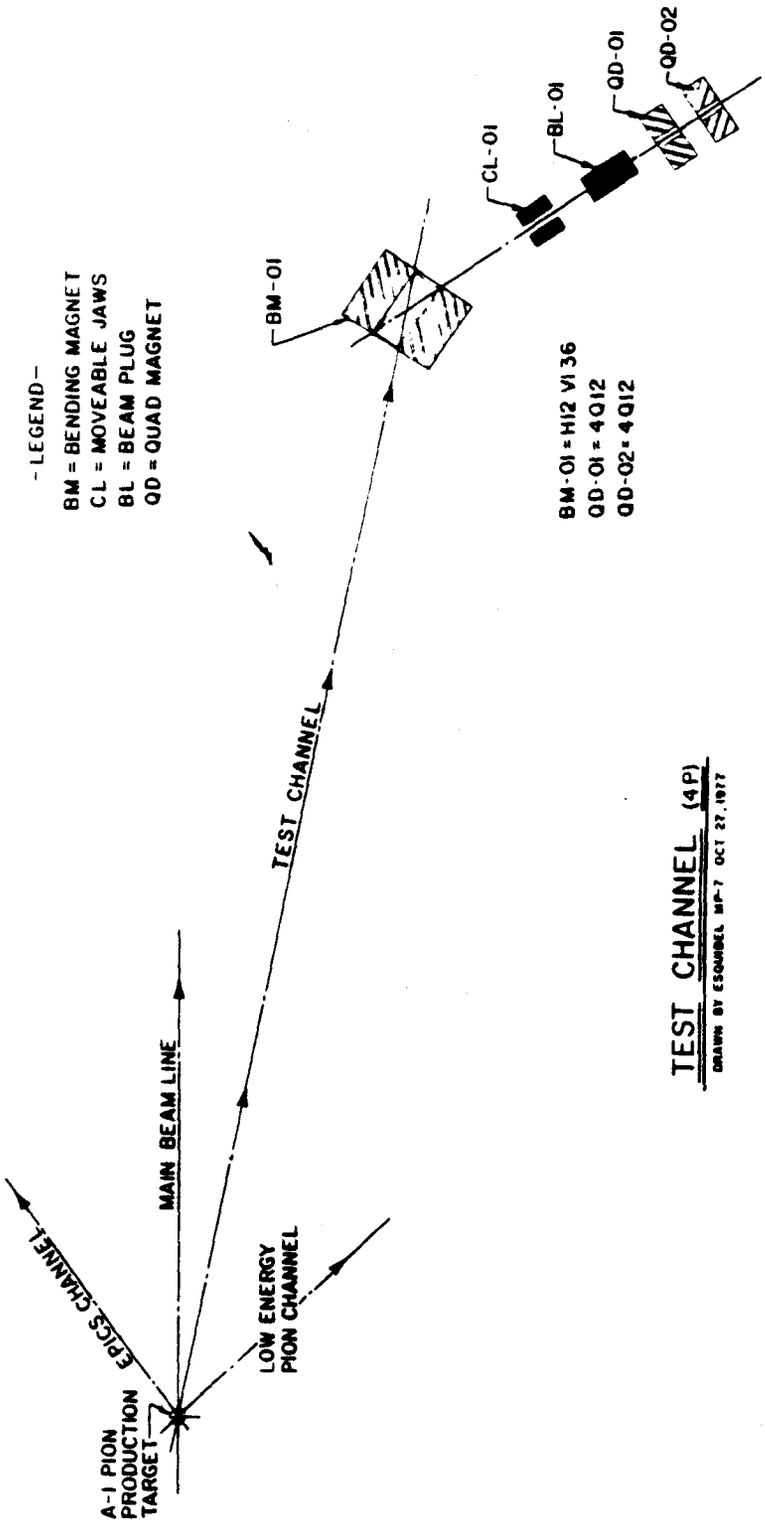

Fig.

Section Number and Title	Rev.	Date Issued
Sec. 6A Experimental Area A	1	December 1980

LAMPF USERS HANDBOOK

Fig. 3. Layout and beam optics of the Target Station A-1 Test Channel.

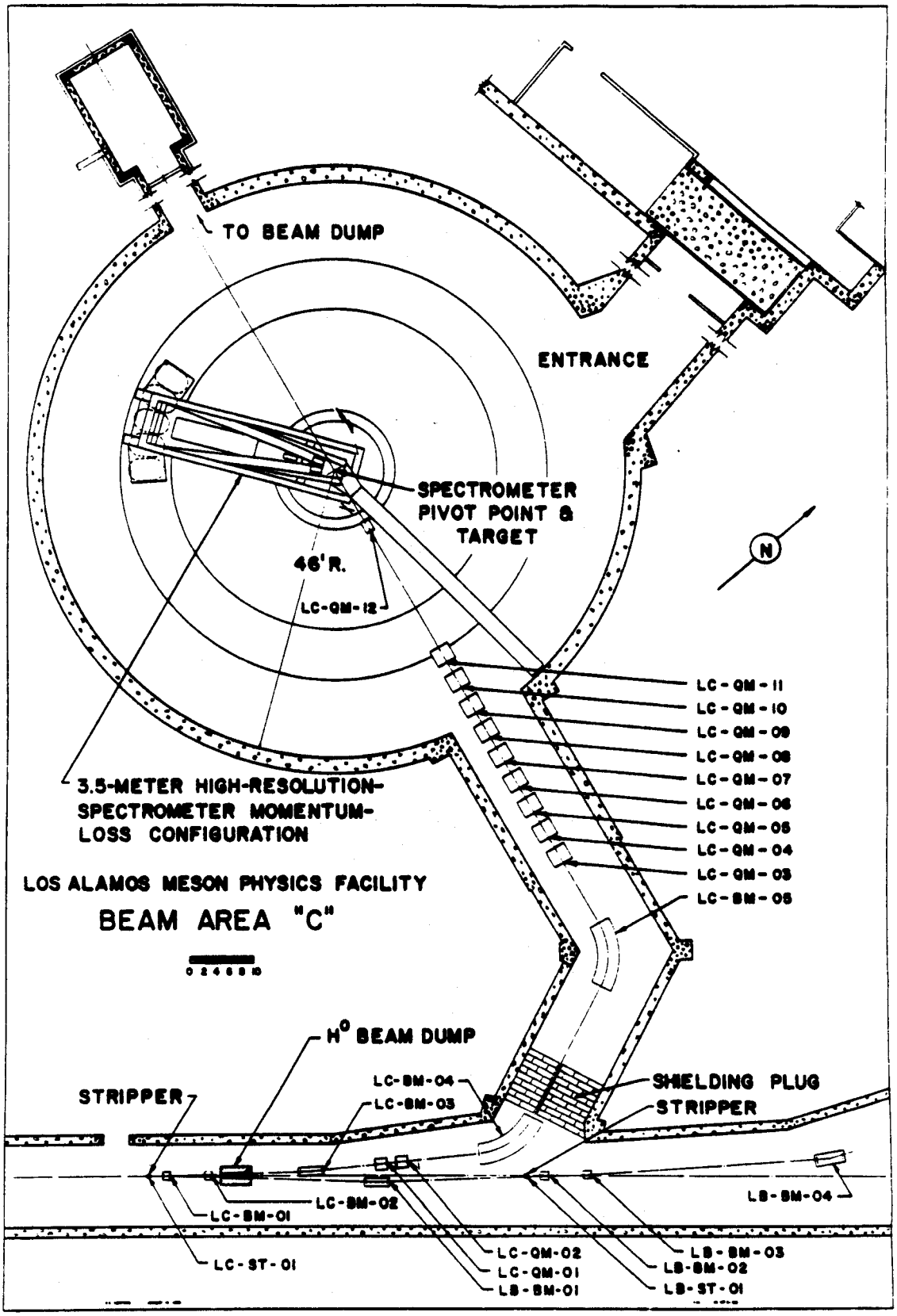

Fig. 4. Layout and beam optics of the Beam Area C HRS External Proton Beam.

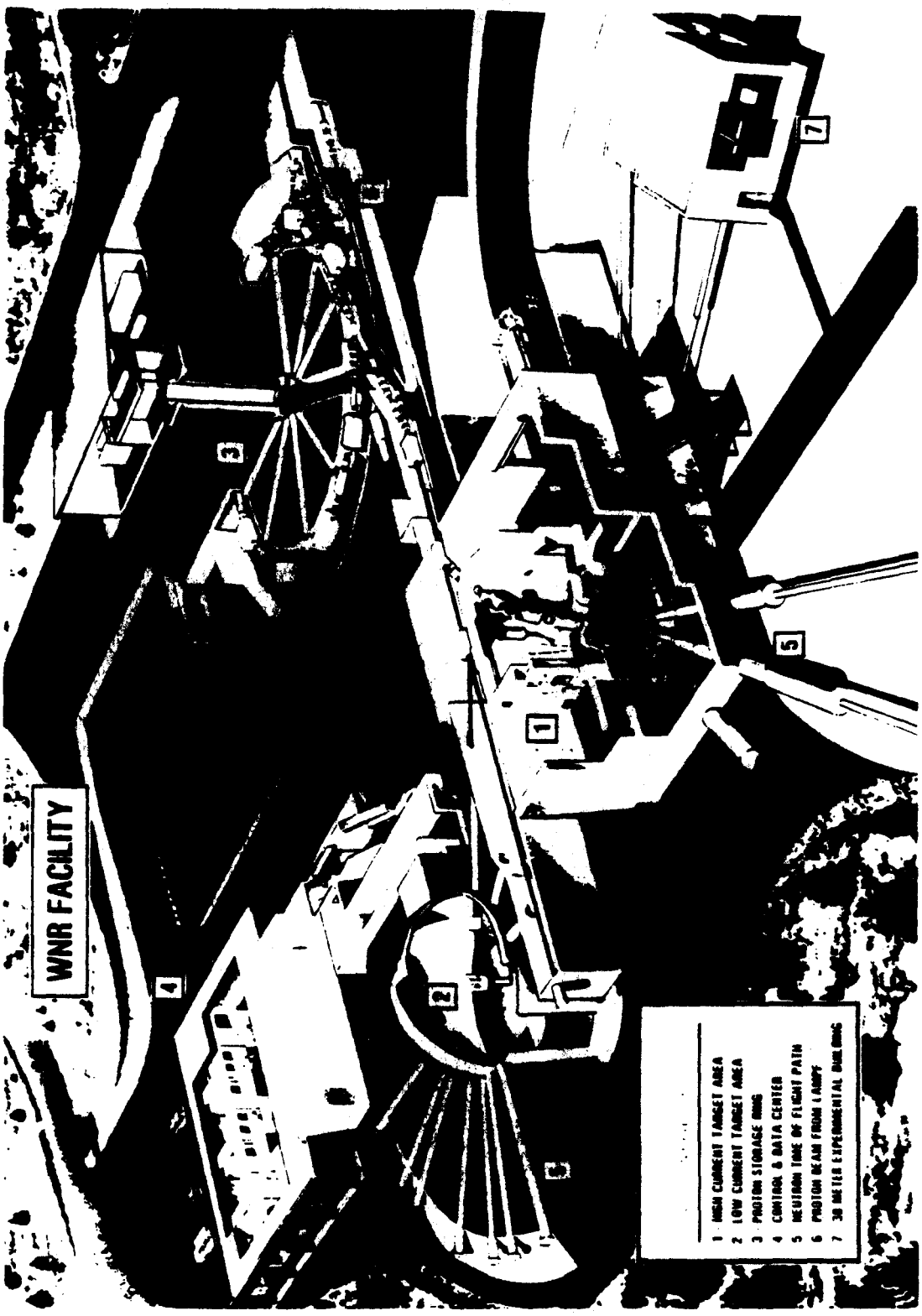

Layout of the WNR facility. The high-current target is located in a vertical proton beam and is viewed by 11 horizontal flight paths. The low-current target is located in a horizontal proton beam; up to 12 flight paths view this target at various angles to the proton beam.

Fig. 5. The WNR and PSR-LANSCE complex.

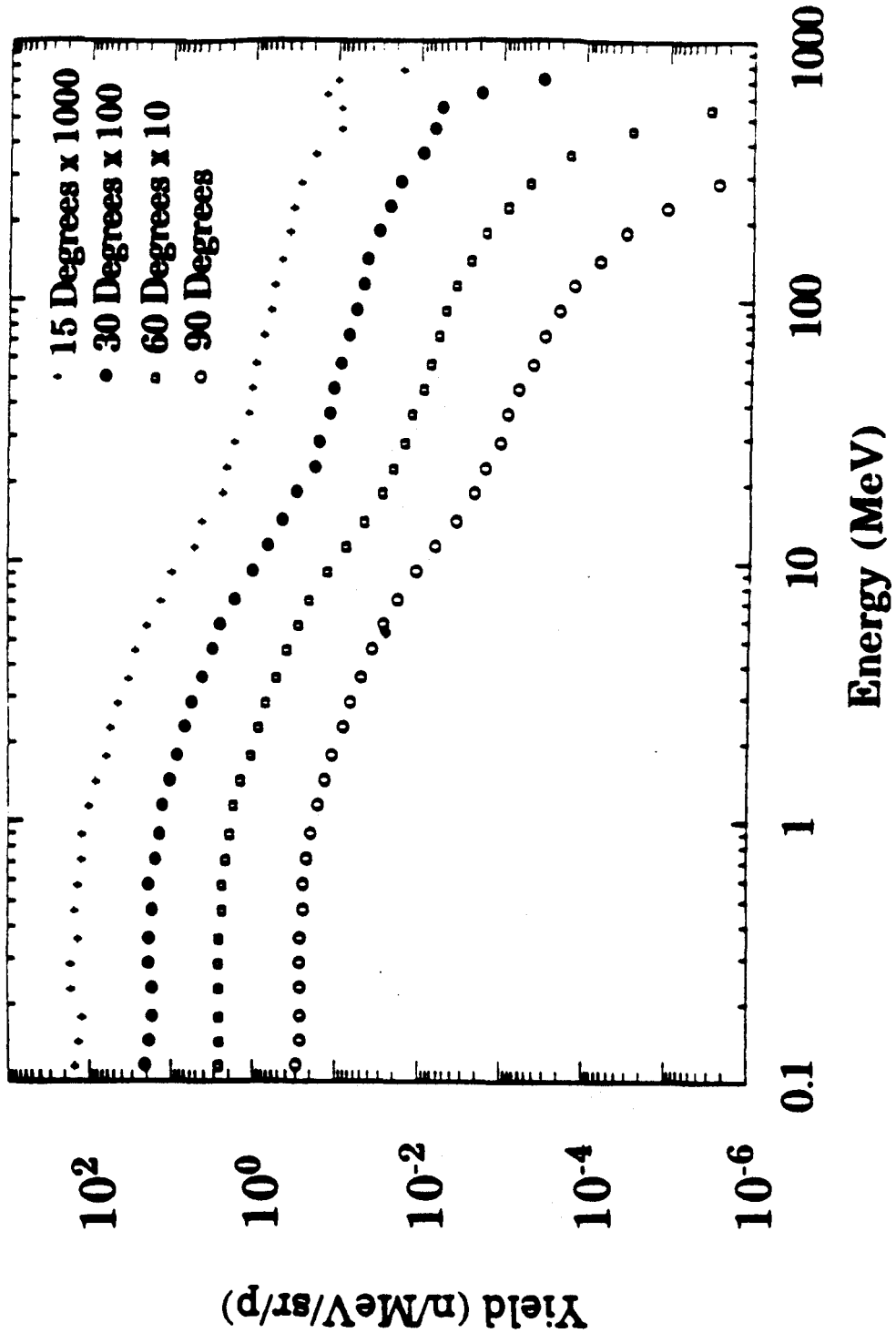

Fig. 6. Calculate neutron spectra as a function of angle. The spallation target is a 3 cm diameter x 7.5 cm long tungsten target. The calculation includes the effect of the stainless steel cooling jacket and the water cooling channels. (Fig. 9 of Appendix 2)

"The Los Alamos National Laboratory Spallation Neutron Sources," P. W. Lisowski, C. D.

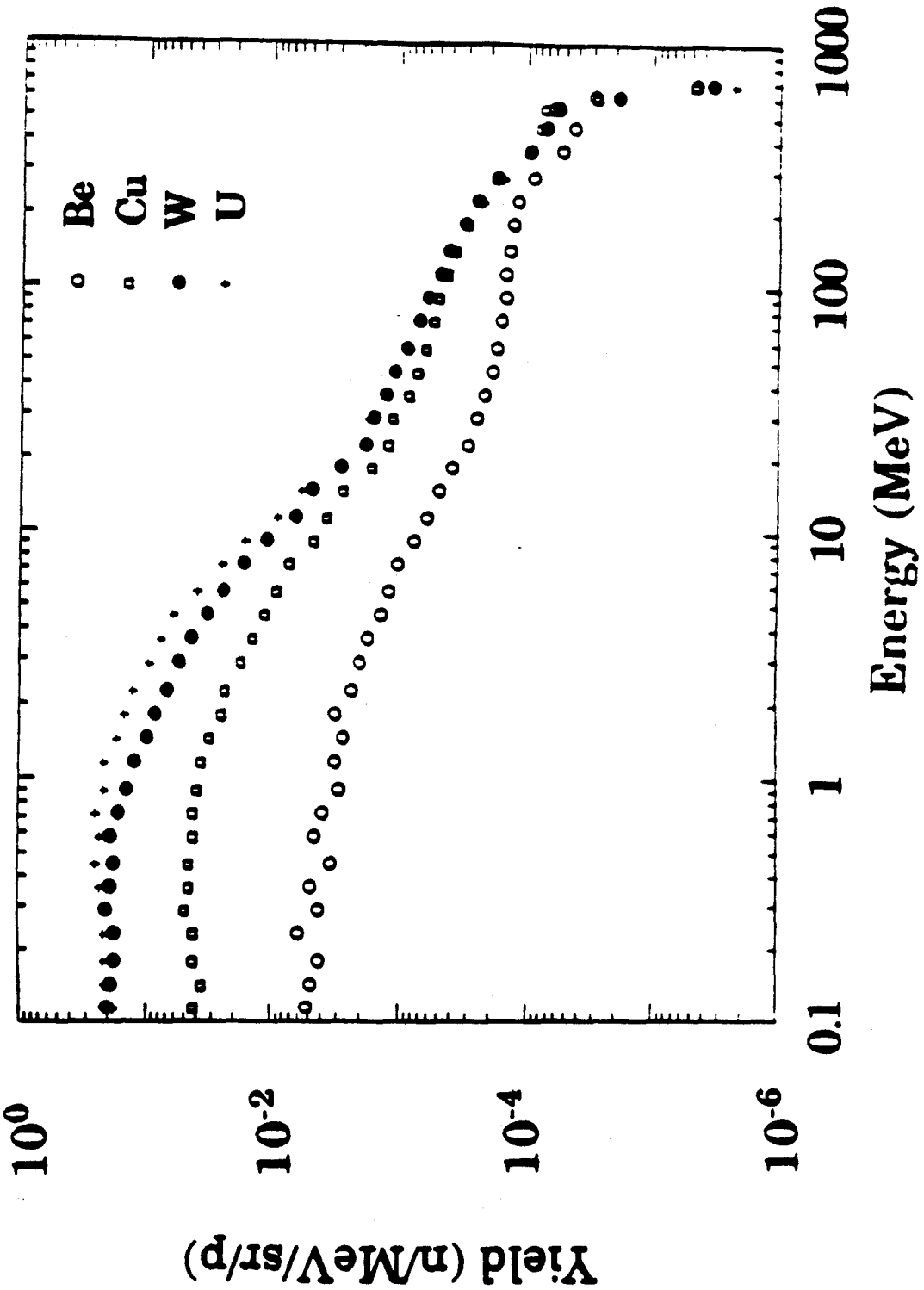

Fig. 7. Calculated neutron yield for WNR targets of berylium, copper, tungsten, and depleted uranium. The target has the same geometry as described in Fig. 7. (Fig. 10 of Appendix 2)

"The Los Alamos National Laboratory Spallation Neutron Sources," P. W. Lisowski, C. D.

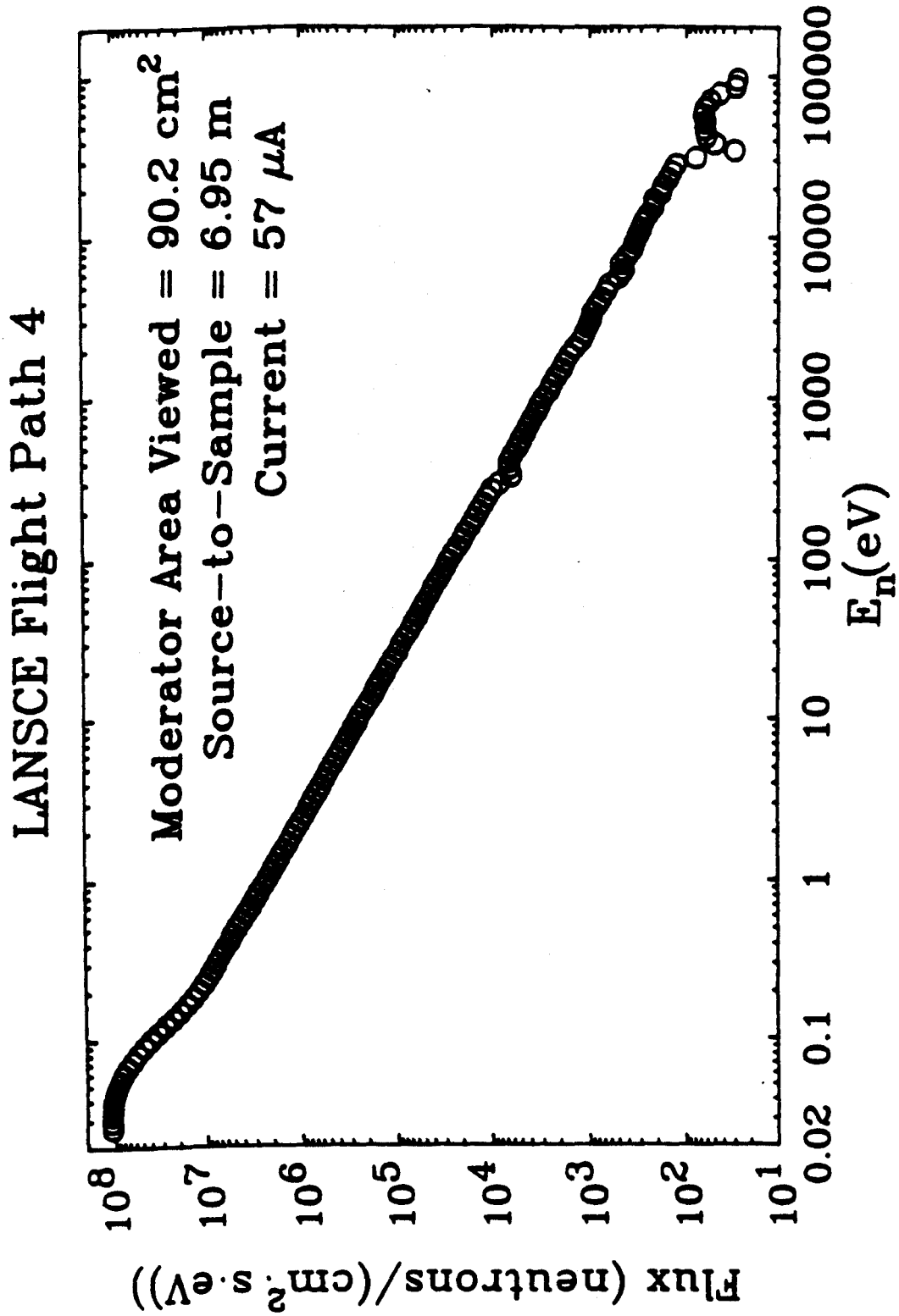

Fig. 8. The measured neutron flux for the LANSCE white neutron source. The realtive uncertainties are smaller than the size of the data points.

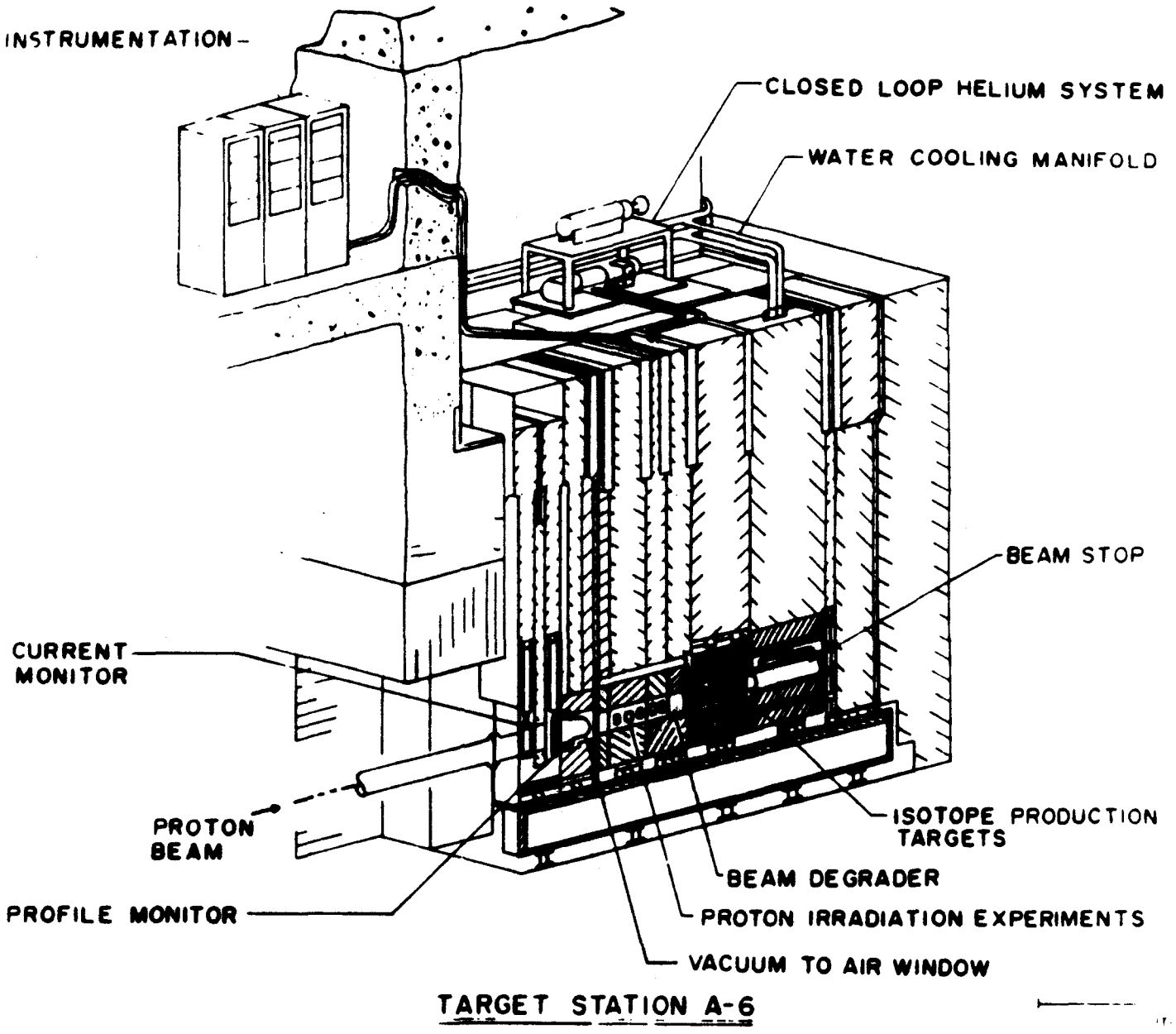

Fig. 9. A prespective view of LAMPF Target Station A-6, which houses the Radiation Effects Facility.

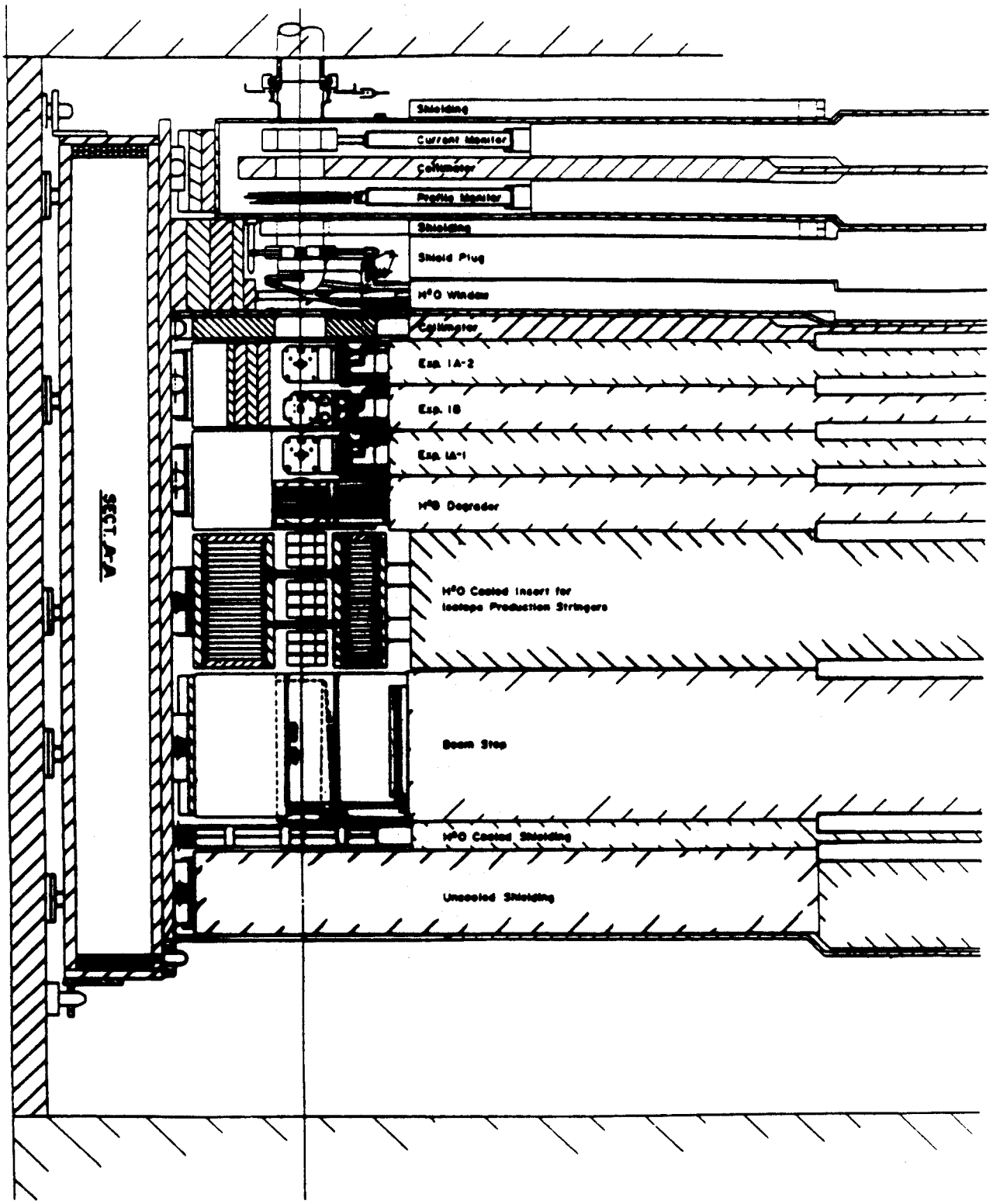

Fig. 10. Elevation view of Target Station A-6.

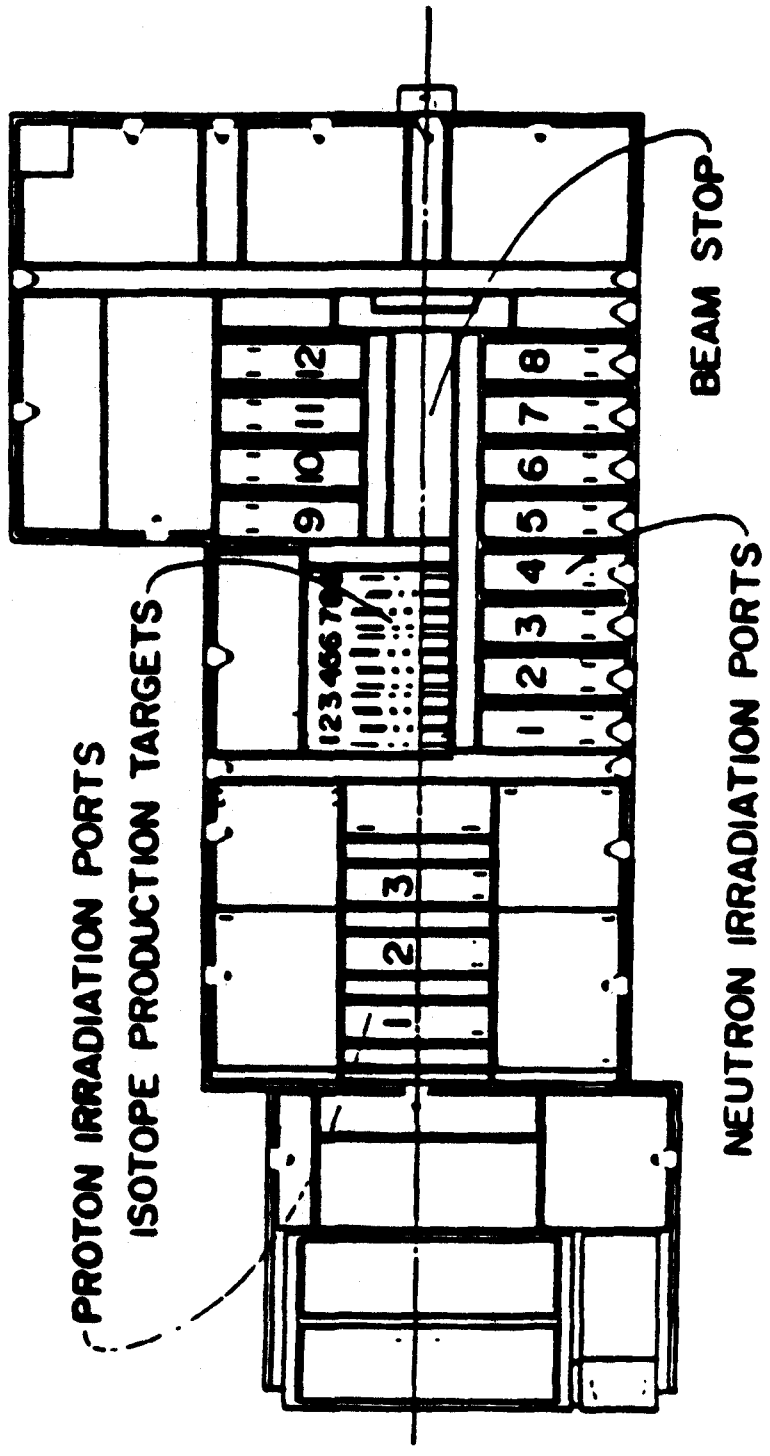

Fig. 11. Plan view of Target Station A-6 and the Radiation Effects Facility irradiation ports.

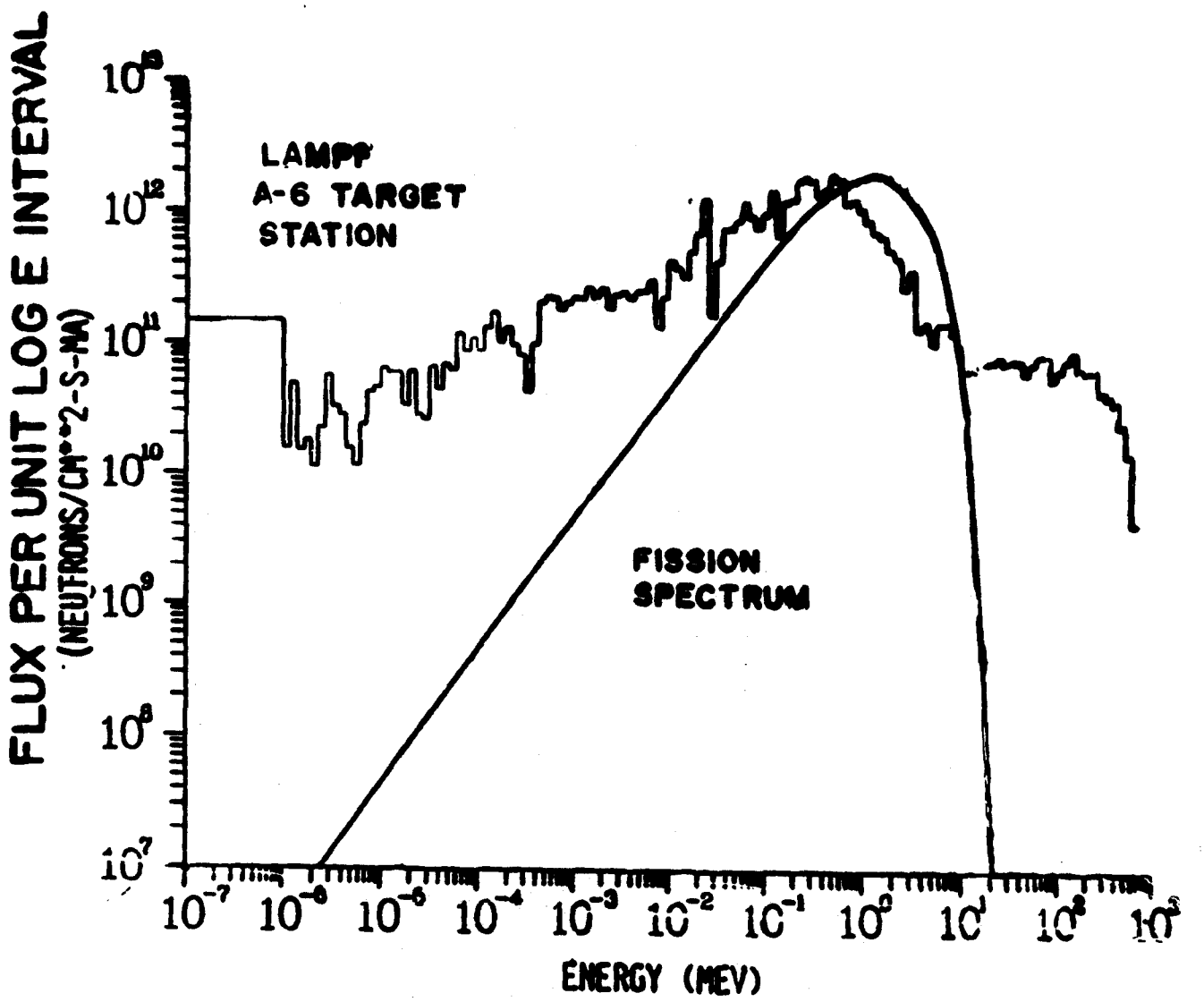

Fig. 12. Neutron flux spectra at the Target Station A-6 irradiation ports. For comparison, a fission spectrum is also shown ito illustrate the high energy (E_n > 10 MeV) flux available at the A-6 facility.

APPENDIX 1

HIGH-ENERGY PION CHANNEL

(P^3)

I. DESCRIPTION

The High-Energy Pion Channel, designated P^3, uses the A-2 production target as its source for the most energetic pions (625 MeV) available at LAMPF. Channel characteristics include high intensity, moderate resolution, low-background contamination, and a well-tailored phase space, transported achromatically to either of two output ports. Each output port contains four quadrupoles which match the channel phase space to a majority of experimental requirements with minimal tuning.

The channel was originally designed to accommodate a wide range of experiments:

- Experiments requiring pion energies in excess of 300 MeV,
- Elementary particle pion physics experiments, and
- Nuclear physics and chemistry experiments with modest resolution requirements.

Upgrading of the channel vacuum system has extended operation into the momentum region below 100 MeV/c. In addition to low-momentum pion operation, the delivery of surface and cloud muon beams has become possible. Preliminary muon beam data are presented along with the pion data.

II. DESIGN

A schematic, plan view of the P^3 channel is depicted in Fig. 1. Secondary charged particles produced at 20° from the A-2 target (5-cm graphite) are collected by

quadrupoles QD-01 and -02. Adjustable jaws (MS-01 and -02) define the solid angle of acceptance. The transmitted beam is momentum analyzed by BM-1 and brought to an intermediate, dispersed focus at the momentum-defining slit (MS-03) by quadrupoles QD-03 and -04. A horizontal target aperture (A-2 collimator) can be inserted to improve momentum resolution by reducing the horizontal target dimension as viewed by the channel.

In order to separate pions from protons in momentum, a variable amount of degrader is inserted. Bending magnet BM-2 transforms the momentum separation into a spatial separation near the second intermediate focus formed by quadrupoles QD-05, -06, -07, and -08. The protons are directed into the proton absorber (PABS). Electrons may similarly be separated and directed into the electron absorber (EABS).

The polarity of BM-3 is chosen to direct the achromatic beam to the selected output port. Additional beam-defining apertures (MS-04, MS-05, MSW, MSE) between the degrader and the experimental area help clean up the beam and define the output phase space.

Quadrupoles QD-09 to -12 in the West leg and QD-13 and -16 in the East leg can be tuned at the user's discretion to provide a wide range of output phase space. This combination of initial high-intensity, adjustable-jaws, and variable-output quadrupoles provides the flexibility required to meet the channel design objectives.

III. CHARACTERISTICS

TABLE I

Target length	5-cm graphite
Production angle	20°
Total length (to a point 1-m downstream of last quadrupole)	19.6 m
Maximum transmitted momentum	750 MeV/c
Maximum π kinetic energy	625 MeV
Maximum solid angle (1% momentum bite)	7 msr
Maximum momentum acceptance FWHM	10%
Minimum resolution (0.5-cm target)	0.2%
Typical resolution (5-cm target)	1.5%
Dispersion at momentum slit:	
West channel tune	1.8 cm/% $\Delta P/P$
East channel tune	1.5 cm/% $\Delta P/P$
First order phase space:	
Horizontal	200π mm-mr
Vertical	250π mm-mr

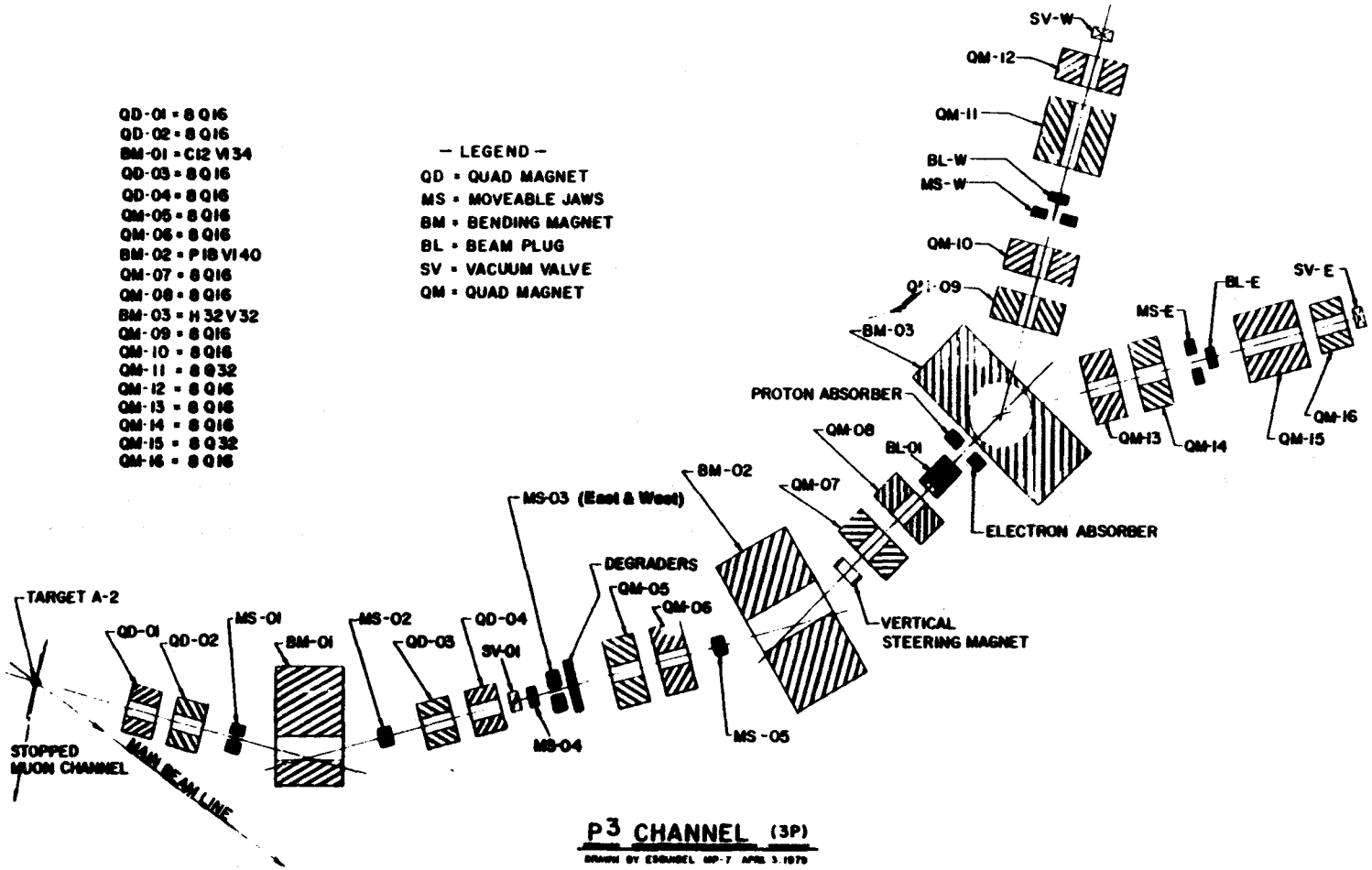
QD-01 = 8 Q16
QD-02 = 8 Q16
BM-01 = C12 V134
QD-03 = 8 Q16
QD-04 = 8 Q16
QM-05 = 8 Q16
QM-06 = 8 Q16
BM-02 = P18 V140
QM-07 = 8 Q16
QM-08 = 8 Q16
BM-03 = H 32 V32
QM-09 = 8 Q16
QM-10 = 8 Q16
QM-11 = 8 Q32
QM-12 = 8 Q16
QM-13 = 8 Q16
QM-14 = 8 Q16
QM-15 = 8 Q32
QM-16 = 8 Q16
— LEGEND —
QD = QUAD MAGNET
MS = MOVEABLE JAWS
BM = BENDING MAGNET
BL = BEAM PLUG
SV = VACUUM VALVE
QM = QUAD MAGNET
SV-W
QM-12
QM-11
BL-W
MS-W
QM-10
QM-09
BM-03
PROTON ABSORBER
QM-08
BL-01
ELECTRON ABSORBER
QM-07
BM-02
VERTICAL STEERING MAGNET
MS-03 (East & West)
DEGRADERS
QM-05
QM-06
MS-05
MS-04
SV-01
QD-04
QD-03
MS-02
BM-01
MS-01
QD-02
QD-01
TARGET A-2
STOPPED MUON CHANNEL
MAIN BEAM LINE
MS-E
BL-E
SV-E
QM-13
QM-14
QM-15
QM-16
P3 CHANNEL (3P)

Fig. 1.

IV. RATES

Pion rates and backgrounds are listed in Table II. The table entries relate to the following conditions:

- solid angle = 7 msr,
- momentum acceptance = 5%,
- 1-mA proton current on 5-cm graphite target,
- sufficient graphite degrader in π^+ beam to give 10-mr multiple scattering at each momentum, and
- π^- data obtained with no degrader.

The muon rates listed in Table III are preliminary measurements, subject to the following conditions:

- solid angle = 7 msr,
- momentum acceptance = 5%, and
- 1-mA proton current on 5-cm graphite.

BIBLIOGRAPHY

1. "A Proposal for P^3, Versatile High-Energy Pion Beam Facility," Los Alamos Scientific Laboratory report LA-4535-MS (September 1970).

2. "Preliminary Report on Some General-Purpose Two-Bend Pion Channels," Los Alamos Scientific Laboratory memo MP6/RJM-1 (April 10, 1970).

3. R. Macek, "A Multiplexed P^3 Channel," Los Alamos Scientific Laboratory memo (September 1970).

4. R. D. Werbeck and R. J. Macek, "Performance of the High-Energy Pion Beam at LAMPF," IEEE Trans. Nucl. Sci. **NS-22**, 1598-1600 (June 1975).

5. R. J. Macek, "Measurements of P^3 Central Momentum Via TOF," Los Alamos Scientific Laboratory report LA-7268-PR (October 1977).

TABLE II

PION RATES

Momentum (MeV/c)	Kinetic Energy (MeV)	π^+/s ($\times 10^8$)	P/π^+	π^+/ALL[a]	π^-/s ($\times 10^8$)	π^-/ALL[a]
100	32				0.01×10^8	0.02
200	104	0.30	0.00	0.68	1.04	0.42
300	191	1.40	0.00	0.95	3.27	0.80
350	237	1.96	0.01	0.98	4.20	0.91
400	284	2.63	0.02	0.996	4.66	0.916
450	332	2.86	0.04	0.999	4.09	0.990
500	380	2.39	0.09	1.000	2.80	1.000
600	476	0.58	0.65	1.000	0.60	1.000
700	574	0.03	18.9	1.000	0.03	1.000

[a]ALL = the nonproton component of the beam.

TABLE III

MUON RATES

Beam	Momentum (MeV/c)	Kinetic Energy (MeV)	μ/s ($\times 10^5$)	e/μ	Degrader
μ^+	28	3.65	21	80	None
μ^-	100	39.8	11.6	41	None
μ^-	100	39.8	2.6	20	0.65-cm carbon
μ^-	100	39.8	1.7	15	0.97-cm carbon

APPENDIX 2

Walter F. Sommer,[1] *Wolfgang Lohmann,*[2] *Karl Graf,*[2] *Ivan K. Taylor,*[1] *and Raymond M. Chavez*[1]

Operating Experience at the Los Alamos Spallation Radiation Effects Facility at LAMPF

REFERENCE: Sommer, W. F., Lohmann, W., Graf, K., Taylor, I. K., and Chavez, R. M., **"Operating Experience at the Los Alamos Spallation Radiation Effects Facility at LAMPF,"** *Influence of Radiation on Material Properties: 13th International Symposium (Part II), ASTM STP 956*, F. A. Garner, C. H. Henager, Jr., and N. Igata, Eds., American Society for Testing and Materials, Philadelphia, 1987, pp. 718–729.

ABSTRACT: Operation of a new irradiation facility at the beam stop (Target Station A-6) at the Clinton P. Anderson Los Alamos Meson Physics Facility (LAMPF) began in May 1985. The facility is now fully operational. A closed-loop water system, a closed-loop helium system, remote handling procedures for activated materials, experiment change-out procedures, and experiment control equipment are all in place.

Experience dictated a change in irradiation capsules from a system that used metal seals to a system that is completely welded. The seals were found to be unreliable and difficult to replace by remote means.

Several materials have been irradiated in the direct 760-MeV proton beam. Material property changes as well as helium production in a variety of materials are being investigated.

A special sample holder that can accommodate transmission electron microscopy (TEM) specimens, isolate them from the cooling medium, maintain fixed temperature, and retain essentially a stress-free state has been developed. Remote handling retrieval of these specimens is being developed.

Activation foil measurements are being made to determine the secondary particle flux and spectrum (charged particles and neutrons) that result from interaction of the direct proton beam with targets at the beam stop. Twelve independent irradiation ports, each with an irradiation volume of 0.12 by 0.25 by 0.50 m, are available for exposing material to this particle flux, primarily neutrons. Two irradiations were completed in this area during the period May through December 1985. The neutron spectrum here resembles a fission spectrum with the addition of neutrons in the MeV energy range (high-energy tail). The maximum neutron flux is about 6×10^{17} n/m^2 s at one of the 12 ports and drops by a factor of about 10 as a minimum at another of the 12 ports.

Three independent ports for proton irradiations are in place. Each has an irradiation volume of about 150 cm^3. The proton beam has a Gaussian intensity profile; the maximum proton flux at the center of the beam is 1.2×10^{14} protons/cm$^2 \cdot$ s. The beam spot has a diameter of approximately 5 cm at 2σ. Four irradiations were completed in this area during the period May through December 1985.

KEY WORDS: protons, spallation neutrons, irradiation facility, irradiation techniques, Los Alamos Meson Physics Facility (LAMPF)

A new facility, in which materials may be exposed to a proton beam of energy ~760 MeV and a neutron flux that results from the interaction of the proton beam with bulk targets and the beam

[1] Associate group leader, senior technician, and senior designer, respectively, Los Alamos National Laboratory, Los Alamos, NM 87545.

[2] Research scientist and engineer, respectively, KFA Jülich GmbH, P.O. Box 1913, D5170, Jülich, West Germany.

stop at the Los Alamos Meson Physics Facility (LAMPF), began operation in May 1985. Several experiments, under controlled temperature conditions, were completed during three LAMPF run cycles between May 1985 and Jan. 1986. An experiment capsule, a closed-loop helium temperature-control system, a closed-loop water temperature control system, and remote-handling procedures for radioactive material have been developed and used successfully. It was also shown that a complete experiment changeover could be accomplished in less than one day. This is of importance because during a nine-week run cycle, the LAMPF accelerator is only idle for one day each two weeks for routine maintenance and some experiments require sample changes in a time frame shorter than nine weeks. Further refinement of the facility will take place during a shut-down period in spring 1986. In the text below, we attempt to summarize our recent experience in using the facility and also to describe the equipment that we feel has proven to be reliable.

Facility Description

The Los Alamos Spallation Radiation Effects Facility (LASREF) is located at the beam-stop area (Target Station A-6) at LAMPF. The design of this facility is modular in that each component and experiment is attached to its own biological shield plug (insert). This can be seen by noting a schematic (Fig. 1) and a photograph (Fig. 2). The biological shield is necessary for containment of the radiation produced along the beamline, at the isotope production bulk targets, and at the beam stop. Services, such as cooling water and instrumentation cabling, are routed through stepped slots in the biological shield to the top of the facility. Instrumentation cabling is further routed

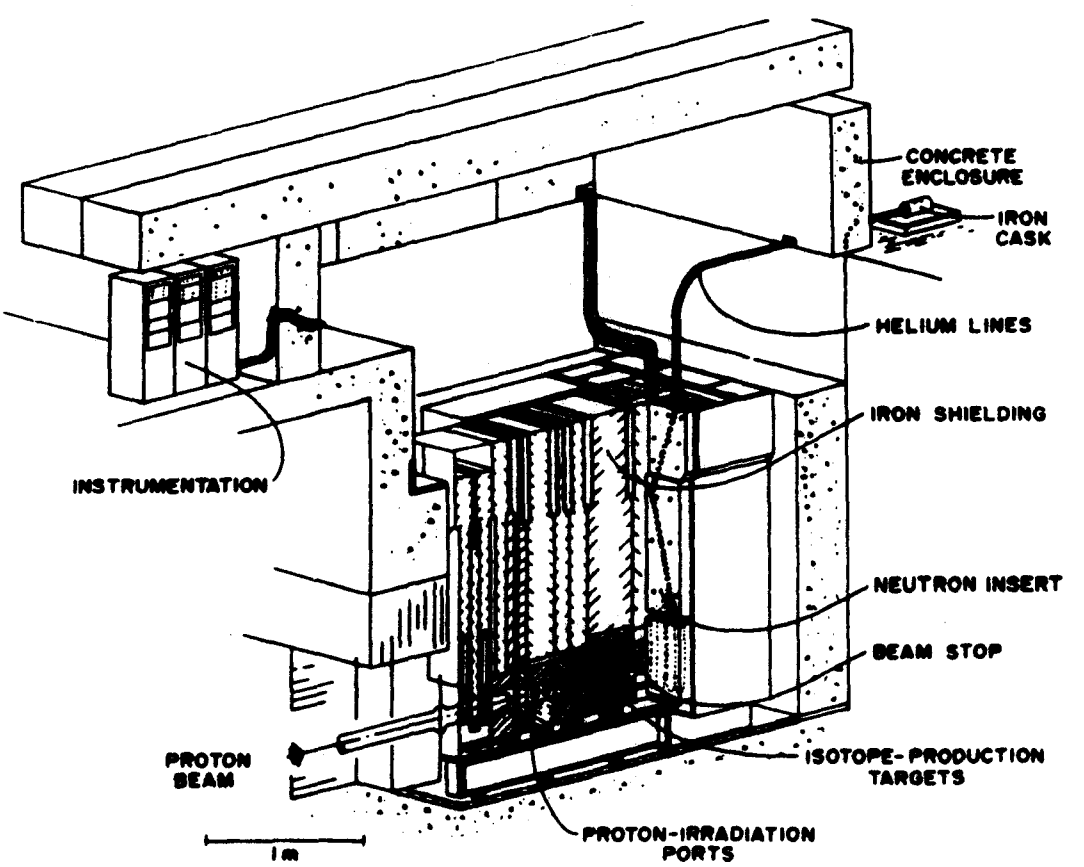

FIG. 1—*Schematic of the Los Alamos Spallation Radiation Effects Facility (LASREF) at LAMPF.*

FIG. 2—*A proton-irradiation insert and capsule.*

through a maze in a secondary containment concrete hut to an area that is accessible when beam is on, where instrumentation cabinets can be located. This can be seen in schematic form in Fig. 1.

Three independent insert locations (proton irradiation inserts) are available for placing capsules in the direct proton beam. Their relationship to other components at Target Station A-6 is shown in a side view in Fig. 3. The irradiation volume for each is about 150 cm^3. It is possible to modify the insert to accommodate more sensitive equipment in a position removed from the beamline where both shielding and distance decrease the particle radiation flux.

Twelve independent insert locations (neutron irradiation inserts) are available for placing capsules in the neutron flux. Figure 4 shows their relationship to other components at Target Station A-6 in a top view and Fig. 5 shows, schematically, their relationship to the neutron-producing targets.

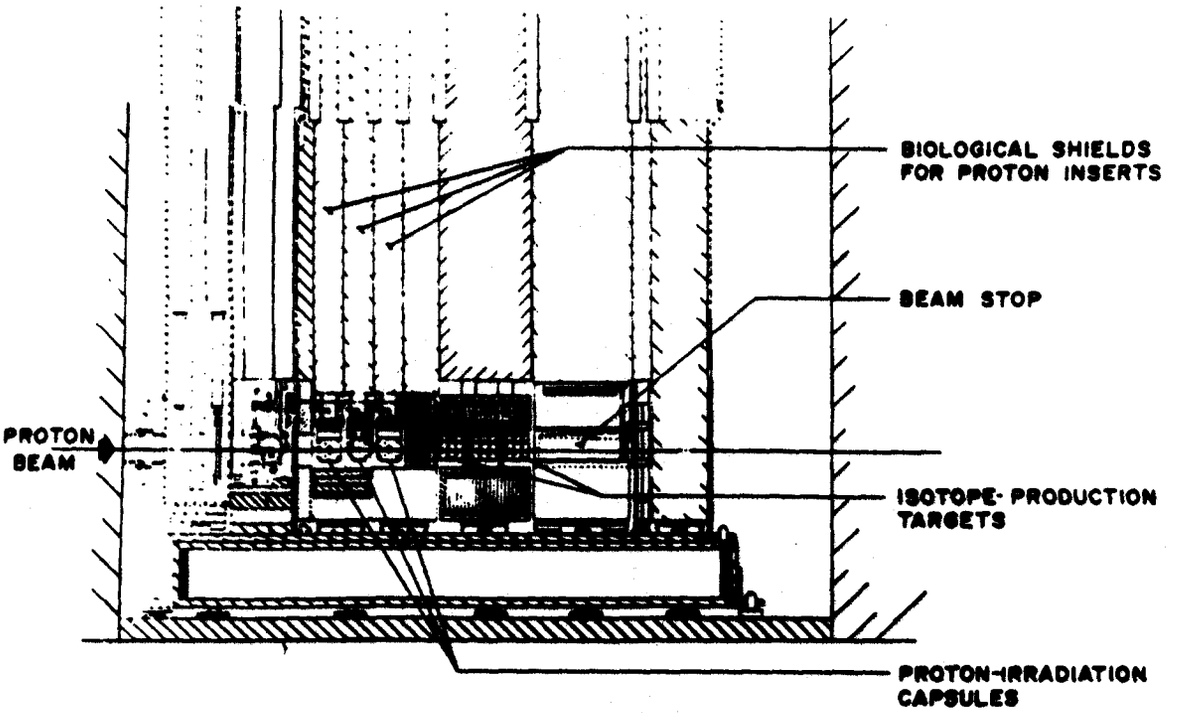

FIG. 3—*Proton-irradiation insert locations relative to other components in Target Station A-6.*

(Protons, in comparable number, are also produced by spallation reactions in the targets but ~90% are absorbed in the target material [*1*,*2*]. This is also the case for other secondary charged particles produced in the targets.) Each insert location has a 12- by 25- by 50-cm volume available for irradiation capsules whose geometry and complexity is left to the discretion of the experimenter.

Although LAMPF accelerates protons to a maximum energy of 800 MeV, interactions with two graphite targets upstream from the facility lowers the energy to about 760 MeV. At a nominal

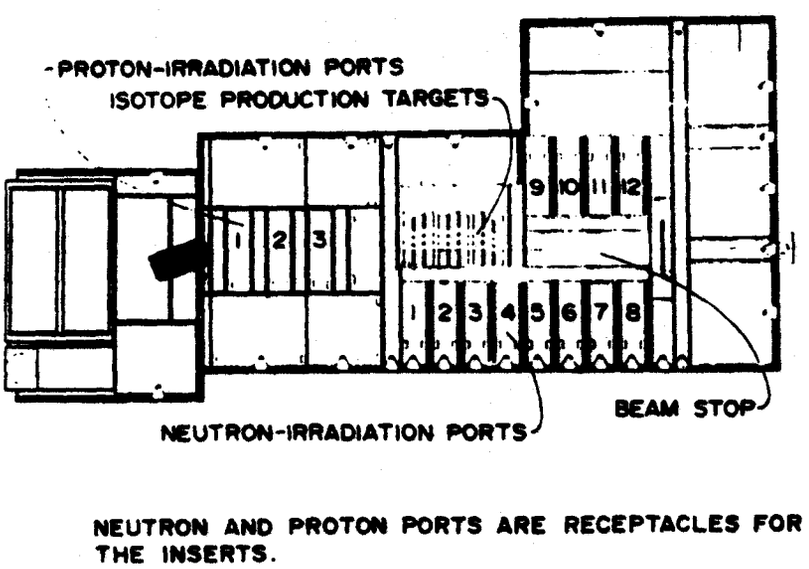

FIG. 4—*Neutron-irradiation insert locations relative to other components in Target Station A-6. This is a top view.*

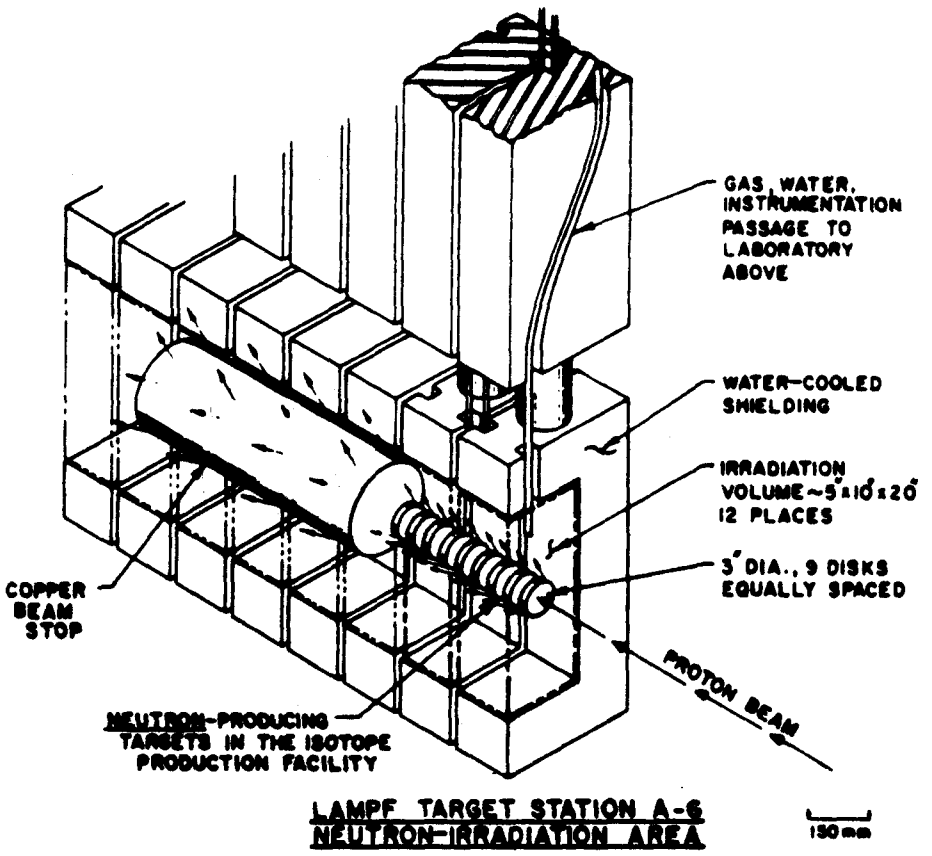

FIG. 5—*Schematic of the relation of neutron-irradiation inserts, 1 through 8, to the neutron-producing targets in Target Station A-6.*

total beam current of 1 mA and a Gaussian-like beam spot size of diameter 5 cm to 2σ (σ is one standard deviation), it has been calculated [*3*] that a displacement rate of 8.4×10^{-7} displacements per atom per second (dpa/s) is obtained in copper metal at the center of the beam. During 1985, the average beam current actually delivered to LASREF was on the order of 0.8 mA and, considering that the beam was available about 80% of the time, the resultant total atomic displacements would be 2.9 dpa in copper metal in one nine-week LAMPF run cycle.

Calculations [*1*] and measurements [*2*][3] have been made of the particle flux and spectrum (Fig. 6) incident on the neutron-irradiation volumes. At position 2 in Fig. 4, the total neutron flux is about 5.5×10^{17} n/m^2 s at 1 mA of proton beam current giving a displacement rate of 4×10^{-8} dpa/s in copper metal [*3*]. For the conditions available during 1985 (0.8 mA and 80% availability), a total atom displacement of 0.14 dpa would be achieved in a nine-week LAMPF run cycle in copper metal. The flux drops along the beamline from position 2 to a minimum at positions 8 and 12, ~10x lower than at position 2. Calculations [*1*] and measurements[3] have also shown that the secondary charged-particle flux at the inner surface (nearest the beamline) of the neutron-irradiation volumes is about 10% of the neutron flux. An additional 1 cm of iron shielding further reduces the charged-particle flux to about 1% of the neutron flux.

A real-time signal of the average beam current being delivered to LASREF is continually available. The signal is compatible with standard data-acquisition equipment.

[3] Davidson, D. R. et al., in this publication, pp. 730–740.

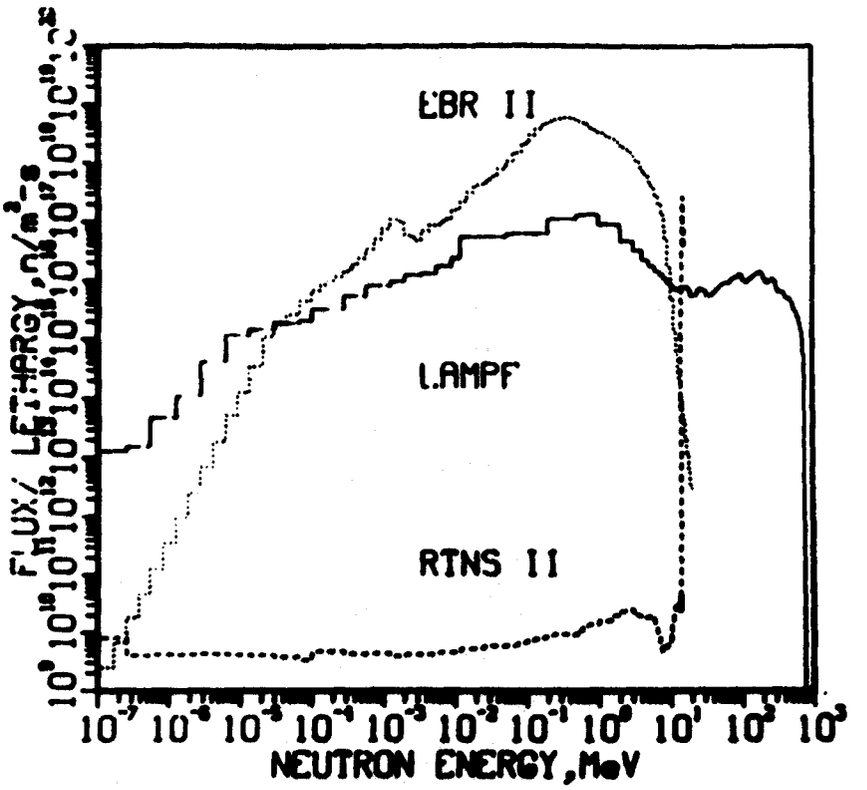

FIG. 6—*Neutron flux and spectrum at Target Station A-6 at neutron-irradiation insert location 2.*

Hardware Description and Performance

Capsules that can survive the radiation environment, provide an atmosphere for controlled conditions of temperature and stress, and allow remote handling and removal of specimens without disturbing the material has been developed and used successfully during 1985. In addition, a "rabbit" system [*4*] that is capable of placing several small capsules (10.3 mm diameter by 21.6 mm long) loaded with foils for activation analyses to determine neutron and charged-particle flux and spectrum was developed and used successfully.

Figure 7 is a pictorial view of a proton irradiation capsule, and the cross-sectional drawing (Fig. 8) shows some of the important details. Note that samples are attached to a finger-like sample holder (materials are selected for appropriate thermal expansion compensation, or one end is left free for unperturbed thermal expansion). This sample holder is attached to a plug with a specially designed weld prep, which in turn is inserted into a tube that directs coolant (in this case, water from a closed-loop water system) over the samples. The proton beam is directed onto the tubes, centered between the plenums, and centered vertically on the group of five tubes. Since the proton beam has a Gaussian intensity profile, there is a gradient in accumulated dose for samples placed in tubes vertically away from the center. This allows some fluence-dependent observations from a single irradiation. The intensity gradient also is present, of course, in the horizontal direction so care must be taken in properly dimensioning the sample gage length so that this gradient does not cause significant ambiguity in the results. There are a total of 13 tubes, in which we have attached 8 samples each; thus a single capsule yields 104 irradiated samples.

Removal of the samples is facilitated by the special weld prep on the plug. By remote means, a special slow-speed grinder removes the weld metal and the entire sample assembly can then be removed from the capsule. This procedure eliminates the excessive vibration and possible mechanical

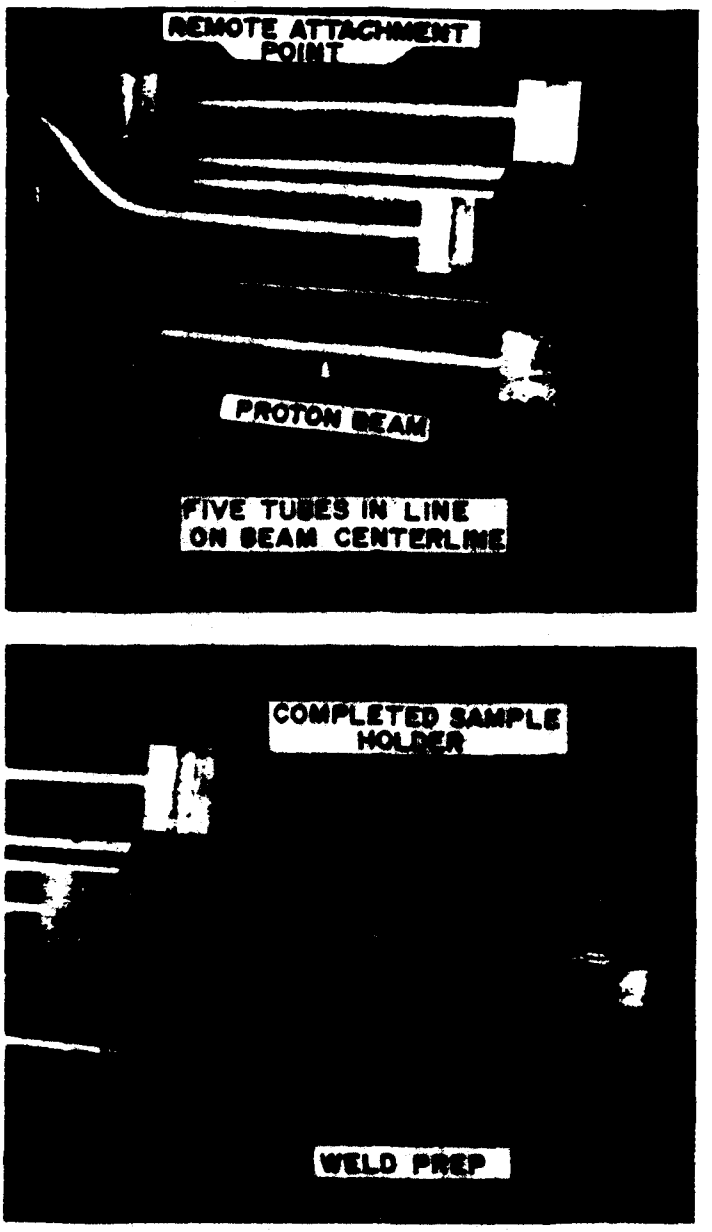

FIG. 7—*Proton-irradiation capsule.*

damage that we encountered in an earlier design that used a bolted flange; removal of the bolts was found to be difficult and metal seals were found to be unreliable.

Another capsule has been developed for use with the closed-loop helium system. Since more than 200 W/cm^3 (in iron) are deposited by beam heating, we found that helium gas alone was not sufficient to maintain a suitable temperature gradient across the samples. The major contribution to the heat load came from the tubes that direct the flow rather than the samples. We therefore designed a double-tube capsule (Fig. 9) in which water flows in the annulus between the tubes and extracts the energy deposited in the tubes and helium, preheated to the temperature needed for the experiment, flows over the samples and extracts the energy deposited in the samples. Installation and remote handling of the specimens is accomplished in a manner identical to that described above.

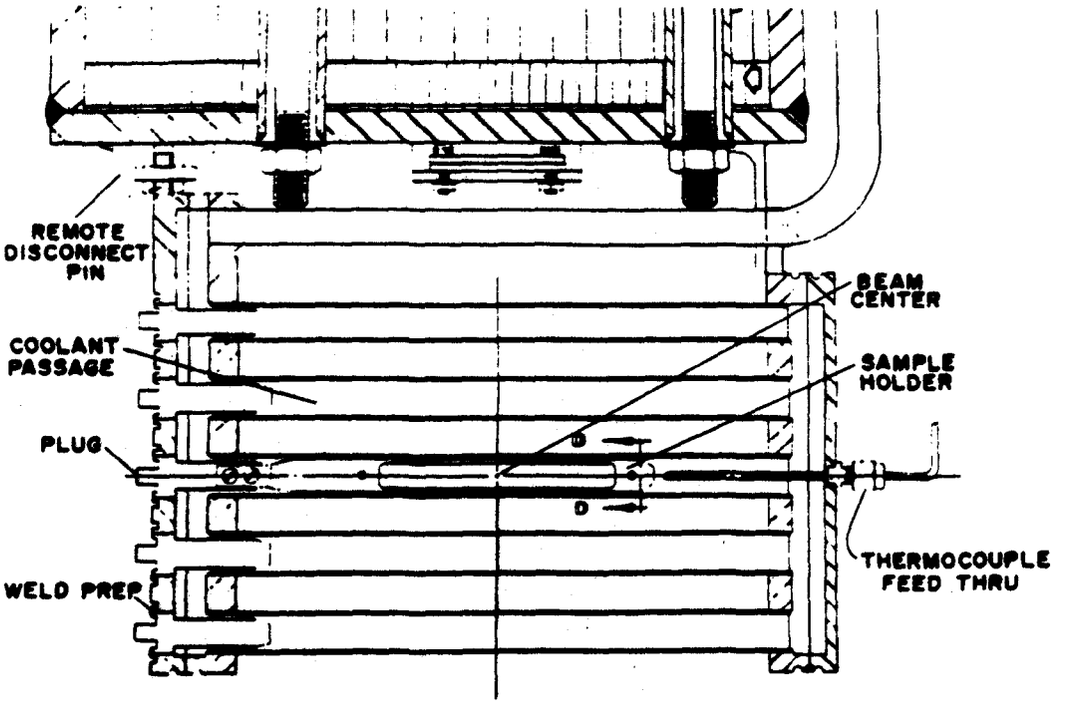

FIG. 8—*Cross section of a proton-irradiation capsule.*

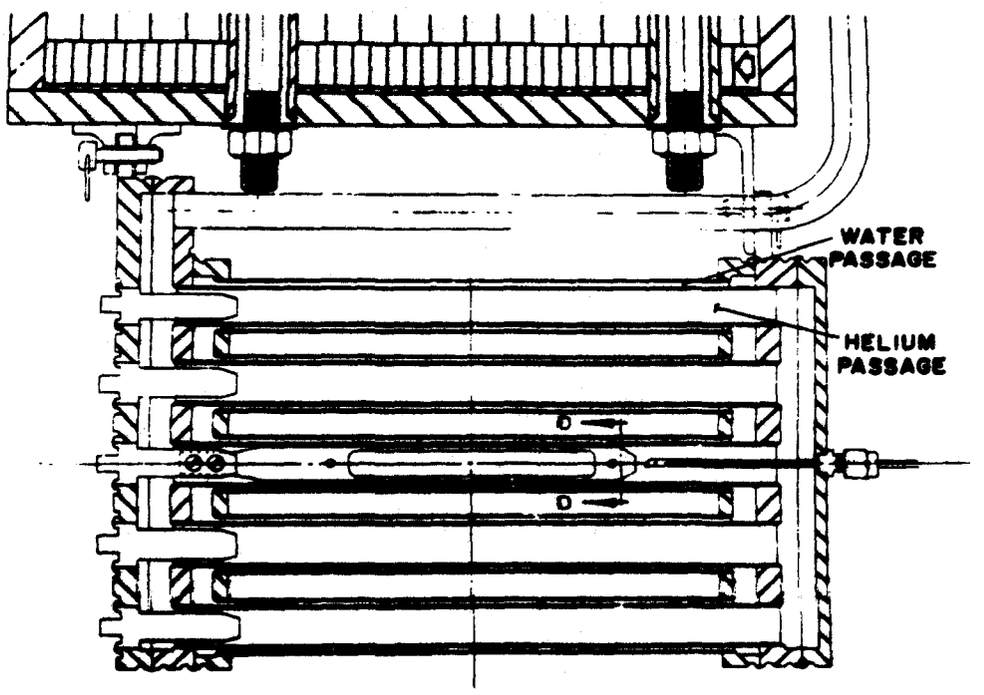

FIG. 9—*Cross section of a proton-irradiation capsule for use with helium or other gas.*

In order to provide a map of the neutron and charged-particle flux in the facility (complex because of the distributed source introduced by the various targets [Fig. 5]), a "rabbit" system capable of placing small capsules containing activation foils (Fig. 10) above and below the beamline and at four locations radially out from the beamline was built and developed [*4*]. The "rabbits" are small cylinders, 10.3 mm in diameter by 21.6 mm long, which house the activation foils. They are pneumatically driven into the irradiation space and, after irradiation, into shield casks outside the concrete enclosure by pressurized helium gas. Several irradiations, in neutron insert Positions 2 and 6, were completed and are now being analyzed[3] as a comparison to earlier work [*1,2*]. The insert that houses the "rabbit" system can be placed in any one of the 12 irradiation locations. It is available for use by the radiation damage community; a nuclear chemistry group studying activation of cosmic material has used the system to learn about material interaction with high-energy (> 100 MeV) neutrons of which ample numbers are available in the facility.

A special capsule that can determine mechanical properties, such as flow stress, fatigue, and creep while the material is being irradiated, was designed and built by the KFA-Jülich group. Central to the successful use of this device is the reliable operation of a stepping motor that loads the samples, a linear variable differential transformer (LVDT) that measures length changes and a load cell that measures load. The internal mechanism of the device is shown in Fig. 11. As a reliability test, we placed identical components on a neutron irradiation insert in Position 7. The motor was used to raise and lower a deadweight onto the load cell while the LVDT recorded the cyclic motion. We found that the devices would properly function in this environment for adequate times. The environment approximates the radiation levels we expect at the proton irradiation insert locations in the areas, outside the beamline, where the devices are planned for use. We found that it is necessary to use mineral-insulated cabling on all inserts used in the facility.

Handling of Radioactive Inserts: Experiment and Sample Changes

It was demonstrated, using existing LAMPF remote handling equipment and other LAMPF systems, that an insert and, hence, an experiment change could be accomplished in a 6-h period.

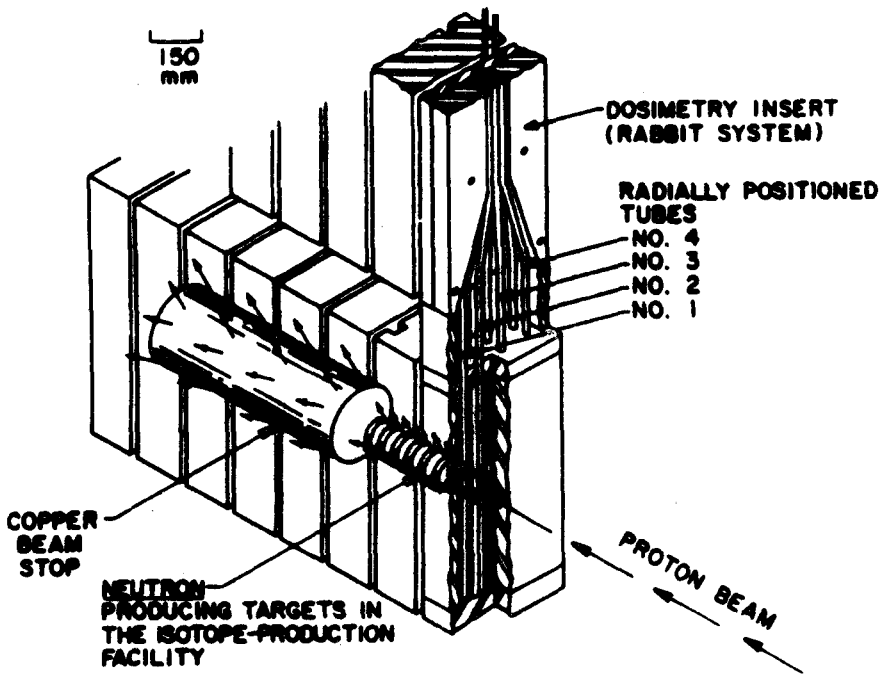

FIG. 10—*"Rabbit" system in place in the neutron-irradiation area.*

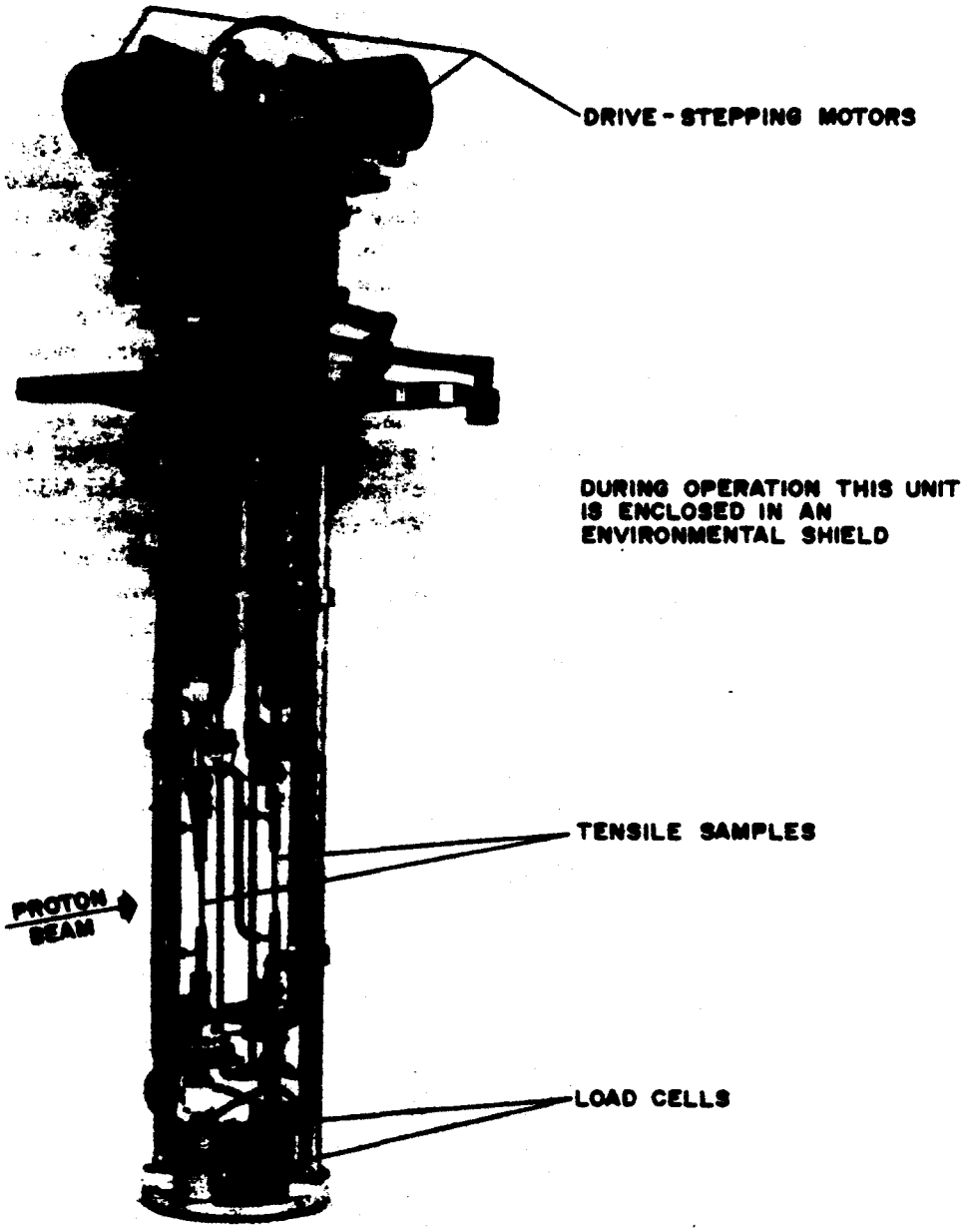

FIG. 11—*Internal mechanism of the in-situ mechanical testing device.*

To facilitate this work, the new experiment is mounted on a new, unirradiated insert and instrumentation, and services are completed and terminated at the top of the insert with the entire unit supported on a special rack in a vertical attitude. Remote handling procedures for sample handling and preparation, for example, of transmission electron microscopy (TEM) samples, are now being developed. With regard to TEM, we developed a special holder that can accommodate 3-mm disks, place them in a tube in a proton-irradiation capsule, isolate them from the cooling medium, and maintain temperature control. This is advantageous when only microstructural evolution study by TEM is desired since it simplifies sample preparation of radioactive material. This device is shown in Fig. 12.

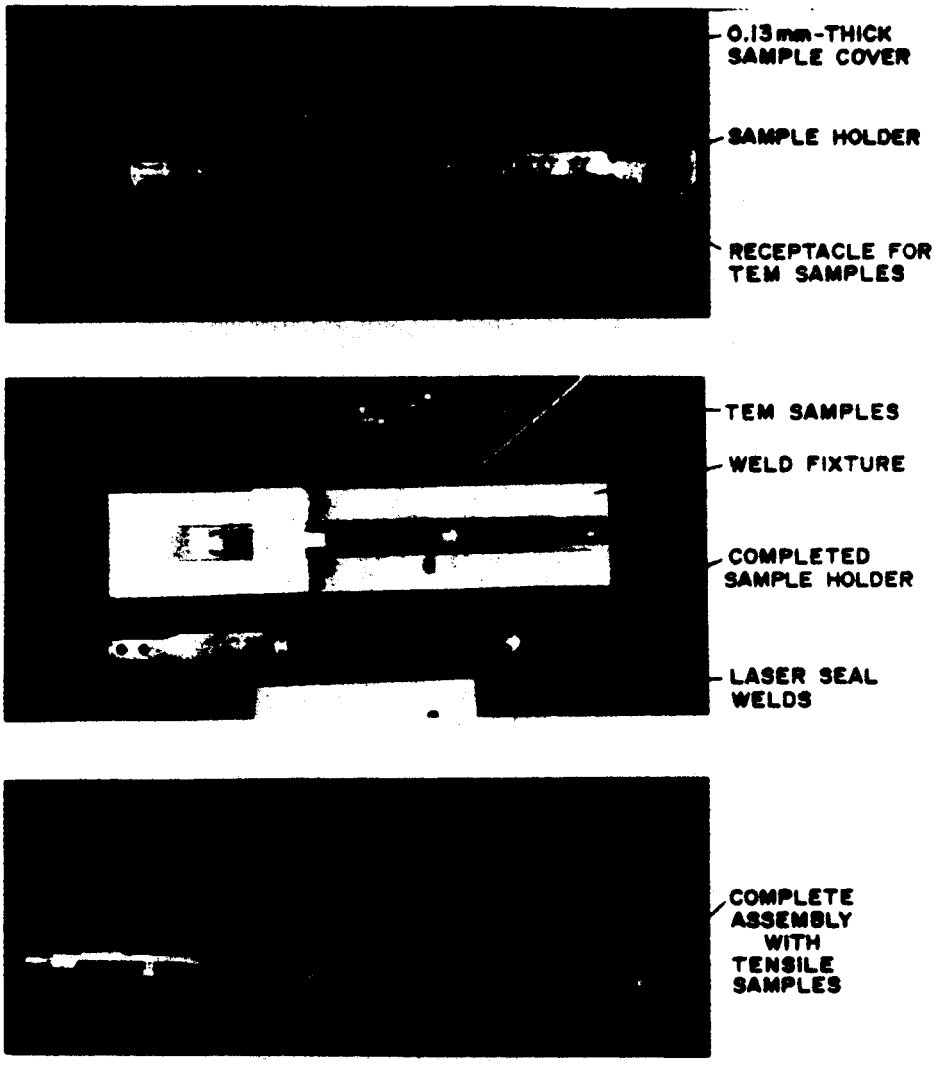

FIG. 12—*Special fixture for irradiating TEM specimens.*

Summary

The LASREF is an operating facility. Equipment necessary for temperature control has been developed. Remote handling capability has been demonstrated. Irradiation capsules have proven reliability. Inquiries relating to the use of the facility can be directed to the authors.

Acknowledgments

The authors thank A. Horsewell for helpful critique and C. Mueller, B. Ortiz, F. M. Gehrmann, S. Lopez, T. Montoya, F. Roybal, A. Maestas, L. Martinez, and the LAMPF Remote Handling and Targeting Section, whose expert technical assistance led to the successful commissioning of our facility.

References

[1] Davidson, D. R., Little, R. C., Sommer, W. F., Bradbury, J. N., and Prael, R. E., "Characterization of the Radiation Environment at a New Proposed Irradiation Facility at LAMPF," *Journal of Nuclear Materials*, Vols. 122 & 123, 1984, pp. 989–994. M. S. Wechsler and W. F. Sommer, "The Radiation Damage Facility at the LAMPF A-6 Target Station," J. Nucl. Mater. 122– 123, 1078–1084 (1984).

[2] Davidson, D. R., Greenwood, L. R., Reedy, R. C., and Sommer, W. F., "Measured Radiation Environment at the Clinton P. Anderson Meson Physics Facility (LAMPF) Irradiation Facility," *Effects of Radiation on Materials: Twelfth International Symposium, STP 870*, F. A. Garner and J. S. Perrin, Eds., American Society for Testing and Materials, Philadelphia, 1985, pp. 1199–1208.

[3] Wechsler, M. S., Davidson, D. R., Greenwood, L. R., and Sommer, W. F., "Calculation of Displacement and Helium Production at the Clinton P. Anderson Meson Physics Facility (LAMPF) Irradiation Facility," *Effects of Radiation on Materials: Twelfth International Symposium, STP 870*, F. A. Garner and J. S. Perrin, Eds., American Society for Testing and Materials, Philadelphia, 1985, pp. 1189–1198.

[4] Davidson, D. R., Sommer, W. F., Taylor, I. K., Brown, R. D., and Martinez, L., " 'Rabbit' System for Activation Foil Irradiations at the Los Alamos Spallation Radiation Effects Facility at LAMPF," LA-UR-85-3630 Revision, abstract accepted for the Second International Conference on Fusion Reactor Materials, Chicago, IL, 13–17 April 1986.

APPENDIX 12

Guidelines for Measurements of Radiation Effects in SSC Semiconductor Detectors and Electronics

Guidelines for Measurements of Radiation Effects in SSC Semiconductor Detectors and Electronics

H. Spieler

1. Specification of Radiation Dose

a) Ionization studies
(e.g. MOSFET V_t, isolation structures)

depends only on liberated charge (deposited energy)

- specify dose in rad

b) Displacement damage
(detector I_b, BJT β vs. I_d, JFET g_m, etc.)

depends on particle type + energy

- specify
  1. fluence (cm^{-2})
  2. particle type
  3. particle energy (or energy range)

2. Measurements on Detectors

a) Specify detector active area and thickness

b) where possible use gated diode structures surrounding detector to allow separation of bulk and surface currents

c) specify temperature

d) provide plots of 1/C vs. V_b (pre- and post-rad)
+ specify operating bias

e) measure charge yield vs. E-field in detector

f) measure shot noise and relate to current (spectrum?)

GET ADEQUATE STATISTICS!

3. Measurements on Transistors
(MOSFETs, JFETs, BJTs)

a) measure V_t shifts at low V_d ($\simeq$ 10 mV)
to facilitate general application

b) measure I_d vs. V_g and g_m vs. I_d from weak
through strong inversion
preferably plot (g_m/I_d) vs. (I_d/W)

c) show g_d vs. V_{ds}

d) Noise:

measure equiv. input noise spectrum through
"1/f" and white noise regimes

when measuring Q_n specify
pulse shaping,
input current,
total input capacitance

GET ADEQUATE STATISTICS!

LBL ^{60}Co Irradiation Facility

Primarily γ-rays (1.17 and 1.33 MeV)

useful for measurement of ionization effects
(some displacement damage)

Dose rate:

r = 1 m:	0.180 rad(Si)/s ≈ 650 rad(Si)/hr
r = 80 cm:	1 krad(Si)/hr
r = 25 cm:	10 krad(Si)/hr (4.2 d for 1 Mrad)

Caution:

Must take proper precautions for accurate dosimetry!

e.g.

1. enclose test device in filter box for equilibration + attenuation of low-energy photons (1.5 mm Pb followed by 0.7 mm Al)

2. high-Z layers toward radiation source to minimize dose enhancement

(see Ma and Dressendorfer, *Ionizing Radiation Effects in MOS Devices and Circuits*)

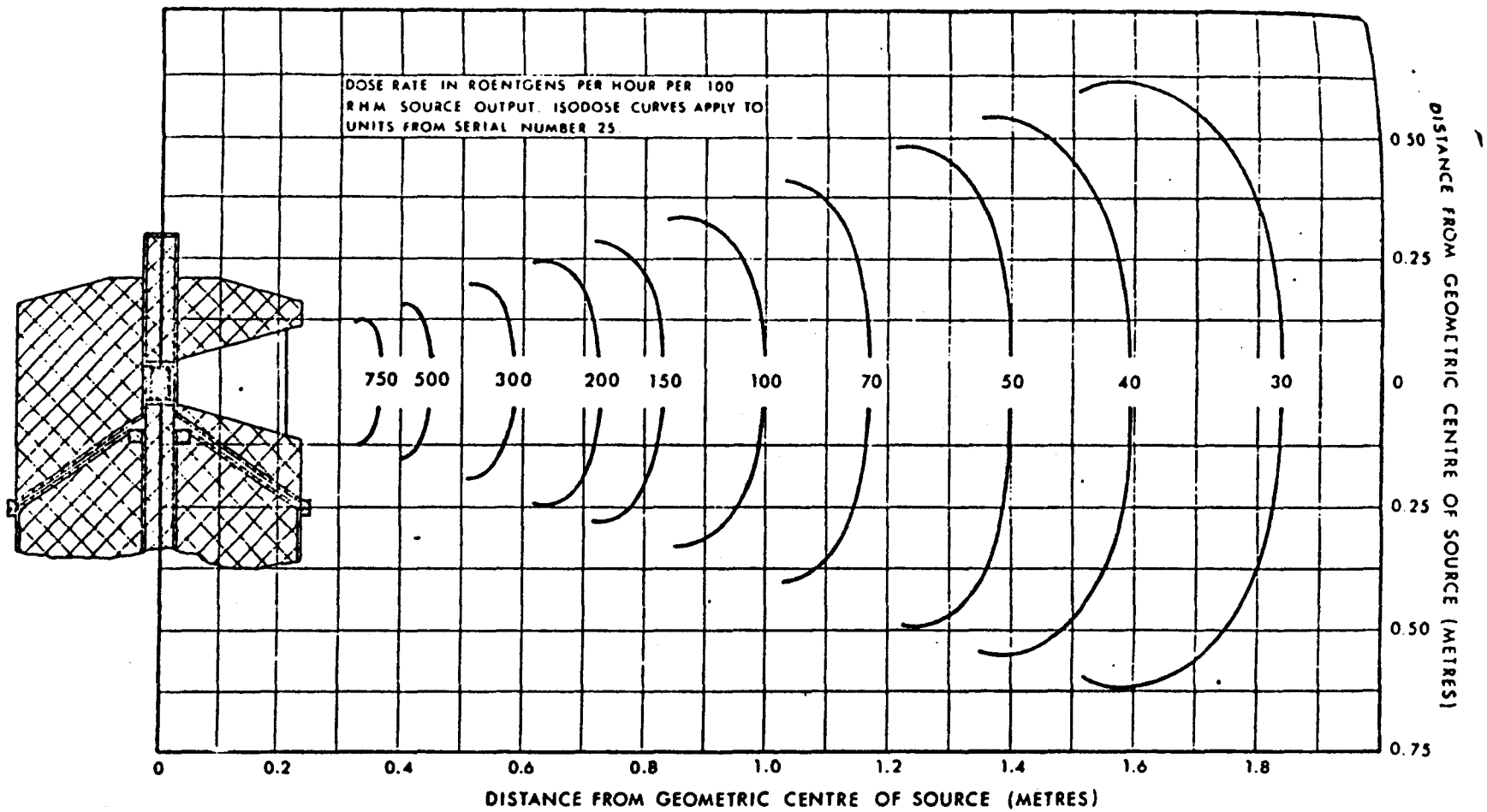

ATOMIC ENERGY OF CANADA LIMITED COMMERCIAL PRODUCTS P.O. BOX 93 OTTAWA	TITLE	GAMMABEAM 150 C ISODOSE CURVES IN AIR VERTICAL PLANE		
	REF. DWG.		REVISED	
THIS DRAWING IS THE PROPERTY OF ATOMIC ENERGY OF CANADA LIMITED, AND IS SUBMITTED FOR CONSIDERATION ON THE UNDERSTANDING THAT THERE SHALL BE NO EXPLOITATION OF ANY INFORMATION CONTAINED HEREIN EXCEPT WITH THE SPECIFIC WRITTEN AGREEMENT OF ATOMIC ENERGY OF CANADA LIMITED.	DATE OCT 17 1968		No J400-X-11	REV.
	DRAWN D.L.B.	CHECKED E.F.R.	APPROVED A.W.G. F.W.	SHEET 1 OF 1

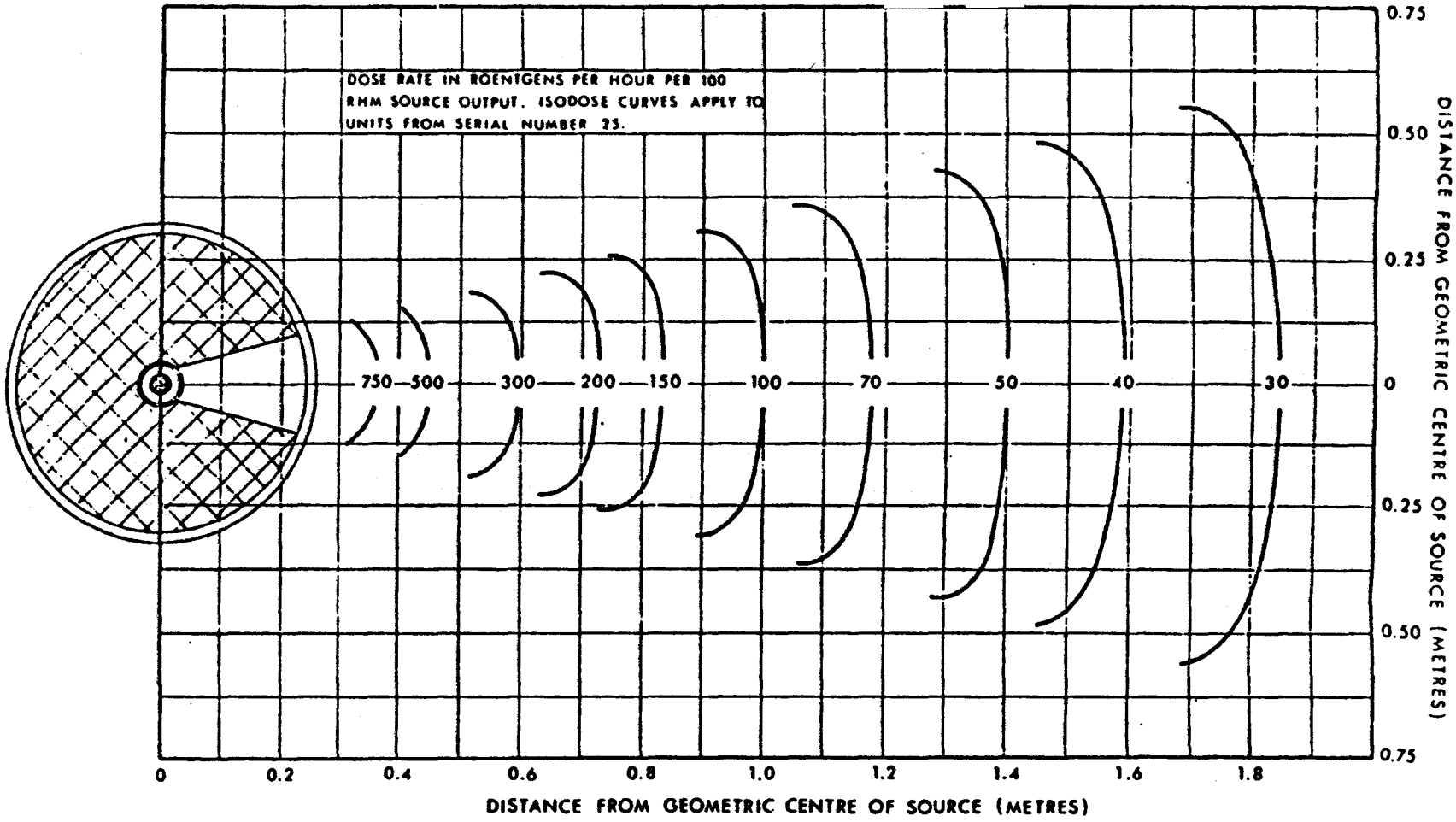

ATOMIC ENERGY OF CANADA LIMITED COMMERCIAL PRODUCTS P.O. BOX 93 OTTAWA	TITLE	GAMMABEAM 150 C ISODOSE CURVES IN AIR HORIZONTAL PLANE			
	REF. DWG.			REVISED	
THIS DRAWING IS THE PROPERTY OF ATOMIC ENERGY OF CANADA LIMITED, AND IS SUBMITTED FOR CONSIDERATION ON THE UNDERSTANDING THAT THERE SHALL BE NO EXPLOITATION OF ANY INFORMATION CONTAINED HEREIN EXCEPT WITH THE SPECIFIC WRITTEN AGREEMENT OF ATOMIC ENERGY OF CANADA LIMITED.	DATE	OCT. 16. 1968		No	REV.
	DRAWN	CHECKED	APPROVED	J400 - X - 10	
	D.L.B.	E.F.R.	A.W.G. F.W.	SHEET 1 OF 1	

APPENDIX 13

Electron Accelerators as Irradiation Facilities

ELECTRON ACCELERATORS AS IRRADIATION FACILITIES

Stan Majewski

CEBAF, Physics Division
Newport News, VA 23606

1. Introduction

At the present phase of planning for plastic scintillator-based detectors at the SSC, one of the crucial questions remains: will the radiation damage be the ultimate obstacle on the way of using this fast, efficient, easy to use and economical active material? This fundamental question of survival must be studied vigorously if the necessary proof of principle is to be delivered on time before the final decisions are to be made. The goal of the present contribution is to focus attention on the lack of satisfactory radiation testing facilities of scintillator samples and detector modules, and to make the point that the existing or planned electron beam sources may fill this gap already in the near future providing appropriate R@D planning by the SSC community is made.

2. Gamma irradiators and their disadvantages

The gamma irradiators remain with neutron irradiators the two main irradiation tools in studies of radiation effects in electronic elements and silicon detectors, as is discussed in many contributions to this meeting. Usually small transversal size beams delivered by these facilities are sufficient for the sample sizes involved and also because of the local character of the damage phenomena in silicon. There are many gamma irradiators located conveniently in the university centers, national laboratories, medical centers, naval research laboratories, etc around the country. The partial list of the gamma irradiators available to the outside users is listed in the contribution to this Task Force meeting by Petersen [Petersen90].

Past and present radiation damage studies of plastic scintillator materials also make use of these gamma irradiators. However, they are limited to small-size samples in a preliminary evaluation phase of radiation resistance studies, usually in the case of new plastic materials. A "classical" example of such an approach is the case of polysiloxane, a radiation-resistant polymer investigated for a plastic scintillator base. In all the studies conducted up to the present, only small-size samples were used [Walker90].

It is well known [Zorn90], that the main effect of radiation on plastic scintillator materials is radiation-induced attenuation due to discoloration (color center formation) of the base plastic material. To study with sufficient precision the effect of this absorption on a final performance of the detector, the real-size samples of fibers,

scintillating plates or waveshifting bars should be used. This in most cases precludes the use of gamma irradiators with their intrinsic limitation to active sample size. In some cases, the researchers attempt to remedy this limitation by use of several gamma sources in the same irradiation chamber or in other more complicated geometry arrangements. However, there still remains the limitation of rather inflexible range of irradiation dose-rates and doses which is not a free parameter but geometry (distance from the source(s)) related.

3. Experimental uses of electron beams in irradiations and the advantages of the technique

In contrast, the electron beams have all the flexibility required to irradiate long or large samples at different, regulated dose rates. The irradiation can be done uniformly over the sample size or following any other preprogrammed dose pattern. This additional and substantial advantage of electron sources will be discussed more in depth later.

The first preliminary irradiation studies of scintillating fiber samples for the SSC detectors were performed quite recently, utilizing the 3 MeV electron Van de Graaff accelerator of the Florida State University in Tallahassee [Majewski89]. In a relatively short time many different mostly 1 mm diameter fiber samples supplied by four major world producers were uniformly irradiated over 50 cm regions and their recoveries were studied in different gas atmospheres. From this comparison, several promising radiation-hard candidates emerged, while many other were found to be not acceptable for further study. An example of obtained results is shown in figure 1. Generally, this was the first convincing demonstration of dramatic differences in resistance limits of different available fiber types. Also, for the first time a clear separation of the attenuation losses and the intrinsic (local) radiation damage was possible by utilizing a method of screening a 1 inch wide fiber section from the electron beam (with a lead brick absorber) during irradiation. Figure 2 shows the result of a scan of some fibers in this region. The step increase at the boundary of the screened section is caused by the difference in scintillation yield in the irradiated fiber and its non-irradiated section. The relative (percentage) value of this step is equal to the percentage loss of the intrinsic (as opposed to long range absorption loss) scintillation yield in the fiber material. Immediately after observing this phenomenon, a succesfull attempt to minimize this local damage effect was made in the green emitting fiber with the 3-hydroxyflavone (3HF) fluor (dye) by increasing concentration of the fluor (Figure 3). This and many other results of that study confirmed that electron beam irradiations are a very efficient and powerful tool in radiation resistance studies.

In a subsequent study with a 80 MeV electron beam of the University of Illinois Microtron [Johnson89, Hertzog90], two small scintillating fiber/lead calorimetric modules were irradiated in an electron beam

and the preliminary results have confirmed that the green emitting 3HF fiber selected in the first study is a much more radiation resistant than the traditional blue emitting fibers. Some results of that study are presented in figure 4 [Hertzog90].

From the past experiences, only briefly described above, and the considerations about planned studies one can prepare a following preliminary list of advantages of electron irradiations :

- generally: possibility to irradiate long and straight samples such as fibers, fiber bunches, light-guide bars, and also large surface scintillator plates, etc.,

- ease and flexibility of control and monitoring of the beam profile and size, with scanning capability by means of standard beam optics elements; for example SSC-type damage profiles can be generated with high energy electron beams (to be discussed below),

- intensity regulation over many orders of magnitude (important in dose-rate studies),

- ease of dose monitoring (in the beam transmission mode) with a simple Faraday cup method.

3.1. Generation of the profile damage "a la SSC"

The most difficult case is the case of scintillation calorimetry at the SSC. Simulation of damage in laboratory conditions is close to impossible, as opposed to the fiber tracker situation, where predictions seem to be relatively straightforward. In our opinion an interesting possibility arises with the availability of higher energy electron beams of the order of many hundred MeV and higher, and is presented here for consideration. From the simulations of the radiation field in the "generic" SSC detector [Groom90], the expected radiation dose depth profile of a combined electromagnetic/hadron scintillating fiber calorimeter (or of a "son-of-Zeus" design, with scintillator/converter plate stack and with waveshifting bars collecting light) is well known. The dose distribution is very non-uniform with a strong and narrow maximum corresponding to a maximum in electromagnetic shower development and a broad, and deeply developed distribution due to the hadronic contribution.

A variation of this idea would be to first irradiate the fiber bunches <u>before</u> inserting them into a calorimetric module, and then testing the resulting performance of the "irradiated module" produced in this indirect way. This method avoids all the difficulty of securing the uniformity of transversal damage at a given depth of the irradiated module. However, it introduces an uncertainty in the time development of the extremely important recovery phase that takes place in fibers after the damage was made. This is caused by very different fiber handling conditions in this case as compared to the real-life

situation, and especially their exposure to air.

This special technique of simulating damage in the SSC conditions, is expected to reproduce better the real situation if applied to the "son-of-Zeus" design. There, the properly pre-irradiated scintillator plates, would be inserted into the stack to form a full "irradiated" calorimetric module. Waveshifting bars, should also be irradiated with the correct depth-dependent dose pattern.

After preparing the fiber module or the plate module, the performance can be first tested with radioactive sources, LEDs, UV-light sources, cosmic rays, and/or the same electron beam used to induce the damage, but turned to a much lower intensity. For example, in the case of the 1 GeV electron beam the average position (depth) of shower maximum for electromagnetic showers is only a "logarithmic" distance away from the expected dose maximum. It will therefore probe the detector module response almost at the most damaged region of this calorimetric module. This beam test can provide crucial information enabling reliable evaluation of damage expected at the SSC, because the gained experimental knowledge can be in turn inserted into simulation programs to predict the effects of the damage on calorimeter detector performance.

Of course, to confirm the conclusions about expected radiation damage effects at the SSC from the damage effects produced and tested in the above proposed way, a "final" test in a high energy beam would be still necessary. However, by following the above procedure the proof of principle can be achieved much faster, as the requested (and difficult to obtain) high energy beam time would be limited to the absolute minimum to test only the final number of preselected solutions, which passed the series of thorough electron beam tests.

3.2. Radiation dosimetry

To secure success of the proposed method a reliable radiation dose dosimetry to calibrate the dose distribution delivered to the plastic material is a must. Fortunately, such a technique exists. It is based on the use of a substance called alanine, the radiation effect on which is evaluated by the Electron Spin Resonace (ESR) method. This, by now well understood and precise dose calibration method, can be applied in the dose range of up to 10 MRad, being therefore an almost perfect match for the dose range used in the scintillator studies. The contribution to this meeting by H. Schoenbacher gives some details on the alanine method and they will not be therefore repeated here.

A set of alanine samples distributed along the irradiated sample, or inserted at several test points into the calorimetric module would provide an experimental dose and dose profile measurement, allowing for a test of the pre-irradiation calculations. Even more, this method can provide control of the total dose and dose profile well before the total planned dose would be delivered, therefore giving an on-line check of the correctness of the irradiation procedure. This

can be achieved by dividing the whole irradiation into two (or more) irradiation periods, with the first, low-dose irradiation period serving as a control irradiation, after which the delivered dose-rate and dose profile would be cross-checked against the calculated (and desired) values. Therefore, if discrepancies are found, the necessary corrections to the irradiation procedure (and to the calculation package) can be made, so that the final result of the total irradiation is as close as possible to the planned one.

4.Available and planned electron beam facilities

In Table I the list of electron irradiation facilities is given in the order of increasing maximum beam energy (see also [Petersen90]). In general, these beams are adapted to deliver radiation doses much higher than the ones needed for the scintillator studies, but in most if not all the cases the dose rate (beam intensity per unit surface) can be lowered to acceptable levels. It is assumed that in the accelerated, time-compressed irradiation studies the highest acceptable equivalent dose rate in a scintillator sample is of the order of 1 Mrad per 5 minutes (up to 5 times higher dose rates were used in some tests), to avoid noticeable heating of material due to energy dissipation in the plastic. This translates into current densities of the order of nanoamps per cm*2 in the case of irradiation of fibers or fiber bunches (for traversing electrons, only a small fraction of their energy is absorbed in the sample material). Total beam current turn down can be accompanied by beam defocussing techniques, including beam scanning, to achieve this goal.

4.1. High energy electron beams

Three high energy electron accelerators are especially promising as possible user friendly irradiation facilities.

The first one is the Bates 1 GeV linac accelerator. Very recently a test facility was proposed there to be used for the SSC detector R@D by several groups from the Boston area [Booth90]. With only a modest upgrade of this facility radiation damage studies can be performed with electron energies up to almost 1 GeV. The only limitation is that the beams will be mostly available in a parasiting mode.

The second facility is being proposed by the Duke University group at the Free Electron Laser laboratory at Duke [Goshaw90]. The proposed facility would be dedicated to detector testing and irradiation studies utilizing the 45 MeV and 1 GeV linacs of the FEL laboratory. The plan is to make beams available on an almost constant percentage beam time basis (about 20 %), and with all the necessary logistical support available for any outside group wishing to use the facility. The proposed beam time structure of the 1 GeV linac can be made to simulate the SSC beam crossing interaction rate of 16 nanoseconds, so the time studies can be made at the same time when testing detector modules for other performance parameters, such as efficiency, energy resolution or radiation resistance limits. The

expected date of completion of the test facility at Duke is by the end of 1991, providing the additional requested funding for the 1GeV test beam will be provided by the DOE and SSC.

Finally, the 4 GeV continuous electron beam accelerator constructed at CEBAF, Newport News, VA will be ready at the beginning of 1994, and it is being discussed what role it can play in the detector R@D for the SSC. It can be assumed that it will be possible to use its beam in some radiation studies, however the details will have to be worked out at a later date.

5. Some comments on test procedures

Several brief comments will be made here on the experimental procedure of radiation damage studies, which is of course interrelated to the problem of selection of appropriate irradiation facilities necessary for a complete and efficient radiation resistance study.

First, one must admit that the present situation is very confusing. There are many experimental results which to a large extent are not consistent with one another. The crucial question of the gas atmosphere effect on the radiation damage and recovery is still to be answered. There is no place here to review these results and discuss in depth the experimental evidence and possible reasons for discrepancies. Such reviews were recently done on other occasions, for example by Zorn [Zorn90]. It is exactly this unsatisfactory present situation that makes the present call for a very vigorous radiation damage R@D programme highly justified, if a proof of principle is to be delivered on time.

However, a list of following general suggestions can be made:

(i) continue tests with small samples (typically 1 cm cube) with gamma beams in a variety of gas conditions (air, argon, nitrogen, oxygen, etc.) and dose-rates (from the extreme of 1 MRad per minute to 1 MRad per 6 months or an even longer period); scintillator samples as well as pure plastic samples and waveshifter samples should be tested (for transmissional damage and recovery); this part of the study is particularly relevant to the plate stack calorimeter design ("son-of-Zeus"),

(ii) increase testing of life-size samples of individual detector elements such as fibers and fiber bunches or scintillator plates, light guides, light couplers, waveshifting bars, and including effects of glues, cladding, etc.; this is when electron beams of several MeV are mostly useful; it can be claimed that some of the most important measurements cannot be made without these flexible irradiation tools, but still a comparison with gamma and fast neutron induced damage should be made for completeness,

(iii) finally, calorimetric modules including mechanical structure, with active material, cladding, glues, epoxies, light guides

and waveshifters, light couplers, etc., and also with gas diffusion channels (as a possible solution to accelerate recovery) should be irradiated and tested in the high energy (many tens of MeV and higher) electron beams (or other high energy beams, if available) as was discussed above in subsection 3.1.; if possible, the irradiations should be performed at different dose rates to be able to extrapolate in a reliable manner the recovery data to the low dose rate SSC conditions,

(iv) to achieve this ultimate goal, the experimental studies should be accompanied by a thorough simulation effort to incorporate all the partial results of measurements and to be able to predict detector behaviour in the SSC conditions; also, at the same time the failure criteria for the detector performance should be defined from the simulation calculations, such as maximum acceptable light loss, attenuation increase, etc. consistent with not compromising detector parameters, such as efficiency, resolution, e/h ratio, etc.; preliminary efforts of this type were already initiated by some groups (Acosta89, Badier90, Gabriel90).

6. Summary

In summary, the combination of testing small scintillator samples irradiated with gamma sources with irradiations of individual fibers, fiber bunches, or scintillator plates and waveshifting bars, and finally of sections of full calorimeter modules in electron beams of up to 1 GeV and higher in energy, is expected to deliver in a relatively short time scale the necessary proof of principle for the plastic scintillator technique applicable to the SSC environment. An important part of the whole procedure is a reliable computer simulation package.

Electron beams in a many MeV energy range are already available and some new beams with interesting parameters and energy in a 1 GeV range may be made available to perform the outlined radiation studies. In view of importance of radiation damage studies for the proposed plastic scintillator detector R@D program, funding of some "user friendly" electron irradiation and test facilities seems to be a necessity in the present situation of a general lack of adequate irradiation and test beams for the SSC detector studies.

Table I

Partial list of electron beam facilities available for radiation studies

Energy	Facility	Location	Comments
2 Mev	Van de Graaff	Brookhaven	
3 MeV	- - - - - - - -	Lehigh U.	
3 MeV	- - - - - - - -	Florida State U.	
22 MeV	linac	Argonne N.L.	
45 MeV	- - -	Duke U.	available from 1990 (see text)
65 MeV	- - -	Naval Res. Lab., DC	
100 MeV	Microtron	U. of Illinois	no beam after 9/1990
100 MeV	linac	Nav. Postgrad. Sch., Monterey, CA	
1 GeV	linac	Bates/MIT	see text
1 GeV	linac	Duke U.	available end 1991 (see text)
4 GeV	2 linac sys.	CEBAF	available beg. 1994

References

Acosta89: D. Acosta et al., The effects of radiation damage on a scintillating fiber calorimeter, UC San Diego, Physics department preprint.

Badier90: J. Badier, Dose profiles/effects on calorimetry, contribution to the Workshop on Radiation Hardness of Plastic Scintillator, FSU, Tallahassee, March 19-21, 1990.

Booth90: Ed Booth, A detector test area at the Bates linac, proposal to the SSC laboratory, and also private communication from Ed Booth, 1990.

Gabriel90: T. Gabriel and T. Handler, Damage simulations, contribution to the Workshop on Radiation Hardness of Plastic Scintillator, FSU, Tallahassee, March 19-21, 1990.

Goshaw90: Al Goshaw et al., A detector test laboratory using a one GeV electron beam at the Duke Free Electron Laser Laboratory, proposal to the SSC laboratory, also private communication from Al Goshaw, 1990.

Groom90: D. Groom, Summary of expected radiation levels in the SSC detectors, contribution to this meeting, and references therein.

Hertzog90: D. W. Hertzog et al., Scintillating fiber calorimetry: performance/survivability, contribution to the Workshop on Radiation Hardness of Plastic Scintillator, FSU, Tallahassee, March 19-21, 1990.

Johnson90: K.F. Johnson et al., High dose calorimetry with scintillating fibers, contribution to the 1989 IEEE Nuclear Science Symposium, San Francisco, January 21-26, 1990.

Majewski89: S. Majewski et al., Radiation damage studies in plastic scintillators with a 2.5 MeV electron beam, Nucl. Instr. and Meth. A281(1989)500.

Petersen90: E. L. Petersen and P. W. Marshall, Standards for electronics radiation testing and remarks about SSC displacement damage testing, contribution to this meeting, also

J. C. Humphreys and C. M. Dozier, Cobalt-60 facilities available for hardness assurance testing, National Bureau of Standards report NBSIR 86-3480, November 1986.

Schoenbacher90: H. Schoenbacher, High-dose dosimetry and standarization of radiation tests, contribution to this meeting, also

F. Coninckx et al., Alanine dosimetry as reference dosimetric system in accelerator radiation environment, presented at the Second International Symposium on ESR Dosimetry and Applications, Munich, October 10-13, 1988, also CERN preprint TIS-CFM/216/CF, February 1989.

Walker90: J. K. Walker, Polysiloxane scintillator, contribution to the Workshop on Radiation Hardness of Plastic Scintillator, FSU, Tallahassee, March 19-21, 1990.

Zorn90: C. Zorn, Studies in the radiation resistance of plastic scintillators. Review and prospects., invited paper presented at the 1989 IEEE Nuclear Science Symposium, San Francisco, January 21-26, 1990.

C. Zorn, Designing a radiation-hard plastic scintillator for high luminosity hadron colliders, contribution to the Workshop on Radiation Hardness of Plastic Scintillator, FSU, Tallahassee, March 19-21, 1990.

Figure captions

1. Comparison of fibers after irradiation to 10 MRad in air and after 8-9 days recovery in air. For each curve, the light output of the fiber at the position of 1.0 inches from its end has been normalized to 1.0.

2. Effect of irradiation on local scintillation yield. Scan of screened region after 10 MRad irradiation in air and 8 days recovery in air of four fiber samples. A "jump" in the attenuation curve is produced by the damage to the local scintillation yield in fiber regions to the left and to the right of the screened unirradiated short fiber section.

3. Comparison of damage to the local scintillation yield after a 100 MRad exposure in air and recovery in air for three different concentrations of 3HF.

4. Pre- and post- irradiation resolution of a small calorimetric module made with 3HF fibers irradiated in a 100 MeV electron beam to approximately 10 MRad (upper figure) and after a 3.5 weeks recovery (lower figure). Note different energy scales.

RECOVERY OF FIBERS

Irradiation 10 Mrad in Air
Recovery 8-9 Days in Air

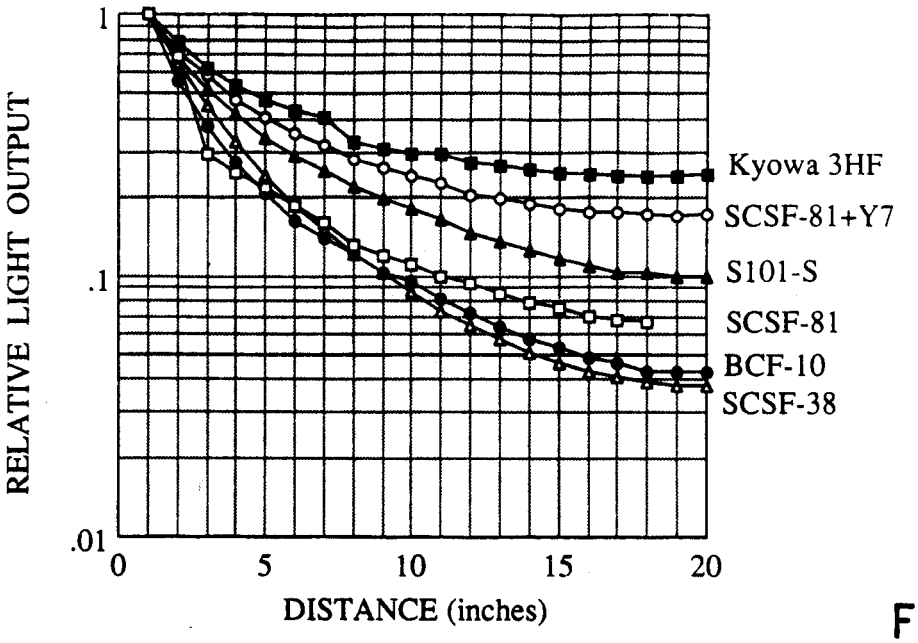

Fig. 1

SCAN OF THE SHADOW AREA

Irradiation: 10 Mrad in Air

Recovery: 8 Days in Air

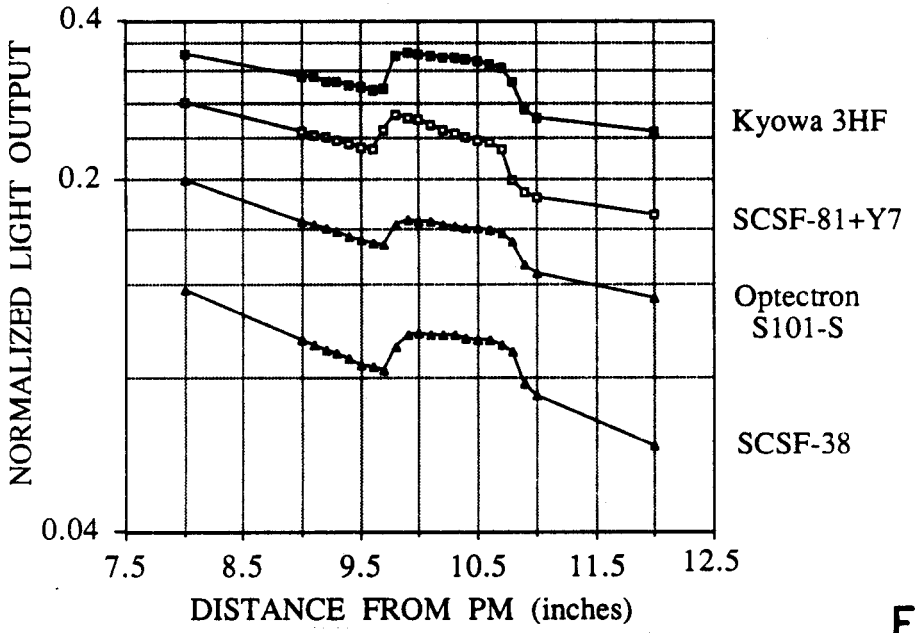

Fig. 2

Loss in Local Scintillation Yield

Bicron 3HF Fibers

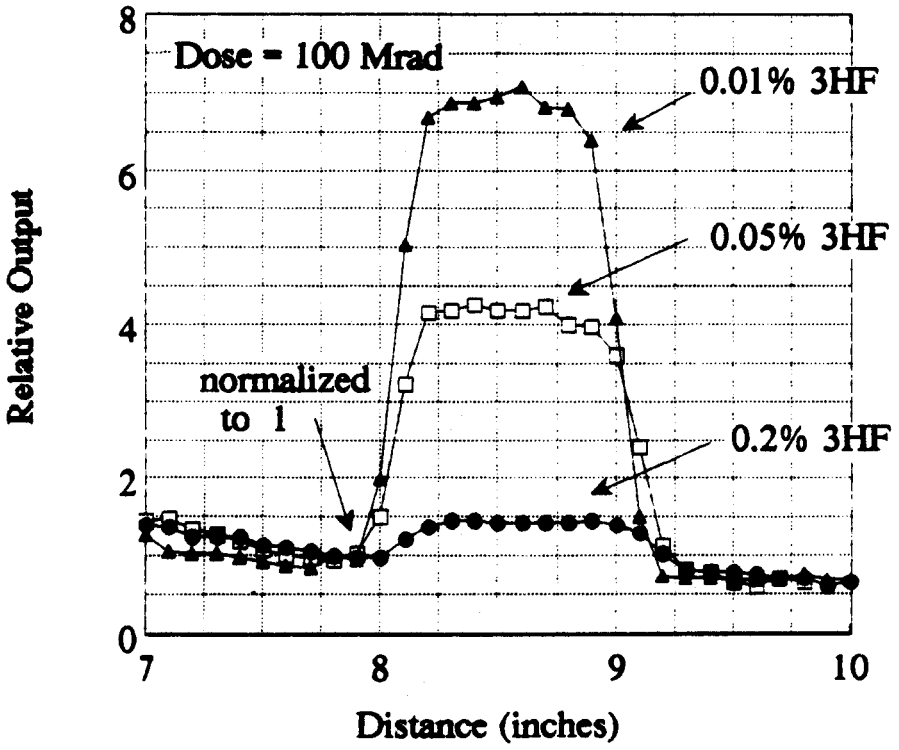

Fig. 3

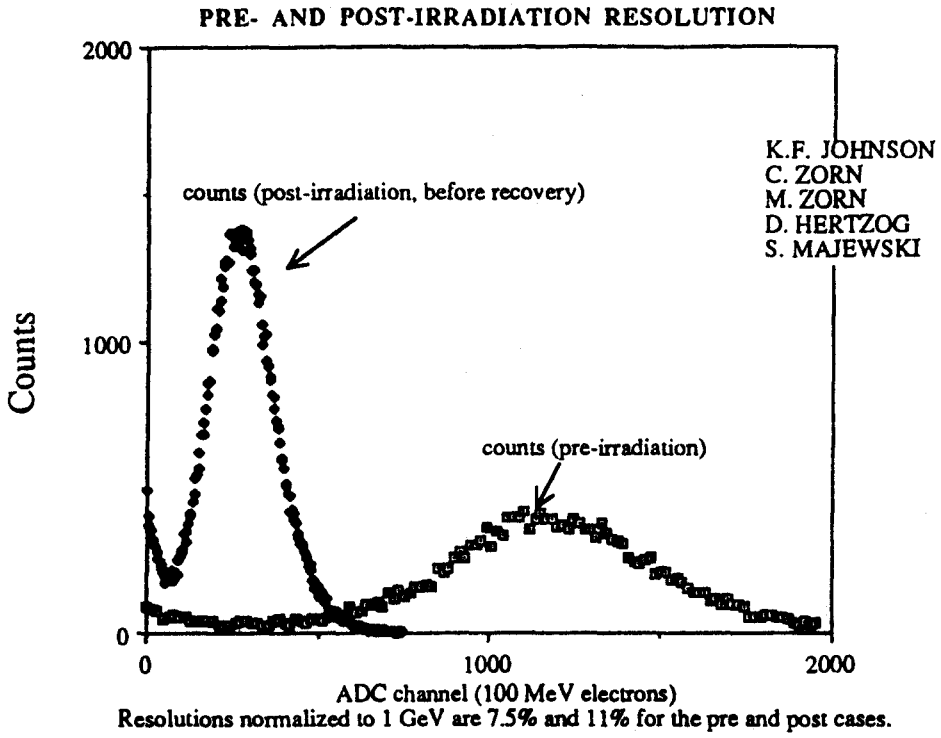
PRE- AND POST-IRRADIATION RESOLUTION
2000
1000
0
Counts
counts (post-irradiation, before recovery)
counts (pre-irradiation)
K.F. JOHNSON
C. ZORN
M. ZORN
D. HERTZOG
S. MAJEWSKI
0
1000
2000
ADC channel (100 MeV electrons)
Resolutions normalized to 1 GeV are 7.5% and 11% for the pre and post cases.

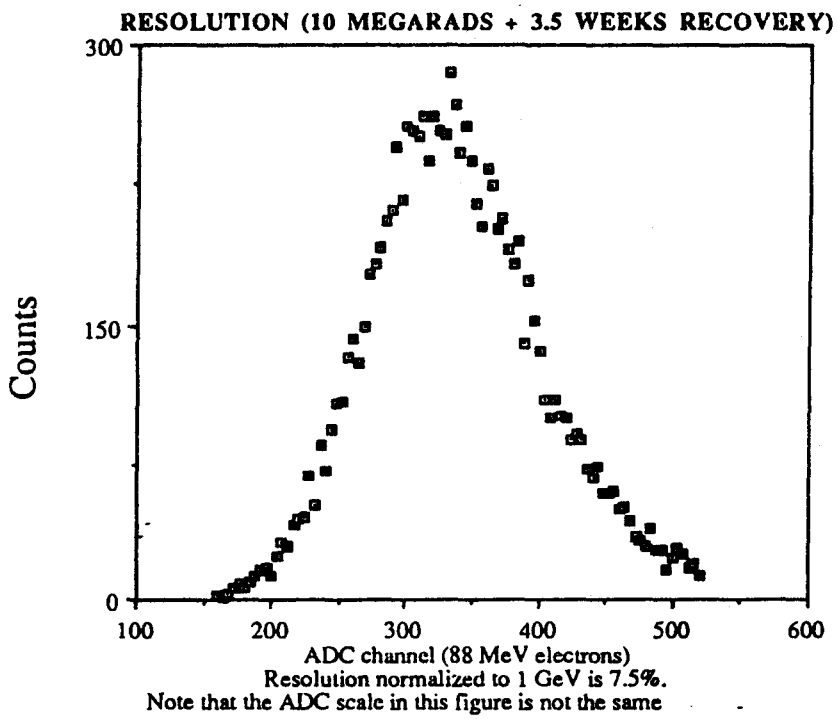
RESOLUTION (10 MEGARADS + 3.5 WEEKS RECOVERY)
300
150
0
Counts
100
200
300
400
500
600
ADC channel (88 MeV electrons)
Resolution normalized to 1 GeV is 7.5%.
Note that the ADC scale in this figure is not the same

Fig. 4

APPENDIX 14

Radiation Displacement Damage Testing at JPL

RADIATION DISPLACEMENT DAMAGE TESTING AT JPL

George Soli
Jet Propulsion Laboratory
California Institute of Technology
4800 Oak Grove Dr. Pasadena, California, 91109

INTRODUCTION

Because of the extreme radiation environment expected in SSC particle detectors, proposed detector read-out chips will require radiation testing. Though the space radiation environment is not as severe, the long duration of deep space exploration missions, and the nature of the detector systems employed, require detector components to be radiation qualified. The detector system of choice is the charge coupled device, CCD, because it increases data quality by orders of magnitude, over older imaging systems. Accomplishments for the CCD this year have produced noise floors below 17 electrons rms and charge transfer efficiencies, CTE, better than 0.999999. This performance is demonstrated by the Fe-55 x-ray spectra shown in figure (1). Unfortunately, optimizing the CCD in these areas has made the detector extremely vulnerable to displacement damage in the space proton environment (1). The CCDs used for displacement damage experiments at JPL are application specific integrated circuits, ASICs. Because specific ASIC design information is available to the radiation experimenter, it is possible to compute the number of vacancies per proton and equate the number to CCD performance degradation.

EXPERIMENT PROCEDURE

For radiation testing a variety of inexpensive chips, available from many manufacturers, a cost effective procedure is to expose the device under test, or DUT, to its expected radiation environment. A LeCroy model TRA1000 preamplifier chip was recently exposed to a gigarad of 2.5 MeV electrons and continued to function at 62mV/microamp (2). But, like many CCDs proposed for space applications, SSC detector read-out chips are likely to be ASICs. An experiment's energy spectrum and fluence is determined from damage computations, and not from the ASICs expected radiation environment. Figure (2) shows Fe-55 line trace plots for two different CCD areas that were exposed to 257 +/-30 and 467 +/-31 keV protons respectively, with both at a fluence of 5E6. Table (1) shows that the charge loss at 257 keV divided by the charge loss at 467 keV equals the ratio of vacancies per proton at the respective energies. Figure (3) defines the trace plots and the charge loss.

SOURCE UTILIZATION

The source most extensively used for CCD displacement damage physics experiments by JPL, is a 5 microcurie Curium-244 alpha source, which is inexpensive and easily handled. The number of displacements produced by each alpha particle is easily computable with commercially available Monte Carlo programs (3). Because the number of vacancies produced by the alpha source is small, a novel method called pocket pumping is employed. This method "pumps" the signal electrons back and forth past the same displacement damage sites until a measurable number are trapped. Small radioactive sources are used to quantify a device specific relationship between displacement damage and signal electron trapping.

The source most used by JPL for proton displacement damage experiments is a six megavolt Tandem Van de Graaff accelerator on the Caltech campus. Experiments using this source are designed as nuclear physics experiments. The CCD is placed in vacuum, and a thin scattering foil, placed far upstream, is used to provide a uniform flux at the CCD. The nuclear physics design is used to produce a monoenergetic beam, which allows the displacement damage to be easily extrapolated to the space environment using Monte Carlo programs, The beam energy and energy straggling are measured with silicon surface barrier detectors and the beam particles counted in plastic scintillator coupled to a photomultiplier tube, PMT.

The extensive displacement damage produced by the high fluences available at the Caltech accelerator verify relationships between displacement damage and performance degradation. The response of the CCD to the low energy, and most damaging, portion of the space proton environment is measured. This extensive damage is used to verify engineering solutions. For CCDs, these include using better silicon to decrease bulk trapping, operating the CCD cold to slow trapping, flooding the CCD with infrared light to fill the traps, in flight damage annealing and designing in lower cross sections.

The high energy source used in displacement damage experiments is the cyclotron at Crocker Nuclear Laboratory, located on the U.C. Davis campus, which can produce 67.5 MeV protons at the CCD. Again, a nuclear physics experiment design is used to produce a monoenergetic beam. Because of the very high fluences required for these higher energy protons to produce significant displacement damage, calibrated Rutherford scattering is used to count protons for fluence control. The counting detectors are also used to measure beam energy and energy straggling. The detectors are BGO coupled to PMTs. These experiments are conducted to verify Monte Carlo displacement damage programs, and extend relationships between displacement damage and performance degradation well into the space proton energy spectrum.

CONCLUSION

For CCDs it is possible to equate charge loss to displacement damage. This damage can be produced with inexpensive sources and extrapolated to the expected radiation environment with Monte Carlo programs. The computations are possible because specific ASIC design information is available to the experimenter.

Radioactive alpha sources are used to quantify a relationship between displacement damage and signal electron trapping in a specific CCD. A high fluence, low energy, proton source is used to relate performance degradation to displacement damage and to verify engineering solutions to CCD radiation damage. Higher energy proton sources are used to verify the Monte Carlo computer programs used to predict CCD displacement damage in a given radiation environment.

Standard experimental nuclear physics methods are used to produce, and verify, that a CCD is exposed to a monoenergetic proton beam. The use of monoenergetic beams allows displacement damage data to be easily compared to Monte Carlo computations.

REFERENCES

(1) J. R. Janesick, G. A. Soli, Proton Damage in Scientific Charge-Coupled Devices, submitted for publication in IEEE Transaction on Nuclear Science, 1990 NSREC.

(2) A. S. Kanofsky, B. Yost, W. Farr, Radiation Effects on Integrated Circuits used in High Energy Research, to be presented at the 1990 IISSC.

(3) TRIM-89, (C) 1989 by J. P. Biersack and J. F. Ziegler

Charge Loss Equated to Displacement Damage

			RATIO	ACTIVE THICKNESS
PROTON ENERGY (keV±FWHM)	257±30	467±31		
CHARGE LOSS (e- ±FWHM)	202±7	38±2	5.29±0.33	
VACANCIES PER PROTON	12±2	0.9±0.3	13.3±5.0	1.00
in active Si	12±2	3.4±0.3	3.5±0.7	1.50

FLUENCE = 5E6

ACTIVE THICKNESS in 1E-4 cm

The CCD is 2E-4 cm of SiO_2 over 2E-5 cm of poly Si over a varying active Si thickness.

All 257 keV protons are stopped at < 1E-4 cm into active Si.

Table (1)

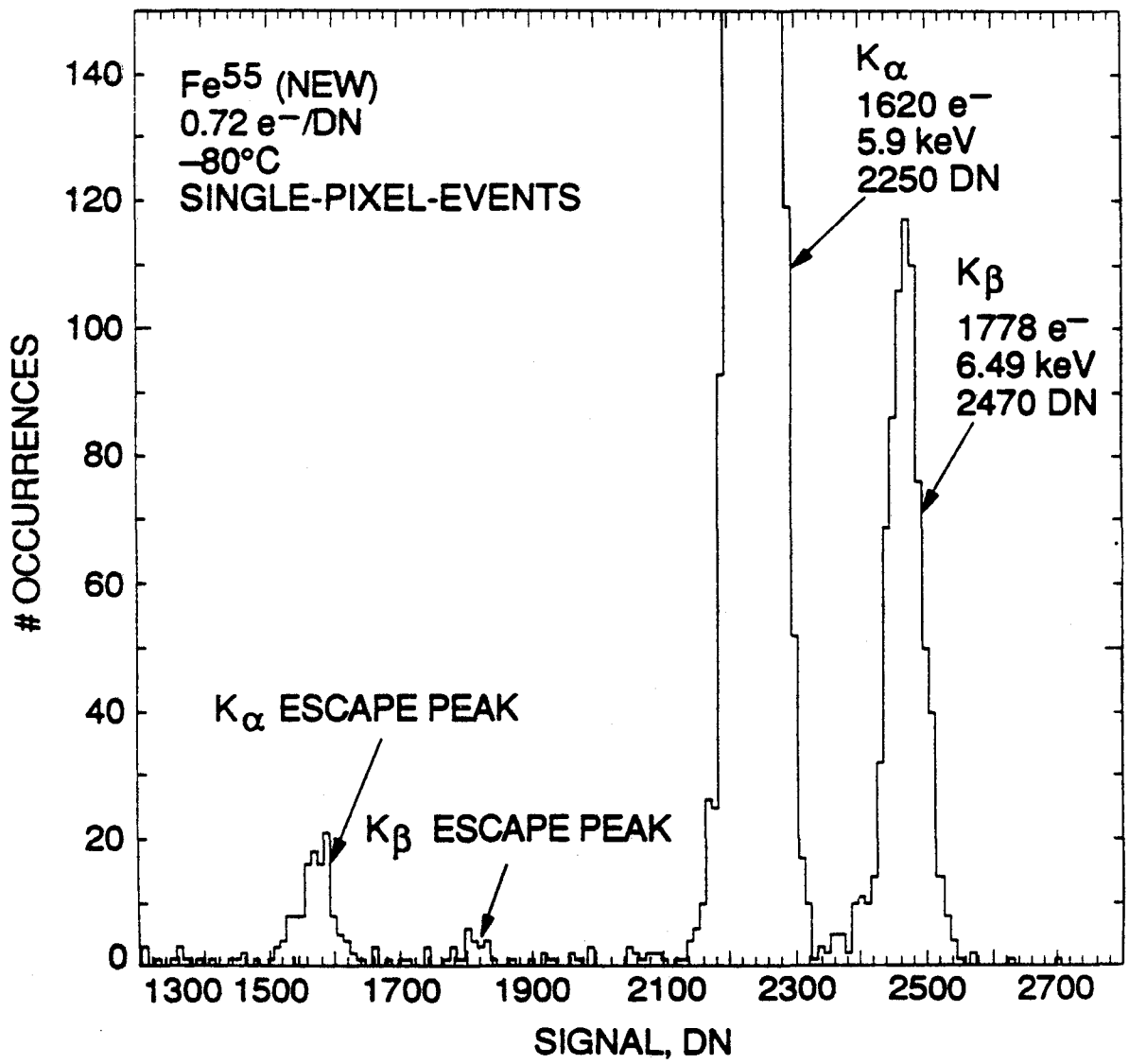
Fe55 (NEW)
0.72 e−/DN
−80°C
SINGLE-PIXEL-EVENTS
Kα
1620 e−
5.9 keV
2250 DN
Kβ
1778 e−
6.49 keV
2470 DN
Kα ESCAPE PEAK
Kβ ESCAPE PEAK
OCCURRENCES
SIGNAL, DN
0
20
40
60
80
100
120
140
1300
1500
1700
1900
2100
2300
2500
2700

Figure (1)

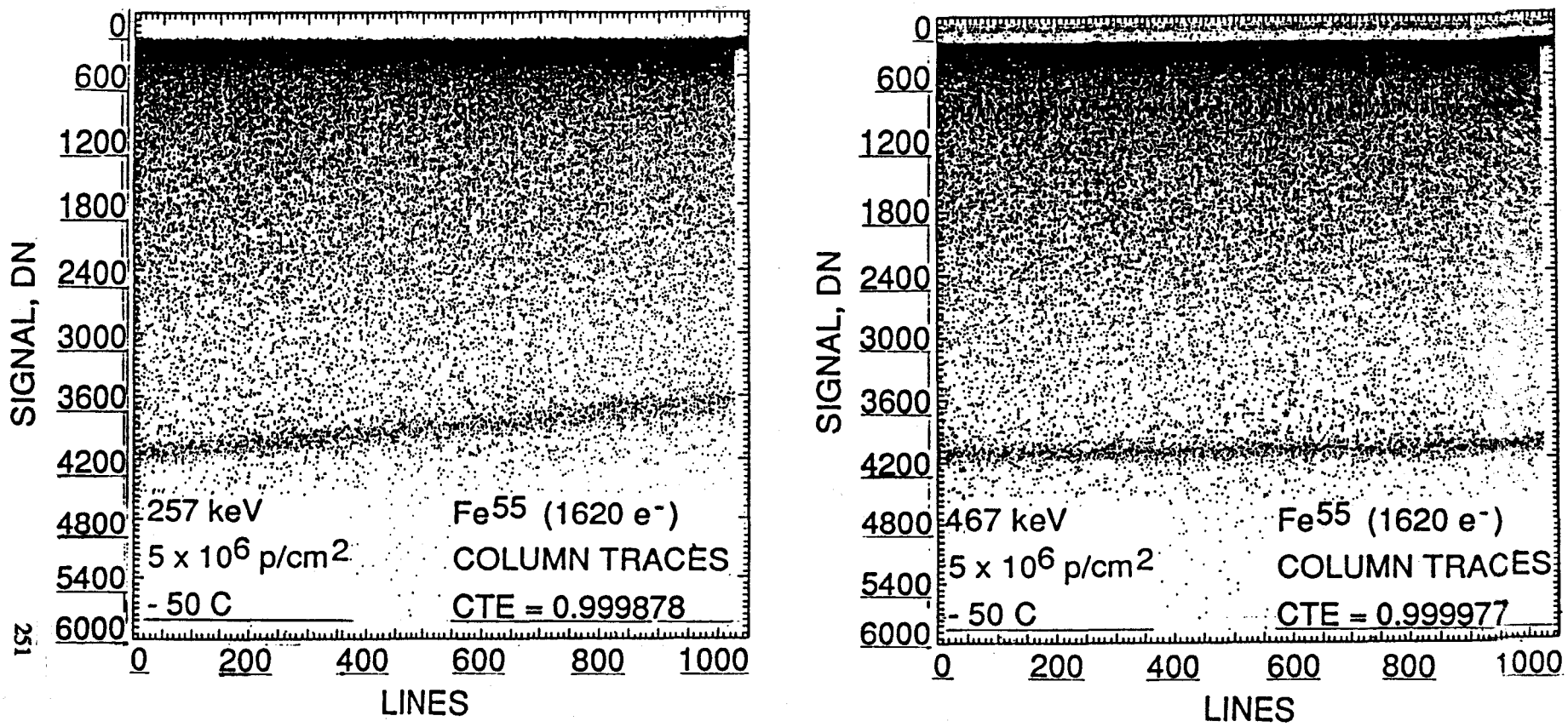
SIGNAL, DN
0
600
1200
1800
2400
3000
3600
4200
4800
5400
6000
257 keV
5 x 10^6 p/cm^2
- 50 C
Fe^55 (1620 e^-)
COLUMN TRACES
CTE = 0.999878
0
200
400
600
800
1000
LINES
SIGNAL, DN
467 keV
5 x 10^6 p/cm^2
- 50 C
Fe^55 (1620 e^-)
COLUMN TRACES
CTE = 0.999977
LINES

Figure (2)

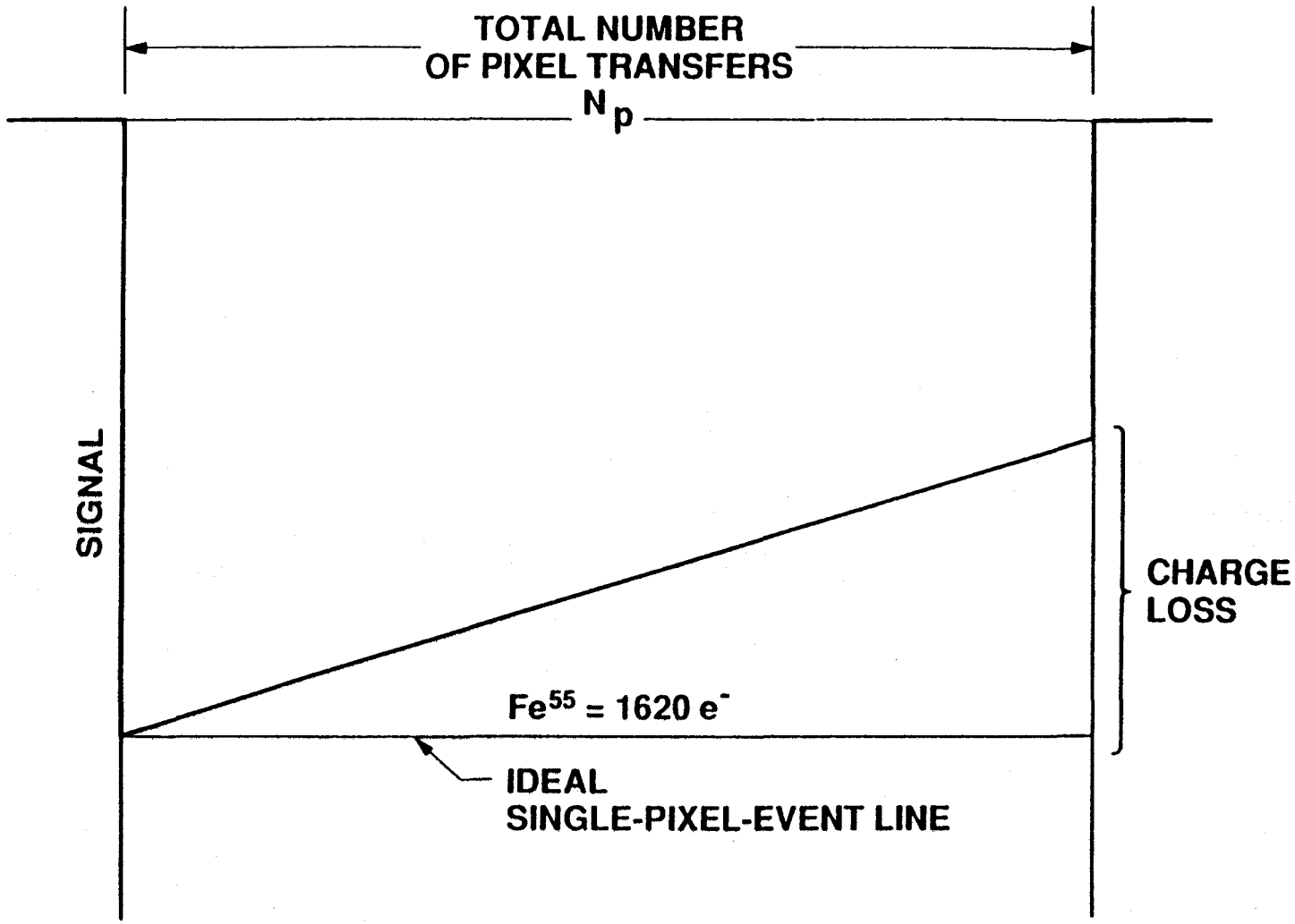

$$CTE = \left[1 - \frac{\text{CHARGE LOSS}}{(1620\ e^-)\ (N_p)} \right]$$

Figure (3)